FLUORESCENT LIGHT-UP PROBES WITH AGGREGATION-INDUCED EMISSION (AIE) CHARACTERISTICS

ZHANG RUOYU

NATIONAL UNIVERSITY OF SINGAPORE

2016

FLUORESCENT LIGHT-UP PROBES WITH AGGREGATION-INDUCED EMISSION (AIE) CHARACTERISTICS

ZHANG RUOYU

(M.S., Dalian Univ. Tech.)

A THESIS SUBMITTED FOR THE DEGREE OF DOCTOR OF PHILOSOPHY

DEPARTMENT OF CHEMICAL & BIOMOLECULAR ENGINEERING

NATIONAL UNIVERSITY OF SINGAPORE

2016

DECLARATION

I hereby declare that the thesis is my original work and it has been written by me in its entirety. I have duly acknowledged all the sources of information which have been used in the thesis.

This thesis has also not been submitted for any degree in any university previously.

_____

ZHANG Ruoyu

31 July 2016

ACKNOWLEDGEMENTS

I would like to take this chance to thank all the people who helped me in the past four years. I would never have been able to finish my thesis without these supports.

I would like to express my sincere gratitude to my supervisor, Prof. Liu Bin, for her guidance, inspiration and encouragement throughout my doctoral study. Prof. Liu has led me to a fascinating world of research and science, in which I got to know how great a scientist can be. Her passion and persistence in scientific research, clear sequence of thought, high efficiency and talent management has deeply impressed me and benefited me not only now but also in the long run.

My genuine thank goes to Dr. Liang Jing, Dr. Feng Guangxue, Dr. Yuan Youyong, Dr. Zhang Chongjing and Dr. Liu Jie for their kind help and guidance during my PhD study. I would like to sincerely thank Dr. Li Kai, Dr. Geng Junlong, Dr. Gao Meng, Dr. Ding Dan, Dr. Cheng Xiamin, Dr. Hu Fang, Mr. Cai Xiaolei, Dr. Wang Long, Dr. Xue Zhaosheng, Mr. Xu Shidang Mr. Guo Bing, Ms. Purnima Naresh Manghnani, Ms. Li Xueqi and Mr. Pan Yutong for their warm help and support in my research work and also my life. Special thank goes to Mr. Boey Kok Hong, Mr. Liu Zhicheng, Ms. Lim Kwee Mei, Ms. Li Fengmei, Dr. Yuan Zeliang, Ms. Lim You Kang, Dr. Yang Liming and other technicians for their supports and assistance.

I also wish to acknowledge National University of Singapore, especially the Department of Chemical & Biomolecular Engineering for providing financial

support for my PhD study. I am also grateful to my thesis advisory committee, Prof. Hong Liang and Prof. Xie Jianping for their valuable suggestion and kind support.

Finally, I would like to express my deepest appreciation to my beloved parents, sister, husband and parents in law for their love, care and understanding. Without them, I could never be here.

TABLE OF CONTENTS

SUMMARY

Fluorescent probes have played a vital role in understanding biological activities, monitoring biological processes and detecting disease markers due to their advantages including high sensitivity and selectivity, versatility and non-invasive functionality, and easy operation. Fluorogenic substances especially organic fluorogens have been explored for construction of bioprobes, on the basis of different mechanisms including photo-induced electron transfer (PET), internal charge transfer (ICT) and fluorescence resonance energy transfer (FRET). However, most of traditional organic fluorogens suffer from a detrimental aggregation-caused quenching (ACQ) phenomenon, which may limit the signal-to-noise ratio. Moreover, only a part of them work in turn-on mode with higher contrast relative to a "dark" background and more accurate results.

A new class of fluorogens has been firstly reported by Tang et al. and has attracted intense research attraction due to their unique aggregation-induced emission (AIE) characteristics. These fluorogens share propeller-shaped structures which undergo intramolecular motion and non-radiative decay when molecularly dissolved. On the other hand, they fluoresce strongly upon aggregation formation or in solid state due to restriction of intramolecular motion (RIM). The unique AIE characteristics make AIEgens ideal candidates for the construction of fluorescence turn-on probes and result in the booming of AIE probes for biosensing and bioimaging. However, the majority of the early AIE probes have been designed based on electrostatic or hydrophobic interactions, which lacks specificity.

In this thesis, AIE-peptide based fluorescence light-up probes are designed and developed for specific biosensing and bioimaging applications by taking advantage of the important biological functions of peptides. Firstly, a general design strategy for the development of AIE probes involving hydrophobic peptide was demonstrated as a proof-of-concept example for thiol detection. Secondly, a red-emissive AIEgen was functionalized with hydrophilic peptide sequences as substrate, which gives fluorescence turn-on upon hydrolysis by chymase in a concentration-dependent manner. The background signal was fine-tuned to optimize the probe performance. In addition, an AIE-peptide conjugate was designed for transferrin receptor (TfR) imaging on the basis of specific receptor-ligand interaction. The AIEgen in this work has reactive oxygen species (ROS) generation ability, making the probe useful for photodynamic ablation of cancer cells. Finally, a novel probe with both AIE and fluorescence resonance energy transfer (FRET) mechanism was developed for the monitoring of cell apoptosis processes. The probe itself is non-emissive due to energy transfer and the dissipation of the acceptor energy through free intramolecular motion of AIEgen, but offers two fluorescent signals responsive to analyte from donor and acceptor moieties, respectively, providing the possibility of self-validation.

LIST OF FIGURES

LIST OF SCHEMES

LIST OF SYMBOLS

AA	amino acids
ABDA	9, 10-anthracenediyl-bis(methylene)dimalonic acid
ACQ	aggregation-caused quenching
AFM	Atomic force microscopy
AIE	aggregation-induced emission
AIEE	aggregation-induced emission enhancement
ATCC	American Type Culture Collection
BBB	blood-brain barrier
BODIPY	boron-dipyrromethene
BSA	bovine serum albumin
BSPOTPE	(1,2-Bis[4-(3-sulfonatopropoxyl)phenyl]-1,2-diphenylethene salt)
CAM	ceric ammonium molybdate
CEA	human carcinoembryonic antigen
CH_3CN	acetonitrile
CLSM	Confocal laser scanning microscopy
Cou	coumarin
Cys	cysteine
dabcyl	4-(dimethylaminoazo)benzene-4-carboxylic acid
DCM	dichloromethane
DDPD	*N*, *N*-dicyclohexyl-1,7-dibromo-3,4,9,10-perylenetetracarboxylic diimide

DIEA, DIPEA	*N*,*N*-diisopropylethylamine
DMEM	Dulbecco's Modified Eagle's Medium
DMF	dimethylformamide
DMSO	dimethyl sulfoxide
DOX	doxorubicin
DSP	dithiobis(succinimidyl propionate)
DTT	dithiothreitol
EA	ethyl acetate
EDANS	(5-((2-Aminoethyl)amino)naphthalene-1-sulfonic acid)
EDC	*N*-(3-dimethylaminopropyl)-*N*′-ethylcarbodiimide hydrochloride
ELISA	enzyme-linked immunosorbent assay
ESI	electrospray ionization
HRMS	high resolution-mass spectrometry
ESIPT	Excited-state intramolecular proton transfer
FRET	fluorescence resonance energy transfer
GSH	glutathione
HBO	2-(2-hydroxy-phenyl)-1,3-benzoxazole
HBTU	*N*,*N*,*N*′,*N*′-tetramethyl-O-(1H-benzotriazol-1-yl)uronium hexafluorophosphate
Hcy	homocysteine
HPLC	high-performance liquid chromatography

HPS	hexaphenylsilole
H_2S	hydrogen sulphide
HSA	human serum albumin
IC_{50}	half-maximal inhibitory concentration
ICT	intramolecular charge transfer
ITC	isothiocyanate
LLS	laser light scattering
MB	molecular beacon
MRI	magnetic resonance imaging
MS-IT-TOF	ion trap-time-of-flight mass spectrometry
MTT	3-(4,5-dimethylthiazol-2-yl)-2,5-diphenylte-trazolium bromide
NBD	7-nitrobenz-2-oxa-1,3-diazole
NHS	N-hydroxysuccinimidyl ester
PCR	polymerase chain reaction
PDT	photodynamic therapy
PeT	photo-induced electron transfer
PET	positron emission tomography
PL	photoluminescence
PNA	peptide nucleic acid
PPh_3	triphenylphosphine
PPi	pyrophosphate anion
ppm	parts per million

PSs	photosensitizers
RB	Rose Bengal
RIM	restriction of intramolecular motion
RIR	restriction of intramolecular rotations
RIV	restriction of intramolecular vibration
ROS	reactive oxygen species
STS	staurosporine
TEA	trimethylamine
Tf	transferrin
TFA	trifluoroacetic acid
TfR	Transferrin receptor
THBA	10, 10', 11, 11'-tetrahydro-5,5'-bidibenzo[a,d] [7]annulenylidene
THz-TDS	terahertz time-domain-spectroscopy
THF	Tetrahydrofuran
TICT	twisted intramolecular charge transfer
TIS	triisopropylsilane
TLC	thin-layer chromatography
TMB	3,3′,5,5′-Tetramethylbenzidine
TMS	tetramethylsilane
TPE	tetraphenylethene
TPS	tetraphenylsilole

CHAPTER 1. INTRODUCTION

1.1 Background

Biosensors are analytical devices for sensing of biomolecules, biological reactions and processes using physicochemical transducers to provide detectable signals. The basic concept of the biosensor was first elucidated by Leyland C. Clark in 1962, by building an "enzyme electrode" for detection of glucose in human samples.[1] On the other hand, fluorescence technique was first used to image cells in the year of 1914 by Provazek.[2] However, fluorescence imaging was limited to fixed samples, which is based on "accumulation" of the fluorescent signal rather than "activation" until the 1980s.[3] The following decades witnessed the prosperity of fluorescent biosensors pioneered by Tsien et al on calcium ions.[4] A wealth of small molecules based fluorescent probes are available in the following decades and become indispensable tools for biological applications. They specifically respond to biological molecules with fluorescence changes either in quantum yield or in wavelength in the absence/presence of the analytes.[5] To achieve recognition in complicate biological systems, probes should possess high affinity to analytes over other interferences, that is, high selectivity. Specific bio/chemo reaction, antibody/antigen immunoreaction, enzyme recognition, peptide nucleic acid (PNA) binding, and ligand/receptor binding have been utilized to develop highly selective probes. Meanwhile, the sensitivity of the probes is determined by the fluorescence signal changes before and after analyte recognition. Mechanisms such as photo-induced electron transfer (PeT), intramolecular charge transfer (ICT) and

fluorescence resonance energy transfer (FRET) are employed to harness the optical properties of fluorescent probes. In terms of working mode, the fluorescence turn-on probes are more advantageous than their turn-off counterparts, as demonstrated by numerous studies.[6, 7, 8] The reasons can be concluded as follows: 1) Turn-on probes enable the measurement of analyte at very low concentration with higher contrast relative to a "dark" background. 2) Turn-on probes are more reliable as turn-off probes may produce false positive signals because many factors other than the target analyte may cause fluorescence quenching. 3) Turn-on probes can provide higher signal-to-background signal, offering higher sensitivity. Additionally, some researchers have made comparisons between turn-on and turn-off assays using the same system and found that, turn-on assay can achieve sensing of analyte in a more direct way.[9] In the following discussion, strategies for development of fluorescent turn-on probes will be discussed.

1.2 Fluorescence turn-on probes based on conventional fluorogens

In this section, strategies for the design of probes based on conventional organic dyes are reviewed, with examples working in turn-on mode. Commonly employed mechanisms include photoinduced electron transfer (PeT), internal charge transfer (ICT), Excited-state intramolecular proton transfer (ESIPT), and fluorescence resonance energy transfer (FRET) while other special cases are also considered.

1.2.1 Turn-on probes based on PeT/ICT/ESIPT mechanism

Photo-induced electron transfer (PeT) mechanism is frequently utilized for the development of fluorescent "turn-on" or "turn-off" probes. In the PeT probes, a fluorogen is connected with an electronegative receptor via a spacer.[10] Excited electron transfers from donor to acceptor and induces fluorescence quenching, which can be recovered by prohibited process. BODIPY dye has been considered as a useful scaffold for the development of fluorescent probes.[11] **Figure 1.1** gives examples of BODIPY-based turn-on probes for the detection of thiols. BODIPY-1, -2 and -3 are developed by modification of ortho-, meta- and para-substituted maleimide moiety as electron acceptors.[12] BODIPY-1 has low quantum yield (Φ) 0.002, which is favorable for construction of turn-on probe, but fluorescence of BODIPY-2 and BODIPY-3 is not quenched effectively with Φ 0.37 and 0.54 (using fluorescein as the reference), indicating the D-A distance is very important. Ma et al. reported BODIPY-4 and BODIPY-5 cysteine detection by employing a stronger electron acceptor 2,4-dinitrobenzenesulfonyl (DNBS) structures.[13] Φ for BODIPY-4 and BODIPY-5 are 0.002 and 0.012, respectively, and their fluorescence shows 54-fold and 300-fold enhancement after reactions with cysteine. These results demonstrate that the distance between the electron donor (D) and the electron acceptor (A) or the donor/acceptor pairs need to be tuned or adjusted carefully to enlarge the signal-to-noise ratio.

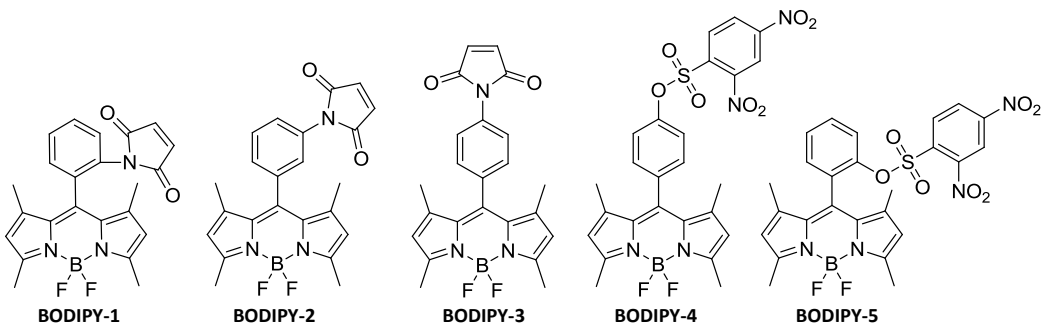

Figure 1.1 Chemical structure of BODIPY based PeT probes for detection of thiols.

In comparison, ICT probes usually show changes not only in fluorescence intensity but also in emission wavelength, which makes ratiometric measurement possible. For example, the electron rich phenanthroimidazole (PI) moiety acts as both a fluorescent dye and electron donor while the aldehyde group was chosen as an electron acceptor (**Figure 1.2A)**. Upon addition of cysteine (Cys) or homocysteine (Hcy), PI-1 shows a blue shift in emission, with gradual decrease at 519 nm and concomitant growth of a new emission band at 394 nm, due to switching off of intramolecular charge transfer (**Figures 1.2 B** and **C**).[14] The results indicate that the addition reaction between Cys/Hcy and the probe lead to the deconjugation of the electron donor-acceptor system and switch off the ICT process, with a blue shift in both absorption and emission spectra.

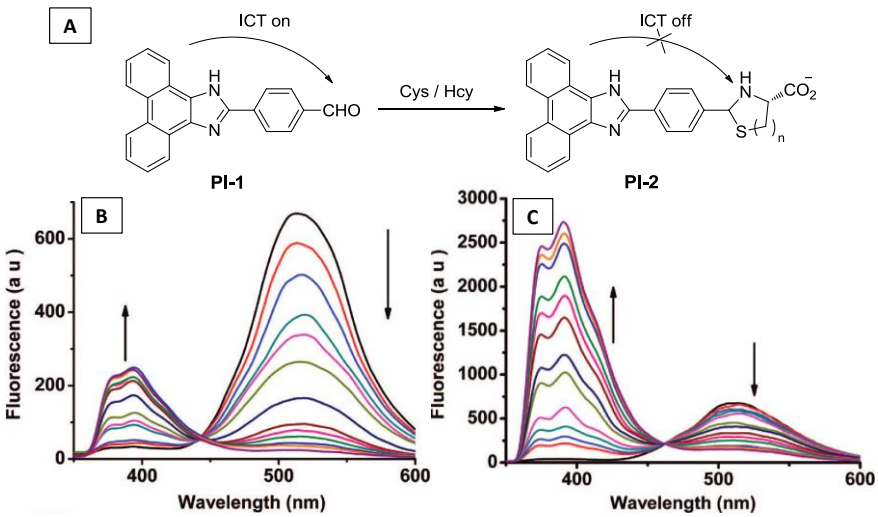

Figure 1.2 (A) Reaction mechanism of PI-1 with Cys and Hcy. Fluorescence spectra of PI-1 upon reaction with increasing concentration of (B) Cys and (C) Hcy.[14] Copyright 2008 American Chemical Society.

Fluorogens with Excited-state intramolecular proton transfer (ESIPT) usually show large Stokes shift which is favorable for the elimination of background signals.[15] **Figure 1.3** shows a ratiometric probe for detection of pyrophosphate anion (PPi) based on a 2-(2-hydroxy-phenyl)-1,3-benzoxazole (HBO) derivative.[16] When Zn^{2+} is added to chelate with the HBO probe, the phenoxide "oxygen" is occupied and the ESIPT process is blocked. The formation of complex of PPi and the two Zn^{2+} releases the phenol moiety, retrieving ESIPT process with fluorescence changing blue (λ_{em} = 420 nm) to green (λ_{em} = 518 nm) color. This method provides a simple and quick way to monitor the pyrophosphate released during DNA polymerase chain reaction (PCR).

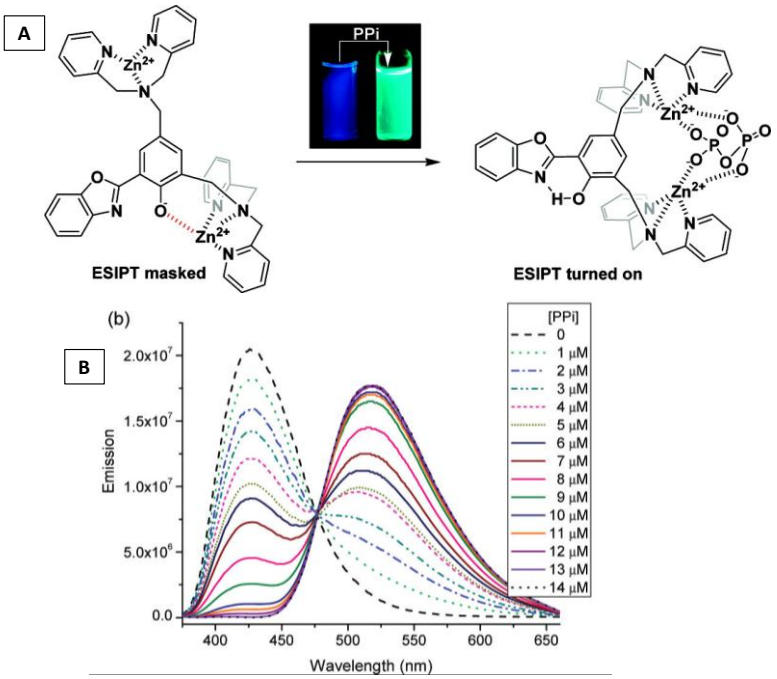

Figure 1.3 (A) Reaction mechanism for pyrophosphate anion (PPi) detection based on ESIPT fluorogen.[16] Copyright 2011 American Chemical Society.

1.2.2 Turn-on probes based on fluorophore/quencher pairs

Incorporation of strong electron-withdrawing groups into fluorogens significantly diminishes the fluorescence, which provides potential for development of turn-on probes. Usually these fluorescence quenchers are connected with the fluorogens through a covalent bond which can be specifically broken upon analyte recognition. For example, **Figure 1.4** demonstrates a turn-on probe for the detection of hydrogen sulfide (H_2S) using dinitrophenyl ether group as a fluorescence quencher.[17] The reducing or nucleophilic properties of H_2S leads to thiolysis of dinitrophenyl ether and evident fluorescence quick turn-on at 555 nm. Other electron-withdrawing groups such as 2,4-dinitrobenzenesulfonyl ether[18, 19] and 7-nitrobenz-2-oxa-1,3-diazole (NBD)[20] ether can also perform as fluorescence quenchers and have been applied for H_2S or cysteine detection.

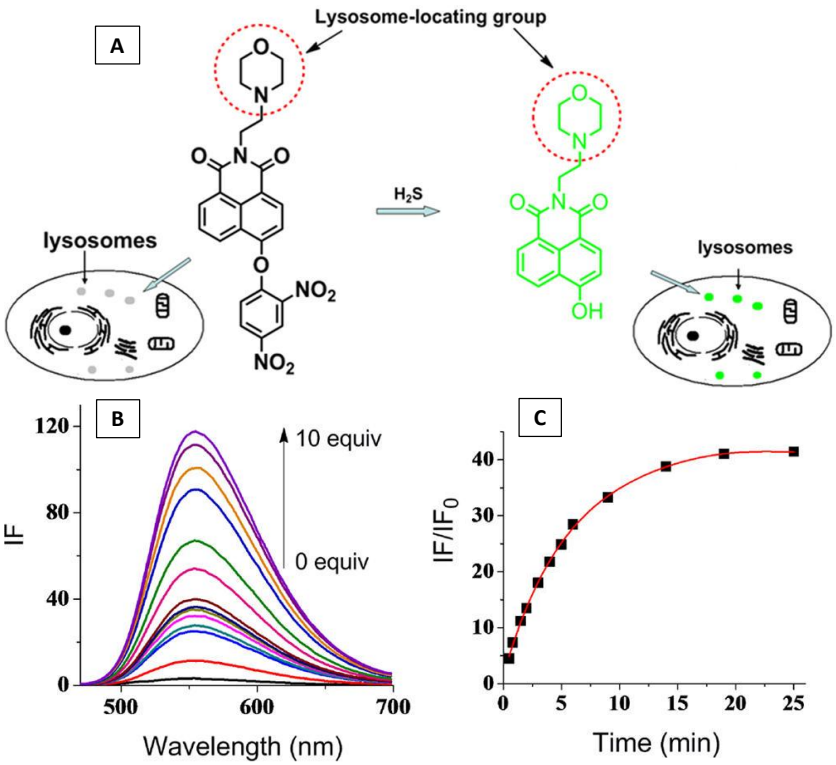

Figure 1.4 (A) Schematic illustration of a turn-on probe for monitoring hydrogen sulfide level in lysosome. (B) PL spectra of Lyso-NHS in the presence of 0-10 equiv. of H_2S in CH_3CN/PBS = 1:9, pH = 7.4 at 37 ^oC. (C) Time-dependent fluorescence intensity of Lyso-NHS at 555 nm with 10 equiv. of H_2S.[17] Copyright 2013 American Chemical Society.

Fluorescent resonance energy transfer (FRET) occurs between a donor molecule (moiety) in its excited state and an acceptor molecule (moiety) in its ground state. FRET has been exploited in ratiometric detection where both donor and acceptor groups are intrinsically fluorescent.[21] In addition, some acceptor chromophores that are intrinsically not fluorescent have been employed for development of turn-on probes. For instance, donor fluorophore (5-((2-Aminoethyl)amino)naphthalene-1-sulfonic acid) (EDANS) and the quencher 4-(dimethylaminoazo)benzene-4-carboxylic acid (dabcyl) are linked by a molecular beacon (MB) molecule **(Figure 1.5 A)**.[22] MBs are synthetic oligonucleotides that have a loop-and-stem structure. The loop portion enables the MB to recognize a

target nucleic acid or a ssDNA binding protein, while the stem portions flanking either side of the probe are complementary to each other (5-7 base pairs usually). Consequently, the fluorescence of the EDANS part is quenched due to formation of stem hybrids that keep the fluorophore and the quencher close to each other, which can be restored by hybridization with target DNA or specific binding with proteins that interact with ssDNA **(Figure 1.5 B)**.[23] Based on the similar principle, FRET-based proteinase probes are developed with turn-on fluorescence upon enzymatic cleavage that separates the fluorophore and the quencher.[24] Design of FRET probes is relatively predictable on the basis of the spectral properties of the donor-acceptor pairs and the distance between them. Förster theories elucidate all the factors that affect the FRET efficiency as indispensable references for the design of FRET probes.[25] The absorbance and emission spectra of common fluorophores and quenchers are summarized in **Figure 1.5C.**[26]

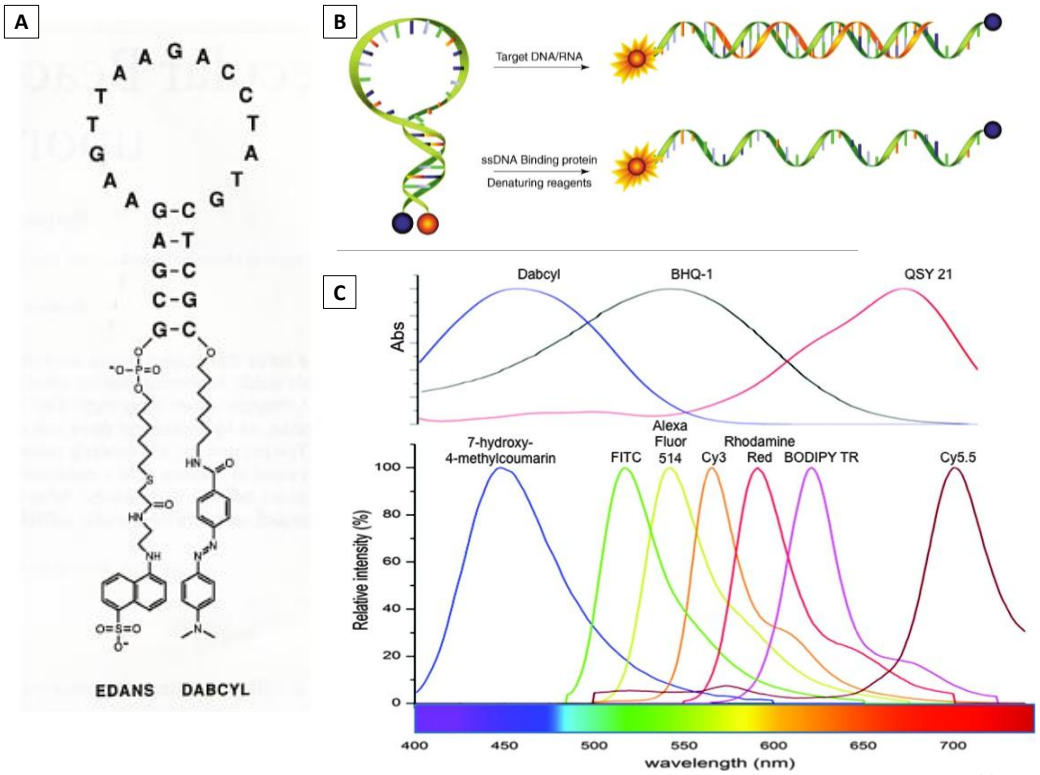

Figure 1.5 A typical example of FRET-based molecular beacon (MB).[22] (B) Mechanism of MB DNA probe operation. MB molecules form stem hybrids which keep the fluorophores close to the quenchers and do not show fluorescence, which fluoresce strongly when the stems move apart upon hybridization with complementary DNA strand or interaction with ssDNA binding proteins.[23] (C) Absorbance and Emission spectra of common fluorophores and quenchers.[26] Copyright 2004 Elsevier Ltd. Copyright 2015, NRC Research Press.

1.2.3 Other examples

In addition to the above examples, some fluorescent probes are designed based on ring-opening of the spirolactam structure, for example, a rhodamine derivative show a red color change and strong fluorescence in acidic solution by activation of a carbonyl group in a spirolactone as shown in **Figure 1.6**. Compound 1 is non-fluorescent and colorless in water-methanol (v/v = 80/20) solution at pH 7, as it exists in the spirocyclic form. The addition of mercuric ion to the solution prompts a 1:1 stoichiometric reaction which results in the formation of ring opened

compound 4. The compound 4 has a large molar absorptivity (logϵ = 4.67) and a high fluorescence quantum yield (Φ = 0.52) with a pink color and a strong yellow fluorescence (λ_{em} = 556 nm).[27] Based on the similar principle, other ligands or analytes that can break the spirolactam ring are designed for turn-on detection of zinc (II),[28] copper (I)[29] and mercury (II)[30] ions and small molecules [31, 32] with significant fluorescence enhancement. However, assays based on this mechanism are somewhat dependent on the solvent system and usually require large fractions of organic solvent.[33]

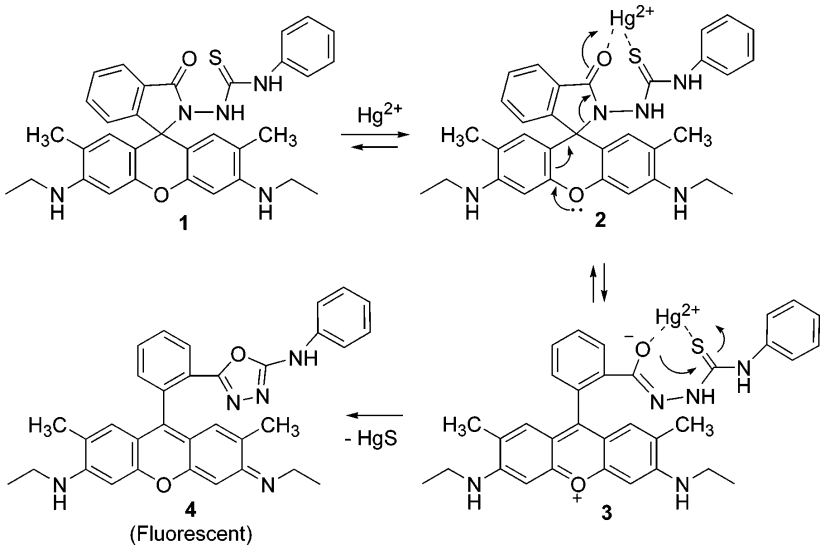

Figure 1.6 Ring-opening reaction of rhodamine derivative for detection of mercuric ion.[27] Copyright 2005 American Chemical Society.

The prosperity of fluorescent probes is due to their advantages including high sensitivity and selectivity, non-destructive visualization, ease of operation, and versatile functionality. However, drawbacks or limitations still exist in each system, thus researchers are always in enthusiastic pursuit to explore advances in fluorescence chemistry and technical discoveries. For example, the constructions of probes based on these mechanisms are relatively unpredictable and empirical

and only a few turn-on probes have been successfully constructed. What is worse, conventional fluorophores suffer from detrimental self-quenching effect, which limit the signal-to-background ratio. For instance, Waggoner et al has found that the quenching of fluorescence is inevitable in development of multiply-labeled fluorescent DNA probe with high labeling density.[34] Thus, it would be ideal if there is one kind of fluorophores which fluoresce strongly even at high concentration without self-quenching.

1.3 AIE fluorogens

1.3.1 Phenomenon and mechanism

As describe above, in order to construct turn-on probes using traditional fluorogens, quenching moieties or groups are needed to achieve "off" state, resulting in complicated probe designs. Moreover, traditional organic fluorogens suffer from a detrimental phenomenon, for example, their fluorescence is weakened at high concentration or aggregated state, which is coined as aggregation-caused quenching (ACQ). **Figure 1.7** gives a vivid demonstration using *N, N*-dicyclohexyl-1,7-dibromo-3,4,9,10-perylenetetracarboxylic diimide (DDPD) as an example. DDPD shows strong fluorescence in its benign solvent THF, but the fluorescence is weakened gradually as the water fractions increase and is almost quenched when water fraction is 70%. This is because fluorogens such as DDPD has a planner aromatic structure which tends to form strong π-π stacking in aggregate state or in concentrated solution. The excimer and exciplexes formation results in nonradiative decay and quenched fluorescence. The detrimental ACQ

effect forces researchers to use dilute solution or low labeling density which will results in low signal-to-noise ratio. It would be ideal if there are fluorogens that do not suffer from ACQ effect can be developed into fluorescence turn-on probes by their intrinsic optical properties.

In 2001, Tang et al observed an interesting phenomenon: when a drop of silole derivative solution was cast on a TLC plate, the wet spot is hardly emissive but the dried spot fluoresces strongly under UV illumination.[35, 36] This intriguing phenomenon signifies that aggregation plays a positive role in the luminescence process of silole compared with its negative role in conventional organic fluorogens. This unique optical property was termed as "aggregation-induced emission" (AIE). As shown in **Figure 1.7,** HPS is non-emissive when molecularly dissolved in THF but shows strong fluorescence upon aggregation formation, for instance, when there is 90% water in the mixture of water/THF.[37] Later on, tetraphenylethene (TPE) was developed and studied intensively. This unique optical property provides a solution to ACQ problem and allows researchers to work with this intrinsic property rather than work against it.

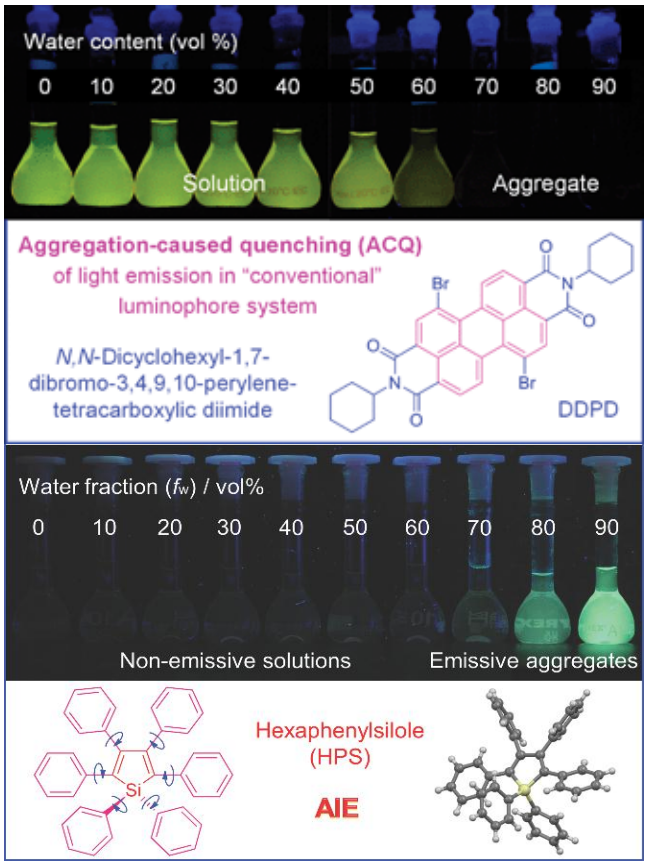

Figure 1.7 Photographs of N,N-dicyclohexyl-1,7-dibromo-3,4,9,10-perylenetetracarboxylic diimide (DDPD) (10 μM) (top) and hexaphenylsilole (HPS) (20 μM) (bottom) in THF/water mixtures with different water fractions under UV illumination.[37, 38] Copyright 2011 The Royal Society of Chemistry. Copyright 2014 WILEY-VCH.

Subsequently, intensive investigations help to deepen the understanding of the luminescence process of AIEgens and several mechanisms have been employed to explain the unique AIE characteristics, including restriction of intramolecular rotations (RIR), twisted intramolecular charge transfer (TICT), J-aggregate formation, E/Z isomerization, etc.[38, 39, 40, 41, 42] However, only indirect experimental evidence has been applied until Pickwell-MacPherson et al. reported the direct evidence with the assistance of terahertz time-domain-spectroscopy (THz-TDS) and solid-state computational simulations.[43] For the first time, the restriction of intramolecular motions was proved to cause the increase in fluorescence intensity

using TPE as an example. As shown in **Figure 1.8,** in dilute solution or molecularly dissolved state, the phenyl rings of TPE undergo dynamic intramolecular motions which consume excited state energy through non-radiative decay pathway. In contrast, the restriction of intramolecular motions (RIM) restricted upon aggregation formation leads to fluorescence recovery. This report provides the mechanism support for most AIE systems. In addition, there is another type of AIEgen, typically, 10, 10', 11, 11'-tetrahydro-5,5'-bidibenzo[a,d] [7]annulenylidene (THBA) which do not have any rotatory elements.[44] In this molecule, two non-coplanar structures are connected by a bendable double bond with formation of an *anti*-conformation. The flexible double bond allows THBA to undergo dynamic vibration in solution state and consumes excited state energy through non-radiative decay pathway. Similarly, the energy decay pathway can be blocked by restriction of intramolecular vibration (RIV) upon aggregation formation, which opens up radiative decay and recovery of fluorescence.[45, 46] So far, these two mechanisms can provide mechanism explanations for most AIE systems and they are named as restriction of intramolecular motion (RIM) collectively.

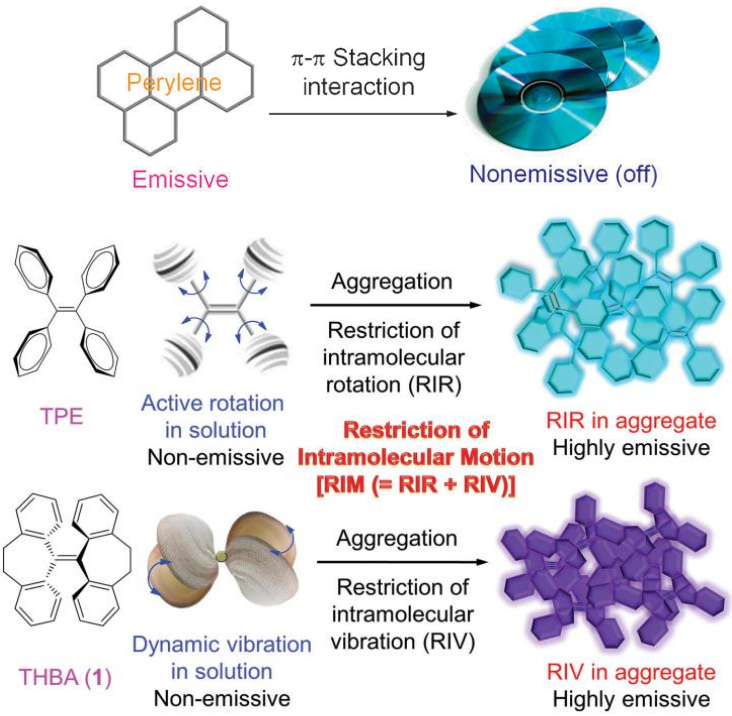

Figure 1.8 Planar fluorogens such as perylene tend to form disc-like aggregate due to strong π- π stacking, which leads to the excimers formation and fluorescence quenching.[37] Propeller-shaped AIEgen such as TPE undergo intramolecular motions and fluorescence quenching when molecularly dissolved, but show strong fluorescence in the aggregation state by restriction of intramolecular motions (RIM). Shell-like AIEgens THBA undergoes dynamic vibration which quenches fluorescence which recovers upon restriction of intramolecular vibration (RIV).[38] Copyright 2011 The Royal Society of Chemistry. Copyright 2014 WILEY-VCH.

1.3.2 AIEgens and functionalization

In addition to the silole molecules firstly reported in 2001 featured with AIE characteristics, more and more molecules are found to be AIE active. Hexaphenylsilole (HPS), tetraphenylsilole (TPS), TPE are still the classic structures with typical AIE features **(Figure 1.9).** Researchers have attempted to convert ACQ fluorogens to AIE fluorogens, but only very limited success has been achieved. For example, N,N-dicyclohexyl-1,7-dibromo-3,4,9,10-perylenetetracarboxylic diimide (DDPD) is an ACQ fluorogen, while TPE-DDPD shows AIE characteristics as two TPE molecules are conjugated to one DDPD.[47, 48]

The majority of AIEgens are still derivatives modified from the above iconic AIE structures.[49] It is noteworthy that the incorporation of dicyanovinyl groups into TPE structure yielded molecules i. e. TPECM in **Figure 1.9** with visible absorption and orange to red emission. Moreover, Liu et al. found that the introduction of dicyanovinyl groups endows TPECM with ROS generation ability upon light irradiation. Thereafter, a series of AIE-based probes for image-guided photodynamic therapy were developed.[50, 51] Later, Liu et al. further fine tune the singlet-triplet energy gap to improve the singlet oxygen generation ability of AIE photosensitizers. The development of these molecules enriches the AIEgen library with versatile functionalities.[52]

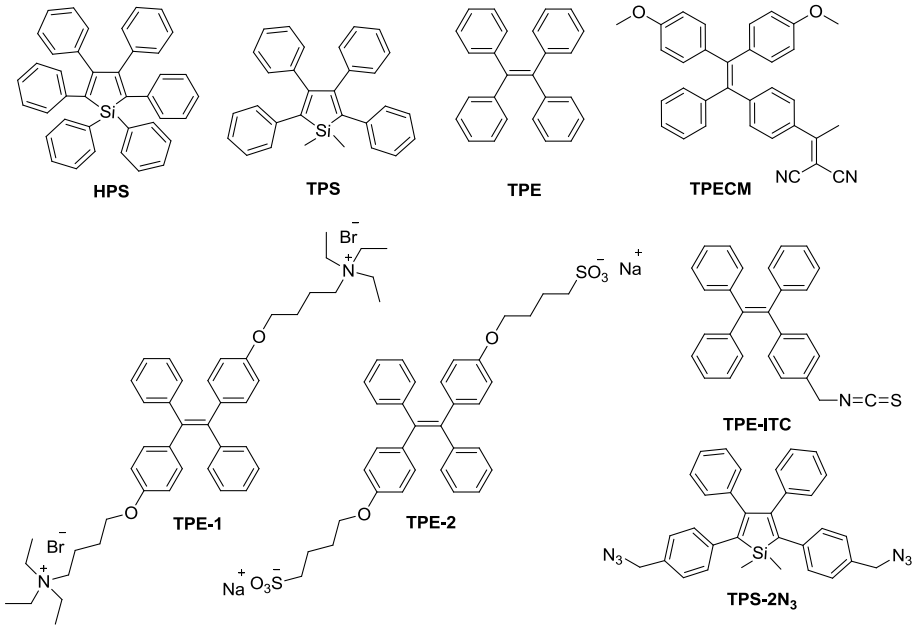

Figure 1.9 Chemical structures of conic AIE fluorogens and their functionalized derivatives.

Good water solubility is one of the most important prerequisites for the development of bioprobes. To disperse AIE molecules into aqueous media, they are chemically modified with ionic groups such as ammonium and sulfonate. These

positively and negatively charged AIE probes are the typical examples of early generation of AIE probes. (TPE-1 and TPE-2 in **Figure 1.9**). Detailed sensing mechanism will be elucidated later in this chapter. Subsequently, AIEgens are functionalized with active moieties to achieve specific interactions with the analytes of interest. For example, TPE-ITC has been synthesized with an isothiocyanate (ITC) group which is reactive to molecules containing amino group.[53] The copper(I)-catalyzed "click chemistry" between azide and alkyne is one of the most commonly used conjugation approach since TPS-$2N_3$ reported by Liu et al.[54] **Figure 1.10** summarized common conjugation chemistry for AIE probes.[55] Copper(I)-catalyzed "click" chemistry is the most widely used conjugation approach thanks to its rapid reaction with minimum side reactions (**Figure 1.10A**). Another merit of alkyne-azide click chemistry is good biorthogonality, which allows reaction occurrence without interference from native biochemical processes. On the other hand, for biolabeling of biomolecules containing amine groups such as proteins and peptides, potential candidates include isothiocyanate (ITC), carboxyl groups or N-hydroxysuccinimidyl ester (NHS) modified AIEgens (**Figure 1.10B-D**). Another popular method for conjugation is the reaction between maleimide and thiol which yields a stable thioester bond (**Figure 1.10E**). It is a good choice for conjugation of AIEgen with peptide sequence containing cysteine.

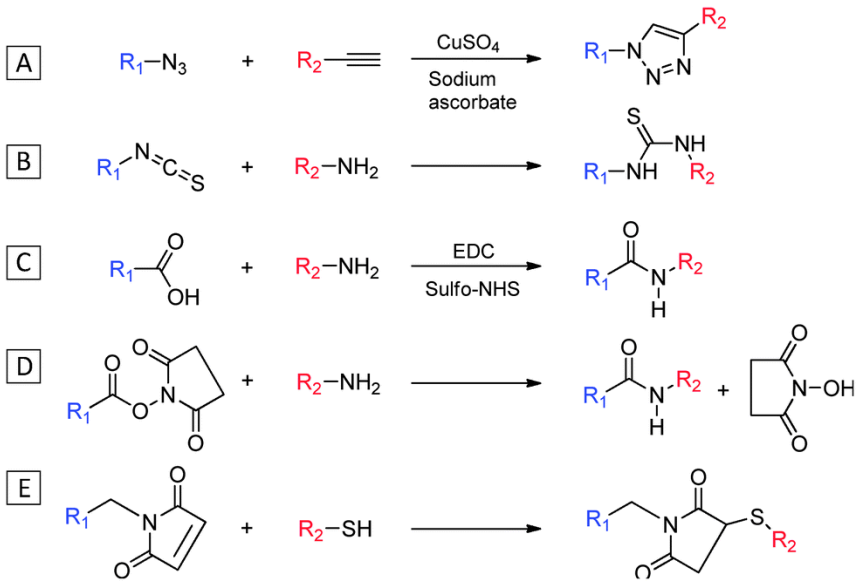

Figure 1.10 Reaction of (A) azide with alkyne, (B)-(D) isothiocyanate, carboxyl, and N-hydroxysuccinimidyl ester with primary amine, and (E) maleimide with sulfhydryls.[55] Reproduced from The Royal Society of Chemistry under a Creative Commons Attribution 3.0 Unported Licence.

1.4 Working principle of AIE probes

In addition to a proper AIEgen, there are three elements to design a light-up AIE probe: The first one is to achieve low background signal by fully exerting the intramolecular motions of AIEgens. Specifically, charged or hydrophilic moieties are introduced to AIEgens to disperse them into aqueous media or to make them molecularly dissolved. Secondly, a proper recognition moiety is needed to allow specific interactions between the probe and the analyte of interest. The specific recognition should induce restriction of intramolecular motions (RIM) which further results in remarkable fluorescence turn-on. Finally, the AIEgen should be properly functionalized, which facilitates further modifications for recognition or hydrophilic moieties, which have been elucidated in details in the above section (1.3.2). Different recognition interactions determine various working mechanism

of the probes. In the following section, some representative AIE light-up probes will be illustrated from the perspective of different working mechanism.

1.4.1 Electrostatic and/or hydrophobic interactions

Early AIEgen based probes are developed by taking advantage of the electrostatic or hydrophobic interactions between charged AIEgens and biological substances. In 2007, by the functionalization of two tertiary amino groups with hexaphenylsilole (HPS) (**Figure 1.11A**), Tang et al. developed A_2HPS which is non-emissive in acidic aqueous media as it is molecularly dissolved. Moreover, they found that the non-emissive A_2HPS shows fluorescence turn-on with the addition of BSA or DNA as well as increase of pH.[56] Inspired by this interesting phenomenon, Zhang et al. developed a label-free turn-on probe for the detection of DNA and nuclease assay with improved selectivity.[57] In their work, they synthesized a silole derivative with a quaternary ammonium moiety (**Figure 1.11A**) and then mixed the probe with different single-strand DNA (ssDNA) and double-strand DNA (dsDNA) sequences with increasing number of bases (pairs). It was found that longer DNA chain will induce more significant fluorescence enhancement of AIE probes when they are incubated in aqueous solution. In addition, a 27-bp dsDNA can induce more evident fluorescence enhancement compared with that induced by a 27-mer ssDNA. The driving force for the interactions between the DNA and the probe is attributed to the electrostatic interaction between positively charged quaternary ammonium moiety and negatively charged phosphate anions in DNA. In addition, the hydrophobic

interaction between phenyl groups in silole structure and the nucleosides in DNA may also contribute to the fluorescence enhancement. Although the interactions between DNA and the probe are based on non-specific electrostatic interactions, Zhang et al. proposed to use nuclease that can cleave DNA sequences into fragments to induce fluorescence decrease. This method can realize the detection of nuclease and its inhibitor screening (**Figure 1.11B**).

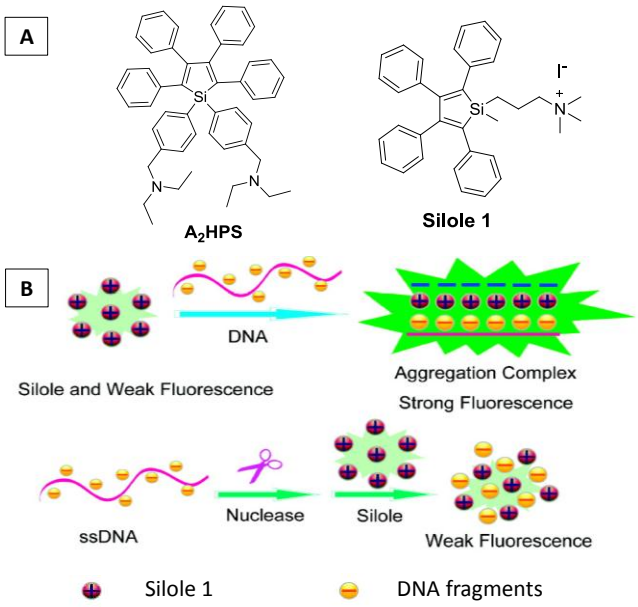

Figure 1.11 (A) The chemical structure of A_2HPS and Silole 1.[56] (B) The schematic illustration of nuclease assays using Silole 1.[57] Copyright 2008 American Chemical Society.

Based on the principle that longer DNA sequences can induce stronger fluorescence enhancement of positively charged AIE probes than their shorter counterpart, Xia et al. have reported quantification of telomerase activity.[58, 59] Telomerase is a ribonucleoprotein that adds a repeated sequence to the 3' end of telomere at the end of chromatid to protect chromosome from deterioration or from fusion with other chromosomes. Researchers have found that elevated levels of telomerase have higher cancer incidence, thus it is of great importance to develop

methods that facilitate the detection of telomerase level. As shown in **Figure 1.12Aa**, the fluorescence of positively charged TPE-Z is very weak when it is incubated with an 18-nt (nucleotides) oligonucleotide, but it increases significantly in the presence of 54-nt oligonucleotide. According to the same principle, TPE-Z fluoresces weakly in the presence of telomerase substrate oligonucleotides (TS primer), but is turned on by increased charges in DNA sequences and strengthened electrostatic interaction during telomere elongation process (**Figure 1.12Ab**).[58] The signal-to-noise ratio (S/N ratio) of this assay is further improved by introducing a quencher group to the 5' end of TS primer (**Figure 1.12B)**. The background signal of Silole-R is effectively quenched by energy transfer from Silole-R to dabcyl (4-(4-(dimethylamino)phenylazo)benzoic acid). With the addition of telomerase, the oligonucleotides are prolonged. Consequently, Silole-R molecules are brought relatively far away from the quencher, leading to the regain of fluorescence.[59] Both of the two assays have been applied for the detection of telomerase activity in cancer cell lines such as E-J, HeLa, MCF-7, and normal cells HLF.

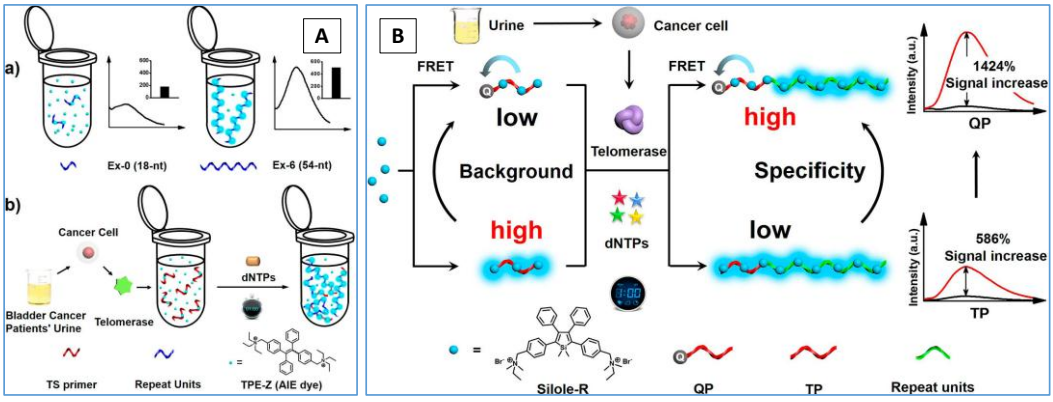

Figure 1.12 (A) (a) Fluorescence turn-on detection of 28-nt and 54-nt ssDNA sequences and schematic illustration of AIE probe for telomerase activity detection. (b) Telomerase substrate oligonucleotides (TS primer) is extended by adding TTAGGG repeat units to the 3'-end to yield telomerase product, which will induce

fluorescence enhancement of TPE-Z.[58] (B) Schematic illustration of telomerase detection with improved selectivity and specificity using Silole-R with the aid of a quencher group Dabcyl labelled at the end of TS primer (denoted as QP) to eliminate background signal.[59] Copyright 2015 American Chemical Society.

In efforts to improve the S/N ratio of AIE-based detection, enzyme-assisted cycle amplification methods represent a promising solution. In 2015, Xia et al. developed an ultrasensitive assay of microRNAs with the aid of exonuclease III which specifically catalyzes the stepwise hydrolysis of mononucleotides from 3'-hydroxyl termini of duplex DNA.[60] An AIE-DNA conjugation was synthesized consisting of a 15-mer single strand DNA and a TPE molecule at the 5' terminus of the DNA. As shown in **Figure 1.13**, the AIE-DNA conjugate is non-emissive in aqueous media, and the subsequent incubation with a target 21-mer microRNA leads to the formation of a duplex DNA strand containing exonuclease III resistant 3' protruding termini. Then, exonuclease III catalyzed hydrolysis of mononucleotides at 3' terminus of TPE-DNA stepwisely, releasing TPE molecules into the solution but leaving the target RNA sequence intact. The point is the target RNA sequence can further hybridize with other TPE-DNA conjugations and repeat the hydrolysis cycle and yield more TPE molecules with recovered fluorescence. The detection limit of this microRNA assay is 1 pM with 40 min incubation at 37 ° C.

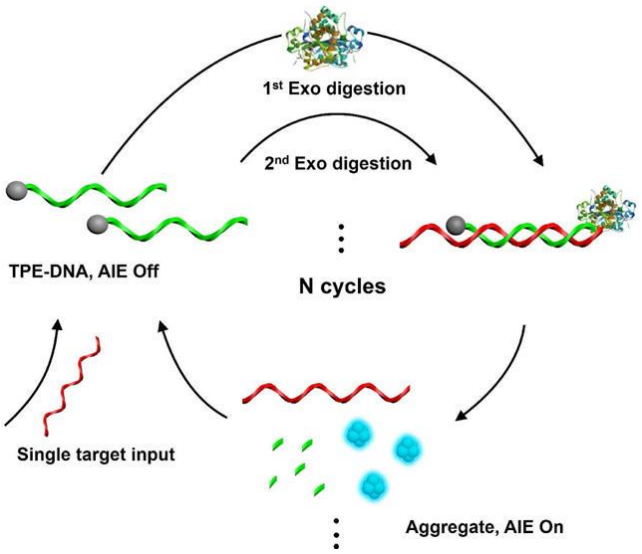

Figure 1.13 Schematic illustration of enzyme-assisted cycle amplified ultrasensitive detection of microRNAs based on AIE probe TPE-DNA.[60] Copyright 2015 American Chemical Society.

Similar to the fluorescence light-up response of cationic AIE probes to DNAs, anionic AIE probes have been applied for the protein detection based on both electrostatic and hydrophobic interactions. As shown in **Figures 1.14A** and **B**, BSPOTPE (1,2-Bis[4-(3-sulfonatopropoxyl)phenyl]-1,2-diphenylethene salt) was synthesized and utilized to monitor human serum albumin (HSA) with a detection limit of 1 nM.[61] The unfolding process of HAS induced by GndHCl was monitored by BSPOTPE. The rationale behind the fluorescence turn on of BSPOTPE responsive to HSA is attributed to hydrophobic effect, charge neutralization and also hydrogen bonding but hydrophobic effect is the most dominant factor. The same probe was also utilized for monitoring of insulin fibrillation, as it is non-emissive with native insulin but shows strong fluorescence with preformed insulin fibril (**Figures 1.14C** and **D**). The probe facilitates in situ monitoring of amyloidogenesis and screening of anti-amyloid inhibitors.[62] Later, another anionic

AIE probe was applied for the human serum proteins detection, for instance, the detection limit for fluorescent imaging for ferritin in gel is 0.78 ng/μL.[63]

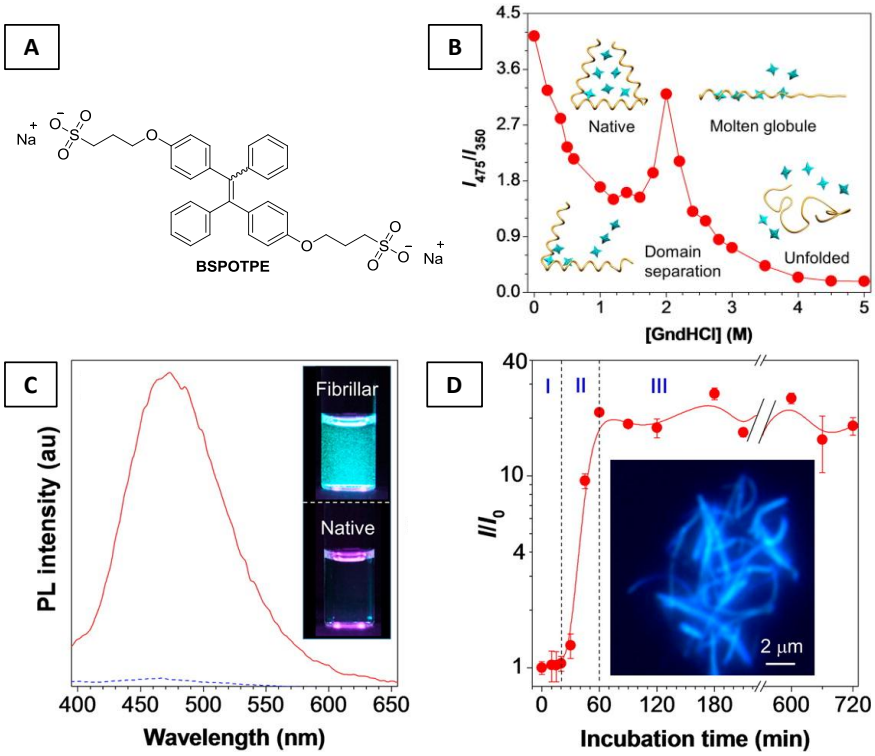

Figure 1.14 (A) Chemical structure of BSPOTPE. (B) Monitoring of HAS unfolding process by changes of I_{475}/I_{350} between HAS and BSPOTPE, which is induced by GndHCl concentration.[61] (C) PL spectra and fluorescent photographs of BSPOTPE in the presence of native and fibrillar forms of bovine insulin. (D) Insulin fibrosis process monitored by the fluorescence change of BSPOTPE.[62] Copyright 2013 American Chemical Society[48]

1.4.2 Hydrogen bonding and complexation

Hydrogen bonding is the electrostatic attraction that occurs between a hydrogen (H) atom and a highly electronegative atom such as nitrogen (N), oxygen (O) or fluorine (F). Sanji et al. reported melamine detection on the basis of multivalent hydrogen-bonding with a TPE derivative functionalized with cyanuric acid moieties. The probe displays turn-on fluorescence upon recognition of melamine and formation of aggregates. Even 1 ppm melamine can induce evident

fluorescence response of the probe, which is observable by naked eye.[64] More recently, Zhang et al. found that (4-(1,2,2-triphenylvinyl)phenoxy)acetic acid (TPE-COOH) forms specific complexation with Al^{3+}. The mechanism behind the specific complexation is attributed to the particular molecular structure of TPE-COOH, which gives high selectivity toward Al^{3+} over other metal ions, as shown in **Figure 1.15**.[65] The detection limit is calculated to be 21.6 nM. Furthermore, the experiments demonstrate that the probe can be used for real-time monitoring of Al^{3+} in living cells with a high signal-to-noise ratio.

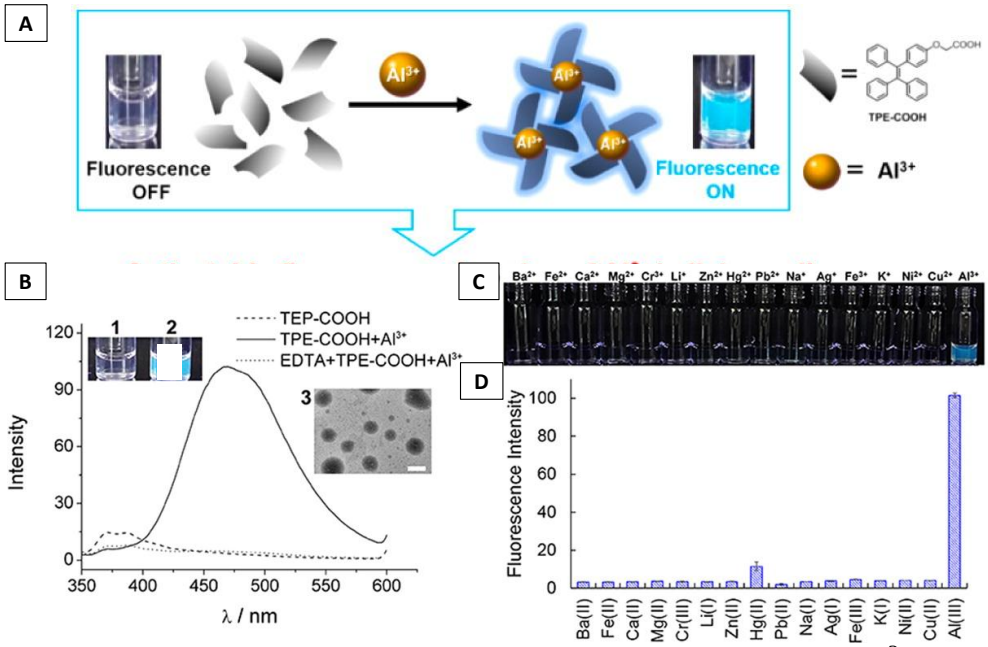

Figure 1.15 (A) Schematic illustration of fluorescence detection of Al^{3+} by TPE-COOH. (B) PL spectra of TPE-COOH in the absence/presence of Al^{3+} and in the presence of EDTA and Al^{3+}. (C) Photographs and (D) fluorescence intensity of the probe TPE-COOH in in the presence of various metal ions in aqueous solutions (2% DMSO, 5% CH_3CN).[65] Copyright 2015 American Chemical Society.

1.4.3 Specific Reactions

Oligomerization reaction occurs between the two cis-diol groups in D-Glucose (Glu) and boronic acid groups, which is not found in any other saccharide

with only one cis-diol unit such as D -Fructose (Fru), D -galactose (Gal), and D -mannose (Man). On the basis of this principle, Tang et al. reported specific detection of Glu based on the fluorescence turn-on upon formation of TPE-2B$(OH)_2$-Glu adducts.[66] It is noteworthy that the fluorescence turn-on of the probe is closely related to the form of the adducts because, monomer, linear oligomer and cyclic oligomer adducts may exits at the same time. Liu et al. reported an AIE probe TPE-Tyr which gives AIE fluorescence upon enzyme-catalyzed cross-linking because H_2O_2 produced by glucose oxidation can transform molecularly dissolved TPE-Tyr to its covalent cross-linking product which shows strong fluorescence (**Figure 1.16**).[67] When the probe TPE-Tyr was applied to human carcinoembryonic antigen (CEA) ELISA kit as a substituent to conventional indicator 3,3′,5,5′-Tetramethylbenzidine (TMB), the assay provides lower detection limit (2.0 ng/mL) compared with 5.0 ng/mL provided by TMB-based ELISA kit.

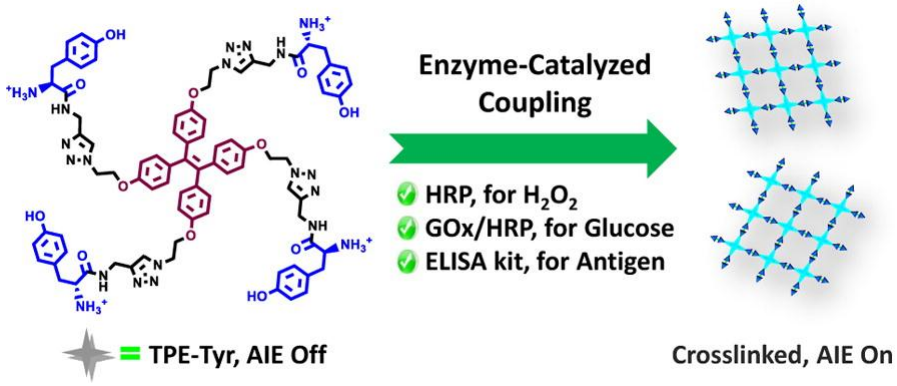

Figure 1.16 Schematic illustration of fluorescence turn-on multi-analyte probe based on TPE-Tyr.[67] Copyright 2014 American Chemical Society

The above two examples represent aggregation-induced by crosslinking reactions, which further restrict the intramolecular motion of AIEgens. There are also some AIE sensors developed based on change of hydrophilicity of AIE probes.

For example, Liu et al has reported an AIE probe for real-time monitoring of cell apoptosis. In this work, they creatively adopted a hydrophilic peptide sequence DEVD which can be specifically hydrolyzed by caspase-3/-7 at the c-terminal of the D near V (**Figure 1.17A**).[68] The conjugation of TPE-DEVD is non-fluorescent in aqueous media but becomes emissive when cleaved by caspase-3/-7. The probe offers real-time imaging of caspase-3/-7 with high signal-to-noise ratio, which has great potential for early diagnosis of diseases and drug screening. Moreover, the success of this probe provides a new strategy for the development of AIE-based probes because specific protein-peptide interaction is prevalent and important in biological systems with high selectivity. Later, Liu et al. synthesized TPE-2DEVD in their E/Z isomers, respectively and applied them to caspase detection. They found that E-TPE-2DEVD binds with caspase-3 more efficiently while Z-TPE-2DEVD exhibited more significant light-up response than its E-counterpart **(Figure 1.17B)**.[69] Very recently, by introducing a self-assembling peptide sequence GFFY, Ding et al. found that the detection limit of the caspase assay can be further improved, because the TPE-GFFYK residues are able to form filamentous network which leads to more effective aggregation-induced emission.[70] In addition to DEVD/caspase-3/7, a wealth of AIE bioprobes have been developed by integration of AIEgens with peptide substrates that can undergo enzymatic hydrolysis.[50, 71, 72]

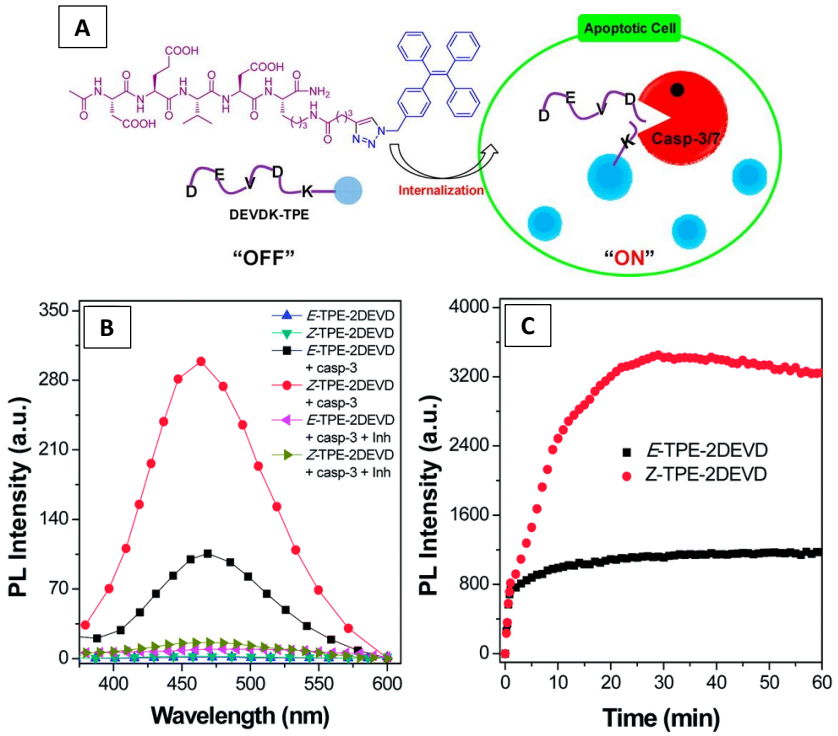

Figure 1.17 (A) Schematic illustration of TPE-DEVD for detection of caspase-3/-7.[68] (B) PL spectra of E- and Z- TPE-2DEVD before and after incubation with caspase-3 in the presence and absence of inhibitor. (C) Time-dependent PL spectra of E- and Z- TPE-2DEVD incubated with caspase-3 from 0 to 60 min. [69] Copyright 2012 American Chemical Society Copyright 2014 The Royal Society of Chemistry.

1.4.4 Specific target binding

In addition to the enzymatic hydrolysis based AIE bioprobes, researchers have also noticed that there are specific binding interactions between some peptides and their corresponding hosts. In 2012, Liu et al. firstly reported a AIE probe for real-time specific detection of integrin $\alpha_v\beta_3$ which is an important biomarker overexpressed in many cancer cells. The probe is developed by conjugation between TPE-2N_3 and azide-functionalized cRGD by click chemistry. TPS-2cRGD is non emissive itself due to its good water solubility. When it is bound to $\alpha_v\beta_3$ integrin, the fluorescence of TPS-2cRGD turns on in a concentration-dependent manner, which is due to aggregation-induced emission induced by RIM mechanism

(Figure 1.18A and B).[54] As shown in **Figure 1.18C**, other proteins can only induce minor fluorescence tur-on compared with $\alpha_v\beta_3$ integrin, indicating the probe is highly specific. The probe was also utilized for membrane stain for $\alpha_v\beta_3$ integrin overexpressed cancer cells, using HeLa as an example. Good overlap between the fluorescence from the probe and a commercial membrane tracker validates the potential of the probe for imaging of $\alpha_v\beta_3$-positive cancer cells. The success of this example leads to the reports of a diverse set of applications of AIE probes for biological sensing and imaging.[73, 74] For example, Zhang et al reported a red-emissive AIE probe TPE-red-2AP2H, which was successfully utilized for imaging of solid tumors. Moreover, as the AIEgen TPE-red has ROS generation ability, the probe is also used for targeted-photodynamic therapy.[73]

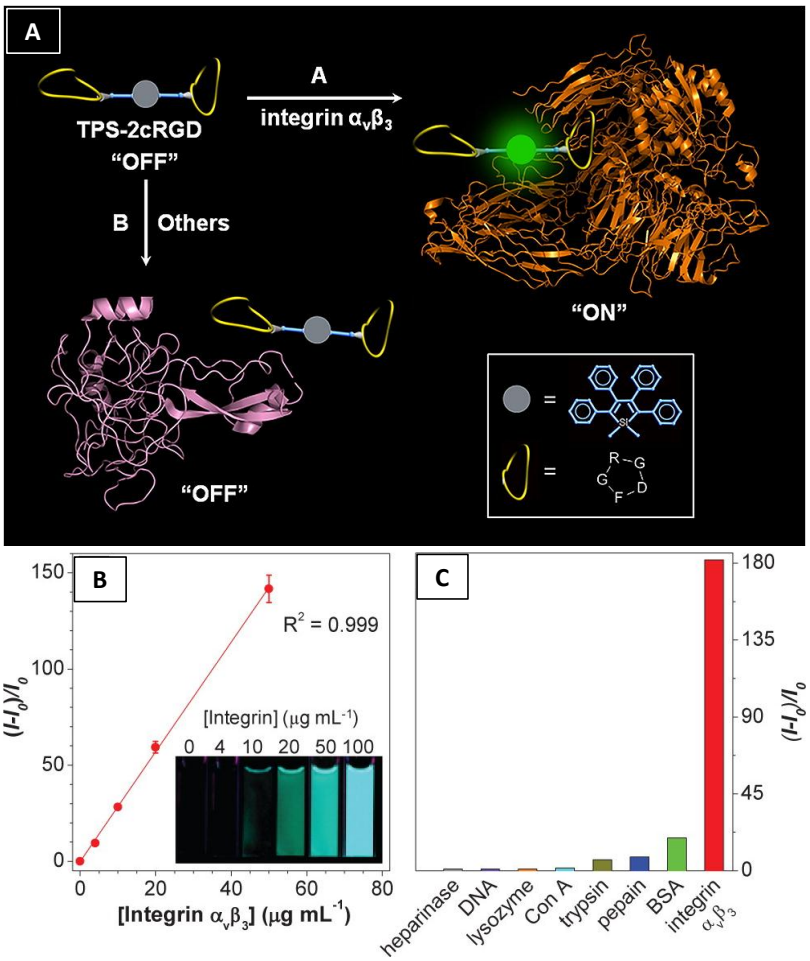

Figure 1.18 (A) Schematic illustration of probe TPS-2cRGD binding with integrin $\alpha_v\beta_3$. (B) plot of fluorescence enhancement of the probe TPS-2cRGD in the presence of integrin $\alpha_v\beta_3$. (C) Fluorescent response of the probe to integrin $\alpha_v\beta_3$ and other proteins and DNA. [54] Copyright 2012 American Chemical Society.

1.4.5 Other examples

In the above examples, all the AIE probes show low fluorescence because they are molecularly dissolved and undergo non-radiative decay through intramolecular motions. Actually, there are examples that integrate AIE characteristics with other luminescence mechanism, which inherit the merits from their parents. For example, Tang et al. synthesized an AIE-active hemicyanine fluorogen TPE-Cy, which facilitates the pH sensing but not suffering from

concentration-quenching.[75] The probe TPE-Cy provides pH sensing in the entire physiological range as the emission color changes from red to blue with increasing pH **(Figure 1.19A).** The successful application of the probe for locating intracellular proton concentration demonstrates its great potential in cell imaging and biomedical application.[76] By functionalization with a maleimide (MI) group, TPE-MI is non-emissive in both solution and the solid state due to photoinduced electron transfer (PET) and nonradiative relaxation. As maleimide groups are readily to react with thiol groups which can block the PET process and lead to the bright blue fluorescence recovery (λ_{em} = 480 nm), TPE-MI was applied for turn-on detection of thiols such as cysteine **(Figure 1.19B)**.[77] The first attempt on combination of AIE characteristics and excited-state intramolecular proton transfer (ESIPT) mechanism can be traced back to 2007 when Yang et al reported a new class of 2-(2'-hydroxyphenyl)benzothiazole-based (HBT-based) compounds that exhibits aggregation-induced emission enhancement (AIEE) and ESIPT mechanism.[78] Liu et al. reported a series of salicyladazine fluorogens that shows "AIE+ESIPT" characteristics and applied them to mitochondrial and lysosomal imaging **(Figure 1.19C)**.[79, 80, 81] By blocking of hydroxyl group by R_1, the fluorescence of salicyladazine is quenched due to destruction of the hydrogen bonding and the free rotation of the N-N bond. R_2 is usually designed as targeting groups. After the occurrence of specific reaction to remove R_1, the probe would be lightened up by reactivation of ESIPT process and RIM.

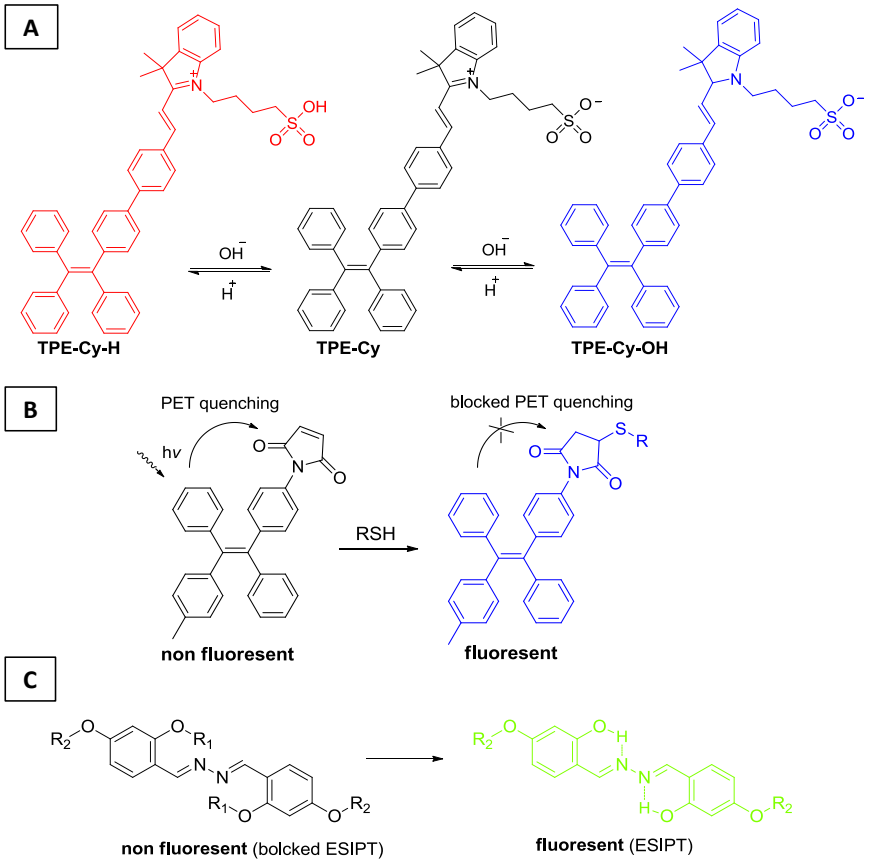

Figure 1.19 (A) TPE-Cy shows strong red emissions at pH 7-10, and nil-to-strong blue emissions at pH 10-14.[75] (B) Thiol turn-on detection based on block of PET process.[77] (C) Fluorescent AIE probe by retrieve of ESIPT process.[81]

1.5 Research Objectives

The discovery of AIE fluorogens has prompted a new cluster of fluorescent bioprobes for detection of ions, small molecules, biomacromolecules, enzyme activity, biomolecule interaction, and biomolecular interactions. Early reports on AIE probes are mainly based on electrostatic interaction or hydrophobic interaction between probes and targets. However, probes based on such working mechanism usually responses to a group of analyte possessing similar electrostatic properties and lacks specificity, which may result in low selectivity or inaccurate results. Although indirect methods can be employed to construct "off-on-off" or "on-off-

on" model to improve detection accuracy, extra stringent requirements need to be met to achieve successful designs. Thus, subsequent reports based on chemical reaction or biological interaction are superior as a group of specific probes.

In this contribution, design and development of fluorescent light-up probes with AIE characteristics are elucidated in details to meet various requirements of biological applications. The specific objectives of this thesis can be summarized as follows:

1. To design a general strategy for fabrication of AIE light-up probes with conjugation to hydrophobic peptide sequences. (Chapter 2)

2. To expand this platform to the development of AIE light-up probe for enzyme detection and analysis of enzyme activity. (Chapter 3)

3. To develop a turn-on AIE probe for recognition of biomolecules based on specific binding. (Chapter 4)

4. To design and develop a turn-on AIE probe based on fluorescence resonance energy transfer (FRET). (Chapter 4)

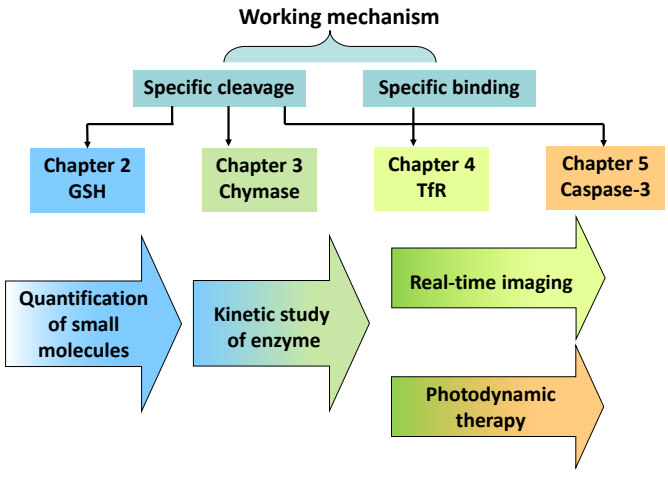

Scheme 1.1 Schematic linkage between technical Chapter 2-5.

1.6 Thesis Outline

The doctoral thesis consists of seven chapters. In Chapter 1, brief background information of fluorescent sensing and existing problems, as well as research objective and thesis outline are provided. Chapter 2 provided literature review on fluorescence turn-on probes developed on conventional fluorogens, followed by a brief review on AIE phenomenon and mechanism, as well as developments of AIE bioprobes from first generation to up-to-date examples. Chapters 3-6 reported four AIE bioprobes for biosensing and bioimaging. The focus is to design AIE bioprobes for versatile sensing tasks by tuning the construction of the probes, providing general principle for AIE bioprobe development and enriching the probe library of AIE probes.

AIE-peptide conjugation has been frequently reported for development of turn-on probes based on hydrophilic peptide ligands, while those based on hydrophobic ligands are not able to offer ideal signal-to-background ratio. Under these circumstances, we proposed a general strategy to fine-tune the AIE characteristics for probe construction, which offers new opportunities for design of AIE turn-on probes based on hydrophobic recognition elements (Chapter 3). Subsequently, Chapter 4 reported an AIE-peptide conjugation for chymase detection on the basis of the conclusion obtained in Chapter 3. The probe shows high sensitivity and selectivity to chymase, a fundamental premise of which is that the signal-to-background ratio is optimized.

Chapter 5 represents a successful example for detection of transferrin receptor (TfR) for cancer diagnosis and therapy. In this work, an AIE probe which is almost non-emissive in aqueous media shows significant light-up in the presence of TfR in a concentration dependent manner. Cellular experiments show that the probe can differentiate TfR-overexpressed cancer cell effectively and can be used for image-guided photodynamic therapy. Chapter 6 provided a novel probe design which integrates an AIEgen with a coumarin to form a FRET pair for turn-on probes with dual signal amplification. Unlike traditional FRET probes, the new generation FRET probe is non-fluorescent by itself due to energy transfer as well as dissipation of the acceptor energy through free molecular motion of AIEgen. The dual turn-on signals allow real-time and self-validated detection with a high signal-to-background ratio. Chapter 7 summarizes conclusions and proposes recommendations for future work.

CHAPTER 2. Fluogen-Peptide Conjugates with Tunable Aggregation-Induced Emission Characteristics for Bioprobe Design

2.1 Introduction

Fluorescence probes have become important tools for shedding light on the interplay between biomolecules and signaling biological processes.[5, 82] By integration of fluorescent molecules and recognition moieties, fluorescent probes provide high selectivity and sensitivity with simple, non-invasive, and easy-to-use formats.[1, 83, 84] Several design strategies such as photo-induced electron transfer (PeT),[13, 85, 86] internal charge transfer (ICT),[87, 88] and fluorescence resonance energy transfer (FRET)[89, 90, 91, 92] have been utilized to develop fluorescence turn-on probes which are highly desirable for biological sensing. The rationale behind this preference is because turn-on probes have higher sensitivity and more accurate results than their turn-off counterparts, especially when trace detection in complicated system is needed.[93, 94, 95]

In recent years, significant research interests have been attracted by a new type of fluorogens with aggregation-induced emission (AIE) characteristics.[35, 36, 45, 96] AIE fluorogens, which have propeller-shaped structure, show weakly fluorescence in solution state, but fluoresces strongly in aggregate state.[37, 97] The mechanism behind this unique optical phenomenon has been attributed to the free motion of the propeller structures (for example, the phenylene rings) in solution state, which consumes the excited state energy by non-radiative decay and leads to

fluorescence quenching.[43] When AIE molecules are aggregated, the intramolecular motion will be restricted, leading to the activation of radiative decay pathway and fluorescence turn-on. Opposite to traditional organic fluorogens which suffer from aggregation-caused quenching (ACQ), AIE fluorogens facilitate the use of highly concentrated solution and enable detection with higher sensitivity and better photobleaching-resistance desirable for biological applications.[48]

A number of bioprobes have been developed based on AIE fluorogens for the sensing of proteins,[98, 99, 100] DNA,[57, 101] heparin,[102, 103] Biological thiols[104, 105, 106, 107] However, most of these assays are taking advantages of the electrostatic and/or hydrophobic interactions between the cationic/anionic AIE derivatives and analytes, which induce fluorescence turn-on by restriction of intramolecular motions (RIM). The working mechanism fundamentally limits their detection selectivity because other charged molecules could easily bring interference. Consequently, most of these assays can only provide reliable response to individual purified analyte in solution. To achieve highly specific detections, recently, we have designed an AIE-peptide conjugate strategy by integration of AIE fluorogens and peptide elements that can specifically recognize biomolecules for integrin[54] level and caspase activity[68, 108, 109, 110] and studies. The same strategy is also proved effective for cancer cell detection.[74] These probes are highly specific and sensitive because 1) they contain hydrophilic ligands which endow the bioprobes good water solubility and disperse the probes in aqueous media as molecular species with extremely low background signals; 2) in the presence of analyte or certain biological event, the fluorescence of AIE fluorogens is recovered with both high selectivity and high

signal output. As the background fluorescence is significantly dependent on the water-solubility of the probe, the performance of the probes is highly dependent on the hydrophilicity of the peptide moiety of each probe. It is very important to understand the effect of peptide moiety on fine-tuning the aggregation-induced emission characteristics of AIE fluorogens.

To build a model to figure out this problem, in this chapter, we propose to synthesize a series of AIE fluorogen-peptide conjugates with different numbers of amino acids (AA) in each sequence. AIE-peptide conjugates TPE-D_n (n = 1−5) were synthesized by covalently conjugating a typical AIE fluorogen TPE and peptide fragments consisting of different numbers of aspartic acid (D). TPE-D_n conjugation with different numbers of D units and their hydrophilicity, optical properties, aggregation sizes and also the AIE characteristics were investigated carefully to find the threshold number of D units needed to achieve the "off" state. As a proof-of-concept, a light-up probe TPE-SS-D_5 was designed for thiol detection by inserting a linker responsive to thiol species between TPE and D_5. This study offers opportunities to facilitate the development of AIE probes and broaden their usage to hydrophobic recognition elements involving applications.

2.2 Experimental

2.2.1 Chemicals and Instruments

Organic solvents including dichloromethane (DCM), dimethylformamide (DMF), acetonitrile (CH_3CN), anhydrous dimethyl sulfoxide (DMSO), 1-octanol

and other chemicals including *N*,*N*-diisopropylethylamine (DIEA), triisopropylsilane (TIS), trifluoroacetic acid (TFA), piperidine, dithiobis(succinimidyl propionate) (DSP), triethylamine (TEA), 1-hydroxybenzotriazole hydrate (HOBt), and glutathione (GSH) were purchased from Sigma-Aldrich. *N*,*N*,*N*′,*N*′-tetramethyl-O-(1H-benzotriazol-1-yl)uronium hexafluorophosphate (HBTU) and Boc-L-aspartic acid(4-tert-butyl)ester were purchased from Biochem and Fluka, respectively. Peptides Asp-Asp (D_2), Asp-Asp-Asp (D_3), Asp-Asp-Asp-Asp (D_4), Asp-Asp-Asp-Asp-Asp (D_5) were customized from GL Biochem Ltd. All chemicals and reagents were used without further purification. Deuterated dimethyl sulfoxide (d_6-DMSO) was purchased from Cambridge Isotope Laboratories. Milli-Q water was supplied by a Milli-Q Plus System (Millipore Corp., USA).

UV-vis absorption spectra and photoluminescence (PL) spectra were recorded on a Shimadzu UV-1700 spectrometer and a Perkin-Elmer LS 55 spectrofluorometer, respectively. The size and size distribution of particles were determined by laser light scattering (LLS) with a particle size analyser (90 Plus, Brookhaven Instruments Co., USA) at a fixed angle of 90^o at room temperature. Atomic force microscopy (AFM) was conducted on a Digital Instrument Nanoscope IIIa scanning probe microscope, operated at the tapping mode. NMR spectra were acquired on a Bruker ARX 400 NMR spectrometer or Varian 600 MHz NMR spectrometer. The separation and purification of the probes were conducted by an Agilent 1100 Series HPLC System. Mass spectra were obtained by a Shimadzu IT−TOF system.

2.2.2 Synthesis and Characterization

Synthesis of 1-[4-(isothiocyanatomethyl)phenyl]-1,2,2-triphenylethene (TPE-NCS)

According to the literature, TPE-N_3 and triphenylphosphine were refluxed with carbon disulfide in distilled dichloromethane with dry nitrogen protection overnight followed by removal of the solvent. The rude product was precipitated with cold ether and washed for three times and finally gave a white solid pure TPE-NCS in 85% yield.[53, 111] ^{1}H NMR, ^{13}C NMR and HRMS confirm the right structure of TPE-NCS with high purity. ^{1}H NMR ($CDCl_3$, 400 MHz): 7.13-6.89 (m, 19H), 4.63 (s, 2H). HRMS (MALDI-TOF) m/z: 403.1386 ($[M]^+$ calcd: 403.1395).

Synthesis of TPE-D_n (n = 1−5)

D-NH_2 was synthesized by solid-phase peptide synthesis strategy using rink amide resin as the solid support. 150 mg of resin (loading ~0.5 mmol/g) was first swelled in DMF for 1 h followed by deprotection in the mixture of piperidine/DMF (v/v = 1/4) for 2 h at room temperature. Then the resin was first separated with piperidine then washed with DMF and DCM and dried thoroughly by high vacuum. The dry resin was then reacted with Boc-L-aspartic acid(4-tert-butyl)ester (92 mg) in the presence of HBTU (4 equiv), HOBt (4 equiv), and DIEA (8 equiv) dissolved in 2.0 mL dry DMF at room temperature for 12 h. Then the resin was filtered and washed with DMF, DCM and DMF, respectively (10 mL X 3 for each solvent), until the filtrate became colourless. After drying under vacuum, the resin was deprotected again with 5 mL of piperidine/DMF (v/v = 1:4). The peptide was finally

cleaved in 3 mL of TFA/TIS/H_2O (v/v/v = 95: 2.5:2.5) for 3 h at room temperature to yield the product of D-NH_2 in 70% yield. (ESI-MS, m/z: 131.0398, ($[M - H]^-$ calcd: 131.0457).

TPE-D was synthesized in a typical reaction. Into TPE-NCS (6.61 mg, 16.4 μmol) and D-NH_2 (3.25 mg, 24.6 μmol) in 0.5 mL DMSO, 3 μL DIEA was added and the mixture was stirred at room temperature for 24 h. The final product was purified by prep-HPLC and lyophilized under vacuum to give the product as white powders in 40% yield (3.51 mg). ^{1}H NMR (DMSO-d_6, 600 MHz): 7.84 (t, J = 6.0 Hz, 1H), 7.13-6.87 (m, 18H), 4.68 (d, J = 6.0 Hz, 2H), 2.48-2.47 (d, 2H, overlap with DMSO-d_6); ESI-MS, m/z: 1093.3503, ($[2M + Na]^+$ calcd: 1093.3757). TPE-D_2 was synthesized from TPE-NCS (7.26 mg, 16.4 μmol) and D_2 (6.67 mg, 24.6 μmol) similarly with a catalytic amount of DIEA in DMSO and purified in the same way to give the product as white powders in 38% yield (4.06 mg). ^{1}H NMR (DMSO-d_6, 600 MHz): 8.20 (m, 2H), 7.69 (d, J = 12.0 Hz, 1H), 7.15-6.90 (m, 19H), 5.15 (s, 2H), 4.57-4.47 (m, 2H), 2.65-2.55 (m, 4H, overlap with DMSO-d_6); ESI-MS, m/z: 652.1965, ($[M + H]^+$ calcd: 652.2117). TPE-D_3 was synthesized from TPE-NCS (5.42 mg, 13.43 μmol) and D_3 (7.31 mg, 20.14 μmol) in 39% yield (4.02 mg); ^{1}H NMR (DMSO-d_6, 600 MHz): 8.29 (d, J = 6.0 Hz, 1H), 8.18-8.04 (m, 1H), 7.88 (d, J = 6.0 Hz, 1H), 7.70 (d, J = 6.0 Hz, 1H), 7.21-6.90 (m, 19H), 5.03 (s, 1H), 4.61-4.48 (m, 3H), 2.73-2.48 (m, 6H, overlap with DMSO-d_6); ESI-MS, m/z: 767.2217, ($[M + H]^+$ calcd: 767.2387).

TPE-D_4 was synthesized from TPE-NCS (4.42 mg, 10.95 μmol) and D_4 (7.85 mg, 16.43 μmol) in 42% yield (4.05 mg); ^{1}H NMR (DMSO-d_6, 600 MHz): 8.29 (d, J = 6.0 Hz, 1H), 8.09 (m, 1H), 7.93 (d, J = 6.0 Hz, 1H), 7.86 (d, J = 6.0 Hz, 1H), 7.67 (d, J = 6.0 Hz, 1H), 7.15-6.90 (m, 19 H), 5.04 (s, 1H), 4.57-4.48 (m, 4H), 2.72-2.48 (m, 8H, overlap with DMSO-d_6); ESI-MS, m/z: 920.1834, ($[M + K]^+$ calcd: 920.2215).

TPE-D_5 was synthesized from TPE-NCS (5.48 mg, 13.57 μmol) and D_5 (12.06 mg, 16.43 μmol) in 40% yield (5.42 mg); ^{1}H NMR (DMSO-d_6, 600 MHz): 8.31 (d, J = 6.0 Hz, 1H), 8.11 (m, 1H), 7.98-7.90 (m, 3H), 7.69 (d, J = 6.0 Hz, 1H), 7.16-6.90 (m, 19 H), 5.05 (s, 1H), 4.54-4.45 (m, 5H), 2.73-2.48 (m, 10H, overlap with DMSO-d_6); ESI-MS, m/z: 1019.2378 ($[M + Na]^+$ calcd: 1019.2745).

Synthesis of 1-[(4-aminomethyl)phenyl]-1,2,2-triphenylethene (TPE-NH_2)

A solution of 1-[(4-azidomethyl)phenyl]-1,2,2-triphenylethene (TPE-N_3) (0.116 g, 0.3 mmol) and triphenylphosphine (0.118 g, 0.45 mmol) in 6 mL anhydrous methanol was added into a 50 mL two-necked round bottle flask under nitrogen protection and refluxed for 12 h followed by cooling down to room temperature and removal of solvent by evaporation under reduced pressure.[112] The crude product was purified by silica-gel chromatography to yield TPE-NH_2 as a white powder in 70% yield (0.13 g). ^{1}H NMR ($CDCl_3$, 400 MHz): 7.13-6.87 (m, 19H), 3.82 (s, 2H), 1.23 (m, 2H), HRMS (MALDI-TOF) m/z: 361.1833 ($[M]^+$ calcd: 361.1830).

Synthesis of TPE-SS-D_5

TPE-SS-D_5 was synthesized according to the literature.[112] Into a mixture of TPE-NH_2 (5.90 mg, 15.22 μmol) and D_5 (8.98 mg, 15.22 μmol) in DMSO (0.5 mL), 2 μL DIEA was added and the mixture was stirred for 10 min at room temperature. Then DSP (6.13 mg, 15.22 μmol) in 0.5 mL DMSO was quickly added and the mixture was stirred for another 24 h at room temperature. The crude product was purified by prep-HPLC and lyophilized to give the product as white powder in 49% yield (8.43 mg). ^{1}H NMR (DMSO-d_6, 600 MHz): 8.34-7.87 (m, 6H), 7.14-6.87 (m, 19H), 4.53-4.44 (m, 5H), 4.17-4.16 (d, 2H), 2.88-2.81 (m, 4H), 2.69-2.41 (m, 14H, overlap with DMSO-d_6), ESI-MS, m/z: 1127.3131, ([M − H]$^-$ calcd: 1127.3014).

Synthesis of TPE-SS-COOH

TPE-SS-COOH was synthesized in a similar way as TPE-SS-D_5 and purified by prep-HPLC (mobile phase A: water with 0.1% TFA, mobile phase B: CH_3CN with 0.1% TFA) and lyophilized under vacuum to give the product as white powder in 30% yield (4.35 mg). ^{1}H NMR (DMSO-d_6, 400 MHz): 8.38 (t, 1H), 6.89-7.15 (m, 19 H), 4.19 (d, 2H), 2.79-3.07 (m, 8H), ESI-MS, m/z: 552.1724, ([M − H]$^-$ calcd: 552.1667).

2.2.3 Investigation on Optical Property, Partition Coefficient and size

Titration of TPE-NCS and TPE-D_n (n = 1−5)

995 μL mixtures of DMSO/H_2O with different water fractions were firstly prepared. Then TPE-NCS and TPE-D_n (n = 1−5) stock solutions were then added into the mixtures to give a final concentration of 10 μM. The PL spectra were obtained using a Perkin-Elmer LS 55 spectrofluorometer.

Measurement of partition coefficient

TPE-D_n (n = 1−5) were dissolved in 1 mL DMSO/H_2O (v/v = 1/199) mixtures (pH=7.0, 1X PBS buffer) at a concentration of 10 μM and then partitioned with 1 mL 1-octanol completely (for 24 h). The concentrations of the TPE-D_n in each phase were determined by absorption spectra using Shimadzu UV-1700 spectrometer.

Laser light scattering measurement

6 μL of 10 mM TPE-NCS stock solution in DMSO was first mixed with 9 μL of DMSO, which was then diluted with 2.985 mL of H_2O to yield a final concentration of 20 μM in 3 mL of DMSO/H_2O (v/v = 1/199). The stock solutions of TPE-D_n (n = 1−5) were prepared in a similar method. The mixture was mixed thoroughly using vortex mixer before LLS measurement using particle size analyser.

Atomic force microscopy measurement

10 μM TPE-NCS and TPE-D_n (n = 1−5) in DMSO/H_2O (v/v = 1/199) were mixed thoroughly using vortex mixer before spin-coating onto freshly cleaved mica surface. Then the samples were dried in drying oven at 65^{o}C for one hour, and kept in vacuum oven for one hour before they were imaged by tapping mode AFM.

2.2.3 General procedure for probe activation by GSH

TPE-SS-D_5 (10 μM) was incubated with 1 mM GSH in 1 mL of DMSO/H_2O (v/v = 1/199) at room temperature and the fluorescence spectra were

measured at different time points (0, 10, 20, 30, 45, 60, 90, 180, 360 min) to obtain time-dependent PL spectra. Next, GSH at different concentrations ranging from 1.0 μM to 1.0 mM were incubated with TPE-SS-D_5 for 3 h before fluorescence intensities were measured. The solutions were excited at 304 nm, and the emission was collected from 390 to 575 nm.

2.3 Results and Discussion

2.3.1 Synthesis of TPE-NCS and TPE-peptide conjugates (TPE-D_n, n = 1−5)

The starting material, 1-[4-(isothiocyanatomethyl)phenyl]-1,2,2-triphenylethene (**TPE-NCS, Scheme S2.1** in **Appendix 1**) was synthesized as reported from 1-[(4-azidomethyl)phenyl]-1,2,2-triphenylethene (TPE-N_3) in 85% yield in the presence of triphenylphosphine (PPh_3) and CS_2 at 40 ^oC overnight. The HRMS and the ^1H NMR, ^{13}C NMR spectra (**Figures S2.1** and **S2.2**) confirmed the right molecular structure of TPE-NCS. The synthesis of 2-diamino-4-oxobutanoic acid (amide terminated aspartic acid, D-NH_2) involves solid phase chemistry as described in **Scheme S2.2** in Appendix 1. Briefly, deprotection of Fmoc group on rink amide resin with 20% piperidine in dimethylformamide (DMF) (v/v = 1/4) for 2 h at room temperature yielded resin with active amine, which was coupled to Boc-L-aspartic acid(4-tert-butyl)ester to afford the aspartic-bearing resin. After deprotection of the amine groups, the product of D-NH_2 for further synthesis was obtained by cleavage from resin.

As shown in **Scheme 2.1,** TPE-D_n (n = 1−5) were synthesized between TPE-NCS and amine functionalized D, D_2, D_3, D_4 and D_5 in the presence of a catalytic amount of triethylamine (TEA) in DMSO at room temperature for 24 h. After purification by HPLC and lyophilization, the products were characterized by ^{1}H NMR and ESI-MS (**Figures S2.3−S2.7**). It is important to note that the terminal group of TPE-D is amide while of the rest are carboxyl for TPE-D_n (n = 2−5). As such, TPE-D_n (n = 1−5) were endowed with 1, 3, 4, 5 and 6 carboxyl groups, respectively, for n = 1, 2, 3, 4, 5.

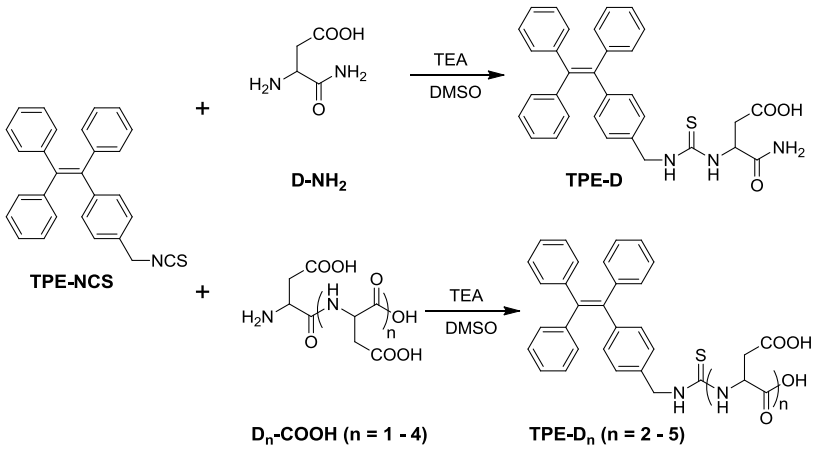

Scheme 2.1 The synthetic route to AIE-peptide conjugates TPE-D_n (n = 1−5). Reprinted with permission from Ref 113.[113] Copyright 2014 American Chemical Society.

2.3.2 Optical Properties

The UV-vis absorption and photoluminescence (PL) spectra of TPE-D_n were measured in the mixture of DMSO and H_2O (v/v = 1/199) at a concentration of 10 μM. The maximum absorption of TPE-NCS is at 314 nm while all the TPE-peptide conjugates TPE-D_n (n = 1−5) have the same absorption maxima at 304 nm, which is 10 nm blue-shifted in comparison with that of TPE-NCS. As seen from

their PL spectra, TPE-NCS shows intense fluorescence at 480 nm **(Figure 2.1).** This is due to aggregate formation in aqueous media, which will be discussed later. Under the same conditions, TPE-D_n (n = 1−5) show similar emission maxima. However, there is an obvious decrease in the PL intensity with the increasing number of D units attached to the TPE. Specifically, for 10 μM TPE-D_n (n = 1−5), if one uses $I_{TPE\text{-}Dn}/I_{TPE\text{-}NCS}$, where $I_{TPE\text{-}Dn}$ is the fluorescence intensity of TPE-D_n and $I_{TPE\text{-}NCS}$ is the fluorescence intensity of TPE-NCS, to describe the fluorescence change, the ratios are 0.70, 0.35 and 0.08 for TPE-D_1, TPE-D_2 and TPE-D_3, respectively (**Figure 2.1B**). The ratios further reduce to 0.03 and 0.01 for TPE-D_4 and TPE-D_5, which emit very weak fluorescence in the same solvent mixture. We hypothesize that the low emission is due to the well-dissolved carboxyl groups that drive the intramolecular rotation of phenyl rings. To validate this hypothesis, we performed a series of tests to examine the dispersion status of TPE-D_n in the mixture of DMSO and H_2O (v/v = 1/199).

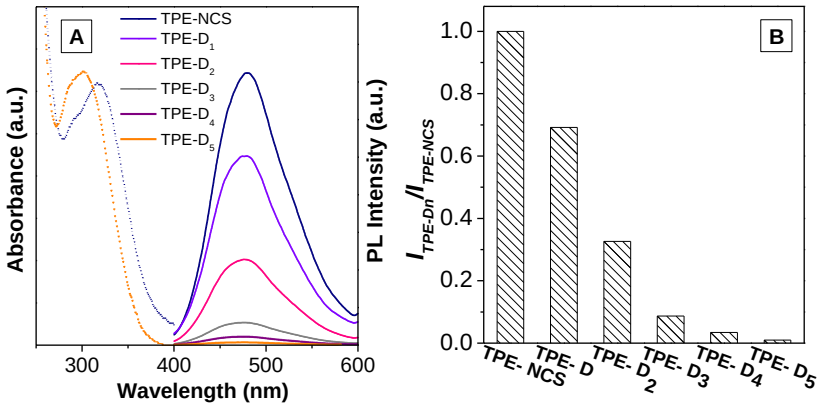

Figure 2.1 (A) UV-vis absorption (dotted line) and PL (solid line) spectra of TPE-NCS and TPE-D_n (n = 1−5); (B) Ratios of PL intensities of TPE-D_n to TPE-NCS (Measured in DMSO/H_2O (v/v = 1/199), λ_{ex} (TPE-NCS) = 314 nm, λ_{ex} (TPE-D_n) = 304 nm, [TPE-NCS] = [TPE-D_n] = 10 μM.) Reprinted with permission from Ref 113.[113] Copyright 2014 American Chemical Society.

2.3.3 AIE properties of TPE-D_n

The AIE properties of TPE-NCS and TPE-D_n (n = 1−5) were studied in DMSO/H_2O mixtures with different water fractions (f_w) to fine tune the solvent polarity and the extent of aggregation. All the PL intensities measured were divided by their maximum PL intensity (that is the PL intensity when f_w = 99.5%), respectively, to get I/I_0 of ranging from 0 to 1 (**Figure 2.2**). Generally, the AIE fluorogens are weakly emissive in good solvents such as DMSO, while the augment of water fraction induces a dramatic fluorescence increase. Accordingly, I/I_0 will experience an upward trend as the water fraction increases. As shown in **Figures 2.2A**, when water fraction (f_w) varies from 0 to 40 vol%, the PL intensity of TPE-NCS remains at a very low level. As f_w changes from 40% to 60%, the PL intensity increases dramatically and I/I_0 goes from less than 0 to 0.8. Afterwards, the PL intensity of TPE-NCS keeps increasing gradually and reaches the maximum at 99.5 vol% water fraction. For TPE-D, its PL intensity remains very weak until f_w reaches 60 vol%. When f_w increases from 60 to 80 vol%, the fluorescence intensity of TPE-D experiences a dramatic increase (I/I_0 increases from 0.05 to 0.9), which is followed by a slow saturation (**Figures 2.2B**). TPE-D_2 and TPE-D_3 also retain the typical AIE characteristics (**Figures 2.2C** and **D**, **Figures S2.8 C** and **D**); their PL intensities increase dramatically after the water fractions reach 70 vol% and 80 vol%, respectively, which continue to increase until f_w is 99.5%. For TPE-D_4 and TPE-D_5, the PL intensities show some increase when f_w is larger than 80% and 90%, respectively, as shown in **Figures 2.2E** and **F**. It is noteworthy that although there is 5-10 fold fluorescence increase for TPE-D_4 and TPE-D_5 at f_w = 99.5% relative to

f_w = 0%, their absolute fluorescence intensities remain low. The results show that the transition points of TPE-D_n at which molecules turn on their fluorescence are shifting to higher f_w with the increasing number of D in the conjugates. This further indicates that with increasing number of D units, the TPE-peptide conjugates tend to show better dispersity in aqueous media.

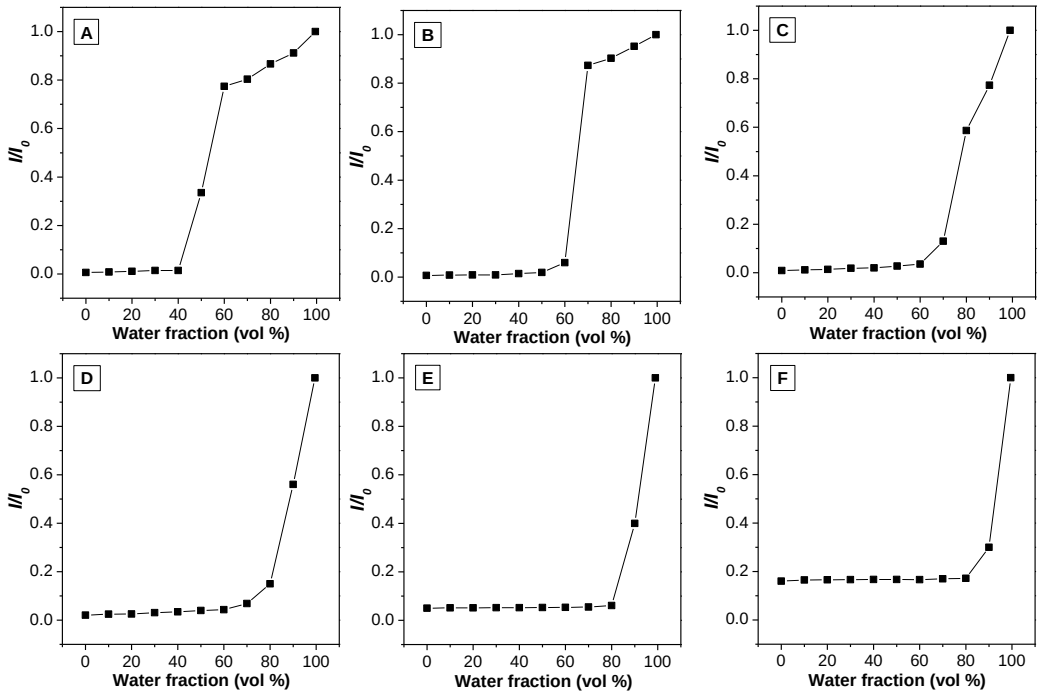

Figure 2.2 Plot of relative PL intensity (I/I_0) for (A) TPE-NCS, (B) TPE-D, (C) TPE-D_2, (D) TPE-D_3, (E) TPE-D_4, and (F) TPE-D_5 versus water fractions (f_w) in the DMSO/H_2O mixtures. I is PL intensity at any f_w and I_0 is the PL intensity measured at f_w = 99.5%. λ_{ex} = 314 nm for TPE-NCS, λ_{ex} = 304 nm for TPE-D_n, [TPE-NCS] = [TPE-D_n] = 10 μM. Reprinted with permission from Ref 113.[113] Copyright 2014 American Chemical Society.

It is well-known that the AIE properties are closely related to the state of fluorogens in solvents, in other words, the extent of aggregation. To explore the sizes of TPE-NCS and TPE-D_n (n = 1−5) aggregates in DMSO/H_2O (v/v = 1/199, 20 μM each), laser light scattering (LLS) and atomic force microscopy (AFM) were employed. As shown in **Figure 2.3A**, the hydrodynamic diameter of TPE-NCS

aggregates is 160 ± 10 nm. In comparison, the hydrodynamic diameter of TPE-D aggregates decreases to 113 ± 8 nm (**Figure 2.3B**). By employing three and four carboxyl groups, the diameters of aggregates of TPE-D_2 and TPE-D_3 further decrease to 50 ± 4 nm and 12 ± 2 nm, respectively **(Figures 2.3C** and **D).** However, the sizes of TPE-D_4 and TPE-D_5 aggregates are too small to be detected precisely by LLS, indicating the good dispersity of the conjugates. These results revealed that peptide moieties could fine-tune the size of aggregates by improving the dispersity and solubility of TPE-D_n in aqueous media.

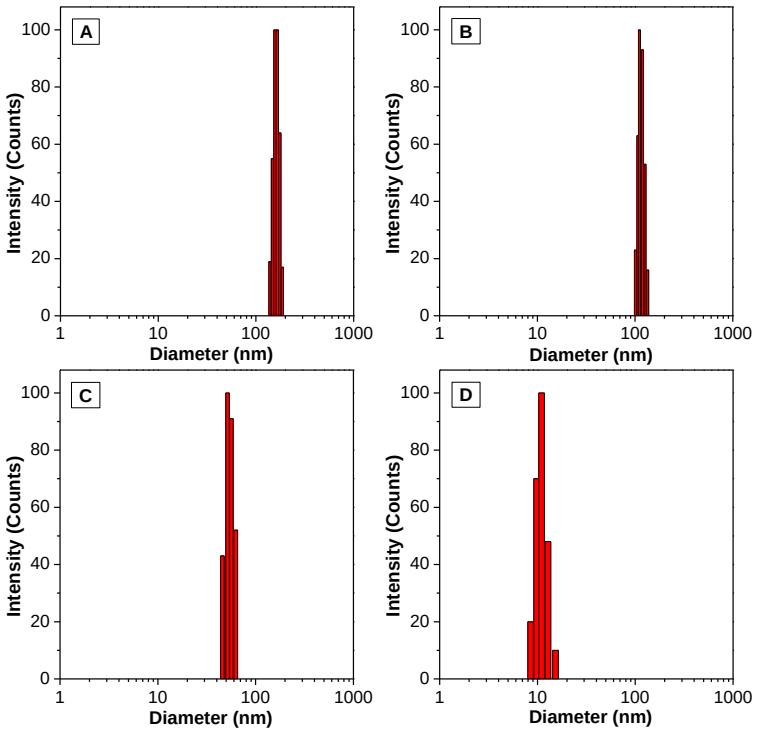

Figure 2.3 Hydrodynamic diameters of (A) TPE-NCS, (B) TPE-D, (C) TPE-D_2 and (D) TPE-D_3 (20 μM) in DMSO/H_2O (v/v = 1/199) measured by LLS. Reprinted with permission from Ref 113.[113] Copyright 2014 American Chemical Society.

The morphology and sizes of the aggregates were further studied by AFM. Suspensions of TPE-NCS and TPE-D_n (n = 1−5) conjugates were firstly prepared in the mixture of DMSO/H2O (v/v = 1/199) at a concentration of 10 μM. Then each

suspension was spin-coated onto freshly cleaved mica surface. All the AFM images were obtained under tapping mode. As shown in Figure 4, the aggregates show high uniformity in size at low magnification. In accordance with LLS results, the heights of TPE-D_n decrease as the number of D units increases, as shown evidently in the height mode (**Figures 2.4 B, E, H, K, N** and **Q)** and 3D mode (**Figures 2.4C, F, I, L, O** and **R**). Specifically, TPE-NCS aggregates are spherical in shape with a height of 30 nm (**Figures 2.4A, B** and **C**). The height of aggregates of TPE-D decreases to 20 nm. By employing three and four carboxyl groups, the heights of TPE-D_2 and TPE-D_3 decrease to 6 nm and 4 nm, respectively, indicating an improvement in dispersion. With five and six carboxyl groups, the height of TPE-D_4 aggregates further decreases to about 1 nm and that for TPE-D_5 is even less than 1 nm. These results imply that with the aid of carboxyl groups, the aggregates of TPE-D_n become increasingly well-dispersed which are most likely attributed to the improvement in hydrophilicity upon introduction of hydrophilic peptide moieties. Combined with PL spectra shown in **Figure 2.1**, the well dispersed small dots of TPE-D_4 and TPE-D_5 on the mica surface demonstrate that five carboxyl groups are sufficient to impart good water-solubility to TPE molecules, as the dimension of the dots is approaching the size of their single molecules.

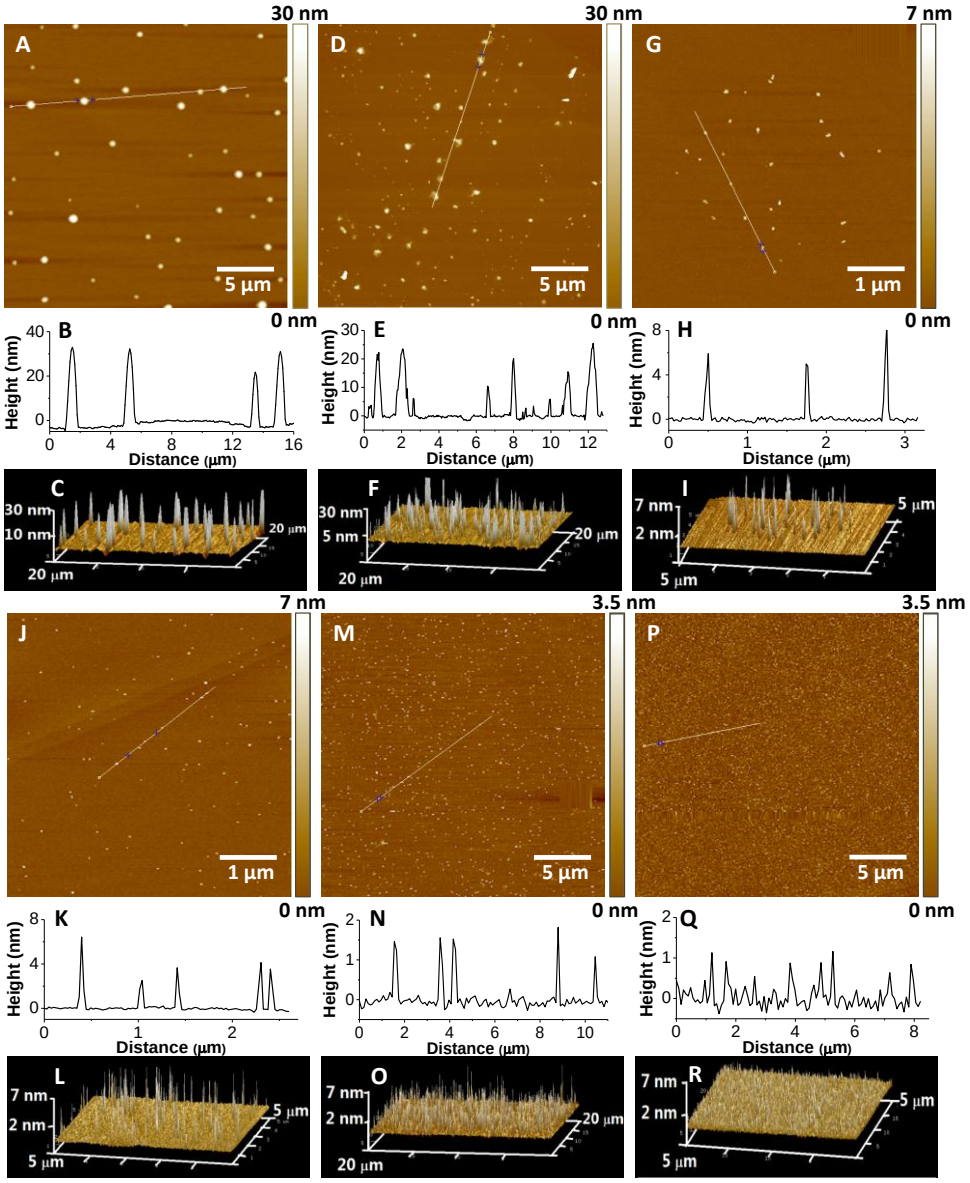

Figure 2.4 AFM images of TPE-NCS (A−C), TPE-D (D−F), TPE-D_2 (G−I), TPE-D_3 (J−L), TPE-D_4 (M−O) and TPE-D_5 (P−Q) after spin-coating their suspensions on mica surface measured by tapping mode. Figures B, E, H, K, N and Q are in height mode. Figures C, F, I, L, O and R are the corresponding 3D mode. Reprinted with permission from Ref 113.[113] Copyright 2014 American Chemical Society.

2.3.4 Measurement of partition coefficients

Partition coefficient is defined as the ratio of concentrations of a compound in a mixture of two immiscible phases at equilibrium.[114, 115, 116] As shown in equation (2.1),

$$Partition\ coefficient = \log \frac{[\text{solute}]_{\text{octanol}}}{[\text{solute}]_{\text{water}}} \qquad \text{Eq. (2.1)}$$

the lipophilicity is reflected by partition coefficient that is equal to the logarithm of the ratio of concentrations in octanol and water, *log P*. Positive values of *log P* stand for hydrophobicity of the compound while negative values represent hydrophilicity. The greater the absolute value, the more hydrophobic or hydrophilic the compound is. In this work, partition coefficients were measured to explore the relationships between the numbers of carboxyl groups and the hydrophilicity of AIE-peptide conjugates. Generally, the *log P* values of TPE-NCS and TPE-D_n follow a linear declining trend in accordance with their numbers of carboxyl groups (**Figure 2.5**). *Log P* of TPE-NCS was measured to be 0.86, indicating its high hydrophobicity. Hydrophobic TPE-NCS molecules form aggregates in water so that they are highly emissive in aqueous media. TPE-D has a *log P* value of ~0.60, indicating that one carboxyl group is able to slightly reduce the hydrophobicity of TPE molecule. With three carboxyl groups, the *log P* of TPE-D_2 was measured to be –0.27, revealing that the molecule is amphiphilic and hydrophilicity is slightly dominant. Accordingly, in **Figure 2.1B**, TPE-D_2 still shows 70% of florescence intensity of TPE-NCS under the same condition. The *log P* values for TPE-D_3 and TPE-D_4 were measured to be –0.63 and –0.81, respectively. The increased

hydrophilicity of both correlated well with their low fluorescence in aqueous media. Finally, the *log P* of TPE-D_5 reaches −1.08, which is clearly a hydrophilic molecule. This agrees with the previous observation that the fluorescence intensity of TPE-D_5 is the lowest in water. The linear trend shown in **Figure 2.5** clearly demonstrates the successful strategy to fine-tune the solubility of TPE fluorogen by peptide conjugation.

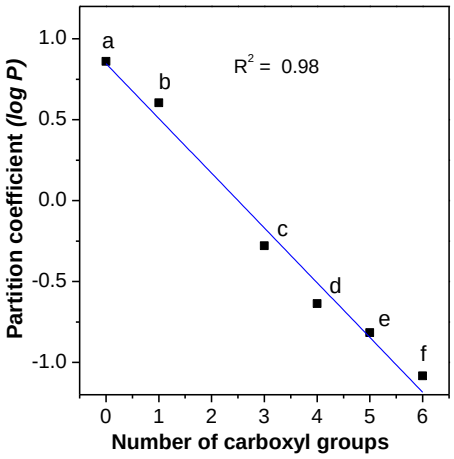

Figure 2.5 Partition coefficients of TPE-NCS (a) and TPE-D_n (b-f for n = 1−5) as a function of the numbers of carboxyl groups they possess. (TPE-NCS, TPE-D, TPE-D_2, TPE-D_3, TPE-D_4 and TPE-D_5 have 0, 1, 3, 4, 5 and 6 carboxyl groups, respectively.) Reprinted with permission from Ref 113.[113] Copyright 2014 American Chemical Society.

2.3.5 Proof-of-concept bioprobe based on TPE-SS-D_5 for thiol detection

The sensing of biological thiols is of great importance due to their vital role in many biological processes and there have been several probes based on AIE fluorogens for thiols detection. However, these probes require high fraction (generally more than 50%) of organic solvents to eliminate background signal. It is highly desirable if one could develop AIE probes that are water-soluble. As discussed above, five carboxyl groups are a threshold to provide sufficient

hydrophilicity to disperse the aggregates of TPE in aqueous media. Considering that TPE-D_5 shows the lowest fluorescence in aqueous media, it was selected to develop a thiol probe as a proof-of-concept. A cleavable thiol responsive linker was inserted between TPE and the peptide moiety so that in the presence of thiols, the hydrophilic peptide moiety can be removed from TPE to recover the fluorescence.

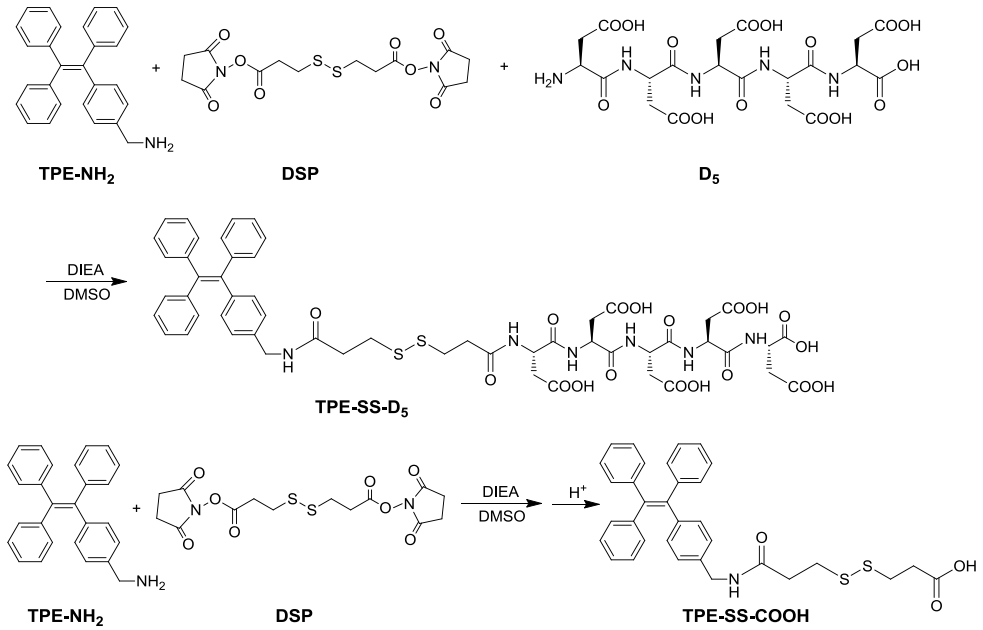

Scheme 2.2 Synthetic route to TPE-SS-D_5 and TPE-SS-COOH. Reprinted with permission from Ref 113.[113] Copyright 2014 American Chemical Society.

As shown in **Scheme 2.2**, two probes, TPE-SS-D_5 and TPE-SS-COOH were developed for thiol detection. The starting material of TPE-NH_2 (1-[(4-aminomethyl)phenyl]-1,2,2-triphenylethene) was synthesized in 70% yield by reducing TPE-N_3 using triphenylphosphine (PPh_3) under nitrogen protection (**Scheme S2.3**). Subsequently, TPE-SS-D_5 was synthesized through conjugation of TPE-NH_2 and D_5 in 49% yield using dithiobis(succinimidyl propionate) (DSP) as the linker. As the disulphide linker is thiol-specific and cleavable, in the presence of thiol species such as dithiothreitol (DTT) or glutathione (GSH), TPE-SS-D_5 is

cleaved to induce the changes in water solubility leading to evident fluorescence turn-on. Another probe TPE-SS-COOH without hydrophilic moiety D_5 was also synthesized in a similar way and exposed to thiol species to make a control for TPE-SS-D_5. The NMR and mass spectra confirmed the right structures of TPE-NH_2, TPE-SS-D_5 and the TPE-SS-COOH. (**Figures S2.9−2.13**)

To examine the potential of the TPE-SS-D_5 probe for thiol detection, glutathione (GSH) was selected as a representative thiol analyte due to its great importance and high concentration in biological system.[52-53] First, 1.0 mM GSH was incubated with 10 μM TPE-SS-D_5 in DMSO/H_2O (v/v = 1/199) mixtures, and the fluorescence spectra were collected at different time points. The fluorescence of TPE-SS-D_5 probe is very weak in aqueous media. It increases significantly within the first 90 min, which is followed by saturation at 180 min (**Figures 2.6A** and **S2.14**). The effect of GSH concentration on the fluorescence of TPE-SS-D_5 was then examined by incubation of the probe with an increasing amount of GSH from 5 μM to 1000 μM for 3h and the corresponding spectra are shown in Figure 6B. Upon addition of GSH, the fluorescence gradually increases due to the cleavage of disulphide bond and aggregates formation in aqueous solution. By plotting the PL intensities at 465 nm for TPE-SS-D_5 against the GSH concentration, a linear line is obtained as shown in Figure 6C, suggesting the potential of using the probe for GSH quantification with a detection limit of 4.26 μM. The concentration dependent experiments were also carried out using 90 min as the incubation time. It shows good linear relationship between the fluorescence intensity and the concentration of GSH (**Figures S2.15A** and **B**). To further confirm the detection

mechanism, reverse-phase HPLC and MS analysis were employed to monitor the fluorescence activation of the detection after incubation of TPE-SS-D_5 with GSH for 3h. TPE-SS-D_5 itself has a retention time of 10.7 min while the cleaved products have retention times of 14.6 min and 15.6 min as shown in **Figures S16A** and **S16B**. The molecular weight of the cleaved species TPE-GSS and TPE-SH (structures shown in **Figures S17−S18**) were confirmed by ESI-MS,[54] which indicate that the fluorescence turn-on is due to the specific cleavage of the disulphide bond and the aggregation of hydrophobic TPE-SH. On the other hand, although TPE-SS-COOH could also be cleaved in the presence of GSH (**Figures S16C** and **S16D**), its fluorescence intensity only shows very minor change due to the subtle variation in hydrophobicity before and after probe cleavage (Figure 6D). These results highlight the importance of the hydrophilic moiety D_5 in the design of light-up probes and also validate the potential of TPE-SS-D_5 probe for thiol detection.

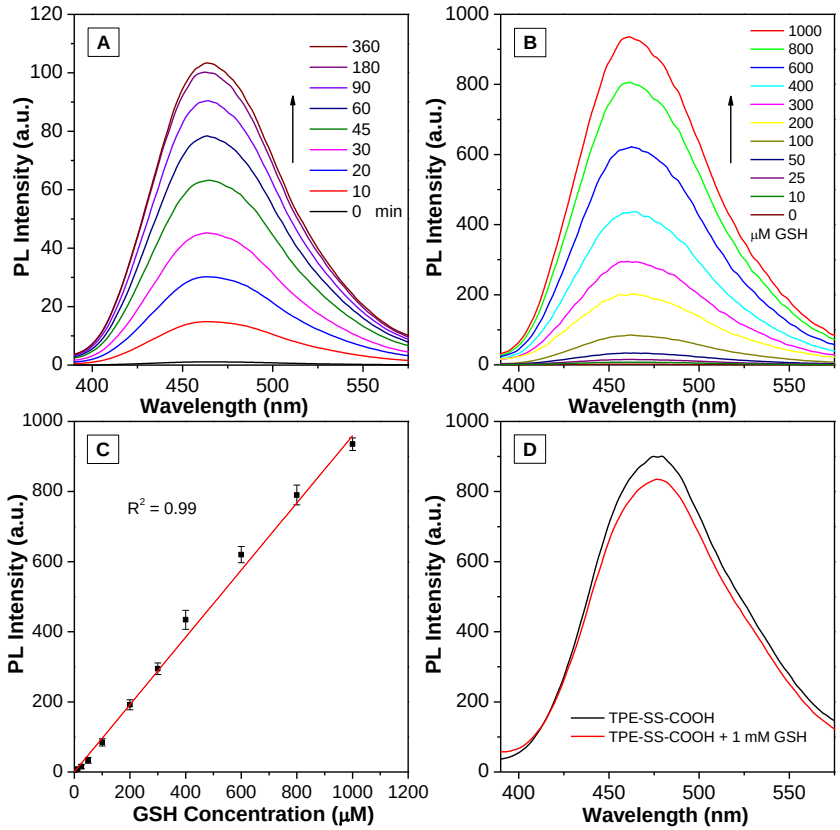

Figure 2.6 . (A) Time-dependent PL spectra of 10 μM TPE-SS-D_5 treated with GSH (1.0 mM); (B) PL spectra of 1.0 mM TPE-SS-D_5 upon addition of increasing amount of GSH from 0 μM to 1000 μM, incubation time: 180 min; (C) Plot of PL intensities of 1.0 mM TPE-SS-D_5 in DMSO/H_2O (v/v = 1/199) at 465 nm versus increasing amount of GSH (mean ± SD, n = 3) and (D) PL spectra of 1.0 mM TPE-SS-COOH upon addition of 0 μM and 1 mM GSH DMSO/H_2O (v/v = 1/199). (λ_{ex} = 304 nm for both TPE-SS-D_5 and TPE-SS-COOH). Reprinted with permission from Ref 113.[113] Copyright 2014 American Chemical Society.

2.4 Conclusion

In summary, we report a general strategy to fine-tune the aggregation-induced emission of TPE-peptide conjugates for the development of fluorescence "turn-on" probes. An iconic AIE fluorogen tetraphenylethene (TPE) was conjugated with peptide fragments containing different numbers of aspartic acid (D) units. Relationships between the numbers of D and the hydrophilicity, optical

properties, and aggregate sizes and the AIE characteristics of TPE-peptide conjugates were investigated carefully. Five carboxyl groups were found to be the threshold to "turn off" the fluorescence of TPE. As a proof-of-concept, TPE-SS-D_5 containing a cleavable disulfide bond was synthesized for thiol turn-on detection. The validated tunable AIE characteristic offers new opportunities to design fluorescence turn-on probes based on hydrophobic recognition elements and AIE fluorogens.

CHAPTER 3. Specific Light-Up Probe with Aggregation-Induced Emission for Facile Detection of Chymase

3.1 Introduction

Chymases are mainly stored and secreted by mast cells, which play critical roles in host defense and inflammatory response.[117] Chymases and other bioactive substances are released into environment when mast cells are activated by allergens and experience degranulation.[118] Chymases are known to promote inflammation, tissue remodeling and hyperresponsiveness and thus have been linked to allergic asthma.[119] Other studies indicate that chymases can modulate immune response and may exert a protective role in preserving airway function in severe asthmatics.[120] In addition, the amount of chymases varies by mast cell type, tissue and mammal of origin.[121] Therefore, direct monitoring of chymases level will help to understand their biological functions. However, existing methods for chymases detection are very limited and generally based on tedious immunohistochemical stains, which require antigens/antibodies.[122, 123, 124, 125] In comparison, peptides have longer shelf-life and higher activity per mass due to their low molecular weight.[126] Moreover, the advent of phage display technology has enriched peptide library and enabled scientists to find peptides that interact with protein targets with high affinity and specificity.[127]

Fluorescent probes have been widely used for sensing of biomolecules and monitoring of biological processes.[1] The past several decades have witnessed the prosperity of bioprobes based on various fluorescent substances including quantum

dots (QDs),[128] fluorescent NPs,[129] conjugated polymers (CPs),[130] and fluorescent dyes[131, 132], etc. Among them, organic fluorescent dyes are the most popular signal reporters. The widely used dyes, such as fluorescein and rhodamine, suffer from aggregation-cased quenching (ACQ), i.e., their fluorescence is quenched at high concentration or in aggregated state.[133] To minimize the ACQ effect, researchers are forced to use dilute solutions, which adds on the risk of photo-bleaching. Moreover, due to their intrinsic fluorescence, dark quenchers such as Black-Hole Quenchers (BHQs), dabcyl and QSY derivatives[134] or graphene oxide (GO),[135] Au-NPs[136] and carbon nanomaterials (CNs)[137] are generally required to construct fluorescence turn-on probes. In view of this, it would be favorable if there is a group of fluorogens that do not suffer from aggregation-caused quenching and can be developed into fluorescence turn-on probes by their intrinsic optical property.

In recent years, significant research efforts have been paid to a group of propeller-shaped fluorogens which fluoresce very weakly when molecularly dissolved but show strong fluorescence in the solid or aggregate state due to the restriction of intramolecular motions (RIM).[43, 49] The fluorogens with aggregation-induced emission (AIE) characteristics are termed as AIEgens, which have been used for the development of fluorescent light-up probes for sensing, imaging and therapeutic applications.[48, 50, 51, 55, 138, 139, 140, 141, 142] The existing AIE light-up probes have been developed based on electrostatic/hydrophobic attraction,[57, 61] hydrogen bonding,[64, 143] site specific reaction,[50, 68, 110] or specific target binding[54, 73, 144] induced fluorescence changes. Among these probes, AIE-peptide conjugates enjoy

substantial popularity and serve as a general strategy for the development of light-up assays.[50, 54, 68, 71, 72, 73, 74, 110, 144]

In this chapter, we report a fluorescent light-up probe for chymase detection. The probe consists of tetraphenylethenethiophene (TPETH), an AIEgen with red-emission in aggregates, and a peptide sequence of Cys-Phe-Thr-Glu-Arg (CFTER), which can be hydrolyzed by chymase.[145] To ensure good solubility of the probe in aqueous media and to minimize the background signal, different numbers of aspartic acids (Asp, D) are linked to the peptide sequence. The probe is almost non-emissive by itself in aqueous media. The presence of chymase will cleave the hydrophilic peptide sequences to result in dramatic solubility change of the probe. The released hydrophobic core of TPETH is able to form aggregates, yielding light-up fluorescence dependent on chymase concentration. The probe offers facile fluorescence light-up chymase detection, which does not require any fluorescent quenchers or washing steps.

3.2 Experimental Section

3.2.1 General Information

Chemicals and solvents including boron tribromide, triphenylphosphine, dichloromethane, hexane, ethyl acetate, acetonitrile (CH_3CN), and dimethyl sulfoxide were purchased from Sigma or Merck. $CFTERD_2$ and $CFTERD_3$ were customized from GL biochem Ltd. Recombinant human chymase, lysozyme, tripsin, cathepsin B, β-glucuronidase, pepsin, bovine serum albumin (BSA), α-

chymotrypsin, and trypsin were ordered from Sigma-Aldrich. Deuterated solvents using tetramethylsilane (TMS) was used as internal reference at 0 ppm (Cambridge Isotope Laboratories Inc.).

NMR spectroscopic characterization was carried out on a Bruker ARX 400 NMR spectrometer and chemical shifts were reported in parts per million (ppm). High resolution mass spectra were obtained by *electrospray* ionization *ion trap/time*-of-*flight mass* manufactured by Shimadzu. HPLC spectra were acquired by Agilent 1100 series HPLC system using 0.1% TFA/H_2O and 0.1% TFA/acetonitrile as eluents. Size and size distribution of AIE aggregates were determined by laser light scattering (LLS). UV−vis absorption spectra were recorded on a Shimadzu UV-1700 spectrometer while the photoluminescence (PL) spectra were measured on a PerkinElmer LS 55 spectrofluorometer. The kinetic analysis of chymase activity was obtained using infinite M200 Pro multimode microplate reader from TECAN.

3.2.2 Synthesis and Characterization

Synthesis of TPETH-2MAL

To the solution of **2** (31.3 mg, 60 μmol) in acetonitrile (3 mL) was added **1** (29.4 mg, 78 μmol) and potassium carbonate (16.8 mg, 120 μmol) as shown in **Scheme S1**. The resulting mixture was stirred at 50 ^oC for 12 h followed by cooling down to room temperature. The residue was removed by filtration. The filtrate was concentrated and purified by silica column chromatography (hexane/EA, v/v = 10/1-3/1) to give the intermediate, which was dissolved in toluene (4 mL) and

refluxed for 20 h. After solvent removal and further purification with column chromatography (hexane/EA = 10/1-3/1), TPETH-2MAL was obtained as a red solid (20.3 mg, 52% yield). ^{1}H NMR (400 MHz, $CDCl_3$) δ 7.82 (dd, J_1 = 1.2 Hz, J_2 = 5.2 Hz, 1H), 7.73 (dd, J_1 = 1.2 hz, J_2 = 5.2 Hz, 1H), 7.10-7.23 (m, 8H), 7.03-7.06 (m, 2H), 6.87-6.93 (m, 4H), 6.68-6.71 (m, 4H), 6.58-6.62 (m, 4H), 3.91 (t, J = 6.0 Hz, 4H), 3.69-3.73 (m, 4H), 2.02-2.08 (m, 4H). ESI-HRMS: m/z $[M+Na]^+$ calcd for $C_{48}H_{36}N_4O_6S$: 819.2248, found: 819.2251.

Synthesis of Probe TPETH-2(CFTERD$_n$), n = 2 or 3

TPETH-2MAL (2 mg, 2.51 μmol), peptide $CFTERD_3$ (6.3 mg, 6.02 μmol) and triphenylphosphine (TPP) (0.79 mg, 3.01 μmol) were dissolved in the mixture of DMSO and PBS buffer (pH = 6.0) with the volume ratio of 8:2. The mixture was further stirred overnight and purified by HPLC. After lyophilization, the product TPETH-2($CFTERD_3$) was obtained as an orange solid (1.8 mg, 25% yield). ESI-HRMS, m/2z $[M+2H]^{2+}$ calcd for $C_{130}H_{158}N_{28}O_{42}S_3$: 1439.5120, found: 1439.5118. Similarly, TPETH-2($CFTERD_2$) was synthesized using TPETH-2MAL and peptide $CFTERD_2$ as the starting materials. After lyophilization, the product TPETH-2($CFTERD_2$) was obtained as an orange solid (2.5 mg, 37% yield). ESI-HRMS, m/2z $[M+2H]^{2+}$ calcd for $C_{122}H_{146}N_{26}O_{36}S_3$: 1324.4850, found: 1324.4855.

3.2.3 PL measurement and enzyme activity investigation

Procedure for measurement of UV-vis and PL spectra

2 μL of 5 mM TPETH-2MAL stock solution in DMSO was firstly mixed with 8 μL of DMSO and 990 μL of PBS buffer to obtain a 10 μM solution. All the PBS buffer used consists of 137 mM NaCl, 2.7 mM KCl, 10 mM Na_2HPO_4, and 1.8 mM Na_2HPO_4 with pH = 7.4. The UV-vis absorption spectra were collected from 300 to 600 nm, while the PL spectra were recorded from 550-800 nm with excitation at 430 nm. The UV-vis and PL spectra of TPETH-2($CFTERD_2$) and TPETH-2($CFTERD_3$) were recorded under the same condition.

Procedure for Light-up Detection of Chymase in Aqueous Solution

5 μL of 5 mM TPETH-2($CFTERD_3$) stock solution in DMSO was mixed with 5 μL of DMSO before dilution with 190 μL of PBS buffer. Then the mixtures were incubated with 0.5, 1, 2, 4, 6 and 12 ng of chymase at 37 ^oC for 3 h, respectively, followed by further dilution with 800 μL of PBS buffer before PL measurement. The solution was excited at 430 nm and the emission spectra were collected from 525 to 775 nm.

Procedure for studying the probe TPETH-2($CFTERD_3$) selectivity over other proteins

Microplate reader was employed to investigate the selectivity of the probe TPETH-2($CFTERD_3$). Specifically, 2 μL of 1 mM TPETH-2($CFTERD_3$) stock solution in DMSO was diluted with 48 μL of PBS buffer, which was subsequently incubated with 1 pmol (in excess) chymase at 37 ^oC for 3 h. The mixture was diluted with 150 μL of PBS buffer before PL measurement. The excitation and emission wavelengths are 430 and 630 nm, respectively. The fluorescence responses of the

probe upon incubation with other proteins were studied under the same condition. All the PBS buffer contains 137 mM NaCl, 2.7 mM KCl, 10 mM Na_2HPO_4, and 1.8 mM Na_2HPO_4 with pH at 7.4. The experiments were carried out three times and the error bars represent standard deviation, n = 3.

To determine the selectivity of the probe TPETH-2(CFTERD_3) to other serine proteases including trypsin and chymotrypsin, 10 μM probe in the mixture of DMSO/PBS (v/v = 1/99) was mixed with 1.5 nM chymase, trypsin and chymotrypsin, respectively. The PL intensity at 630 nm was recorded every 30 min with excitation at 430 nm.

Procedure for kinetic study of chymase

The kinetic analysis of chymase activity was also carried out on 96-well plates using microplate reader with excitation at 430 nm and the PL intensities were collected at 630 nm. Firstly, in 200 μL of the mixture of DMSO/PBS (v/v = 1/99), 0, 0.5, 2.5, 5.0, 10.0, 20.0, and 35.0 μM TPETH-2(CFTERD_3) was incubated with 6.6 nM chymase at 37 ^oC for 3 h, respectively. The PL intensity was subsequently measured and plot against the probe concentration. Secondly, the probe at different concentrations of 2, 4, 8, 10, 50, 100, and 200 μM was incubated with 6.6 nM chymase, respectively. The PL intensity was monitored every 30 min and plotted against the incubation time. For kinetic experiments with high probe concentrations, incubation at required concentration followed by dilution was conducted before PL measurement at each time point.

3.3 Results and discussion

3.3.1 Probe design and synthesis

As shown in **Scheme 3.1**, the probe is designed based on three elements. Firstly, the signal reporter TPETH is a fluorescent core with AIE characteristics. It is functionalized with two maleimide groups (MAL) for further conjugation. Secondly, a peptide sequence of Cys-Phe-Thr-Glu-Arg (CFTER) consists of the recognition moiety FTER and a cysteine as anchor unit, which is reactive to maleimide groups. Thirdly, to obtain significant signal-to-background ratio, hydrophilic aspartic acid (Asp or D) pendant is added to the peptide sequence. Two or three aspartic acids are modified to the N-terminal of arginine (R) to obtain $CFTERD_2$ or $CFTERD_3$ and the subsequent conjugation with TPETH-2MAL yields the probes TPETH-2($CFTERD_2$) or TPETH-2($CFTERD_3$). In the absence of chymase, the probes are expected to be well-dispersed in aqueous media and show weak fluorescence, that is, the OFF state. In contrast, chymase can specifically cleave at the C-terminal of phenylalanine and generate hydrophobic core TPETH-2C, leading to fluorescence light-up in aqueous medium due to RIM.

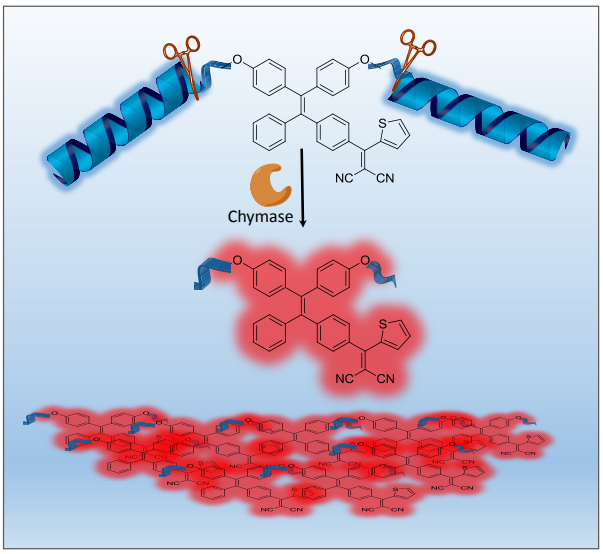

Scheme 3.1 Schematic illustration of working mechanism of the probe TPETH-2(CFTERD$_n$), n = 2 or 3 for chymase sensing.

As shown in **Scheme 3.2**, TPETH-2OH was synthesized according to our previous report.[146] It further underwent alkylation with compound **1** in the presence of potassium carbonate in acetonitrile, followed by subsequent deprotection in toluene to yield TPETH-2MAL as red solid in 53.4% yield after silica gel chromatography. The ^{1}H NMR and MS spectra confirmed the right structure with high purity (**Figures S3.1** and **S3.2** in **Appendix 2**). TPETH-2MAL was further reacted with CFTERD$_2$ or CFTERD$_3$ overnight in the mixture of DMSO and PBS buffer (pH = 6.0) mixture to yield TPETH-2(CFTERD$_2$) or TPETH-2(CFTERD$_3$). The final products were purified using HPLC and characterized by high resolution electrospray ionization-mass spectrometry (ESI-HRMS) (**Figures S3.3-S3.6**).

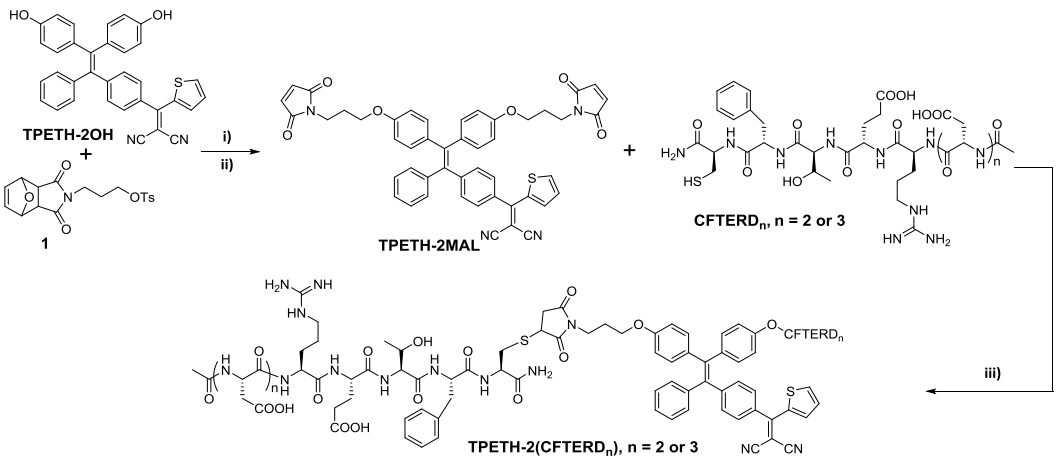

Scheme 3.2 Synthetic routes to TPETH-2MAL and TPETH-2($CFTERD_n$), n = 2 or 3. Reaction condition: i) K_2CO_3/acetonitrile; ii) toluene/reflux; iii) DMSO/PBS (pH = 6.0).

3.3.2 Optical Properties

The optical properties of TPETH-2MAL, TPETH-2($CFTERD_2$) and TPETH-2($CFTERD_3$) were studied in the mixture of dimethyl sulfoxide (DMSO) and PBS buffer (v/v = 1/99). As shown in **Figure 3.1**, both TPETH-2MAL and the probes share the similar UV-vis absorption spectra, with one peak at 340 nm and the shoulder peak centered at 440 nm. Likewise, their PL spectra are located at around 630 nm. At the same concentration of 10 μM, the PL intensities of TPETH-2($CFTERD_2$) and TPETH-2($CFTERD_3$) are 25% and 0.03% as that of TPETH-2MAL in the mixture of DMSO/PBS (v/v = 1/99). The inset photographs illustrate the fluorescence difference between TPETH-2MAL and the probes. Laser light scattering (LLS) results confirm that TPETH-2MAL forms aggregates in the aqueous media with an effective diameter of around 95 nm (**Figure S3.7**). In contrast, no LLS signal was detected from the TPETH-2($CFTERD_3$) solution, suggesting that it has good water-solubility. The PL spectra of TPETH-2MAL were measured in the mixture of DMSO and water with water different fractions to

investigate its AIE characteristics and the results are shown in **Figures 3.1B** and **S3.8**. The fluorescence of TPETH-2MAL remains very weak when the water fraction is less than 30%. It becomes slightly emissive when the water fraction reaches 40%. There is a dramatic fluorescence enhancement when the water fraction increases from 40% to 50%. A steady increase in fluorescence intensity is observed when the water fraction changes from 50% to 99%. The results prove that the fluorescence of TPETH can be revitalized upon restriction of intramolecular motions. Considering the ionic strength is a very important factor in bioassays, the PL intensity of the probe in different PBS buffers was measured and the results (**Figure S3.9**) show that the probe stays non-emissive in aqueous media with different ionic strength.

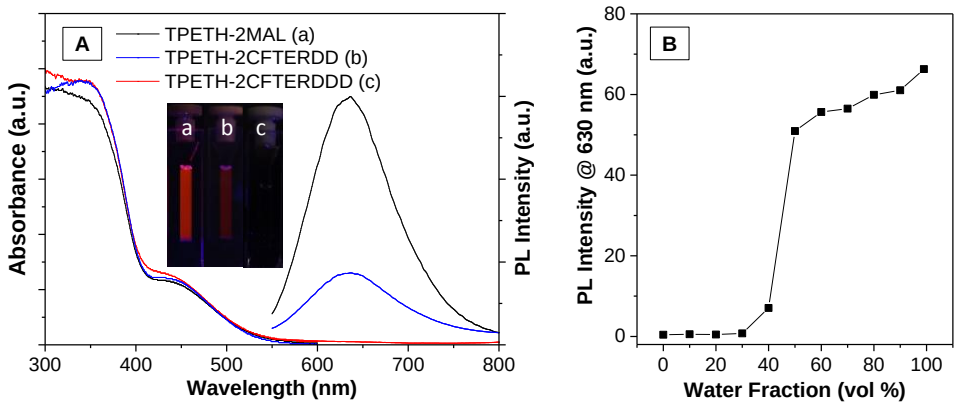

Figure 3.1 (A) UV-vis absorption and Photoluminescence (PL) spectra of TPETH-2MAL (black) and TPETH-2(CFTERD$_n$), n = 2 (blue) or 3 (red) in DMSO/PBS buffer (v/v = 1/99); (B) the plot of emission peak intensities of TPETH-2MAL in DMSO/H_2O solvent mixture with increasing water fractions. (λ_{ex} = 430 nm, [TPETH-2MAL] = [TPETH-2(CFTERD$_n$)] = 10 μM, n = 2 or 3).

3.3.3 Detection of Chymase

As shown in **Figure 3.1A**, TPETH-2(CFTERD$_3$) has a lower background signal than TPETH-2(CFTERD$_2$). As a consequence, TPETH-2(CFTERD$_3$) was

chosen as the chymase probe for further detailed studies. To test the potential of TPETH-2(CFTERD$_3$) for quantification of chymase, the probe was incubated with different amount of chymase and the PL spectra were recorded. Specifically, 25 μM of TPETH-2(CFTERD$_3$) was incubated with 0.5, 1, 2, 4, 6 and 12 ng/mL of chymase in 200 μL of PBS buffer (pH = 7.4) solution at 37 ^{o}C for 3 h, then each sample was diluted to 1 mL and their PL spectra were measured. As shown in **Figure 3.2A**, the probe only weakly fluoresces in aqueous solution, however, after incubation with chymase, obvious concentration-dependent fluorescence enhancement is observed. The PL intensities at 630 nm were plotted against the chymase concentration and the results are summarized in **Figure 3.2B**. A linear trend is found in the range of 0-9.0 ng/mL, which gives a detection limit of 0.1 ng/mL. The product of chymase hydrolysis was analyzed by HPLC and a peak with absorbance at 430 nm was observed as shown in **Figure S3.10**. The product peak has a retention time of 9.5 min, indicating that its hydrophobicity is increased as compared to that for TPETH-2(CFTERD$_3$) (8.8 min), as shown in **Figure S3.5.** HRMS results confirm that chymase cleaves the probe at the C-terminal of phenylalanine (F). The HRMS spectrum of the cleavage product of TPETH-2C is shown in **Figure S3.11**.

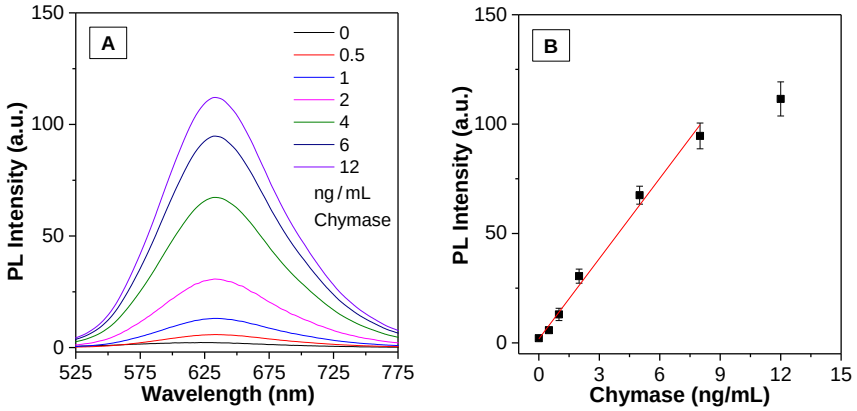

Figure 3.2 (A) PL spectra of 25 μM TPETH-2(CFTERD$_3$) responsive to increasing amount of chymase at the concentration of 0.5, 1, 2, 4, 6 and 12 ng/mL in DMSO/PBS buffer (v/v = 1/99); (B) PL intensities of the probe TPETH-2(CFTERD$_3$) at 630 nm in the presence of different amount of chymase.

The selectivity of TPETH-2(CFTERD$_3$) is evaluated by incubation of the probe with chymase and other proteins such as lysozyme, cathepsin B, β-glucuronidase, pepsin, and BSA. Among them, BSA represents a common interferant which may lead to non-specific binding while the rest of proteins belong to hydrolytic enzymes. 10 μM of the probe TPETH-2(CFTERD$_3$) was incubated with chymase and other proteins at the same concentration of 10 nM, respectively. From **Figure 3.3**, the probe shows around 48-fold PL enhancement in response to chymase, but it remains nearly non-emissive in the presence of other proteins (**Figure 3.3, c-g**). Moreover, the mixture of lysozyme, cathepsin B, β-glucuronidase, pepsin and BSA cannot induce evident fluorescence light-up of the probe (**Figure 3.3, h**). In comparison, when chymase was added into the mixture, significant fluorescence turn-on is observed (**Figure 3.3, i**). The results show that the probe TPETH-2(CFTERD$_3$) can serve as a highly specific probe for chymase detection, even in the presence of a variety of interference substances.

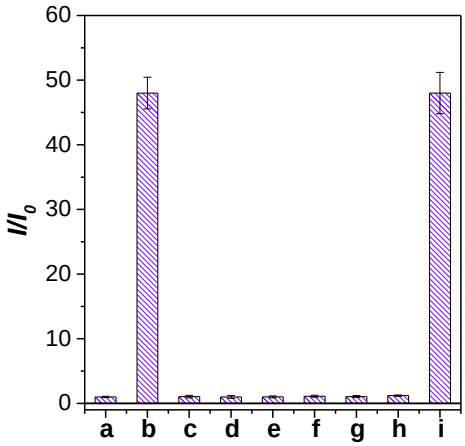

Figure 3.3 PL enhancement of (a) the probe TPETH-2(CFTERD$_3$) alone or the probe incubated with different enzymes or other proteins including (b) chymase, (c) lysozyme, (d) cathepsin B, (e) β-glucuronidase, (f) pepsin, and (g) BSA, the mixture of all these proteins without chymase (h) and with chymase (i). I_0 and I are fluorescence intensities of the probe TPETH-2(CFTERD$_3$) in the absence and presence of protein used. [TPETH-2(CFTERD$_3$)] = 10 μM, chymase and other enzymes or proteins share the same concentration of 10 nM. Error bars represent standard deviation, n = 3.

It is important to note that chymase, trypsin and chymotrypsin are all serine proteases. Trypsin cleaves c-terminal to arginine (R),[147] while chymotrypsin and chymase are both chymotryptic peptidases, which share the similar cleavage site at phenylalanine (F). The selectivity of the probe was further evaluated for these proteases and the PL intensity of the probe was recorded every 30 min. **Figure 3.4** shows that although trypsin cleaves at arginine, its hydrolysis effect to TPETH-2(CFTERD$_3$) does not lead to obvious fluorescence change. In comparison, chymotrypsin at the same concentration (1.5 nM) shows some fluorescence turn-on while more than 45-fold increase of fluorescence intensity is observed for chymase. It is also found that the hydrolysis of the probe by chymase occurs very quickly in the first 30 min, which slows down thereafter and the process finished within 3 hours. To highlight the importance of molecular probe design, the

selectivity of TPETH-2(CFTERD$_2$) for chymase detection was also investigated. As shown in **Figure S12A**, TPETH-2(CFTERD$_2$) only gives 3-fold fluorescence turn-on upon incubation with chymase, which is considerably less than that for TPETH-2(CFTERD$_3$). In addition, as shown in **Figures S3.12A** and **B**, the selectivity comparison between TPETH-2(CFTERD$_3$) and TPETH-2(CFTERD$_2$) in response to chymase was also studied. In these experiments, both TPETH-2(CFTERD$_2$) and TPETH-2(CFTERD$_3$) are incubated separately with enzymes including chymase, chymotrypsin or trypsin, respectively. Herein, I_0 and I stand for the fluorescence intensity of the probe in the absence and presence of enzymes used. Here R is defined as the fluorescence enhancement, which equals to I/I_0. The $R_{chymase}/R_{chymotrypsin}$ is 5 for TPETH-2(CFTERD$_3$), while it is only 3 for TPETH-2(CFTERD$_2$). The results clearly show that the introduction of two D_3 to the probe is essential in realizing high detection selectivity.

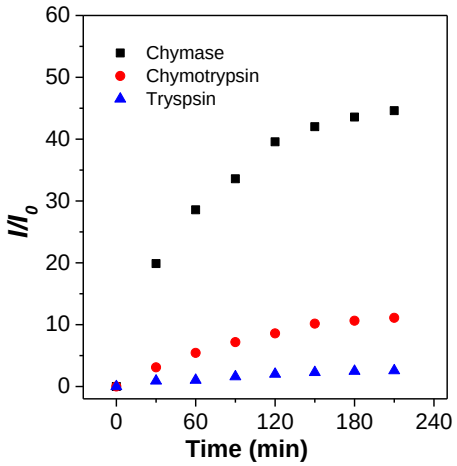

Figure 3.4 PL enhancement of the probe (10 μM) upon incubation with different enzymes including chymase, chymotrypsin, and trypsin at the same concentration of 1.5 nM. I_0 and I are fluorescence intensities of the probe TPETH-2(CFTERD$_3$) in the absence and presence of enzymes used.

The kinetics of chymase on the probe of TPETH-2($CFTERD_3$) was evaluated by Michaelis-Menten model,[148] which has been used for prediction of product formation for more than one hundred years. Michaelis-Menten model states that the rate of an enzymatic reaction increases as the concentrations of substrate increase. The initial reaction rate (V_0) of an enzymatic reaction can be expressed by $V_0 = (V_{max}[S])/(K_m + [S])$, where [S] is the substrate concentration and here the substrate is TPETH-2($CFTERD_3$). K_m is named as Michaelis constant, which is the substrate concentration at which the reaction rate reaches half of the maximum. K_m equals to the product of k_{cat} and enzyme concentration $[E]_0$, where k_{cat} is defined as the maximum amount of substrate hydrolyzed per unit enzyme per unit time. V_{max} and K_m are two kinetic parameters, which is different for each enzyme-substrate pair. In this experiment, the PL intensities of the probe at different concentrations upon incubation with the same concentration of chymase (6.6 nM) were recorded every 30 min and the results are summarized in **Figure 3.5A**. Then the reaction rate expressed in fluorescence intensity per unit time is converted to concentration per unit time using a calibration plot (**Figure 3.5B**). **Figure 3.5C** illustrates the Michaelis–Menten saturation curve for chymase hydrolysis. By taking the reciprocal of the Michaelis–Menten curve, Lineweaver-Burk double reciprocal plot is obtained (**Figure 3.5D**). Lineweaver-Burk plot can be expressed as $1/V = (K_m/V_{max})(1/[S])+1/V_{max}$, where 1/V and 1/[S] are variables. Based on the slop and intercept of the fitted line in Figure 5D, the k_{cat} and K_m are determined to be 21.0 s^{-1} and 0.69 mM, respectively, which are similar to the previous report of 19.7 s^{-1} and

0.64 mM in the same buffer system.[145] The enzymatic efficiency, which equals to k_{cat}/K_m, is calculated to be 30.5 s^{-1} mM^{-1}.

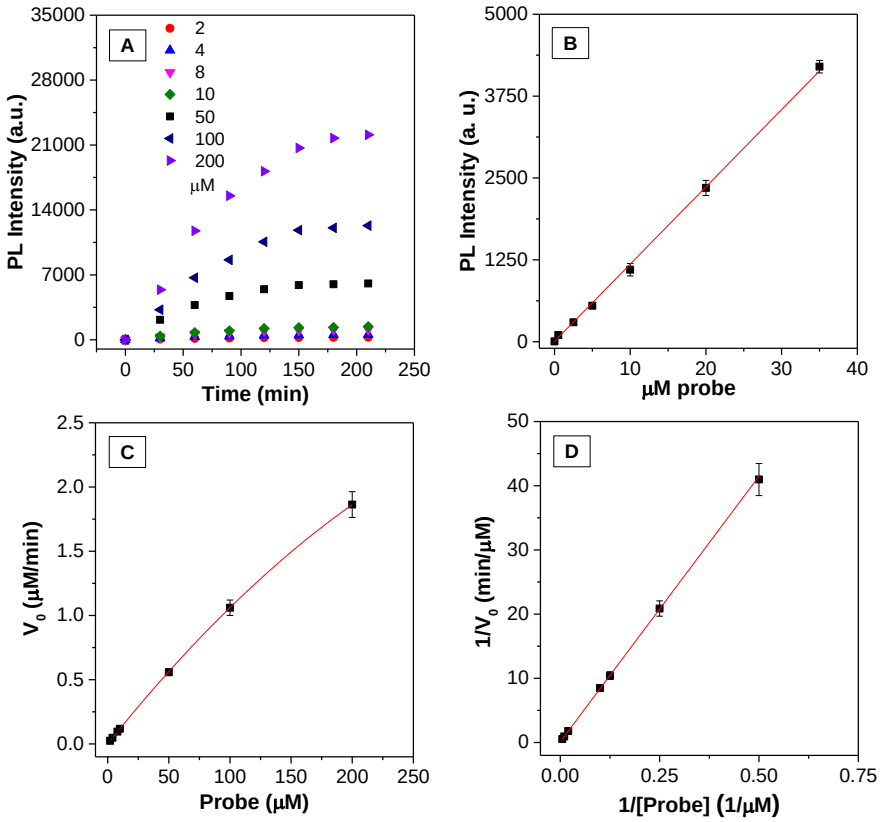

Figure 3.5 (A) Time-dependent PL intensity of the probe TPETH-2(CFTERD$_3$) at different concentrations (2—200 μM) upon incubation with 6.6 nM chymase. (B) Plot of PL intensity of TPETH-2(CFTERD$_3$) at different concentration (0—35 μM) after incubation with excess chymase (6.6 nM) measured every 30 min in PBS buffer (pH = 7.4). (C) Plot of initial reaction rate (V_0) against the probe concentration and (D) the Lineweaver-Burk plot for the reaction between the probe and chymase.

3.3 Conclusion

In summary, a specific light-up probe is developed by covalently conjugation of AIEgen TPETH-2MAL and peptide CFTERD$_3$ to yield the probe TPETH-2(CFTERD$_3$). The six aspartic acids (D) in the peptide sequence endows the probe with good hydrophilicity and low background signal in aqueous media.

Meanwhile, the probe can be cleaved by chymase and produces hydrophobic product TPETH-2C, which lights up in aqueous media due to the restriction of intramolecular motion. The fluorescence intensity follows a linear trend against chymase concentration between 0-9.0 ng/mL with a detection limit of 0.1 ng/mL. The probe not only shows excellent selectivity among common proteins like trypsin, BSA, lysozyme, etc, but also can differentiate chymase from chymotrypsin and trypsin from the family of E.C. 3.4.21. In comparison, the probe with four aspartic acids TPETH-2($CFTERD_2$) shows poor selectivity as well as low fluorescence turn-on ratio, which emphasizes the importance of probe design in realizing high signal-to-background ratio. The successful example of the probe TPETH-2($CFTERD_3$) for real-time chymase quantification will encourage further development of more molecular probes simply by changing the dye or peptide sequences.

CHAPTER 4. Real-time Specific Light-up Sensing of Transferrin Receptor (TfR): Image-guided Photodynamic Ablation of Cancer Cells through controlled Cytomembrane Disintegration

4.1 Introduction

Transferrin receptor (TfR), a transmembrane glycoprotein, is upregulated by metabolic demand due to its vital role in cellular respiration and iron transport.[149, 150] Although TfR is ubiquitously expressed on normal cells, increased expression level is observed on cells with higher proliferation rate. The TfR expression level can even be correlated with tumor stage or cancer progression, thus the detection and qualification of TfR can facilitate the precise cancer diagnosis at early stage. Moreover, upon binding with transferrin (Tf), the TfR/Tf complex could be internalized in clathrin-coated pits through endocytosis.[151] The intrinsic endocytosis pathway can even help to cross biological barriers such as blood-brain barrier (BBB),[152, 153] which emphasized the importance of TfR as a delivery vector for therapeutic reagents. To realize direct visualization of TfR, fluorescent dyes and nanoparticles have been functionalized with TfR-targeting ligands for targeted imaging of cancer cells.[154, 155] Moreover, anticancer reagents such as chemodrugs have been co-loaded into the nanoparticles to realize diagnosis and therapy at the same time.[156, 157, 158] However, the performance of chemodrugs is often blocked by the inherent genetic resistance or resistance acquired following continuous

exposure to cells.[159, 160] Alternative strategies are thus of interest to improve the therapeutic performance in cancer cell ablation.

Photodynamic therapy (PDT) using photosensitizers (PSs) with intrinsic fluorescence is undoubtedly an effective method regardless of drug resistance. As PSs can only be activated to generate highly toxic and short-lived reactive oxygen species (ROS) upon light illumination, they offer high spatiotemporal precision.[161, 162] The precise image-guided PDT also facilitates studies on delivery kinetics, subcellular response and therapeutic efficacy.[163, 164, 165] The insight into site-dependent photodynamic efficacy has also prompted the organelle-targeting therapy, *e.g.*, mitochondria and lysosome-targeted PDT.[166, 167, 168] To minimize the side effect of PSs to normal cells, researchers have developed pre-quenched PSs which are subsequently activated after binding with the target.[169, 170] However, traditional PSs, such as porphyrin derivatives, are highly hydrophobic with rigid planar structures that tend to form aggregates in aqueous media through π-π stacking.[171] This resulted in quenched fluorescence and reduced phototoxicity which affected the imaging quality and PDT performance.[172, 173] In view of this, to realize TfR-targeted precise diagnostic and therapeutic applications, it is highly desirable to develop photoactive probes that are non-emissive by themselves but become highly fluorescent upon specific protein and cell recognition.

Recently, a group of propeller-shaped fluorogens that show aggregation-induced emission (AIE) characteristics have attracted significant research attention.[37, 97] AIEgens are almost non-emissive when molecularly dissolved, but

show strong fluorescence in solid or aggregate state due to restriction of intramolecular motions (RIM).[43, 49] Taking advantage of the unique AIE characteristics, both AIE light-up probes and AIE nanoparticles have been developed for biosensing and bioimaging.[48, 55, 138, 139, 174] So far, AIEgens have been designed to conjugate with hydrophilic moieties to yield light-up probes which show fluorescence turn-on upon target recognition either through specific binding[54, 61, 73, 175] or cleavage reaction.[68, 71, 72, 110] More recently, some AIEgens with phototoxicity were developed, yielding a group of probes for activatable photodynamic therapy, drug and gene delivery.[50, 51, 52, 72, 142, 176] In contrast to conventional fluorophores that suffer from aggregation-caused quenching (ACQ), AIEgens offer fluorescence turn-on and effective PDT in the presence of target, showing great promise in both diagnostic and therapeutic applications.[50, 72]

In this contribution, we report a probe for specific light-up sensing of TfR and image-guided photodynamic killing of cancer cells. The probe TPETH-2T7 is a conjugation between the red-emissive AIEgen tetraphenylethenethiophene (TPETH) and a TfR-targeting peptide T7 (His-Ala-Ile-Tyr-Pro-Arg-His, HAIYPRH).[177] T7 peptide rather than transferrin (Tf) is selected as the targeting ligand for TfR due to the following reasons: 1) T7 has a high affinity which is comparable to that of Tf to TfR; [177, 178] 2) The binding site of T7 to TfR is different from that of Tf to TfR, thus avoiding competition from endogenous Tf; [179] 3) there have been reports that receptor targeting proteins lose their activity due to formation of biomolecule corona or disruption of structure during conjugation or surface modification.[144, 180, 181] The hydrophilic T7 moiety enables the probe TPETH-2T7

to stay non-emissive in aqueous media, which offers fluorescence light-up response upon complexation with TfR for image-guided photodynamic ablation of cancer cells.

4.2 Experimental Section

4.2.1 General Information

Chemicals including copper (II) sulphate, sodium ascorbate, dimethyl sulfoxide (DMSO), trifluoroacetic acid (TFA), acetonitrile (CH_3CN), hexane, dichloromethane (DCM), and ethyl acetate (EA), 3-azidopropyl 4-methylbenzenesulfonate, potassium carbonate, 9, 10-anthracenediyl-bis(methylene)dimalonic acid (ABDA) was purchased from Sigma-Aldrich and 3-(4,5-dimethylthiazol-2-yl)-2,5-diphenylte-trazolium bromide (MTT) was ordered from TCI. Bovine serum albumin (BSA), holo-transferrin (Tf), lysozyme from human milk and pepsin from porcine gastric mucosa were ordered from Sigma-Aldrich. All the chemicals and reagents were used without further purification. Compound 1 was synthesized according to reported procedures.[49] Recombinant Human TfR protein was purchased from R&D system with catalog number of 2474-TR. Alkyne-HAIYPRH peptide (Acetyl-His-Ala-Ile-Tyr-Pro-Arg-His-NH_2, peptide T7) was ordered from GL biochem Ltd. Deuterated solvents using tetramethylsilane (TMS) was used as internal reference at 0 ppm (Cambridge Isotope Laboratories Inc.). Dulbecco's Modified Eagle's Medium (DMEM) was used as cell culture medium and is ordered from National University Medical

Institutes in Singapore. Alexa Fluor® 488 Conjugated transferrin (T-13342), Hoechst 33342 were purchased from ThermoFisher Scientific and used directly.

NMR spectroscopic characterization was carried out on a Bruker ARX 400 NMR spectrometer and chemical shifts were reported in parts per million (ppm). The molecular mass spectra were acquired using ion trap-time-of-flight mass spectrometry (MS-IT-TOF, Shimadzu). HPLC spectra were obtained using an Agilent 1100 Series HPLC System using 0.1% TFA/H_2O and 0.1% TFA/acetonitrile as eluents. Size and size distribution of AIE aggregates were determined by laser light scattering (LLS). UV−vis absorption spectra were recorded on a Shimadzu UV-1700 spectrometer while the photoluminescence (PL) spectra were measured on a PerkinElmer LS 55 spectrofluorometer.

4.2.2 Synthesis

Synthesis of TPETH-2N_3

To 8 mL of acetonitrile solution containing 102 mg (0.2 mmol) compound 2 was added 120 mg of 3-azidopropyl 4-methylbenzenesulfonate (0.47 mmol) and 138 mg of potassium carbonate (1.0 mmol). After being stirred for 12 h at 60 ^oC, the reaction mixture was cooled down to room temperature and filtered to remove the undissolved solid. The filtrate was concentrated and separated with column chromatography (hexane/ethyl acetate = 50/1 to 5/1) to give the desired product as red solid (80 mg, 58.0%). ^1H NMR (400 MHz, Acetone-d_6) δ 8.17 (dd, J_1 = 1.2 Hz, J_2 = 4.8 Hz), 7.78 (dd, J_1 = 1.2 Hz, J_2 = 4.0 Hz), 7.35-7.39 (m, 3H), 7.12-7.24 (m,

7H), 6.96-7.03 (m, 4H), 6.74-6.78 (m, 4H), 4.08 (m, 4H), 3.58 (m, 4H), 2.02-2.08 (m, 4H). m/z: $[M+Na]^+$, calcd for $C_{40}H_{32}N_8O_2S$, 711.2261; found, 711.2262.

Synthesis of probe TPETH-2T7 through "click" reaction

TPETH-2N_3 (3 mg, 4.48 μmol) and alkyne-HAIYPRH (alkyne-T7, 11.54 mg, 11.2 μmol) were dissolved in DMSO and H_2O mixture with the volume *ratio of* 1:1. Sodium ascorbate (3.33 mg, 16.8 μmol) and copper sulphate (1.79 mg, 11.2 μmol) were added into the mixture to initiate the click reaction. The mixture was further stirred for another 24 h to complete the reaction and then purified by semi-prep HPLC. After lyophilization, the product TPETH-2HAIYPRH (TPETH-2T7) was obtained in 91% yield and characterized by ^{1}H NMR and HRMS. ^{1}H NMR (400 MHz, DMSO-d_6), δ (TMS, ppm): 9.01-8.93 (m, 4H), 8.29-8.25 (m, 3H), 8.18-8.09 (m, 9H), 7.91-7.89 (d, *J* = 8.0 Hz, 2H), 7.84 (s, 2H), 7.67-7.62 (m, 3H), 7.38-7.34 (s, 9H), 7.26 (s, 2H), 7.21-7.17 (m, 3H), 7.25-7.10 (m, 4H), 7.05-7.01 (m, 6H), 6.92-6.84 (m, 4H), 3.72-6.68 (m, 4H), 6.62-6.60 (d, *J* = 8.0 Hz, 4H), 4.62-4.16 (m, overlaps with DMSO-d_6), 3.91-3.88 (t, *J* = 4.0 Hz, 4H), 3.66-3.64 (d, *J* = 8.0 Hz, 2H), 3.47-3.46 (s, 2H), 3.16-3.08 (m, 8H), 3.02-2.94 (m, 6H), 2.87-2.81 (m, 4H), 2.71-2.63 (m, 2H), 2.21-2.18 (t, *J* = 6.0 Hz, 4H), 2.02-1.98 (m, 2H), 1.79-1.78 (m, 10H), 1.71-1.60 (m, 6H), 1.55-1.43 (m, 5H), 1.36-1.24 (m, 3H), 1.19-1.18 (d, *J* = 4.0 Hz, 5H), 1.02-0.95 (m, 2H), 0.77-0.71 (m, 12H). HRMS (ESI-MS): m/2z $[M+2H]^{2+}$ calcd for $C_{136}H_{170}N_{40}O_{22}S$: 1373.6562; found: 1373.6571.

4.2.3 Titration Experiment

Procedure for light-up sensing of TfR in solution.

2 μL of 10 mM TPETH-2T7 stock solutions in DMSO was first diluted to 10 μM in a mixture of DMSO and PBS buffer (v/v = 1/99). The PBS buffers used in this Chapter contain 13.7 mM NaCl, 0.27 mM KCl, 0.8 mM Na_2HPO_4, and 0.2 mM KH_2PO_4. Then an increasing amount of recombinant human TfR protein was added into the probe solution to yield the final concentrations from 0 to 100 μg/mL. The PL spectra were collected from 500 to 800 nm with excitation at 430 nm. The selectivity of the probe was determined by incubation of 10 μM probe with 100 μg/mL other proteins including pepsin, BSA, lysozyme, Tf, and the mixture of TfR and Tf, respectively, following the similar procedure used for the sensing of TfR.

Procedure for $^1O_2$ detection and $^1O_2$ quantum yield measurement

In 1 mL of the mixture of DMSO and PBS buffer (v/v = 1/99), 10 μM of TPETH-2T7 and 100 μg/mL of TfR were incubated for 20 min. Then into the mixture, 5 μL of 20 mM 9, 10-anthracenediyl-bis(methylene) dimalonic acid (ABDA) stock solution in DMSO was added. UV-vis absorption spectra were recorded after the probe was exposed to a white light source (400-800 nm) with a power density of 250 mW/cm^2.

The $^1O_2$ quantum yield was measured using Rose Bengal (RB) as the reference photosensitizer and calculated using the following equation (4.1):

$$\phi_{probe} = \phi_{\mathrm{RB}} \frac{K_{probe} A_{RB}}{K_{RB} A_{probe}} \qquad (4.1)$$

Where K_{probe} and K_{RB} are the decomposition rate constants of ABDA in the presence of the probe and RB, respectively. Φ_{RB} is the $^1O_2$ quantum yield of RB

(Φ_{RB} = 0.75 in water). A_{probe} and A_{RB} represent the integration area of absorption bands ranging from 400-800 nm of the probe and RB, respectively. 100 μM ABDA in 1 mL of the probe solution was exposed to white light irradiation (400-800 nm) with a power density of 250 mW/cm^2. The natural logarithm of the absorbance ratio (A_0/A) of ABDA at 380 nm was plotted against irradiation time and the slope is regarded as the decomposition rate.

4.2.4 Cell Culture and Imaging

MDA-MB-231 human breast cancer cells and NIH 3T3 cells were supplied by American Type Culture Collection (ATCC). The cells were cultured in DMEM ordered from Invitrogen containing 10% FBS and 1% penicillin streptomycin at 37 °C in a humidified environment containing 5% CO_2. Before experiments, the cells were pre-cultured to reach confluence.

MDA-MB-231 human breast cancer cells and NIH 3T3 cells were cultured in 8-well chamber according to the above mentioned procedure and incubated with probe TPETH-2T7 as described above. Cell nuclei stain by Hoechst 33342 was carried out following the standard protocol of the manufacturer (Thermo Scientific) and imaged immediately by confocal microscope. Images were taken upon excitation at 405 nm using optical filters with a band pass of 430-470 nm. For images of probe stained cells, the emission was collected above 560 nm with excitation at 405 nm. As for cells incubated with Tf-Alexa Fluor® 488 conjugate, images were taken with excitation at 488 nm and the signal was collected with a band pass of 505-525 nm optical filter.

Cytotoxicity studies.

MTT (3-(4,5-dimethylthiazol-2-yl)-2,5-diphenyl-tetrazolium bromide) assays were used to evaluate the cell viability of MDA-MB-231 and NIH 3T3 cells exposed to probe TPETH-2T7 in dark or under light irradiation. Cells were first incubated with TPETH-2T7 for 0.5 hour in dark, then undergone MTT assays to yield dark toxicity results, or exposed to (400 - 800 nm) white light irradiation for 5 min to obtain light toxicity. In addition, another group of MDA-MB-231 cells were incubated for 0.5 h first followed by removal of free probe and continuous culture for 4 h to allow the probe to be uptaken by cells before white light irradiation. All the cells were first incubated in 96-well plate (Costar, IL, USA) then washed with PBS buffer twice before light irradiation at a power density of 100 mW cm^{-2}. After incubation for another 24 h, 100 μL of 0.5 mg mL^{-1} MTT in PBS buffer was added into each well. After further incubation for 3h, the supernatant was discarded and the precipitate was dissolved in 100 μL of DMSO with gentle shaking. The absorbance of MTT at 570 nm was determined by microplate reader (Genios Tecan) using cells without any treatment as a control.

4.3 Results and Discussion

4.3.1 Probe design and synthesis

As shown in **Scheme 4.1**, Compound 1 was prepared according to our previous report.[72] Demethylation of compound 1 using boron tribromide gave compound 2 in 97% yield. Compound 2 was further reacted with 3-azidopropyl 4-methylbenzenesulfonate in the presence of potassium carbonate to afford TPETH-

$2N_3$ in 81% yield. The HRMS, ^{1}H NMR spectra confirmed the right chemical structure of TPETH-$2N_3$ (**Figures S4.1** and **S4.2** in **Appendix 3**) with high purity. The probe TPETH-2T7 was synthesized by conjugating TPETH-$2N_3$ to alkyne-T7 through a copper-catalyzed click reaction and was separated and purified by HPLC in 46% yield. The chemical structures of TPETH-$2N_3$ and TPETH-2T7 were confirmed by ^{1}H NMR and HRMS, as shown in **Figures S4.3 - S4.5**, respectively. As each T7 peptide sequence contains three positively charged amino acids (His and Arg), the probe TPETH-2T7 is expected to be molecularly dissolved in aqueous media to yield low fluorescence. Upon specific binding with TfR, the probe should light up due to RIM, which is the AIE characteristic of TPETH.

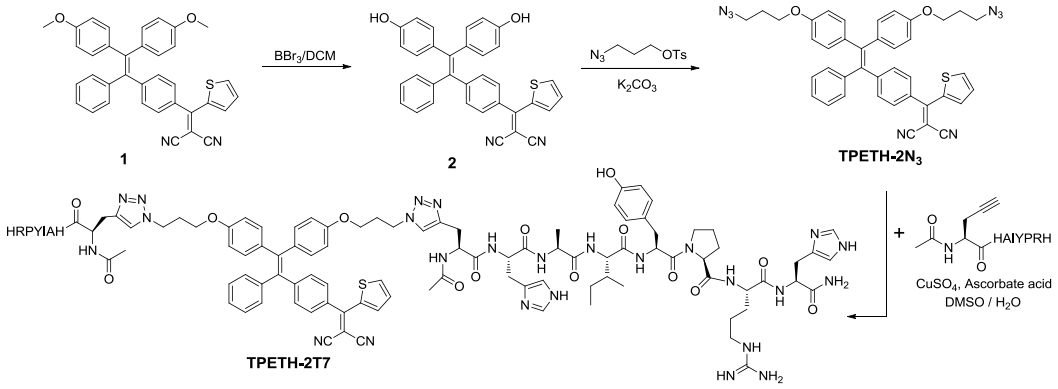

Scheme 4.1 The synthetic routes to AIEgen TPETH-$2N_3$ and the probe TPETH-2T7. Reprinted with permission from Ref 144.[144] Copyright 2016 American Chemical Society.

4.3.2 Optical properties and titration experiments

The UV-vis absorption and photoluminescence (PL) spectra of TPETH-$2N_3$ and TPETH-2T7 were measured in the mixture of dimethyl sulfoxide (DMSO)/H_2O (v/v = 1/99) and the results are shown in **Figure 4.1A**. TPETH-$2N_3$ has two absorption peaks at 360 nm and 430 nm. The first is attributed to TPE and the

second is due to intramolecular charge transfer (ICT) transition induced by the thiophene substituted dicyanovinyl group. As expected, TPETH-2N_3 (10 μM) emits strong red fluorescence with an emission maximum at 635 nm. The hydrophobic TPETH-2N_3 formed aggregates in aqueous media and the laser light scattering (LLS) results showed that they had an effective diameter of 104 ± 10 nm (**Figure S4.6**). In comparison, no LLS signal was collected for TPETH-2T7, suggesting that the probe was dissolved as molecular species in aqueous solution. The AIE characteristics of TPETH-2N_3 were investigated by measuring its PL spectra in the mixture of DMSO and water with different fractions. TPETH-2N_3 is almost non-emissive in pure DMSO when water fraction is 0%, which becomes brighter with increasing water fraction beyond 20%. The fluorescence intensity reaches a maximum when there is 70% water in the DMSO/water mixture (**Figures 4.1B** and **S4.7**). In addition, as shown in **Figure 4.1C**, the emission maxima shift from 600 to 635 nm when water fractions vary from 30% to 100%, which is attributed to the effect of polar solvent on the intramolecular charge transfer characteristics of TPETH-2N_3. In comparison, TPETH-2T7 shows faint fluorescence at the same concentration in aqueous media, which is desirable for light-up sensing of TfR.

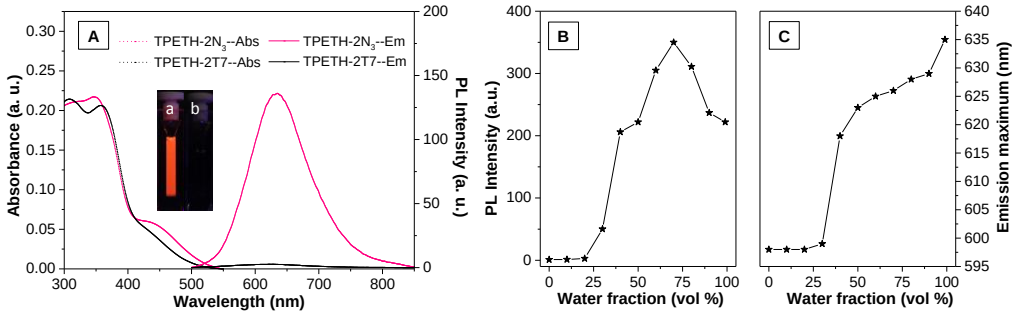

Figure 4.1 (A) UV-vis absorption and photoluminescence (PL) spectra of TPETH-2N_3 (red) and TPETH-2T7 (black) in DMSO/PBS buffer (v/v = 1/99); (B) plots of

emission peak intensities and (C) emission maxima of TPETH-2N_3 in DMSO/H_2O mixture with increasing water fractions. λ_{ex} = 430 nm, [TPETH-2N_3] = [TPETH-2T7] = 10 μM. Reprinted with permission from Ref 144.[144] Copyright 2014 American Chemical Society.

Light-up TfR detection and photodynamic activity

The potential of TPETH-2T7 for light-up sensing of TfR and its photodynamic activity were subsequently investigated in DMSO/PBS (v/v = 1/99) buffer. **Figure 4.2A** shows that 10 μM TPETH-2T7 only faintly fluoresces in the DMSO/PBS buffer mixture. It lights up gradually in the presence of increasing amount of TfR. The PL intensities at 635 nm against the TfR concentrations are plotted in **Figure 4.2B**, showing a linear trend in the range of 0-100 μg/mL with a R^2 = 0.98. The detection limit was calculated to be 0.45 μg/mL by (3σ/k), where σ and k represent the standard deviation of the blank sample and the slope of fluorescence intensity over TfR concentration, respectively. The highly sensitive fluorescence turn-on upon TfR recognition is due to the formation of probe/TfR complex, which leads to restriction of intramolecular motions.

The selectivity of TPETH-2T7 to TfR was confirmed by incubation of the probe with other proteins such as pepsin, BSA, lysozyme, which have isoelectric point (pI) values of 2.9, 4.8 and 11.35, respectively. Transferrin (Tf) is also studied because the endogenous Tf practically exists and might affect the formation of T7/TfR complex through binding with TfR. As shown in **Figure 4.2C**, only TfR can induce prominent fluorescence enhancement, proving that the complexation between TPETH-2T7 and TfR is highly specific. Moreover, the presence of Tf does not affect the binding of the probe to TfR, as the fluorescent signal is similar to that

in the presence of TfR alone. The time-dependent PL change of the probe in the presence of TfR was examined and the results show that the probe fluorescence is enhanced quickly within the first 10 min of incubation (**Figure S4.9**). The quick response, high selectivity and sensitivity endow the probe with great potential for real-time cellular imaging.

The photodynamic activity of the probe was subsequently evaluated with a chemical method using ABDA as the indicator. Exposure to $^1O_2$ will induce consumption of ABDA to result in its absorbance decrease. The probe was first incubated with TfR for 20 min. The ABDA stock solution in DMSO was subsequently added into the mixture and exposed to white light irradiation at 250 mW/cm^2. **Figures 4.2D** and **S4.10A** show that the absorbance of ABDA decreases significantly upon exposure to white light for 0 to 120 seconds. The $^1O_2$ quantum yield of TfR/TPETH-2T7 complex was calculated to be 0.92 using Rose Bengal (RB) as the standard PS, indicating the photodynamic activity of the probe is very high (**Figure S4.10**).

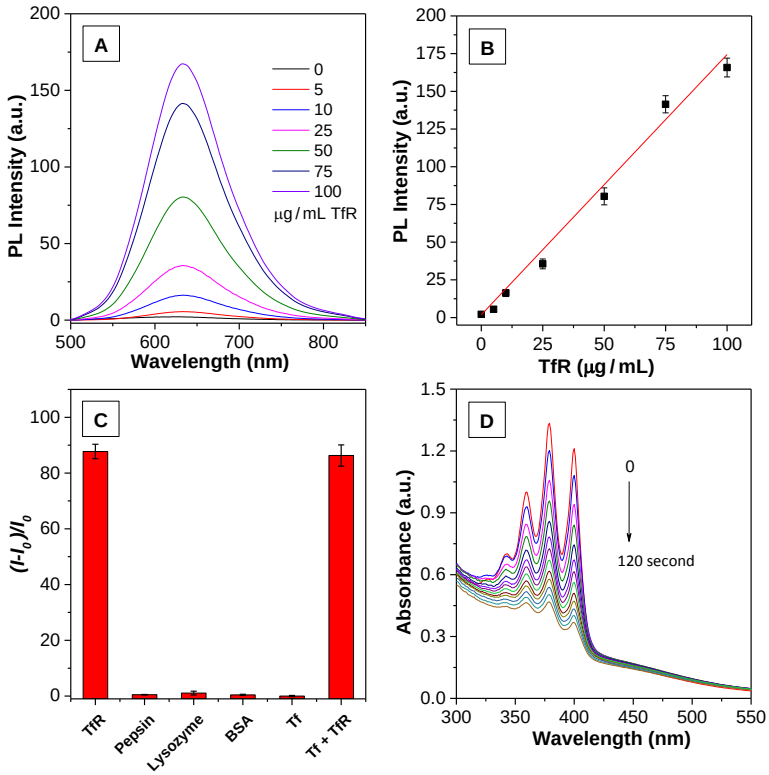

Figure 4.2 (A) Photoluminescence (PL) spectra of TPETH-2T7 upon addition of increasing amount of TfR at the concentrations of 0, 5, 10, 25, 50, 75 and 100 μg/mL in DMSO/PBS buffer (v/v = 1/99). (B) Plots of PL intensity at 635 nm of TPETH-2T7 against increasing concentration of TfR. (C) PL intensity enhancement upon incubation with TfR and other proteins including pepsin, lysozyme, BSA, transferrin (Tf) and the mixture of Tf and TfR [protein] = 100 μg/mL. (D) UV-vis spectra of 100 μM ABDA (for monitoring of $^1O_2$ generation) mixed with 10 μM TPETH-2T7 with different exposure time to white light irradiation (400-800 nm). [TPETH-2T7] = 10 μM, error bars represent standard deviation, n = 3. Reprinted with permission from Ref 144.[144] Copyright 2016 American Chemical Society.

4.3.3 Cell experiments

Targeted-bioimaging and photodynamic therapy

To study the potential of TPETH-2T7 for light-up detection of TfR *in vitro*, the probe was incubated with MDA-MB-231 breast cancer cells as a TfR-positive model and NIH 3T3 cells as a negative control with a low TfR-expression level. Confocal laser scanning microscopy (CLSM) images of MDA-MB-231 and NIH

3T3 cells were taken after incubation of the probe with live cells for 0.5 h and the images are shown in **Figure 4.3**. As can be seen, NIH 3T3 cells only show very weak fluorescence. In sharp contrast, strong fluorescence is collected from MDA-MB-231 cell membrane, indicating that the probe is able to differentiate TfR-overexpressed cancer cells from normal ones. In addition, a commercial fluorescent Tf-Alexa Fluor® 488 conjugate was applied to MDA-MB-231 cells under the same condition. The excellent overlap between the probe and the TfR tracker manifests that the specific binding occurs between TPETH-2T7 and TfR, corroborating that the probe can be used for light-up sensing of TfR.

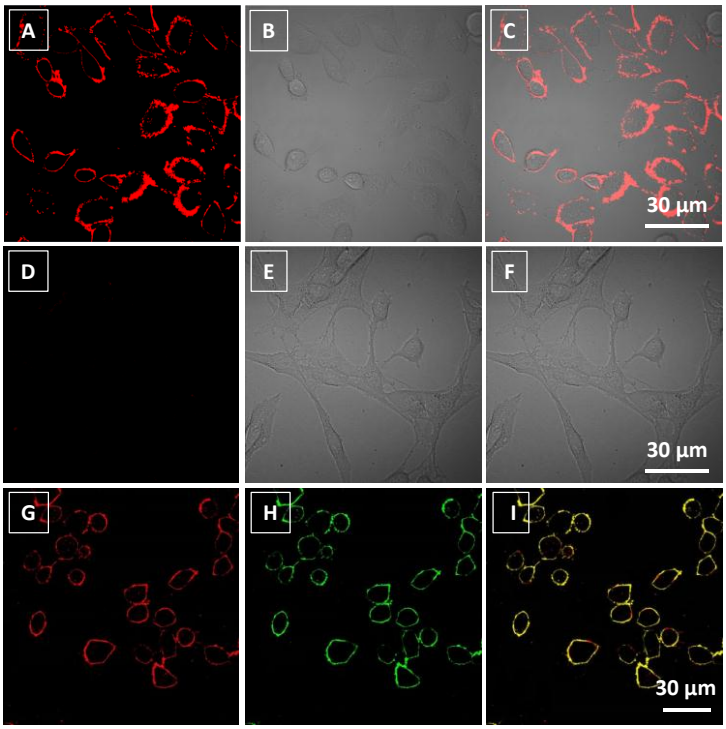

Figure 4.3 CLSM images of the probe TPETH-2T7 (10 µM) incubated with (A-C, G-I) MDA-MB-231 and (D-F) NIH 3T3 cells for 0.5 h. CLSM images of MDA-MB-231 cells stained by (G) TPETH-2T7 and (H) Tf-Alexa Fluor® 488 conjugate and (I) their overlay image. The images were taken with excitations at (A, D, G) 405 nm and (H) 488 nm using optical filters with band passes of (A, D, G) above 560 nm and (H) 505-525 nm. Reprinted with permission from Ref 144.[144] Copyright 2016 American Chemical Society.

Good discrimination ability of the probe to cancer cells against normal cells is highly desirable for effective photodynamic therapy. In addition, ideal PSs should exert high toxicity upon light irradiation but remain silent in the dark to maximize the therapeutic performance and minimize the side effect. To evaluate the potential of the probe for targeted-photodynamic killing of cancer cells, the phototoxicity and dark toxicity of TPETH-2T7 were investigated by standard MTT assay using MDA-MB-231 and NIH 3T3 cells as models for TfR-overexpressed and normal cells, respectively. The absorbance of formazan solutions was recorded and normalized to those of untreated cells. The probe was first incubated for 0.5 h with both cell lines in dark. The cell viability was subsequently determined with or without light irradiation. Quantitative data show that TPETH-2T7 exerts no evident toxicity to MDA-MB-231 and NIH 3T3 cells in dark even when the probe concentration is up to 100 nM (**Figure 4.4A**). In contrast, upon light irradiation, the probe shows a concentration-dependent cytotoxicity when incubated with MDA-MB-231 cells as shown in **Figure 4.4B**. The half-maximal inhibitory concentration (IC_{50}) to MDA-MB-231 cells is about 9.5 μM while only very limited toxicity is observed for NIH-3T3 cells. The results indicate that the probe remain biocompatible in the dark and can exert severe toxicity to MDA-MB-231 cells upon light irradiation but show very limited phototoxicity to NIH 3T3 cells.

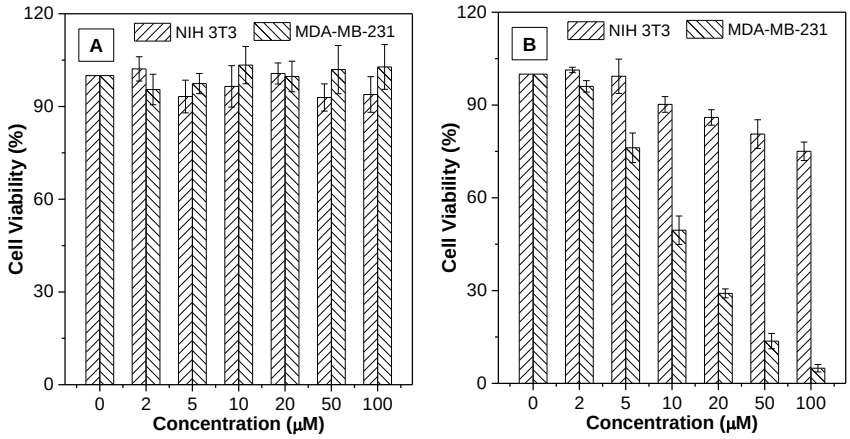

Figure 4.4 Viability of NIH 3T3 and MDA-MB-231 cells pre-incubated with TPETH-2T7 (A) in the dark or (B) with white light irradiation (400-800 nm) for 5 min at the power density of 100 mW/cm^{-2}. Reprinted with permission from Ref 144.[144] Copyright 2016 American Chemical Society.

Subcellular site-dependent response

The above results show the usefulness of TPETH-2T7 as a TfR-targeted probe for cancer cell imaging and therapy. TfR is not only accessible on the cell surface but can also be internalized into cell cytoplasm by endocytosis pathway, which makes TfR as an important delivery vector for therapeutic reagents. To investigate the therapeutic performance of the probe at different subcellular locations, TPETH-2T7 was incubated with MDA-MB-231 cells under different conditions and the cell viability was also monitored.

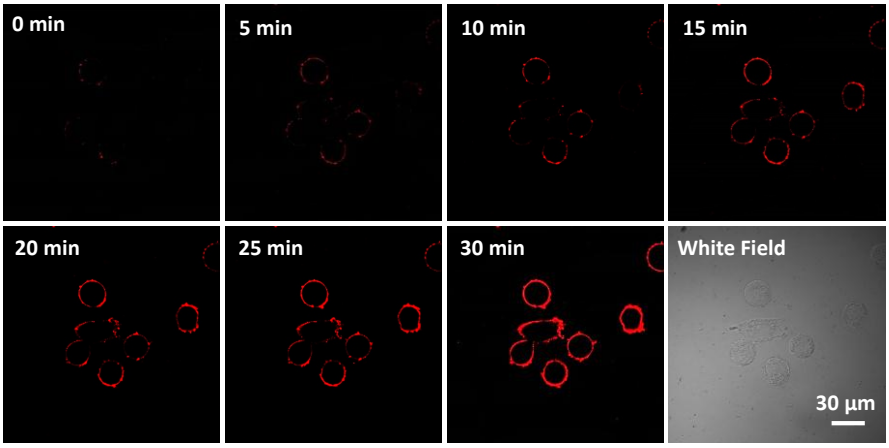

Figure 4.5 Real-time light-up monitoring of TfR on MDA-MB-231 cell membrane with incubation time for 0 to 30 min. [TPETH-2T7] = 10 μM, incubation time = 30 min. Reprinted with permission from Ref 144.[144] Copyright 2016 American Chemical Society.

First, MDA-MB-231 cells were incubated with TPETH-2T7 and CLSM images were taken with different incubation time. **Figure 4.5** shows that as the incubation time elapses, the probe gradually turns on its red fluorescence, which outlines the cell membrane within 10-15 min and reaches a maximum at 30 min. The dark background signal and good light-up behavior with increasing incubation time validate the usefulness of TPETH-2T7 as a promising tool for studying the probe interaction with TfR and tracking of TfR in a real-time manner. The same procedure was also applied to another batch of MDA-MB-231 cells with probe stain for 30 min, which was followed by removal of the free probe and further incubation for another 4 hours to investigate the internalization of the probe. The CLSM images in **Figure S4.11** show that the red fluorescence from the probe is mainly localized around nuclei using Hoechst 33342 as cell nuclei stain, indicating the occurrence of cellular internalization. In the following experiments, the probe TPETH-2T7 was controlled to stay on the cell membrane or in cytoplasm and the PDT effect under the two circumstances were investigated.

The PDT performance of the probe on the cell membrane and in cytoplasm was subsequently studied. White light irradiation was exposed to MDA-MB-231 cells when the probe is located on the cell membrane and in cytoplasm, respectively, and the PDT efficacy was evaluated by cell viability. **Figure 4.6A** shows that the PDT effect is more profound when TfR/probe complex is located on the cell membrane rather than in cytoplasm. The rationale behind this interesting phenomenon is revealed by CLSM image shown in (**Figure 4.6B**). Before light irradiation, the probe is localized on the cell membrane. After 5-min light irradiation, multiple protuberances (arrows in **Figure 4.6B (c))** appear on the membrane of MDA-MB-231 cells. The dramatic morphology changes provide direct evidence of cytomembrane damage. In contrast, when TPETH-2T7 was localized in cytoplasm and exposed to white light for the same period of time, no obvious change was observed. The results emphasize the importance of activation sites of PSs and the membrane disruption in cancer cells ablation.[182, 183] In contrast, after TfR/probe complexes were uptaken into the cells, more exposure time is needed to achieve the same toxic effects. These results show that the optimal activation site for TfR-targeted PDT is on the cytomembrane rather than in cytoplasm.

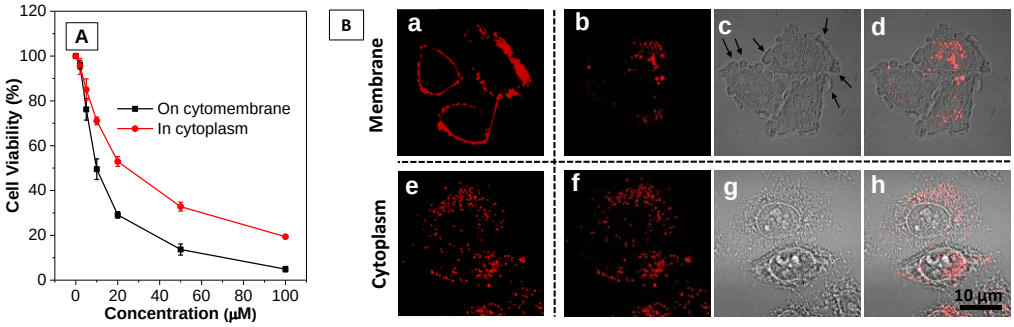

Figure 4.6 (A) Viabilities of MDA-MB-231 cells upon exposure to white light irradiation for 5.0 min when the probe is on cytomembrane (red) or in the cytoplasm (black); (B) CLSM images showing the white light induced cell morphology changes when the probe localized on cytomembrane (a-d) or in the cytoplasm (e-f) after 5 min light irradiation. (a) and (e): before light irradiation; (b) and (f): after light irradiation; (c) and (g) are the bright field images of (b) and (f), respectively. (d) and (h) are the overlay images for (b) and (f) with their respective bright field. Reprinted with permission from Ref 144.[144] Copyright 2016 American Chemical Society.

4.4 Conclusion

In summary, a new probe of TPETH-2T7 with aggregation-induced emission characteristics is designed and synthesized by conjugation of an AIE PS TPETH and a TfR-targeting peptide T7. The probe turns on its red fluorescence upon specific binding with TfR to restrict the intramolecular motion (RIM) within TPETH. A linear trend in PL intensity against TfR concentration ranging from 0-100 μg/mL is obtained with a detection limit of 0.45 μg/mL. Cellular experiments show that the probe can discriminate TfR-overexpressed cancer cells against normal cells with a high contrast. As compared to other existing TfR detection probes, the unique fluorescence turn-on response of our probe makes it possible to study the probe interaction with TfR and tracking of TfR in a real-time manner. When the probe was applied for image-guided photodynamic cancer cell ablation, it was found that the PDT performance was superior when the probe was localized

on the cell membrane than that in cytoplasm. This study thus represents a good example of optimizing subcellular locations for receptor-targeted PDT activation.

CHAPTER 5. FRET Probe with AIEgen as the Energy Quencher: Dual Signal Turn-on for Self-Validated Caspase Detection

5.1 Introduction

Fluorescent probes have attracted increasing attention in biomedical research due to their high sensitivity, good selectivity, non-invasiveness and the capability of real-time detection.[84, 184, 185] Fluorescence turn-on probes are superior to turn-off probes due to their lower background signal and higher signal output.[186] Fluorescence resonance energy transfer (FRET) is one of the most widely exploited mechanisms for the design of fluorescence turn-on probes, which have been successfully utilized in sensing, imaging, environmental monitoring, and medical diagnosis.[187] Two strategies have been generally utilized to design FRET probes. One is to conjugate a fluorescent dye with a quencher (donor-quencher model) and the other is to link two fluorescent dyes which can form the donor-acceptor pair (donor-acceptor model).[188] Once these FRET probes are exposed to the analytes, the seperation between the donor and quencher/acceptor leads to readable signals. While the donor-quencher model exhibits single fluorescent signal output, the donor-acceptor model shows donor fluorescence turn-on at the expense of the acceptor emission. The single fluorescent signal turn-on can only provide limited information, which is sometimes insufficient for accurate detection.[189] Recently, several “always on” probes with different image modalities have been developed for self-validated bioimaging in order to provide more accurate results.[189] Up to

now, a variety of biological probes based on fluorescence imaging, magnetic resonance imaging (MRI), positron emission tomography (PET) and photoacoustic imaging have been actively explored to offer dual signal output in one study. [190, 191, 192, 193, 194, 195] However, single fluorescence turn-on probes with a dual signal output upon encountering a specific analyte have not been reported yet. It is thus of great interest to develop a single fluorescent probes with dual signal turn-on at different emission wavelengths for self-validated sensing and imaging, which remains challenging.

In Recent years, fluorogens with aggregation-induced emission characteristics (AIEgens) have attracted considerable attention in biosensing and bioimaging.[49, 50, 52, 55, 80, 96, 110, 196, 197, 198, 199, 200] Opposite to the traditional fluorophores that show a notorious phenomenon known as aggregation caused quenching (ACQ),[201] AIEgens are non-emissive in molecularly dissolved state but can be induced to emit strongly in aggregates due to the restriction of intramolecular rotations (RIR) and prohibition of energy dissipation *via* non-radiative channels.[37] Based on this unique property, several fluorescence turn-on probes have been developed for detection and imaging of various analytes.[55] These probes are generally based on AIEgens conjugated to hydrophilic recognition elements. When the AIE probes are well-dissolved in aqueous media, the background fluorescence is very low. Upon specific analyte recognition, the probes are cleaved to release the hydrophobic AIEgens and yield bright fluorescence. As compared to traditional FRET probes which require dual labelling to realize fluorescence turn-on, these singly labelled AIE probes show high simplicity, which makes them very useful in

the development of multifunctional probes for monitoring of multiple processes in one go.[55] These successful examples have motivated us to explore whether the energy dissipation of AIEgens could affect other fluorophores conjugated to the probe. In this case, it would offer a new generation of energy quenchers, which is able to fluorescence once it is separated from the energy donor and offers for the first time a dual signal turn-on probe for self-validated biosensing and bioimaging.

As a proof of concept, in this contribution, we report a fluorescent probe based on coumarin (Cou) as energy donor and an AIEgen as the energy quencher conjugated *via* an Asp-Glu-Val-Asp (DEVD) substrate for caspase-3 detection (**Scheme 5.1**).[170, 202, 203, 204, 205] The probe itself is non-fluorescent due to the energy transfer and dissipation of the acceptor energy through free motion of AIEgens. Upon addition of caspase-3, it displays strong green fluorescence of Cou due to the separation of donor-acceptor and intense red fluorescence of AIEgen due to the aggregation of the released AIEgen residue. This dual fluorescent signal turn-on can be used for caspase-3 detection both in solution and in cells, which opens new avenues for the development of next generation self-validated FRET probes with high signal-to-background ratio and fluorescence amplification.

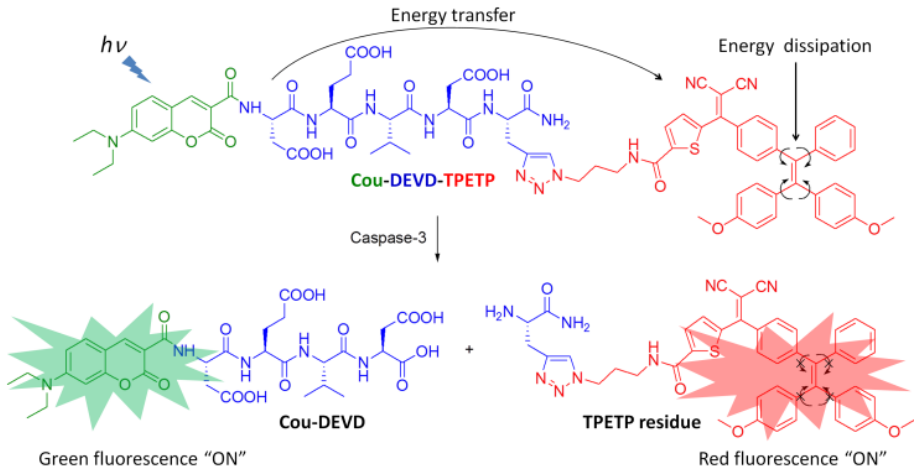

Scheme 5.1 Schematic illustration of the FRET probe using AIEgen as energy quencher with dual signal output for self-validated caspase-3 detection. Reprinted with permission from Ref 206 [206] under a Creative Commons Attribution 3.0 Unported Licence.

5.2 Experimental Section

5.2.1 General Information

Cisplatin, doxorubicin (DOX), trifluoroacetic acid (TFA), 7-(diethylamino)coumarin-3-carboxylic acid *N*-succinimidyl ester (Cou-NHS), *N*-(3-dimethylaminopropyl)-*N*′-ethylcarbodiimide hydrochloride (EDC), *N*-hydroxysuccinimide (NHS), *N*, *N*-diisopropylethylamine (DIPEA), triethylamine (TEA), *N,N,N′,N′*-tetramethyl-*O*-(1*H*-benzotriazol-1-yl)uronium hexafluorophosphate, *O*-(benzotriazol-1-yl)-*N,N,N′,N′*-tetramethyluronium hexafluorophosphate (HBTU), copper(II) sulfate ($CuSO_4$), sodium ascorbate, anhydrous dimethyl sulfoxide (DMSO), anhydrous *N*, *N*-Dimethylformamide (DMF), 3-(4,5-dimethylthiazol-2-yl)-2,5-diphenyltetrazolium bromide (MTT) and other chemicals were all purchased from Sigma-Aldrich or Alfa Aesar and used as received without further purification. Tetrahydrofuran (THF) and dichloromethane

were dried by distillation using sodium as drying agent and benzophenone as indicator. All non-aqueous reactions were carried out under nitrogen atmosphere in oven-dried glassware. Deuterated solvents with tetramethylsilane (TMS) as internal reference were purchased from Cambridge Isotope Laboratories Inc.. Alkyne-functionalized DEVD (Asp-Glu-Val-Asp) peptide was purchased from GL Biochem Ltd (Shanghai).

Dulbecco's Modified Essential Medium (DMEM) is a commercial product of Invitrogen. Milli-Q water was supplied by Milli-Q Plus System (Millipore Corporation, United States). Phosphate-buffer saline (PBS, 10×) buffer with pH = 7.4 is a commercial product of 1st BASE (Singapore). Milli-Q water (18.2 MΩ) was used to prepare the buffer solutions from the 10× PBS stock buffer. 1× PBS contains NaCl (137 mM), KCl (2.7 mM), Na_2HPO_4 (10 mM), and KH_2PO_4 (1.8 mM). Recombinant human caspase-3 was purchased from R&D Systems. Caspase-3/-7 inhibitor 5-[(*S*)-(+)-2-(methoxymethyl)pyrrolidino]sulfonylisatin was purchased from Calbiochem. Staurosporine (STS) was purchased from Biovision. Cleaved caspase-3 (Asp175) (5A1E) rabbit mAb (#9664) was purchased from Cell Signaling. Mouse anti-rabbit IgG-TR (sc-3917) was purchased from Santa Cruz. SYTO® orange, fetal bovine serum (FBS) and trypsin-EDTA solution were purchased from Life Technologies.

NMR spectra were measured on a Bruker ARX 300/400/500 NMR spectrometer. Chemical shifts are reported in parts per million referenced with respect to residual solvent ($CDCl_3$ = 7.26 ppm and $(CD_3)_2SO$ = 2.50 ppm) for ^1H

NMR and ($CDCl_3$ = 77.0 ppm and $(CD_3)_2SO$ = 40.0 ppm) for ^{13}C NMR. The extent of reaction was monitored by thin layer chromatography (TLC) using Merck 60 F254 pre-coated silica gel plates with fluorescent indicator UV254. After the plates were subjected to elution in the TLC chamber, the spots were visualized under UV light or using the appropriate stain (I_2, $KMnO_4$, ninhydrin or ceric ammonium molybdate (CAM)). Flash column chromatography was carried out using Merck silica gel (0.040-0.063). A 0.1% trifluoroacetic acid solution in H_2O and acetonitrile was used as the eluent for high-performance liquid chromatography (HPLC) experiments (Agilent). Mass spectra were recorded on Agilent 5975 DIP-MS for electron impact (EI) and the AmaZon X LC-MS for electrospray ionization (ESI). Particle size and size distribution were determined by laser light scattering (LLS) with a particle size analyzer (90 Plus, Brookhaven Instruments Co., United States) at a fixed angle of 90° at room temperature. TEM images were obtained from a JEOL JEM-2010 transmission electron microscope with an accelerating voltage of 200 kV. UV-vis absorption spectra were taken on a Shimadzu Model UV-1700 spectrometer. Photoluminescence (PL) spectra were measured on a Perkin-Elmer LS 55 spectrofluorometer. All UV and PL spectra were collected at 24 ± 1 °C.

5.2.2 Synthesis

Synthesis of 4,4'-(2-(4-Bromophenyl)-2-phenylethene-1,1-diyl)bis(methoxybenzene) (compound 1) To a solution of bis(4-methoxyphenyl)methanone (3.8 g, 16 mmol), (4-bromophenyl)(phenyl)methanone (5.3 g, 20 mmol) and zinc dust (5.9 g, 91 mmol) in dry THF (80 mL), $TiCl_4$ (5. 0

mL, 46 mmol) was added dropwise under Argon atmosphere at 0 ^{o}C. After addition was complete, the reaction was warm to room temperature and refluxed overnight. Then the reaction was quenched with saturated aqueous sodium bicarbonate (50 mL) and extracted with ethyl acetate (100 mL × 3). The combined extracts were washed with brine and dried over anhydrous magnesium sulphate. The solution was concentrated *in vacuo* and purified by column chromatography to give product **1** as a yellowish solid. (3.0 g, 40%). ^{1}H NMR (300 MHz, $CDCl_3$) δ 7.16 – 7.10 (m, 2H), 7.08 – 6.97 (m, 4H), 6.97 – 6.88 (m, 3H), 6.88 – 6.76 (m, 6H), 6.62 – 6.49 (m, 4H), 3.68 (s, 3H), 3.65 (d, *J* = 1.1 Hz, 3H); ^{13}C NMR (151 MHz, $CDCl_3$) δ 158.42, 158.34, 143.93, 143.45, 140.93, 136.16, 136.08, 133.19, 132.69, 132.66, 131.49, 130.99, 127.95, 126.45, 120.16, 113.35, 113.17, 55.27, 55.24.

Synthesis of N^2, N^5-dimethoxy-N^2,N^5-dimethylthiophene-2,5-dicarboxamide (compound 2) To a solution of thiophene-2,5-dicarboxylic acid (4.4 g, 20 mmol) and *N*,*O*-dimethylhydroxylamine hydrochloride (7.8 g, 80 mmol) in DMF (10 mL) was added HBTU (23 g, 60 mmol) and TEA (17 mL) at 0 ^{o}C. After 1 hr, the reaction was allowed to warm to room temperature and stirred at room temperature overnight. After DMF was removed by distillation *in vacuo*, the residue was extracted with ethyl acetate (100 mL × 3). The combined extracts were washed with brine (100 mL) and dried over anhydrous magnesium sulphate. The solution was concentrated *in vacuo* to give residue which was purified by column chromatography to give product **2** as a white solid. (4.78 g, 92%). ^{1}H NMR (300 MHz, $CDCl_3$) δ 7.89 (s, 2H), 3.79 (s, 6H), 3.39 (s, 6H); ^{13}C NMR (75 MHz, $CDCl_3$) δ 161.85, 138.38, 133.18, 61.61, 33.03.

Synthesis of 5-(4-(2,2-bis(4-methoxyphenyl)-1-phenylvinyl)benzoyl)-*N*-methoxy-*N*-methylthiophene-2-carboxamide (compound 3) To a solution of compound **1** (1.7 g, 3.6 mmol) in dry THF (30 mL) was added butyllithium (1.6 M, 2.7 mL) at -78 ^{o}C. After the reaction was stirred at -78 ^{o}C for 1 hr, compound **2** (0.62 g, 2.4 mmol) in dry THF (9.0 mL) was added. Then the reaction was warmed to room temperature slowly and stirred at room temperature overnight. The reaction was quenched by aqueous ammonium chloride (50 mL) and extracted with ethyl acetate (60 mL × 3). The combined extracts were washed with brine and dried over anhydrous magnesium sulphate. After volatiles was removed *in vacuo*, the resulted residue was purified by column chromatography to give the product **3** as a yellow solid. (0.66 g, 31%). ^{1}H NMR (400 MHz, $CDCl_3$) δ 7.93 (d, *J* = 4.1 Hz, 1H), 7.64 (d, *J* = 8.3 Hz, 2H), 7.54 (d, *J* = 4.0 Hz, 1H), 7.21 – 7.08 (m, 5H), 7.03 (dd, *J* = 7.6, 2.0 Hz, 2H), 6.98 – 6.89 (m, 4H), 6.72 – 6.57 (m, 4H), 3.82 (s, 3H), 3.74 (d, *J* = 3.5 Hz, 6H), 3.40 (s, 3H); ^{13}C NMR (101 MHz, $CDCl_3$) δ 188.37, 161.47, 158.64, 158.47, 149.63, 147.94, 143.70, 142.17, 138.78, 138.10, 135.85, 135.80, 134.93, 134.50, 132.91, 132.77, 132.69, 131.61, 131.49, 129.07, 128.03, 126.57, 113.35, 113.16, 61.96, 55.22, 55.20, 33.15. LRMS (ESI): m/z = 590.21 [M+H^{+}], calc for ($C_{36}H_{32}NO_5S$): m/z = 590.20; HRMS (ESI): m/z = 612.1813 [M+Na^{+}], calc for ($C_{36}H_{31}NNaO_5S$): m/z = 612.1815.

Synthesis of 5-(4-(2,2-bis(4-methoxyphenyl)-1-phenylvinyl)benzoyl)thiophene-2-carboxylic acid (compound 4) To a solution of compound **6** (95 mg, 0.16 mmol) in methanol-water (3:1, 50 mL) was added sodium hydroxide (32 mg, 0.81 mmol). Then the reaction was stirred at room

temperature overnight. After removal of methanol, the reaction mixture was acidified by 1 *N* HCl to pH 2~3. The mixture was extracted with dichloromethane (10 mL × 3). The combined solution was dried over anhydrous magnesium sulphate and concentrated *in vacuo* to give a residue which was purified by column chromatography to give product **4** as a yellow oil. (72 mg, 82%). ^{1}H NMR (300 MHz, $CDCl_3$) δ 8.30 (s, 1H), 7.85 (d, *J* = 4.0 Hz, 1H), 7.66 (d, *J* = 8.1 Hz, 2H), 7.59 (d, *J* = 4.0 Hz, 1H), 7.23 – 7.12 (m, 5H), 7.09 – 7.02 (m, 2H), 6.96 (d, *J* = 8.3 Hz, 4H), 6.69-6.64 (m, 4H), 3.75 (d, *J* = 3.6 Hz, 6H); ^{13}C NMR (75 MHz, $CDCl_3$) δ 187.33, 166.12, 158.48, 158.29, 149.85, 149.09, 143.47, 142.16, 137.83, 135.63, 135.56, 134.26, 134.19, 133.47, 132.61, 132.54, 131.54, 131.32, 128.97, 127.89, 126.44, 113.21, 113.00, 55.07, 55.03. LRMS (ESI): m/z = 545.03 [M-H$^+$], calc for ($C_{34}H_{25}O_5S$): m/z = 545.14; HRMS (ESI): m/z = 545.1434 [M-H$^+$], calc for ($C_{34}H_{25}O_5S$): m/z = 545.1428.

Synthesis of *N*-(3-azidopropyl)-5-(4-(2,2-bis(4-methoxyphenyl)-1-phenylvinyl)benzoyl)thiophene-2-carboxamide (compound 5) To a stirring solution of compound **4** (72 mg, 0.13 mmol) and HBTU (76 mg, 0.20 mmol) in DMF (3. 0 mL) was added 3-azidopropan-1-amine (26 mg, 0.26 mmol) and triethylamine (55 µL, 0. 40 mmol) at room temperature. The reaction was stirred at room temperature overnight. After the reaction was complete, DMF was removed *in vacuo*. The residue was dissolved in dichloromethane (10 mL) and washed with water (5 mL) and brine (5 mL). The organic layer was dried over anhydrous magnesium sulphate and concentrated *in vacuo* to give a residue which was purified by column chromatography to give the product **5** as a yellow oil. (70 mg, 84%). ^{1}H

NMR (400 MHz, $CDCl_3$) δ 7.63 (d, *J* = 8.1 Hz, 2H), 7.55 (s, 1H), 7.53 (s, 1H), 7.16 (m, 5H), 7.06 – 7.00 (m, 2H), 6.96-6.93 (m, 4H), 6.69 – 6.54 (m, 4H), 6.42-6.39 (m, 1H), 3.75 (s, 6H), 3.55 (q, *J* = 6.3 Hz, 2H), 3.46 (t, *J* = 6.3 Hz, 2H), 1.94-1.89 (m, 2H); ^{13}C NMR (151 MHz, $CDCl_3$) δ 187.48, 161.40, 158.69, 158.53, 149.83, 146.24, 144.68, 143.72, 142.28, 138.08, 135.86, 135.80, 134.70, 133.93, 132.81, 132.73, 131.70, 131.52, 129.07, 128.72, 128.08, 126.62, 113.41, 113.20, 55.29, 55.25, 49.74, 38.22, 28.79; LRMS (ESI): m/z = 628.9 [$M+H^+$], calc for ($C_{37}H_{32}N_4O_4S$): m/z = 629.2; HRMS (ESI): m/z = 651.2051 [$M+Na^+$], calc for ($C_{37}H_{32}N_4NaO_4S$): m/z = 651.2036.

Synthesis of *N*-(3-azidopropyl)-5-(1-(4-(2,2-bis(4-methoxyphenyl)-1-phenylvinyl)phenyl)-2,2-dicyanovinyl)thiophene-2-carboxamide (TPETP-N_3) To a solution of compound **5** (70 mg, 0.11 mmol) and malononitrile (9.6 mg, 0.14 mmol) in dry dichloromethane (2 mL) at 0 ºC. After 30 min of stirring at 0 ºC, pyridine (31 µL, 0.39 mmol) was added and stirred for another 30 min at 0 ºC. Then the mixture was heated to 40 ºC for 4 hrs. The reaction was cooled to room temperature and quenched with water and extracted with dichloromethane (5 mL × 3). The combined extracts were dried over anhydrous magnesium sulphate. The solution was concentrated *in vacuo* to give residue which was purified by column chromatography to give product **TPETP-N_3** (*N*-(3-azidopropyl)-5-(1-(4-(2,2-bis(4-methoxyphenyl)-1-phenylvinyl)phenyl)-2,2-dicyanovinyl)thiophene-2-carboxamide) as a red solid. (65 mg, 88%). ^1H NMR (300 MHz, $CDCl_3$) δ 7.79 (d, *J* = 4.0 Hz, 1H), 7.52 (d, *J* = 4.2 Hz, 1H), 7.22 – 7.11 (m, 7H), 7.06 (dd, *J* = 7.5, 2.1 Hz, 2H), 7.00 – 6.89 (m, 4H), 6.77 – 6.59 (m, 4H), 6.40 (s, 1H), 3.75 (s, 6H),

3.55 (q, *J* = 6.4 Hz, 2H), 3.46 (t, *J* = 6.3 Hz, 2H), 1.99 – 1.82 (m, 2H); ^{13}C NMR (75 MHz, $CDCl_3$) δ 164.22, 160.50, 158.65, 158.45, 149.43, 146.85, 143.08, 142.71, 141.73, 137.60, 135.41, 135.05, 132.85, 132.72, 132.59, 131.71, 131.36, 129.25, 128.50, 128.04, 126.59, 114.11, 113.39, 113.30, 113.07, 55.21, 55.10, 49.58, 38.19, 28.56; LRMS (ESI): m/z = 699.2 [M+Na^+], calc for ($C_{40}H_{32}N_6NaO_3S$): m/z = 699.2; HRMS (ESI): m/z = 699.2163 [M-H^+], calc for ($C_{40}H_{32}N_6NaO_3S$): m/z = 699.2149.

Synthesis of TPETP-DEVD. TPETP-N$_3$ (5 mg, 7.38 μmol) and DEVD-alkyne (5.04 mg, 8.83 μmol) were firstly dissolved in DMSO/H_2O (v/v = 10:1) and mixed thoroughly. Into the mixture, sodium ascorbate (0.6 mg, 3.0 μmol) and copper sulphate (0.8 mg, 1.5 μmol) were added to initiate the click reaction and the mixture was shaken at room temperature for another 24 h. The product TPETP-DEVD was purified by prep-HPLC and further characterized by ^{1}H NMR and HRMS. ^{1}H NMR (400 MHz, DMSO-*d*$_6$), δ (TMS, ppm): 8.88 (t, *J* = 4.0 Hz, 1H), 8.52 (d, *J* = 8.0 Hz, 1H), 8.24 (d, *J* = 8.0 Hz, 1H), 7.96 (d, *J* = 8.0 Hz, 1H), 7.83 (d, *J* = 8.0 Hz, 1H), 7.80 (d, *J* = 4.0 Hz, 1H), 7.74 (s, 1H), 7.62 (d, *J* = 4.0 Hz, 1H), 7.30 (d, *J* = 8.0 Hz, 2H), 7.15-7.11 (m, 3H), 7.07-7.04 (m, 4H), 6.98 (d, *J* = 8.0 Hz, 2H), 6.85 (d, *J* = 8.0 Hz, 2H), 6.79 (d, *J* = 8.0 Hz, 2H), 6.66 (t, *J* = 8.0 Hz, 4H), 4.48 (t, *J* = 8.0 Hz, 1H), 4.36-4.27 (m, 4H), 4.09-4.05 (t, *J* = 8.0 Hz, 2H), 3.62 (d, *J* = 4.0 Hz, 6H, overlap with DMSO-*d*$_6$), 3.23-3.18 (m, 2H), 3.03-2.98 (dd, *J* = 4.0 Hz, 1H), 2.88-2.82 (m, 1H), 2.78-2.72 (m, 1H), 2.66-2.55 (m, 2H), 2.5 (m, 2H, overlap with DMSO-*d*$_6$), 2.26-2.13 (m, 2H), 2.03-1.96 (m, 2H), 1.89-1.82 (m, 2H), 1.71-1.65 (m, 1H), 0.76-0.70 (m, 6H). HRMS (ESI-MS): m/2z [M-2H]$^{2-}$ calcd for $C_{63}H_{67}N_{12}O_{14}S$: 622.2198; found: 622.2204.

Synthesis of Cou-DEVD-TPETP. TPETP-DEVD (4 mg, 2.68 μmol) was firstly dissolved in 500 μL dry DMSO and mixed with DIPEA (1 μL), then Cou-NHS (1.2 mg, 3.22 μmol) was added into the mixture and the reaction was continued for another 24 h. The product was purified by prep-HPLC to yield Cou-DEVD-TPETP as orange powder in 52% yield, which was further characterized by ^{1}H NMR and HRMS. ^{1}H NMR (400 MHz, DMSO-d_6), δ (TMS, ppm): 9.11 (d, J = 8.0 Hz, 1H), 8.85 (m, 1H), 8.57 (d, J = 4.0 Hz, 1H), 8.19-8.12 (dd, J = 8.0 Hz, 2H), 7.95 (d, J = 8.0 Hz, 1H), 7.78 (t, J = 8.0 Hz, 2H), 7.61 (m, J = 12.0 Hz, 3H), 7.29 (d, J = 8.0 Hz, 2H), 7.13-7.03 (m, 7H), 6.97-6.94 (d, J = 12.0 Hz, 2H), 6.84-6.72 (m, 5H), 6.65-6.56 (m, 5H), 4.72 (d, J = 4.0 Hz, 1H), 4.44 (d, J = 8.0 Hz, 1H), 4.29 (m, 4H), 4.02 (t, J = 8.0 Hz, 1H), 3.62-3.59 (m, 6H, overlap with DMSO-d_6), 3.2 (m, 3H), 3.04-2.99 (m, 1H), 2.88-2.8 (m, 1H), 2.65-2.60 (m, 3H), 2.48 (m, 4H, overlap with DMSO-d_6), 2.19-2.13 (m, 2H), 2.00-1.97 (m, 2H), 1.89-1.82 (m, 2H), 1.74-1.63 (m, 1H), 1.07-1.05 (t, J = 8.0 Hz, 6H), 0.71 (t, J = 8.0 Hz, 6H). HRMS (ESI-MS): m/z $[M+H]^+$ calcd for $C_{77}H_{80}N_{13}O_{17}S$: 1490.5510; found: 1490.5530.

5.2.3 Enzymatic assay

DMSO stock solutions of Cou-DEVD-TPETP were diluted with a mixture of DMSO and PBS (v/v = 1/99) to 10 μM. Next, the probe was incubated with caspase-3 at 37 °C and the change of fluorescence intensity of Cou and TPETP were measured. The PL spectra of Cou were collected from 425 to 570 nm under

excitation at 405 nm; The PL spectra of TPETP were collected from 570 to 820 nm under excitation at 405 nm.

5.2.4 Cell experiments

Cell Culture. Human cervix carcinoma HeLa cells and human breast cancer MDA-MB-231 cells were provided by American Type Culture Collection (ATCC). The cells were cultured in DMEM medium containing 100 μg mL^{-1} streptomycin, 10% heat-inactivated FBS, 100 U mL^{-1} penicillin, and maintained in a humidified incubator with 5% CO_2 at 37 °C.

Confocal Imaging. HeLa and MDA-MB-231 cells were cultured in 8-well chambers (Thermo Scientific) at 37 °C. After 80% confluence, the culture medium was removed and washed twice with 1× PBS. After incubation with the probe for 4 h at 37 °C, the cells were washed twice with 1× PBS buffer and treated with 1 μM apoptosis inducers (STS, cisplatin or DOX) for different time. The cells were then washed twice with 1× PBS and the cell nuclei were live stained with SYTO® orange, following the standard protocols of the manufacturer (Life Technologies) and imaged immediately by confocal microscope (CLSM, Zeiss LSM 410, Jena, Germany). For colocalization with active caspase-3 antibody, the cells were fixed with 3.7% formaldehyde in 1× PBS for 15 min at room temperature, washed twice with cold 1× PBS again, and permeabilized with 0.1% Triton X-100 in 1× PBS for 10 min. The cells were then blocked with 2% BSA in 1× PBS for 30 min and washed twice with 1× PBS. The cells were subsequently incubated with a mixture of anti-caspase-3 antibody/PBS (v/v = 1/99) for 1 h at room temperature, washed

once with 1× PBS buffer, and then incubated with mouse anti-rabbit IgG-TR (0.8 μg mL^{-1}) in 1× PBS for 1 h, followed by washing with 1× PBS. For SYTO® orange detection, the excitation wavelength was 543 nm and the emission filter was 610−640 nm; for Cou detection, the excitation wavelength was 405 nm, and the emission filter was 505−525 nm; for TPETP detection, the excitation was 405 nm and the emission was collected above 650 nm.

Flow Cytometry Study. HeLa and MDA-MB-231 cells in 24-well plate (Costar, IL, USA) were precultured overnight and incubated with the probe for the designated time and treated with 1 μM apoptosis inducers (STS, cisplatin or DOX) for different time. After incubation, the cells were washed with 1× PBS and treated with trypsin, washed with medium twice and subjected to flow cytometry analysis using Cyan-LX (DakoCytomation). The cells without any treatment were used as control. The mean fluorescence was determined by counting 10,000 events.

Cytotoxicity Studies. MTT assays were used to assess the cell viability of HeLa and MDA-MB-231 cells after incubation with the probe. The cells in 96-well plates (Costar, IL, USA) were incubated with the probe for designated time in the dark. The cells were further incubated in fresh medium for 48 h and washed with 1× PBS. Then MTT in 1× PBS solution (100 μL, 0.5 mg mL^{-1}) was added into each well. After incubation for 3 h, the supernatant was discarded and the precipitate was dissolved in DMSO (100 μL) with gentle shaking. The absorbance of MTT at 570 nm was monitored by the microplate reader (Genios Tecan). The cells without any treatment were used as control.

5.3 Results and Discussion

Recently, some AIEgens with red emission have been developed for bioimaging and tetraphenylethenethiophene (TPETP) was selected for this study.[72, 73, 142, 207] The synthetic route to the azide-functionalized TPETP (TPETP-N_3) and the probe Cou–DEVD–TPETP is shown in **Scheme 5.2.** Compound **1** was synthesized by McMurry reaction between bis(4-methoxyphenyl)methanone and (4-bromophenyl)(phenyl)methanone in the presence of $TiCl_4$ and Zn. Subsequently, compound **1** was reacted with compound **2** in the presence of butyllithium to yield compound **3.** The carboxyl group of compound **3** was deprotected by sodium hydroxide in a methanol–water mixture, which was further reacted with 3-azidopropan-1-amine to yield compound **5**. Compound **5** was further reacted with malononitrile on a SiO_2 support to produce azide-functionalized TPETP (TPETP-N_3). The "click" reaction between TPETP-N_3 and alkyne-functionalized DEVD catalyzed by copper(II) sulfate ($CuSO_4$) and sodium ascorbate (Na Asc) afforded amine terminated TPETP–DEVD, which was further reacted with 7-(diethylamino) coumarin-3-carboxylic acid N-succinimidyl ester (Cou-NHS) in the presence of *N*,*N*-diisopropylethylamine (DIPEA) to give Cou–DEVD–TPETP in a 52% yield after HPLC purification. Detailed characterization data are shown in **Figure S5.1-5.8** in **Appendix 4**. The AIE property of TPETP-N_3 was confirmed by studying its PL spectra in DMSO or DMSO/water mixtures (v/v = 1/99). As shown in **Figure S5.9A**, TPETP-N_3 is almost non-fluorescent in DMSO which should be due to the easy intramolecular rotations of the TPE phenyl rings in benign solvents.[49]

However, TPETP-N_3 in DMSO/water mixtures (v/v = 1/99) is highly fluorescent, which shows 110-fold brighter fluorescence than that in DMSO. The increase in fluorescence intensity is attributed to the aggregation of TPETP-N_3, which restricts the intramolecule motion when the water fraction is increased. The formation of TPETP-N_3 aggregates in aqueous media was also confirmed by laser light scattering (LLS) measurements and transmission electron microscopy (TEM) image (**Figures S5.9B** and **C**), while there is no LLS signal detected in DMSO solution. The absorption and emission spectra of Cou and TPETP-N_3 are shown in **Figure S5.10**. The emission of Cou and the absorption of TPETP-N_3 shows a perfect spectral overlap, indicating that they could form an energy transfer pair.

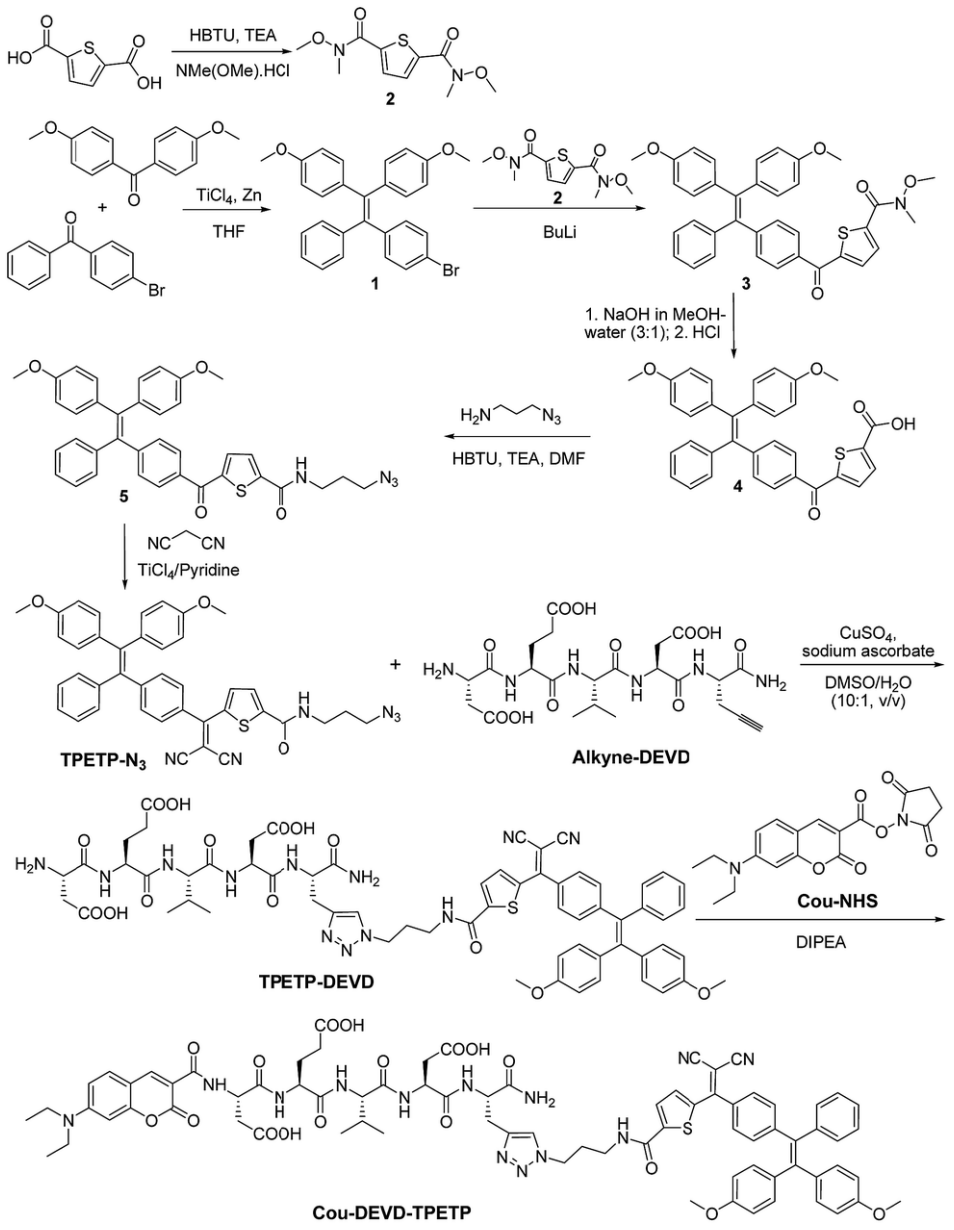

Scheme 5.2 Synthetic route to the probe Cou–DEVD–TPETP. HBTU: *O*-(benzotriazol-1-yl)-*N*,*N*,*N*′,*N*′-tetramethyluronium hexafluorophosphate; TEA: triethylamine; $TiCl_4$: titanium(IV) chloride; Zn: zinc; THF: tetrahydrofuran; BuLi: butyllithium; DMF: *N*,*N*-dimethylformamide; DIPEA: *N*,*N*-diisopropylethylamine; Cou-NHS: 7-(diethylamino)coumarin-3-carboxylic acid *N*-succinimidyl ester. Reprinted with permission from Ref 206 [206] under a Creative Commons Attribution 3.0 Unported Licence.

To validate the energy transfer between Cou and TPETP-N_3, the optical properties of Cou, TPETP-N_3 and Cou-DEVD-TPETP were studied in DMSO/PBS

buffer (v/v = 1/99). Cou and TPETP-N_3 have absorption maxima at 445 and 470 nm, with emission maxima at 465 and 665 nm, respectively (**Figure S5.10).** As both Cou and TPETP-N_3 show obvious absorption at 405 nm, it offers the possibility of dual signal collection upon a single wavelength excitation. As shown in **Figure 5.1A**, upon excitation at 405 nm, both Cou and TPETP-N_3 are highly fluorescent while Cou-DEVD-TPETP emits very weakly, which indicates that the probe has extremely low background signal as designed. The rationale behind the fluorescence quenching of Cou and TPETP parts in the probe is due to energy transfer from the former to the latter, and the dissipation of the AIEgen energy through free motion of the molecules. The fluorescence of the probe remains weak in aqueous media with different ionic strength or in cell culture medium (**Figure S5.11**). Upon addition of caspase-3, the cleavage of DEVD separates Cou-DEVD away from the proximity of TPETP. This leads to the recovering of the green fluorescence of Cou and synchronously allows the formation of TPETP residue aggregates with red fluorescence turn-on. As shown in **Figure 5.1B**, upon treatment with caspase-3 at different concentrations for 1 h at 37 °C, the emissions of Cou-DEVD and TPETP residue exhibit concentration-dependent turn-on at 465 nm and 665 nm, respectively. When the probe was treated with 200 pM caspase-3 for 1 h, the fluorescence of Cou-DEVD and TPETP residue showed 55- and 37- fold increase compared to their intrinsic emission in the probe, respectively. In addition, the peak PL intensities of Cou and TPETP are shown in **Figure S5.12**, which correlate linearly to the concentration of caspase-3 with $R^2 = 0.97$, indicating that the enzyme concentration can be quantified through monitoring the PL intensity

changes of Cou and TPETP. In addition, in the presence of the caspase-3 inhibitor 5-[(S)-(+)-2-(methoxymethyl)pyrrolidino]sulfonylisatin, the probe remains weakly emissive even after the treatment with caspase-3. A kinetic analysis of the enzymatic reaction was also carried out by incubating caspase-3 with different concentrations of Cou–DEVD– TPETP at 37 ^{O}C. As shown in **Figure S5.13**, the Michaelis constant (K_M) and kinetic constant (k_{cat}) were calculated to be 7.70 m M and 2.69 $^{-1}$, which are comparable to the previous FRET probe.[202] The specific cleavage of DEVD by caspase-3 was further confirmed by a reverse phase HPLC and mass spectrometry study through the formation of Cou–DEVD and the TPETP residue (**Figure S5.14**).

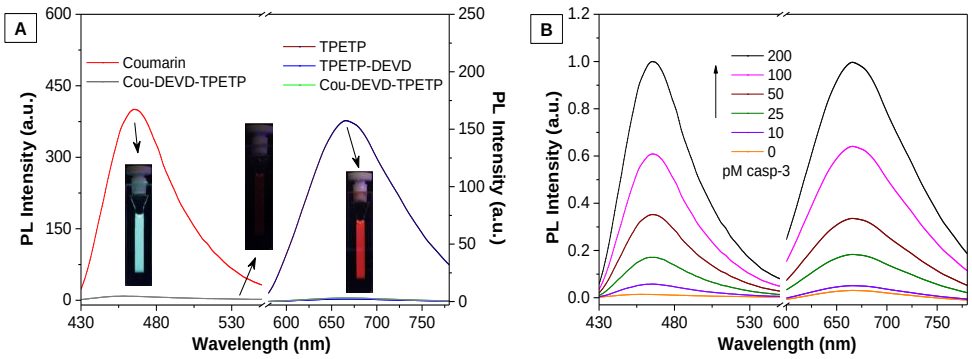

Figure 5.1 (A) Photoluminescence (PL) spectra of Cou, TPETP-N_3 and Cou-DEVD-TPETP (10 μM) in DMSO/PBS buffer (v/v = 1/99). (B) PL spectra of Cou-DEVD-TPETP (10 μM) upon incubation with different concentrations of caspase-3 (λ_{ex}: 405 nm, emission collected from 430 – 550 nm is from the Cou-DEVD and that at 600 – 780 nm is from the TPETP residue). Reprinted with permission from Ref 206 [206] under a Creative Commons Attribution 3.0 Unported Licence.

The selectivity of the probe was studied by incubating the probe with different caspase enzymes as well as several proteins including lysozyme, pepsin, bovine serum albumin and trypsin. As shown in **Figure 5.2A** and **S15A**, only the probe treated with caspase-3/-7 displays a significant fluorescence increase,

confirming the specificity of the probe for caspase-3/-7. The time-dependent fluorescence change of the probe after incubation with caspase-3/-7 and a cell lysate of normal and apoptotic cells was also studied. As shown in **Figure 5.2B**, a quick and steady fluorescence increase at both 465 and 665 nm is observed when caspase-3 is added. On the other hand, the HeLa cells were induced to undergo apoptosis by the treatment of staurosporine (STS), a commonly used apoptosis inducer,[208] and the cell lysates were incubated with the probe. As shown in **Figure S5.15**, the fluorescent signals at both wavelengths increase along with incubation time which is similar to the solution study shown in **Figure 5.2B**. In contrast, no fluorescence change is observed when the probe is incubated with the HeLa cell lysate without STS treatment, indicating that the probe is stable with cellular proteins and it can be specifically recognized by the caspase enzyme with self-validation.

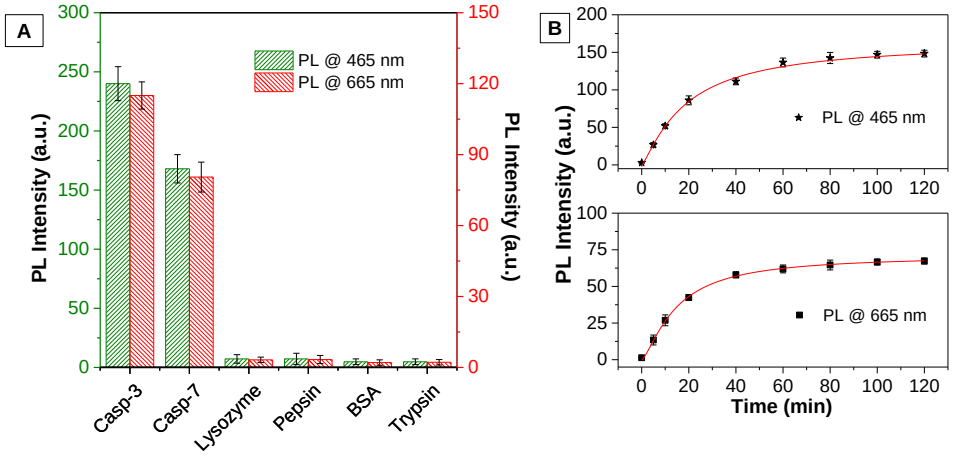

Figure 5.2 PL intensities monitored at both 465 and 665 nm for Cou–DEVD–TPETP (10 mM) upon treatment with various proteins; (B) time-dependent PL intensities for Cou–DEVD–TPETP (10 mM) upon addition of caspase-3 (λ_{ex}: 405 nm). Reprinted with permission from Ref 206 [206] under a Creative Commons Attribution 3.0 Unported Licence.

To explore the potential of using Cou–DEVD–TPETP for caspase imaging in live cells, the probe was incubated with HeLa and MDA-MB-231 cells and subsequently treated with STS. The fluorescence changes at both wavelengths were monitored by confocal laser scanning microscopy. As shown in **Figure 5.3** and **S5.16**, the fluorescent signals of Cou–DEVD and the TPETP residue increase gradually and synchronously with the cellular apoptotic progress upon addition of STS. The fluorescence changes after STS treatment were also confirmed by flow cytometric analysis (**Figure 5.3E** and **F**). These results clearly support the idea that the probe with dual signal turn-on can be used for the self-validation of caspase-3 activation and for real-time monitoring of the apoptosis process in live cells.

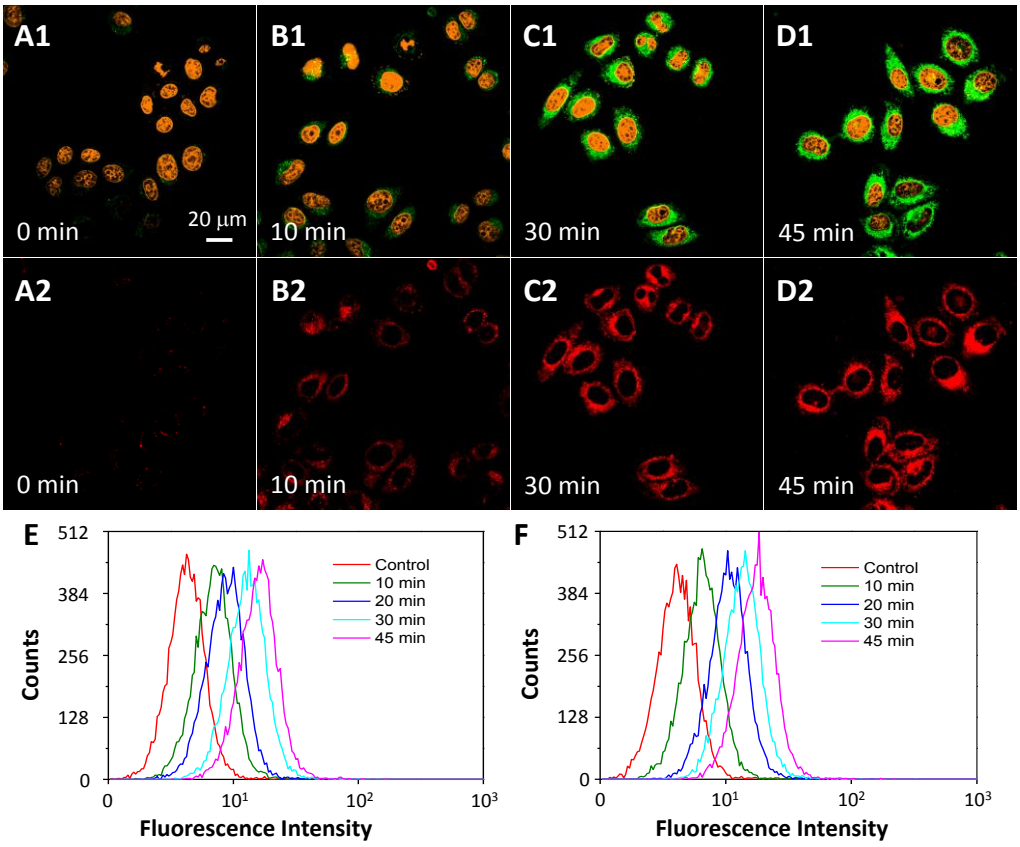

Figure 5.3 Confocal images of Cou–DEVD–TPETP (10 mM) incubated HeLa cells upon treatment with STS (1 m M) for different times. Green fluorescence (Cou–

DEVD, Ex: 405 nm; Em: 505 – 525 nm); orange fluorescence (nucleus dyed with SYTO® orange, Ex: 543 nm, Em: 610–640 nm); A1–D1 are the overlay images of the fluorescence of Cou and SYTO® orange; red fluorescence (TPETP residue, A2–D2, Ex: 405 nm, Em: >650 nm). (E and F) Flow cytometric analysis of Cou–DEVD (E) and the TPETP residue (F) fluorescence in HeLa cells after treatment with STS (1 mM). Reprinted with permission from Ref 206 [206] under a Creative Commons Attribution 3.0 Unported Licence.

To further confirm that the probe can image cell apoptosis, HeLa cells were co-stained with an anti-caspase-3 primary antibody and a Texas Red-labeled secondary antibody. As shown in **Figure 5.4A**, the fluorescence of Cou–DEVD and the TPETP residue in HeLa cells with STS treatment overlaps well with the immuno fluorescence signals from Texas Red. However, when the cells are pretreated with the caspase-3/-7 inhibitor, both intensities are greatly reduced while the fluorescence of Texas Red remains (**Figure 5.4B**). This is because the activity of the caspase-3/-7 enzyme is prohibited upon inhibitor treatment, but the apoptosis process is not affected. Similar results were also observed in MDA-MB-231 cells (**Figure S5.17**). Overall, these results further confirm the caspase-3/-7 specific turn-on of the probe fluorescence in cells.

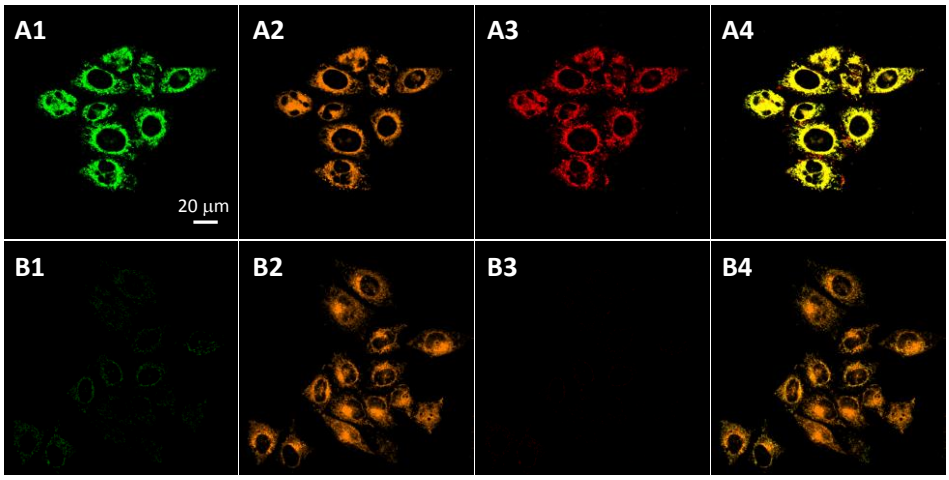

Figure 5.4 Confocal images of apoptotic HeLa cells treated with Cou–DEVD–TPETP (10 mM) in the absence (A) and presence (B) of the caspase-3 inhibitor and

stained with an anti-caspase-3 primary antibody and a Texas Red-labeled secondary antibody. Green fluorescence (Cou–DEVD, A1, B1, Ex: 405 nm; Em: 505 – 525 nm); orange fluorescence (Texas Red, A2, B2, Ex: 543 nm, Em: 610 – 640 nm); red fluorescence (TPETP residue, A3, B3, Ex: 405 nm, Em: >650 nm); A4 and B4 are the overlay images of A1–A3 and B1–B3, respectively. Due to the low absorbance of TPETP at 543 nm, its emission spectral overlap with Texas Red is negligible. Reprinted with permission from Ref 206 [206] under a Creative Commons Attribution 3.0 Unported Licence.

It is known that most drugs induce cell death through the apoptosis pathway.[209] 13 To verify the potential of this probe for self-validated drug screening, the probe incubated cells were treated with several cell apoptosis inducing drugs and the apoptosis-inducing capabilities were evaluated by monitoring the fluorescent signal changes. As shown in **Figure 5.5**, the strongest fluorescence of Cou–DEVD and the TPETP residue is observed when the cells are treated with STS, while a moderate fluorescence is observed when the cells are treated with the anticancer drug doxorubicin (DOX) or cisplatin. The cells treated with Na Asc show the lowest fluorescence, indicating that Na Asc is not a good apoptosis inducer. Similar results were also observed in MDA-MB-231 cells (**Figure S5.18**), revealing the generality of the probe. To test whether the probe could be used to quantify the capability of different drugs in inducing cell apoptosis, the cells were further treated with different amounts of Na Asc, cisplatin, DOX and STS and the fluorescent signals were studied. As shown in **Figure 5.5C**, the fluorescent signals of Cou– DEVD and the TPETP residue intensify synchronously with the drug concentration for all the four drugs. It should be noted that the probe (up to 25 m M) does not show any obvious cytotoxicity to both cells after 48 h incubation (**Figure S5.19**). Collectively, these results indicate that Cou–DEVD–TPETP can quantitatively analyze the capability of different drugs to induce cell apoptosis in

living cells with self-validation, which offers a new opportunity to accurately evaluate the efficiency of new anticancer drugs.

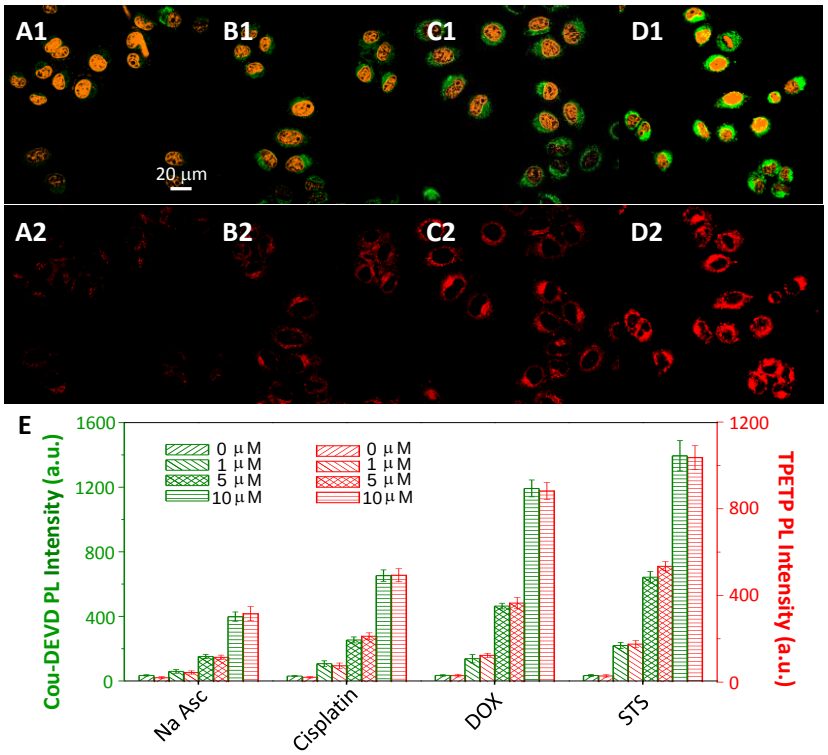

Figure 5.5 Confocal images of Cou–DEVD–TPETP (10 m M) incubated HeLa cells upon treatment with (A) sodium ascorbate (Na Asc), (B) cisplatin, (C) DOX and (D) STS. Green fluorescence (Cou–DEVD, Ex: 405 nm; Em: 505–525 nm); orange fluorescence (nucleus dyed with SYTO® orange, Ex: 543 nm, Em: 610–640 nm); A1–D1 are the overlay images of the fl uorescence of Cou and SYTO® orange; red fluorescence (TPETP residue, A2 – D2, Ex: 405 nm, Em: >650 nm). (E) PL intensities of Cou–DEVD and the TPETP residue in HeLa cells treated with Na Asc, cisplatin, DOX and STS at different concentrations. Reprinted with permission from Ref 206 [206] under a Creative Commons Attribution 3.0 Unported Licence.

5.4 Conclusion

In summary, we developed a simple but unique fluorescent probe with a dual signal turn-on for accurate caspase-3 detection with self-validation. Thanks to the unique property of AIEgen, the fluorescence of the probe is initially quenched,

but a two-signal turn-on is produced upon interaction with the caspase-3 enzyme. The dual-signal turn-on enables real-time monitoring of caspase-3 activity in solution and in live cells with a high efficiency, which has been utilized for self-validated enzyme detection and drug screening. Compared to traditional FRET probes that show a single fluorescence turn-on upon interaction with the analytes, the probe developed in this work using AIEgen as the energy quencher does not complicate the probe design, but offers for the first time a two-signal turn-on upon analyte recognition. In addition, this is the first time that the energy quencher could change its role to a signal reporter upon analyte recognition. Our design strategy for the AIEgen based FRET probe can be generalized to other probes simply by changing DEVD to another cleavable substrate, which will open new avenues for self-validated diagnosis, imaging and drug screening applications. For real practical applications, there is a need to evaluate the in vivo cytotoxicity and design probes with a longer absorption and emission wavelength.

CHAPTER 6. Conclusions and Recommendations

6.1 Conclusions

In summary, we have designed a series of fluorescence light-up probes based on fluorogens with aggregation-induced emission (AIE) characteristics for the detection of biomolecules and imaging of cancer cells. These probes are highly specific and sensitive because of the following reasons: (1) The signal reporters have unique AIE characteristics, which only show negligible fluorescence when molecularly dissolved but fluoresces strongly upon aggregation, offering possibility of fluorescence "OFF" and "ON". (2) The probes have peptide sequences that allows the occurrence of specific recognition event, which will further induce the changes of solubility and direct restriction of intramolecular motions (RIM). (3) The overall hydrophilicity of the probes is fine-tuned by addition of hydrophilic amino acid such as aspartic acid, in order to obtain significant signal-to-background ratio. In addition to these elements, AIEgens are modified with functional groups that facilitate effective conjugation with minimum side reactions. In addition, by modifying the chemical structures of AIEgens, they can be constructed into sensors with different excitation/emission maxima and functions, for example, ROS generation ability, for various detection and imaging tasks.

First, we reported a general strategy to fine tune the aggregation-induced emission (AIE) characteristics of AIE−peptide conjugates for the development of fluorescence "turn-on" probes. As the numbers of carboxyl groups increase from

one to six, the fluorescence intensity of TPE-D_n (n = 1 − 5) in aqueous media gradually decreased. Five carboxyl groups were found to be the threshold to "turn off" the fluorescence of TPE. Then, a proof-of-concept bioprobe TPE-SS-D_5 was used to validate our design by incorporating a cleavable disulfide linker between the hydrophilic moiety D_5 and TPE. The hydrophilic peptide moiety renders the AIE probe water-solubility, which allows it to be used in aqueous media with low background signal and offers a high fluorescence turn-on response to analyte. In addition, this strategy offers an effective solution to overcome the existing limitation of ligand selection for AIE probe design, enabling the development of more versatile bioprobes with hydrophobic recognition elements. The single labeling of the AIE probe also offers simplicity and reduces cost as compared to fluorophore and quencher dual labeled probes for realizing light-up sensing.

Second, a light-up probe TPETH-2(CFTERD_3) for specific detection of chymase was developed by covalent conjugation of AIEgen TPETH-2MAL and peptide CFTERD_3. The probe has low fluorescent signal in aqueous media, but its solubility can be changed after hydrolysis by chymase, giving significant fluorescence turn-on with a high signal to noise (S/N) ratio. The probe has excellent selectivity to chymase but not to other proteins and can effectively differentiate chymase from other enzymes (e.g. chymotrypsin and trypsin) in the same family (E.C. 3.4.21). The detection limit is calculated to be 0.1 ng/mL in PBS buffer with a linear range of 0-9.0 ng/mL. In comparison, the probe with four aspartic acids TPETH-2(CFTERD_2) shows poor selectivity as well as low fluorescence turn-on ratio, which emphasizes the importance of probe design in realizing high signal-to-

background ratio. TPETH-2(CFTERD$_3$) thus represents a simple turn-on probe for chymase detection, with real-time and direct readout and also excellent sensitivity and selectivity.

Thirdly, a light-up probe TPETH-2T7 was developed by conjugating a red-emissive photosensitizer with aggregation-induced emission (AIE) characteristics to a TfR-targeting peptide T7. The probe is almost non-emissive by itself, but it gives concentration-dependent turn-on fluorescence in the presence of TfR ranging from 0-100 μg/mL with a detection limit of 0.45 μg/mL. Cellular experiments show that the probe specifically binds to TfR-overexpressed cancer cells and can discriminate TfR-overexpressed cancer cells against normal cells with a high contrast. Real-time imaging results reveal that the probe stains the MDA-MB-231 cell membrane in 30 min, which is followed by probe internalization. Experiments on image-guided photodynamic cancer ablation show that the therapeutic performance is better when TPETH-2T7 is localized on the cell membrane as compared to that being internalized into cells. Furthermore, confocal laser scanning microscopy (CLSM) study reveals that cytomembrane disintegration allows quick ablation of MDA-MB-231 cells.

Finally, we reported a self-validated fluorescent probe which is composed of a coumarin fluorophore as energy donor and a fluorogen with aggregation-induced emission characteristics (AIEgen) as energy quencher linked through a caspase-3 specific peptide substrate. Unlike the traditionally widely studied fluorescence resonance energy transfer (FRET) probes, our new generation of

FRET probe itself is non-fluorescent due to energy transfer as well as the dissipation of the acceptor energy through free molecular motion of the AIEgen. Upon interaction with caspase-3, the probe displays strong green and red fluorescent signals synchronously due to the separation of donor-quencher and aggregation of the released AIEgen. The fluorescence turn-on with dual signal amplification allows real-time and self-validated enzyme detection with high signal-to-background ratio, providing a good opportunity to accurately monitor various biological processes in real-time manner.

In conclusion, we have developed an AIE-peptide conjugation strategy for construction of light-up probes. Unlike probes based on traditional organic fluorogens that suffer from aggregation-caused quenching (ACQ), aggregation becomes advantageous for development of AIE probes. Meanwhile, by manipulation of the AIE characteristics, fluorescence "OFF" and "ON" with high signal-to-noise ratio can be obtained, which facilitate the development of light-up sensors with more accurate results and avoid false positive signals. Compared with traditional turn-on probes, the design of AIE-based light-up probes is more straightforward and does not require the introduction of fluorescence quenchers, which significantly facilitate and simplifies the probe development. Moreover, these turn-on probes realize real-time detection and imaging of biomolecules because no extra washing steps are required. The FRET probe (Chapter 5) in this thesis, is more like a combination of FRET probe and a turn-on probe. It realizes fluorescence off state by integration of FRET process and also fluorescence decay

by free intramolecular motions. The presence of target induces the dual color fluorescence turn-on, which facilitate self-validation.

On the other hand, the advent of phage display technology has greatly enriched the peptide library and offers alternatives that can interact with protein targets with high affinity and specificity. By fully utilizing peptides as recognition elements, more AIE-peptide probes can be developed for the sensing of various targets. In general, the low toxicity, good photostability and tunable emission color endow the AIE probes good biocompatibility, and excellent versatility for various sensing tasks and sensing systems. Other properties such as ROS generation ability will endow AIE-based probes with functionality for theranostic applications.

6.2 Recommendations

We have successfully demonstrated the design and development of AIE-peptide based probes, which are highly sensitive, specific and versatile and can be utilized for various sensing tasks. Generally, fluorescent probes consist of two main parts: the signaling and recognition moieties, which determine the sensitivity and selectivity of the probes, respectively. In this thesis, two AIEgens TPE and TPETH with blue and red emission colors have been used. In comparison, TPETH which emits at around 630 nm is more suitable for biological applications because they can avoid the interferences from the blue autofluorescence prevalently produced in biological systems. Moreover, in further studies that involve *in vivo* applications, near-infrared (NIR) dyes that have emission in the range of 650-1350 nm are highly desirable, due to their effective tissue penetration depth. Researchers have paid

great efforts to develop such AIE fluorogens, though there are very limited successful examples now.

In addition, imaging/therapeutic application that can realize accurate targeting on the organelle level is in highly demanding. Different organelle plays various functions in the cells. Understanding their functionality and taking full advantage of their functions will surely benefit scientific research. For example, studies have shown that mitochondrion play important role in cell apoptosis. It is thus an important target for photodynamic therapy. Also, there are some mitochondria-targeting peptide sequences reported. By combination of two different peptide sequences, a tadem probe that can first target cancer cells then locate the photosensitizers to mitochondria will significantly improve the efficiency of the PDT process.

In the parallel to the booming of AIEgens in biological applications, in recent years, point-of-care diagnostics have emerged as valuable tools for on-site detections due to their advantages such as rapidness, low cost, simplicity and great accessibility. On the other hand, some new AIEgens have been developed by integration of other mechanism such as ESIPT. Typical AIE fluorogens are non-emissive when molecularly dissolved, which endows the hydrophilic AIE probes with extremely low background signals. However, most of them are limited in applications in aqueous media due to the high background signal in solid state. In comparison, AIE-ESIPT fluorogens show weak emission when proton transfer is blocked, regardless of whether the molecules are in molecular or solid state. Once

upon the deprotection of proton donor and the formation of intramolecular hydrogen bonds, strong fluorescence is restored by both proton transfer and RIM. Such AIE-ESIPT fluorogens have great potential in paper-based assays, not only for the simplest dipstick assays, but also for lateral flow assays and even complicated microfluidic paper-based analytical devices. These models will broaden the application of AIEgens to mass manufacture industry, for example pre-diagnosis by urine samples.

In this thesis, peptides that can achieve targeting or recognition functions have been chosen to conjugate with AIE fluorogens due to their ease of synthesis and conjugation, availability of peptide library and great potential in delivery of biological information. The working mechanism of AIE-peptide conjugates falls into two categories: enzymatic hydrolysis induced changes of hydrophilicity or specific binding induced restriction of intramolecular motions. The probes based on enzymatic hydrolysis can not only be utilized for monitoring enzyme level, they can also be used for screening of enzyme inhibitors, which is very promising in drug development because many drug take effect by blocking enzymes' activity or regulating metabolic imbalance. The success of AIE-peptide probes for enzyme detection has fully validated that they can contribute to the studies on enzyme inhibitors in the future. In addition, some enzyme reactions produce measurable fluorescence for sensing of product formation, which can be regarded as chemiluminescence. By combination of these inherent bioreaction, dual signals for self-validation or cascade light-up probes that does not require excitation laser probably can be designed. On the other hand, probes based on specific binding

between peptide and protein pairs, such as cRGD and $\alpha_v\beta_3$ integrin, have succeed in recognition of proteins. In the future, they may also take part in screening peptide sequences for protein recognition.

In addition to peptides, other recognition moieties such as DNAs are promising candidates for the development of AIE probes. For example, there is a type of single strand oligonucleotide named as aptamer, which can specifically bind with ions and proteins. Considering aptamers have good hydrophilicity, they can be conjugated with AIEgens to yield probes with extremely low background signals. In the presence of targets, aptamers will become rigid and restrict the intramolecular motions of AIEgens, leading to fluorescence turn-on. Similarly, as single strand DNA is hydrophilic and flexible, the DNA-AIE conjugates must be nonemissvie in aqueous media, but the fluorescence can be regained upon hybridization with their complimentary strands due to the formation of rigid double strand DNA. By taking advantage of the recognition ability of ssDNA and aptamer, a new type of AIE probes can be designed. Moreover, there are a wealth of nucleic acid related enzymes, which plays important roles in the investigation of DNA. By properly design AIE-based assays with these enzyme, more powerful probes can be developed and fully exert the potential of AIEgens for biological applications.

In practical detections, the target of analyte usually exists in a very complicated system containing various interferents. In addition, detections of multi-analyte in one go are frequently needed. In view of this, multiplex detection is a promising solution to this problem. As described above, both DNA and peptide

can be introduced for design of AIE probes. We all know that DNA and peptides are existing in biological systems and take effect respectively without being affected by each other. As mentioned, more and more AIEgens with different emission color have been designed and reported. There are also abundant options to realize recognition and/or signaling. By combination of these two types of candidates, a wealth of probes for multiplex detections can be developed to meet the demand of assays for complicated samples and real samples.

AIEgens are easy to be synthesized and modified, additional functions such as therapeutic applications can be embedded in to AIE-based probes. For example, in this thesis, the TPETH-2T7 is a successful example that combines the detection, imaging and photodynamic therapy into one probe. In this regard, this type of probes can satisfy the requirement of theranostics, which integrates the specific targeting, fluorescence detection of disease markers and therapy/treatment into one model. Theranostics has undergone great prosperity in cancer research because they hampered the cancer growth during diagnostic procedure. In view of this, AIEgens with multi-functionalities or other therapeutic drugs, multi-model AIE probes can be developed.

References

1. Turner AP. Biosensors: sense and sensibility. *Chem Soc Rev*, 2013, **42**(8)**:** 3184-3196.

2. Darken MA. Natural and induced fluorescence in microscopic organisms. *Appl Microbiol*, 1961, **9**(4)**:** 354-360.

3. Terai T, Nagano T. Fluorescent probes for bioimaging applications. *Curr Opin Chem Biol*, 2008, **12**(5)**:** 515-521.

4. Grynkiewicz G, Poenie M, Tsien RY. A new generation of Ca^{2+} indicators with greatly improved fluorescence properties. *J Biol Chem*, 1985, **260**(6)**:** 3440-3450.

5. Ueno T, Nagano T. Fluorescent probes for sensing and imaging. *Nat Methods*, 2011, **8**(8)**:** 642-645.

6. Rurack K, Kollmannsberger M, Resch-Genger U, Daub J. A selective and sensitive fluoroionophore for HgII, AgI, and CuII with virtually decoupled fluorophore and receptor units. *J Am Chem Soc*, 2000, **122**(5)**:** 968-969.

7. McQuade DT, Hegedus AH, Swager TM. Signal amplification of a "turn-on" sensor: Harvesting the light captured by a conjugated polymer. *J Am Chem Soc*, 2000, **122**(49)**:** 12389-12390.

8. Fan L-J, Jones WE. A highly selective and sensitive inorganic/organic hybrid polymer fluorescence "turn-on" chemosensory system for iron cations. *J Am Chem Soc*, 2006, **128**(21)**:** 6784-6785.

9. Pinto MR, Schanze KS. Amplified fluorescence sensing of protease activity with conjugated polyelectrolytes. *Proc Natl Acad Sci U S A*, 2004, **101**(20)**:** 7505-7510.

10. Daly B, Ling J, de Silva AP. Current developments in fluorescent PET (photoinduced electron transfer) sensors and switches. *Chem Soc Rev*, 2015, **44**(13)**:** 4203-4211.

11. Kowada T, Maeda H, Kikuchi K. BODIPY-based probes for the fluorescence imaging of biomolecules in living cells. *Chem Soc Rev*, 2015, **44**(14)**:** 4953-4972.

12. Matsumoto T, Urano Y, Shoda T, Kojima H, Nagano T. A thiol-reactive fluorescence probe based on donor-excited photoinduced electron transfer: key role of ortho substitution. *Org Lett,* 2007, **9**(17)**:** 3375-3377.

13. Guo H, Jing Y, Yuan X, Ji S, Zhao J, Li X, *et al*. Highly selective fluorescent OFF–ON thiol probes based on dyads of BODIPY and potent intramolecular electron sink 2, 4-dinitrobenzenesulfonyl subunits. *Org Biomol Chem,* 2011, **9**(10)**:** 3844-3853.

14. Lin W, Long L, Yuan L, Cao Z, Chen B, Tan W. A ratiometric fluorescent probe for cysteine and homocysteine displaying a large emission shift. *Org Lett,* 2008, **10**(24)**:** 5577-5580.

15. Zhao J, Ji S, Chen Y, Guo H, Yang P. Excited state intramolecular proton transfer (ESIPT): from principal photophysics to the development of new chromophores and applications in fluorescent molecular probes and luminescent materials. *Phys Chem Chem Phys,* 2012, **14**(25)**:** 8803-8817.

16. Chen W-H, Xing Y, Pang Y. A highly selective pyrophosphate sensor based on ESIPT turn-on in water. *Org Lett,* 2011, **13**(6)**:** 1362-1365.

17. Liu T, Xu Z, Spring DR, Cui J. A lysosome-targetable fluorescent probe for imaging hydrogen sulfide in living cells. *Org Lett,* 2013, **15**(9)**:** 2310-2313.

18. Tang Y, Yang HR, Sun HB, Liu SJ, Wang JX, Zhao Q, *et al*. Rational design of an "OFF-ON" phosphorescent chemodosimeter based on an iridium(III) complex and its application for time-resolved luminescent detection and bioimaging of cysteine and homocysteine. *Chem Eur J,* 2013, **19**(4)**:** 1311-1319.

19. Yang XF, Wang L, Xu H, Zhao M. A fluorescein-based fluorogenic and chromogenic chemodosimeter for the sensitive detection of sulfide anion in aqueous solution. *Anal Chim Acta,* 2009, **631**(1)**:** 91-95.

20. Hammers MD, Pluth MD. Ratiometric measurement of hydrogen sulfide and cysteine/homocysteine ratios using a dual-fluorophore fragmentation strategy. *Anal Chem,* 2014, **86**(14)**:** 7135-7140.

21. Whitney M, Savariar EN, Friedman B, Levin RA, Crisp JL, Glasgow HL, *et al*. Ratiometric activatable cell-penetrating peptides provide rapid in vivo readout of thrombin activation. *Angew Chem Int Ed Engl,* 2013, **52**(1)**:** 325-330.

22. Tyagi S, Kramer FR. Molecular beacons: probes that fluoresce upon hybridization. *Nat Biotechnol,* 1996, **14**(3)**:** 303-308.

23. Tan W, Wang K, Drake TJ. Molecular beacons. *Curr Opin Chem Biol,* 2004, **8**(5)**:** 547-553.

24. Hu HY, Gehrig S, Reither G, Subramanian D, Mall MA, Plettenburg O, *et al.* FRET-based and other fluorescent proteinase probes. *Biotechnol J,* 2014, **9**(2)**:** 266-281.

25. Valeur B, Berberan-Santos MN. *Molecular fluorescence: principles and applications*. John Wiley & Sons, 2012.

26. Chen Y, Tsao K, Keillor JW. Fluorogenic protein labelling: a review of photophysical quench mechanisms and principles of fluorogen design. *Can J Chem,* 2015, **93**(4)**:** 389-398.

27. Yang Y-K, Yook K-J, Tae J. A rhodamine-based fluorescent and colorimetric chemodosimeter for the rapid detection of Hg^{2+} ions in aqueous media. *J Am Chem Soc,* 2005, **127**(48)**:** 16760-16761.

28. Han Z-X, Zhang X-B, Li Z, Gong Y-J, Wu X-Y, Jin Z, *et al.* Efficient Fluorescence Resonance Energy Transfer-Based Ratiometric Fluorescent Cellular Imaging Probe for Zn^{2+} Using a Rhodamine Spirolactam as a Trigger. *Anal Chem,* 2010, **82**(8)**:** 3108-3113.

29. Taki M, Iyoshi S, Ojida A, Hamachi I, Yamamoto Y. Development of Highly Sensitive Fluorescent Probes for Detection of Intracellular Copper(I) in Living Systems. *J Am Chem Soc,* 2010, **132**(17)**:** 5938-5939.

30. Song F, Watanabe S, Floreancig PE, Koide K. Oxidation-Resistant Fluorogenic Probe for Mercury Based on Alkyne Oxymercuration. *J Am Chem Soc,* 2008, **130**(49)**:** 16460-16461.

31. Qu D-Y, Chen J-L, Di B. A fluorescence "switch-on" approach to detect hydrazine in aqueous solution at neutral pH. *Anal. Methods,* 2014, **6**(13)**:** 4705-4709.

32. Lippert AR, New EJ, Chang CJ. Reaction-based fluorescent probes for selective imaging of hydrogen sulfide in living cells. *J Am Chem Soc,* 2011, **133**(26)**:** 10078-10080.

33. Kim HN, Lee MH, Kim HJ, Kim JS, Yoon J. A new trend in rhodamine-based chemosensors: application of spirolactam ring-opening to sensing ions. *Chem Soc Rev,* 2008, **37**(8)**:** 1465-1472.

34. Randolph JB, Waggoner AS. Stability, specificity and fluorescence brightness of multiply-labeled fluorescent DNA probes. *Nucleic Acids Res,* 1997, **25**(14)**:** 2923-2929.

35. Luo J, Xie Z, Lam JW, Cheng L, Chen H, Qiu C, *et al.* Aggregation-induced emission of 1-methyl-1, 2, 3, 4, 5-pentaphenylsilole. *Chem Commun,* 2001(18)**:** 1740-1741.

36. Tang B, zhan x, Lee PPS, Liu Y, Daoben Z. Efficient blue emission from siloles. *J Mater Chem,* 2001, **11**(12)**:** 2974-2978.

37. Hong Y, Lam JW, Tang BZ. Aggregation-induced emission. *Chem Soc Rev,* 2011, **40**(11)**:** 5361-5388.

38. Mei J, Hong Y, Lam JW, Qin A, Tang Y, Tang BZ. Aggregation-Induced Emission: The Whole Is More Brilliant than the Parts. *Adv Mater,* 2014, **26**(31)**:** 5429-5479.

39. Yin S, Peng Q, Shuai Z, Fang W, Wang Y-H, Luo Y. Aggregation-enhanced luminescence and vibronic coupling of silole molecules from first principles. *Phys. Rev. B,* 2006, **73**(20)**:** 205409.

40. Li Z, Dong Y, Mi B, Tang Y, Häussler M, Tong H, *et al.* Structural control of the photoluminescence of silole regioisomers and their utility as sensitive regiodiscriminating chemosensors and efficient electroluminescent materials. *J Phys Chem B,* 2005, **109**(20)**:** 10061-10066.

41. Kokado K, Chujo Y. Multicolor tuning of aggregation-induced emission through substituent variation of diphenyl-o-carborane. *J Org Chem,* 2010, **76**(1)**:** 316-319.

42. Chen J, Law CC, Lam JW, Dong Y, Lo SM, Williams ID, *et al.* Synthesis, light emission, nanoaggregation, and restricted intramolecular rotation of 1, 1-substituted 2, 3, 4, 5-tetraphenylsiloles. *Chem Mater,* 2003, **15**(7)**:** 1535-1546.

43. Parrott EP, Tan NY, Hu R, Zeitler JA, Tang BZ, Pickwell-MacPherson E. Direct evidence to support the restriction of intramolecular rotation hypothesis for the mechanism of aggregation-induced emission: temperature resolved terahertz spectra of tetraphenylethene. *Mater Horiz,* 2014, **1**(2)**:** 251-258.

44. Luo J, Song K, long Gu F, Miao Q. Switching of non-helical overcrowded tetrabenzoheptafulvalene derivatives. *Chem Sci,* 2011, **2**(10)**:** 2029-2034.

45. Chi Z, Zhang X, Xu B, Zhou X, Ma C, Zhang Y, *et al.* Recent advances in organic mechanofluorochromic materials. *Chem Soc Rev,* 2012, **41**(10)**:** 3878-3896.

46. Zhou X, Li H, Chi Z, Zhang X, Zhang J, Xu B, *et al.* Piezofluorochromism and morphology of a new aggregation-induced emission compound derived from tetraphenylethylene and carbazole. *New J Chem,* 2012, **36**(3)**:** 685-693.

47. Zhao Q, Li K, Chen S, Qin A, Ding D, Zhang S, *et al.* Aggregation-induced red-NIR emission organic nanoparticles as effective and photostable fluorescent probes for bioimaging. *J Mater Chem,* 2012, **22**(30)**:** 15128.

48. Ding D, Li K, Liu B, Tang BZ. Bioprobes based on AIE fluorogens. *Acc Chem Res,* 2013, **46**(11)**:** 2441-2453.

49. Mei J, Leung NL, Kwok RT, Lam JW, Tang BZ. Aggregation-Induced Emission: Together We Shine, United We Soar! *Chem Rev* 2015, **115**(21)**:** 11718-11940.

50. Yuan Y, Zhang CJ, Gao M, Zhang R, Tang BZ, Liu B. Specific Light-Up Bioprobe with Aggregation-Induced Emission and Activatable Photoactivity for the Targeted and Image-Guided Photodynamic Ablation of Cancer Cells. *Angew Chem Int Ed,* 2015, **54**(6)**:** 1780-1786.

51. Zhang C-J, Hu Q, Feng G, Zhang R, Yuan Y, Lu X, *et al.* Image-guided combination chemotherapy and photodynamic therapy using a mitochondria-targeted molecular probe with aggregation-induced emission characteristics. *Chem Sci,* 2015, **6**(8)**:** 4580-4586.

52. Xu S, Yuan Y, Cai X, Zhang C-J, Hu F, Liang J, *et al.* Tuning the singlet-triplet energy gap: a unique approach to efficient photosensitizers with aggregation-induced emission (AIE) characteristics. *Chem Sci,* 2015, **6**(10)**:** 5824-5830.

53. Wang Z, Chen S, Lam JW, Qin W, Kwok RT, Xie N, *et al.* Long-term fluorescent cellular tracing by the aggregates of AIE bioconjugates. *J Am Chem Soc,* 2013, **135**(22)**:** 8238-8245.

54. Shi H, Liu J, Geng J, Tang BZ, Liu B. Specific detection of integrin αvβ3 by light-up bioprobe with aggregation-induced emission characteristics. *J Am Chem Soc,* 2012, **134**(23)**:** 9569-9572.

55. Liang J, Tang BZ, Liu B. Specific light-up bioprobes based on AIEgen conjugates. *Chem Soc Rev,* 2015, **44**(10)**:** 2798-2811.

56. Dong Y, Lam JWY, Qin A, Li Z, Liu J, Sun J, *et al.* Endowing hexaphenylsilole with chemical sensory and biological probing properties by attaching amino pendants to the silolyl core. *Chem Phys Lett,* 2007, **446**(1-3)**:** 124-127.

57. Wang M, Zhang D, Zhang G, Tang Y, Wang S, Zhu D. Fluorescence turn-on detection of DNA and label-free fluorescence nuclease assay based on the aggregation-induced emission of silole. *Anal Chem,* 2008, **80**(16)**:** 6443-6448.

58. Lou X, Zhuang Y, Zuo X, Jia Y, Hong Y, Min X, *et al.* Real-Time, Quantitative Lighting-up Detection of Telomerase in Urines of Bladder Cancer Patients by AIEgens. *Anal Chem,* 2015, **87**(13)**:** 6822-6827.

59. Zhuang Y, Zhang M, Chen B, Duan R, Min X, Zhang Z, *et al.* Quencher Group Induced High Specificity Detection of Telomerase in Clear and Bloody Urines by AIEgens. *Anal Chem,* 2015.

60. Min X, Zhuang Y, Zhang Z, Jia Y, Hakeem A, Zheng F, *et al.* Lab in a Tube: Sensitive Detection of MicroRNAs in Urine Samples from Bladder Cancer Patients Using a Single-Label DNA Probe with AIEgens. *ACS Appl Mater Interfaces,* 2015, **7**(30)**:** 16813-16818.

61. Hong Y, Feng C, Yu Y, Liu J, Lam JWY, Luo KQ, *et al.* Quantitation, visualization, and monitoring of conformational transitions of human serum albumin by a tetraphenylethene derivative with aggregation-induced emission characteristics. *Anal Chem,* 2010, **82**(16)**:** 7035-7043.

62. Hong Y, Meng L, Chen S, Leung CWT, Da L-T, Faisal M, *et al.* Monitoring and inhibition of insulin fibrillation by a small organic fluorogen with aggregation-induced emission characteristics. *J Am Chem Soc,* 2012, **134**(3)**:** 1680-1689.

63. Wang F, Wen J, Huang L, Huang J, Ouyang J. A highly sensitive "switch-on" fluorescent probe for protein quantification and visualization based on aggregation-induced emission. *Chem Commun,* 2012, **48**(59)**:** 7395-7397.

64. Sanji T, Nakamura M, Kawamata S, Tanaka M, Itagaki S, Gunji T. Fluorescence "Turn-On" Detection of Melamine with Aggregation-Induced-Emission-Active Tetraphenylethene. *Chem Eur J,* 2012, **18**(48)**:** 15254-15257.

65. Gui S, Huang Y, Hu F, Jin Y, Zhang G, Yan L, *et al.* Fluorescence turn-on chemosensor for highly selective and sensitive detection and bioimaging of Al(3+) in living cells based on ion-induced aggregation. *Anal Chem,* 2015, **87**(3)**:** 1470-1474.

66. Liu Y, Deng C, Tang L, Qin A, Hu R, Sun JZ, *et al.* Specific detection of D-glucose by a tetraphenylethene-based fluorescent sensor. *J Am Chem Soc,* 2011, **133**(4)**:** 660-663.

67. Wang X, Hu J, Zhang G, Liu S. Highly selective fluorogenic multianalyte biosensors constructed via enzyme-catalyzed coupling and aggregation-induced emission. *J Am Chem Soc,* 2014, **136**(28)**:** 9890-9893.

68. Shi H, Kwok RTK, Liu J, Xing B, Tang BZ, Liu B. Real-Time Monitoring of Cell Apoptosis and Drug Screening Using Fluorescent Light-Up Probe with Aggregation-Induced Emission Characteristics. *J Am Chem Soc,* 2012, **134**(43)**:** 17972-17981.

69. Liang J, Shi H, Kwok RT, Gao M, Yuan Y, Zhang W-H, *et al.* Distinct Optical and Kinetic Responses from E/Z Isomers of Caspase Probes with Aggregation-Induced Emission Characteristics. *J Mater* Chem B, 2014, **2**, 4363-4370.

70. Han A, Wang H, Kwok RT, Ji S, Li J, Kong D, *et al.* Peptide-Induced AIEgen Self-Assembly: A New Strategy to Realize Highly Sensitive Fluorescent Light-Up Probes. *Anal Chem,* 2016, **88**(7)**:** 3872-3878.

71. Wang Y, Chen Y, Wang H, Cheng Y, Zhao X. Specific Turn-On Fluorescent Probe with Aggregation-Induced Emission Characteristics for SIRT1 Modulator Screening and Living-Cell Imaging. *Anal Chem,* 2015, **87**(10)**:** 5046-5049.

72. Yuan Y, Zhang C-J, Kwok RTK, Xu S, Zhang R, Wu J, *et al.* Light-Up Probe for Targeted and Activatable Photodynamic Therapy with Real-Time In Situ Reporting of Sensitizer Activation and Therapeutic Responses. *Adv Funct Mater,* 2015, **25**(42)**:** 6586-6595.

73. Hu F, Huang Y, Zhang G, Zhao R, Yang H, Zhang D. Targeted bioimaging and photodynamic therapy of cancer cells with an activatable red fluorescent bioprobe. *Anal Chem,* 2014, **86**(15)**:** 7987-7995.

74. Huang Y, Hu F, Zhao R, Zhang G, Yang H, Zhang D. Tetraphenylethylene Conjugated with a Specific Peptide as a Fluorescence Turn-On Bioprobe for the Highly Specific Detection and Tracing of Tumor Markers in Live Cancer Cells. *Chem Eur J,* 2014, **20**(1)**:** 158-164.

75. Chen S, Liu J, Liu Y, Su H, Hong Y, Jim CKW, *et al.* An AIE-active hemicyanine fluorogen with stimuli-responsive red/blue emission: extending the pH sensing range by "switch + knob" effect. *Chemi Sci,* 2012, **3**(6)**:** 1804.

76. Chen S, Hong Y, Liu Y, Liu J, Leung CW, Li M, *et al.* Full-range intracellular pH sensing by an aggregation-induced emission-active two-channel ratiometric fluorogen. *J Am Chem Soc,* 2013, **135**(13)**:** 4926-4929.

77. Liu Y, Yu Y, Lam JW, Hong Y, Faisal M, Yuan WZ, *et al.* Simple biosensor with high selectivity and sensitivity: thiol-specific biomolecular probing and intracellular imaging by AIE fluorogen on a TLC plate through a thiolene click mechanism. *Chem Eur J,* 2010, **16**(28)**:** 8433-8438.

78. Qian Y, Li S, Zhang G, Wang Q, Wang S, Xu H, *et al.* Aggregation-induced emission enhancement of 2-(2'-hydroxyphenyl) benzothiazole-based excited-state intramolecular proton-transfer compounds. *J Phys Chem B,* 2007, **111**(21)**:** 5861-5868.

79. Gao M, Hu Q, Feng G, Tang BZ, Liu B. A fluorescent light-up probe with "AIE+ ESIPT" characteristics for specific detection of lysosomal esterase. *J Mater Chem B,* 2014, **2**(22)**:** 3438-3442.

80. Hu Q, Gao M, Feng G, Liu B. Mitochondria-targeted cancer therapy using a light-up probe with aggregation-induced-emission characteristics. *Angew Chem Int Ed Engl,* 2014, **53**(51)**:** 14225-14229.

81. Gao M, Sim CK, Leung CW, Hu Q, Feng G, Xu F, *et al.* A fluorescent light-up probe with AIE characteristics for specific mitochondrial imaging to identify differentiating brown adipose cells. *Chem Commun,* 2014, **50**(61)**:** 8312-8315.

82. Lavis LD, Raines RT. Bright ideas for chemical biology. *ACS Chem Biol,* 2008, **3**(3)**:** 142-155.

83. Schäferling M. The art of fluorescence imaging with chemical sensors. *Angew Chem Int Ed,* 2012, **51**(15)**:** 3532-3554.

84. Stich MI, Fischer LH, Wolfbeis OS. Multiple fluorescent chemical sensing and imaging. *Chem Soc Rev,* 2010, **39**(8)**:** 3102-3114.

85. Callan JF, de Silva AP, Magri DC. Luminescent sensors and switches in the early 21st century. *Tetrahedron,* 2005, **61**(36)**:** 8551-8588.

86. Kaur K, Saini R, Kumar A, Luxami V, Kaur N, Singh P, *et al.* Chemodosimeters: an approach for detection and estimation of biologically and medically relevant metal ions, anions and thiols. *Coord Chem Rev,* 2012, **256**(17)**:** 1992-2028.

87. Goswami S, Sen D, Das NK. A new highly selective, ratiometric and colorimetric fluorescence sensor for Cu2+ with a remarkable red shift in absorption and emission spectra based on internal charge transfer. *Org Lett,* 2010, **12**(4)**:** 856-859.

88. Qian X, Xiao Y, Xu Y, Guo X, Qian J, Zhu W. "Alive" dyes as fluorescent sensors: fluorophore, mechanism, receptor and images in living cells. *Chem Commun,* 2010, **46**(35)**:** 6418-6436.

89. Sapsford KE, Berti L, Medintz IL. Materials for fluorescence resonance energy transfer analysis: beyond traditional donor–acceptor combinations. *Angew Chem Int Ed,* 2006, **45**(28)**:** 4562-4589.

90. Carlson HJ, Campbell RE. Genetically encoded FRET-based biosensors for multiparameter fluorescence imaging. *Curr Opin Biotechnol,* 2009, **20**(1)**:** 19-27.

91. Liu B, Bazan GC. Homogeneous fluorescence-based DNA detection with water-soluble conjugated polymers. *Chem Mater,* 2004, **16**(23)**:** 4467-4476.

92. Shao J, Sun H, Guo H, Ji S, Zhao J, Wu W, *et al.* A highly selective red-emitting FRET fluorescent molecular probe derived from BODIPY for the detection of cysteine and homocysteine: an experimental and theoretical study. *Chemi Sci,* 2012, **3**(4)**:** 1049-1061.

93. Sabelle S, Renard P-Y, Pecorella K, de Suzzoni-Dézard S, Créminon C, Grassi J, *et al.* Design and synthesis of chemiluminescent probes for the detection of cholinesterase activity. *J Am Chem Soc,* 2002, **124**(17)**:** 4874-4880.

94. Thomas SW, Joly GD, Swager TM. Chemical sensors based on amplifying fluorescent conjugated polymers. *Chem Rev,* 2007, **107**(4)**:** 1339-1386.

95. Jun ME, Roy B, Ahn KH. "Turn-on" fluorescent sensing with "reactive" probes. *Chem Commun,* 2011, **47**(27)**:** 7583-7601.

96. Zhang X, Zhang X, Tao L, Chi Z, Xu J, Wei Y. Aggregation induced emission-based fluorescent nanoparticles: fabrication methodologies and biomedical applications. *J Mater Chem B,* 2014, **2**(28)**:** 4398.

97. Hong Y, Lam JW, Tang BZ. Aggregation-induced emission: phenomenon, mechanism and applications. *Chem Commun,* 2009(29)**:** 4332-4353.

98. Tong H, Hong Y, Dong Y, Häussler M, Li Z, Lam JW, *et al.* Protein detection and quantitation by tetraphenylethene-based fluorescent probes with aggregation-induced emission characteristics. *J Phys Chem B,* 2007, **111**(40)**:** 11817-11823.

99. Tong H, Hong Y, Dong Y, Häußler M, Lam JW, Li Z, *et al.* Fluorescent "light-up" bioprobes based on tetraphenylethylene derivatives with aggregation-induced emission characteristics. *Chem Commun,* 2006(35)**:** 3705-3707.

100. Chen J, Jiao H, Li W, Liao D, Zhou H, Yu C. Real-time fluorescence turn-on detection of alkaline phosphatase activity with a novel perylene probe. *Chem Asian J,* 2013, **8**(1)**:** 276-281.

101. Li Y, Kwok RT, Tang BZ, Liu B. Specific nucleic acid detection based on fluorescent light-up probe from fluorogens with aggregation-induced emission characteristics. *RSC Adv,* 2013, **3**(26)**:** 10135-10138.

102. Wang M, Zhang D, Zhang G, Zhu D. The convenient fluorescence turn-on detection of heparin with a silole derivative featuring an ammonium group. *Chem Commun,* 2008(37)**:** 4469-4471.

103. Kwok RTK, Geng J, Lam JWY, Zhao E, Wang G, Zhan R, *et al.* Water-soluble bioprobes with aggregation-induced emission characteristics for light-up sensing of heparin. *J Mater Chem B,* 2014, **2**(26)**:** 4134.

104. Li X, Zhang X, Chi Z, Chao X, Zhou X, Zhang Y, *et al.* Simple fluorescent probe derived from tetraphenylethylene and benzoquinone for instantaneous biothiol detection. *Anal Methods,* 2012, **4**(10)**:** 3338-3343.

105. ZhiáSun J, ZhongáTang B. Discriminative fluorescence detection of cysteine, homocysteine and glutathione via reaction-dependent aggregation of fluorophore-analyte adducts. *J Mater Chem,* 2012, **22**(33)**:** 17063-17070.

106. Mei J, Wang Y, Tong J, Wang J, Qin A, Sun JZ, *et al.* Discriminatory Detection of Cysteine and Homocysteine Based on Dialdehyde-Functionalized Aggregation-Induced Emission Fluorophores. *Chem Eur J,* 2013, **19**(2)**:** 613-620.

107. Lou X, Hong Y, Chen S, Leung CW, Zhao N, Situ B, *et al.* A selective glutathione probe based on AIE fluorogen and its application in enzymatic activity assay. *Sci Rep*, 2014, **4:** 4272.

108. Shi H, Zhao N, Ding D, Liang J, Tang BZ, Liu B. Fluorescent light-up probe with aggregation-induced emission characteristics for in vivo imaging of cell apoptosis. *Org Biomol Chem*, 2013, **11**(42)**:** 7289-7296.

109. Ding D, Liang J, Shi H, Kwok RT, Gao M, Feng G, *et al.* Light-up bioprobe with aggregation-induced emission characteristics for real-time apoptosis imaging in target cancer cells. *J Mater Chem B*, 2014, **2**(2)**:** 231-238.

110. Yuan Y, Kwok RT, Tang BZ, Liu B. Targeted Theranostic Platinum (IV) Prodrug with a Built-In Aggregation-Induced Emission Light-Up Apoptosis Sensor for Noninvasive Early Evaluation of Its Therapeutic Responses in Situ. *J Am Chem Soc*, 2014, **136**(6)**:** 2546-2554.

111. Tang L, Jin JK, Qin A, Zhang Yuan W, Mao Y, Mei J, *et al.* A fluorescent thermometer operating in aggregation-induced emission mechanism: probing thermal transitions of PNIPAM in water. *Chem Commun*, 2009(33)**:** 4974-4976.

112. Yuan Y, Kwok RT, Feng G, Liang J, Geng J, Tang BZ, *et al.* Rational design of fluorescent light-up probes based on an AIE luminogen for targeted intracellular thiol imaging. *Chem Commun*, 2014, **50**(3)**:** 295-297.

113. Zhang R, Yuan Y, Liang J, Kwok RT, Zhu Q, Feng G, *et al.* Fluorogen-peptide conjugates with tunable aggregation-induced emission characteristics for bioprobe design. *ACS Appl Mater Interfaces*, 2014, **6**(16)**:** 14302-14310.

114. Shiu WY, Mackay D. A critical review of aqueous solubilities, vapor pressures, Henry's law constants, and octanol–water partition coefficients of the polychlorinated biphenyls. *J Phys Chem Ref Data*, 1986, **15**(2)**:** 911-929.

115. Miller MM, Wasik SP, Huang GL, Shiu WY, Mackay D. Relationships between octanol-water partition coefficient and aqueous solubility. *Environ Sci Technol*, 1985, **19**(6)**:** 522-529.

116. Levin VA, Dolginow D, Landahl HD, Yorke C, Csejtey J. Relationship of octanol/water partition coefficient and molecular weight to cellular permeability and partitioning in S49 lymphoma cells. *Pharm Res*, 1984, **1**(6)**:** 259-266.

117. Madjene LC, Pons M, Danelli L, Claver J, Ali L, Madera-Salcedo IK, *et al.* Mast cells in renal inflammation and fibrosis: Lessons learnt from animal studies. *Mol Immunol*, 2015, **63**(1)**:** 86-93.

118. Amin K. The role of mast cells in allergic inflammation. *Respir Med*, 2012, **106**(1)**:** 9-14.

119. Bradding P, Walls AF, Holgate ST. The role of the mast cell in the pathophysiology of asthma. *J Allergy Clin Immunol*, 2006, **117**(6)**:** 1277-1284.

120. Waern I, Jonasson S, Hjoberg J, Bucht A, Åbrink M, Pejler G, *et al.* Mouse mast cell protease 4 is the major chymase in murine airways and has a protective role in allergic airway inflammation. *J Immunol*, 2009, **183**(10)**:** 6369-6376.

121. Caughey GH. Mast cell tryptases and chymases in inflammation and host defense. *Immunol Rev*, 2007, **217**(1)**:** 141-154.

122. Suzuki T, Kaki H, Naya S, Murayama S, Tatsui A, Nagai A, *et al.* Recombinant human chymase produced by silk-worm-baculovirus expression system: application for chymase detection kit. *Jpn J Pharmacol*, 2002, **90**(3):210-213.

123. Beil WJ, Pammer J. In situ detection of the mast cell proteases chymase and tryptase in human lung tissue using light and electron microscopy. *Histochem Cell Biol*, 2001, **116**(6)**:** 483-493.

124. Jolly S, Detilleux J, Coignoul F, Desmecht D. Enzyme-histochemical detection of a chymase-like proteinase within bovine mucosal and connective tissue mast cells. *J Comp Pathol*, 2000, **122**(2)**:** 155-162.

125. Shimizu Y, Suga T, Maeno T, Tsukagoshi H, Kawata T, Narita T, *et al.* Detection of tryptase−, chymase+ cells in human CD34+ bone marrow progenitors. *Clin Exp Allergy*, 2004, **34**(11)**:** 1719-1724.

126. Ladner RC, Sato AK, Gorzelany J, de Souza M. Phage display-derived peptides as therapeutic alternatives to antibodies. *Drug Discov Today*, 2004, **9**(12)**:** 525-529.

127. Goldman ER, Pazirandeh MP, Mauro JM, King KD, Frey JC, Anderson GP. Phage-displayed peptides as biosensor reagents. *J Mol Recogn*, 2000, **13**(6)**:** 382-387.

128. Wu P, Yan XP. Doped quantum dots for chemo/biosensing and bioimaging. *Chem Soc Rev,* 2013, **42**(12)**:** 5489-5521.

129. Yao J, Yang M, Duan Y. Chemistry, biology, and medicine of fluorescent nanomaterials and related systems: new insights into biosensing, bioimaging, genomics, diagnostics, and therapy. *Chem Rev,* 2014, **114**(12)**:** 6130-6178.

130. Li K, Liu B. Water-soluble conjugated polymers as the platform for protein sensors. *Polym Chem,* 2010, **1**(3)**:** 252-259.

131. Beija M, Afonso CA, Martinho JM. Synthesis and applications of Rhodamine derivatives as fluorescent probes. *Chem Soc Rev,* 2009, **38**(8)**:** 2410-2433.

132. Yuan L, Lin W, Zheng K, Zhu S. FRET-based small-molecule fluorescent probes: rational design and bioimaging applications. *Acc Chem Res,* 2013, **46**(7)**:** 1462-1473.

133. Henderson G. The effects of absorption and self-absorption quenching on fluorescent intensities. *J Chem Educ,* 1977, **54**(1)**:** 57.

134. Marras SA. Selection of fluorophore and quencher pairs for fluorescent nucleic acid hybridization probes. *Methods Mol Biol,* 2006, 335**:** 3-16.

135. Yang S, Wang C, Liu C, Wang Y, Xiao Y, Li J, *et al.* Fluorescence Modulation by Absorbent on Solid Surface: An Improved Approach for Designing Fluorescent Sensor. *Anal Chem,* 2014, **86**(15)**:** 7931-7938.

136. Wang H, Wang Y, Jin J, Yang R. Gold nanoparticle-based colorimetric and "turn-on" fluorescent probe for mercury (II) ions in aqueous solution. *Anal Chem,* 2008, **80**(23)**:** 9021-9028.

137. Li F, Pei H, Wang L, Lu J, Gao J, Jiang B, *et al.* Nanomaterial-Based Fluorescent DNA Analysis: A Comparative Study of the Quenching Effects of Graphene Oxide, Carbon Nanotubes, and Gold Nanoparticles. *Adv Funct Mater,* 2013, **23**(33)**:** 4140-4148.

138. Wang M, Zhang G, Zhang D, Zhu D, Tang BZ. Fluorescent bio/chemosensors based on silole and tetraphenylethene luminogens with aggregation-induced emission feature. *J Mater Chem,* 2010, **20**(10)**:** 1858-1867.

139. Li K, Qin W, Ding D, Tomczak N, Geng J, Liu R, *et al.* Photostable fluorescent organic dots with aggregation-induced emission (AIE dots) for noninvasive long-term cell tracing. *Sci Rep,* 2013, **3**, 1150.

140. Qin W, Li K, Feng G, Li M, Yang Z, Liu B, *et al.* Bright and Photostable Organic Fluorescent Dots with Aggregation-Induced Emission Characteristics for Noninvasive Long-Term Cell Imaging. *Adv Funct Mater,* 2014, **24**(5)**:** 635-643.

141. Yuan Y, Xu S, Cheng X, Cai X, Liu B. Bioorthogonal Turn-On Probe Based on Aggregation-Induced Emission Characteristics for Cancer Cell Imaging and Ablation. *Angew Chem Int Ed Engl,* 2016, **55**(22)**:** 6457-6461.

142. Yuan Y, Zhang CJ, Liu B. A Photoactivatable AIE Polymer for Light-Controlled Gene Delivery: Concurrent Endo/Lysosomal Escape and DNA Unpacking. *Angew Chem Int Ed,* 2015, **54**(39)**:** 11419-11423.

143. Hong Y, Häuβler M, Lam JW, Li Z, Sin KK, Dong Y, *et al.* Label-Free Fluorescent Probing of G-Quadruplex Formation and Real-Time Monitoring of DNA Folding by a Quaternized Tetraphenylethene Salt with Aggregation-Induced Emission Characteristics. *Chem Eur J,* 2008, **14**(21)**:** 6428-6437.

144. Zhang R, Feng G, Zhang CJ, Cai X, Cheng X, Liu B. Real-Time Specific Light-Up Sensing of Transferrin Receptor: Image-Guided Photodynamic Ablation of Cancer Cells through Controlled Cytomembrane Disintegration. *Anal Chem,* 2016, **88**(9)**:** 4841-4848.

145. Raymond WW, Su S, Makarova A, Wilson TM, Carter MC, Metcalfe DD, *et al.* α2-Macroglobulin capture allows detection of mast cell chymase in serum and creates a reservoir of angiotensin II-generating activity. *J Immunol,* 2009, **182**(9)**:** 5770-5777.

146. Zhang CJ, Feng G, Xu S, Zhu Z, Lu X, Wu J, *et al.* Structure-Dependent cis/trans Isomerization of Tetraphenylethene Derivatives: Consequences for Aggregation-Induced Emission. *Angew Chem Int Ed,* 2016, **55**(21)**:** 6192-6196.

147. Olsen JV, Ong S-E, Mann M. Trypsin cleaves exclusively C-terminal to arginine and lysine residues. *Mol Cell Proteomics,* 2004, **3**(6)**:** 608-614.

148. Copeland RA. *Enzymes: a practical introduction to structure, mechanism, and data analysis*. John Wiley & Sons, 2004.

149. Tros de Ilarduya C, Düzgünes N. Delivery of therapeutic nucleic acids via transferrin and transferrin receptors: lipoplexes and other carriers. *Expert Opin Drug Deliv,* 2013, **10**(11)**:** 1583-1591.

150. Tortorella S, Karagiannis TC. Transferrin receptor-mediated endocytosis: a useful target for cancer therapy**.** *J Membr Biol,* 2014, **247**(4)**:** 291-307.

151. Daniels TR, Delgado T, Helguera G, Penichet ML. The transferrin receptor part II: targeted delivery of therapeutic agents into cancer cells. *Clin Immunol,* 2006, **121**(2)**:** 159-176.

152. Gabathuler R. Approaches to transport therapeutic drugs across the blood-brain barrier to treat brain diseases. *Neurobiol Dis,* 2010, **37**(1)**:** 48-57.

153. Ying X, Wen H, Lu WL, Du J, Guo J, Tian W, *et al.* Dual-targeting daunorubicin liposomes improve the therapeutic efficacy of brain glioma in animals. *J Control Release,* 2010, **141**(2)**:** 183-192.

154. Zhang M-Z, Yu R-N, Chen J, Ma Z-Y, Zhao Y-D. Targeted quantum dots fluorescence probes functionalized with aptamer and peptide for transferrin receptor on tumor cells. *Nanotechnology,* 2012, **23**(48)**:** 485104.

155. Cao C, Wang X, Cai Y, Sun L, Tian L, Wu H, *et al.* Targeted In Vivo Imaging of Microscopic Tumors with Ferritin-based Nanoprobes Across Biological Barriers. *Adv Mater,* 2014, **26**(16)**:** 2566-2571.

156. Han L, Huang R, Liu S, Huang S, Jiang C. Peptide-Conjugated PAMAM for Targeted Doxorubicin Delivery to Transferrin Receptor Overexpressed Tumors. *Mol Pharm,* 2010, **7**(6)**:** 2156-2165.

157. Daniels TR, Bernabeu E, Rodríguez JA, Patel S, Kozman M, Chiappetta DA, *et al.* The transferrin receptor and the targeted delivery of therapeutic agents against cancer. *Biochim Biophys Acta,* 2012, **1820**(3)**:** 291-317.

158. Kuang Y, An S, Guo Y, Huang S, Shao K, Liu Y, *et al.* T7 peptide-functionalized nanoparticles utilizing RNA interference for glioma dual targeting. *Int J Pharm,* 2013, **454**(1)**:** 11-20.

159. Coley HM. Mechanisms and strategies to overcome chemotherapy resistance in metastatic breast cancer. *Cancer Treat Rev,* 2008, **34**(4)**:** 378-390.

160. Dawar S, Singh N, Kanwar RK, Kennedy RL, Veedu RN, Zhou SF, *et al.* Multifunctional and multitargeted nanoparticles for drug delivery to overcome barriers of drug resistance in human cancers. *Drug Discov Today,* 2013, **18**(23-24)**:** 1292-1300.

161. Dolmans DE, Fukumura D, Jain RK. Photodynamic therapy for cancer. *Nat Rev Cancer,* 2003, **3**(5)**:** 380-387.

162. Price M, Reiners JJ, Santiago AM, Kessel D. Monitoring singlet oxygen and hydroxyl radical formation with fluorescent probes during photodynamic therapy. *Photochem Photobiol,* 2009, **85**(5)**:** 1177-1181.

163. Agostinis P, Berg K, Cengel KA, Foster TH, Girotti AW, Gollnick SO, *et al.* Photodynamic therapy of cancer: an update. *CA Cancer J Clin,* 2011, **61**(4)**:** 250-281.

164. Kelkar SS, Reineke TM. Theranostics: combining imaging and therapy. *Bioconjugate Chem,* 2011, **22**(10)**:** 1879-1903.

165. Takeuchi Y, Ichikawa K, Yonezawa S, Kurohane K, Koishi T, Nango M, *et al.* Intracellular target for photosensitization in cancer antiangiogenic photodynamic therapy mediated by polycation liposome. *J Control Release,* 2004, **97**(2)**:** 231-240.

166. Bhattacharyya A, Dixit A, Mitra K, Banerjee S, Karande AA, Chakravarty AR. BODIPY appended copper(ii) complexes of curcumin showing mitochondria targeted remarkable photocytotoxicity in visible light. *Med Chem Commun,* 2015, **6**(5)**:** 846-851.

167. Li D, Li L, Li P, Li Y, Chen X. Apoptosis of HeLa cells induced by a new targeting photosensitizer-based PDT via a mitochondrial pathway and ER stress. *Onco Targets Ther,* 2015, **8:** 703-711.

168. He L, Li Y, Tan C-P, Ye R-R, Chen M-H, Cao J-J, *et al.* Cyclometalated iridium(iii) complexes as lysosome-targeted photodynamic anticancer and real-time tracking agents. *Chem Sci,* 2015, **6**(10)**:** 5409-5418.

169. Tian J, Ding L, Xu H-J, Shen Z, Ju H, Jia L, *et al.* Cell-specific and pH-activatable rubyrin-loaded nanoparticles for highly selective near-infrared photodynamic therapy against cancer. *J Am Chem Soc,* 2013, **135**(50)**:** 18850-18858.

170. Lovell JF, Chan MW, Qi Q, Chen J, Zheng G. Porphyrin FRET acceptors for apoptosis induction and monitoring. *J Am Chem Soc,* 2011, **133**(46)**:** 18580-18582.

171. Sekkat N, Bergh Hvd, Nyokong T, Lange N. Like a bolt from the blue: phthalocyanines in biomedical optics. *Molecules,* 2011, **17**(1)**:** 98-144.

172. Park SY, Baik HJ, Oh YT, Oh KT, Youn YS, Lee ES. A smart polysaccharide/drug conjugate for photodynamic therapy. *Angew Chem Int Ed,* 2011, **50**(7)**:** 1644-1647.

173. Jang WD, Nishiyama N, Zhang GD, Harada A, Jiang DL, Kawauchi S, *et al.* Supramolecular nanocarrier of anionic dendrimer porphyrins with cationic block copolymers modified with polyethylene glycol to enhance intracellular photodynamic efficacy. *Angew Chem,* 2005, **117**(3)**:** 423-427.

174. Kwok RT, Leung CW, Lam JW, Tang BZ. Biosensing by luminogens with aggregation-induced emission characteristics. *Chem Soc Rev,* 2015, **44**(13)**:** 4228-4238.

175. Zhang R, Kwok RT, Tang BZ, Liu B. Hybridization induced fluorescence turn-on of AIEgen–oligonucleotide conjugates for specific DNA detection. *RSC Adv,* 2015, **5**(36)**:** 28332-28337.

176. Yuan Y, Zhang CJ, Liu B. A platinum prodrug conjugated with a photosensitizer with aggregation-induced emission (AIE) characteristics for drug activation monitoring and combinatorial photodynamic-chemotherapy against cisplatin resistant cancer cells. *Chem Commun,* 2015, **51**(41)**:** 8626-8629.

177. Lee JH, Engler JA, Collawn JF, Moore BA. Receptor mediated uptake of peptides that bind the human transferrin receptor. *Eur J Biochem,* 2001, **268**(7)**:** 2004-2012.

178. Oh S, Kim BJ, Singh NP, Lai H, Sasaki T. Synthesis and anti-cancer activity of covalent conjugates of artemisinin and a transferrin-receptor targeting peptide. *Cancer Lett,* 2009, **274**(1)**:** 33-39.

179. Barth BM, Sharma R, Altınogˇlu EI, Morgan TT, Shanmugavelandy SS, Kaiser JM, *et al.* Bioconjugation of calcium phosphosilicate composite nanoparticles for selective targeting of human breast and pancreatic cancers in vivo. *ACS nano,* 2010, **4**(3)**:** 1279-1287.

180. Salvati A, Pitek AS, Monopoli MP, Prapainop K, Bombelli FB, Hristov DR, *et al.* Transferrin-functionalized nanoparticles lose their targeting capabilities when a biomolecule corona adsorbs on the surface. *Nat Nanotechnol,* 2013, **8**(2)**:** 137-143.

181. Deng ZJ, Liang M, Monteiro M, Toth I, Minchin RF. Nanoparticle-induced unfolding of fibrinogen promotes Mac-1 receptor activation and inflammation. *Nat Nanotechnol,* 2011, **6**(1)**:** 39-44.

182. Kim J, Santos OA, Park JH. Selective photosensitizer delivery into plasma membrane for effective photodynamic therapy. *J Control Release,* 2014, **191:** 98-104.

183. Hsieh YJ, Wu CC, Chang CJ, Yu JS. Subcellular localization of Photofrin determines the death phenotype of human epidermoid carcinoma A431 cells triggered by photodynamic therapy: when plasma membranes are the main targets. *J Cell Physiol,* 2003, **194**(3)**:** 363-375.

184. Zheng J, Yang R, Shi M, Wu C, Fang X, Li Y, *et al.* Rationally designed molecular beacons for bioanalytical and biomedical applications. *Chem Soc Rev,* 2015, **44**(10)**:** 3036-3055.

185. Yang Z, Cao J, He Y, Yang JH, Kim T, Peng X, *et al.* Macro-/micro-environment-sensitive chemosensing and biological imaging. *Chem Soc Rev,* 2014, **43**(13)**:** 4563-4601.

186. Chan J, Dodani SC, Chang CJ. Reaction-based small-molecule fluorescent probes for chemoselective bioimaging. *Nat Chem,* 2012, **4**(12)**:** 973-984.

187. Li J, Cheng F, Huang H, Li L, Zhu JJ. Nanomaterial-based activatable imaging probes: from design to biological applications. *Chem Soc Rev,* 2015, **44**(21)**:** 7855-7880.

188. Sapsford KE, Berti L, Medintz IL. Materials for fluorescence resonance energy transfer analysis: beyond traditional donor-acceptor combinations. *Angew Chem Int Ed Engl,* 2006, **45**(28)**:** 4562-4589.

189. Lee DE, Koo H, Sun IC, Ryu JH, Kim K, Kwon IC. Multifunctional nanoparticles for multimodal imaging and theragnosis. *Chem Soc Rev,* 2012, **41**(7)**:** 2656-2672.

190. Rolfe BE, Blakey I, Squires O, Peng H, Boase NR, Alexander C, *et al.* Multimodal polymer nanoparticles with combined 19F magnetic resonance and optical detection for tunable, targeted, multimodal imaging in vivo. *J Am Chem Soc,* 2014, **136**(6)**:** 2413-2419.

191. Harrison VS, Carney CE, MacRenaris KW, Waters EA, Meade TJ. Multimeric Near IR-MR Contrast Agent for Multimodal In Vivo Imaging. *J Am Chem Soc,* 2015, **137**(28)**:** 9108-9116.

192. Sun Y, Ma X, Cheng K, Wu B, Duan J, Chen H, *et al.* Strained cyclooctyne as a molecular platform for construction of multimodal imaging probes. *Angew Chem Int Ed Engl,* 2015, **54**(20)**:** 5981-5984.

193. Wang Y, Song S, Liu J, Liu D, Zhang H. ZnO-functionalized upconverting nanotheranostic agent: multi-modality imaging-guided chemotherapy with on-demand drug release triggered by pH. *Angew Chem Int Ed Engl,* 2015, **54**(2)**:** 536-540.

194. Wu X, Lin B, Yu M, Yang L, Han J, Han S. A carbohydrate-grafted nanovesicle with activatable optical and acoustic contrasts for dual modality high performance tumor imaging. *Chem Sci,* 2015, **6**(3)**:** 2002-2009.

195. Wu Q, Cheng Q, Yuan S, Qian J, Zhong K, Qian Y, *et al.* A cell-penetrating protein designed for bimodal fluorescence and magnetic resonance imaging. *Chem Sci,* 2015, **6**(11)**:** 6607-6613.

196. Guan W, Zhou W, Lu C, Tang BZ. Synthesis and Design of Aggregation-Induced Emission Surfactants: Direct Observation of Micelle Transitions and Microemulsion Droplets. *Angew Chem Int Ed Engl,* 2015, **54**(50)**:** 15160-15164.

197. Xue X, Zhao Y, Dai L, Zhang X, Hao X, Zhang C, *et al.* Spatiotemporal drug release visualized through a drug delivery system with tunable aggregation-induced emission. *Adv Mater,* 2014, **26**(5)**:** 712-717.

198. Li K, Liu B. Polymer-encapsulated organic nanoparticles for fluorescence and photoacoustic imaging. *Chem Soc Rev,* 2014, **43**(18)**:** 6570-6597.

199. Shao A, Xie Y, Zhu S, Guo Z, Zhu S, Guo J, *et al.* Far-Red and Near-IR AIE-Active Fluorescent Organic Nanoprobes with Enhanced Tumor-Targeting Efficacy: Shape-Specific Effects. *Angew Chem Int Ed Engl,* 2015, **54**(25)**:** 7275-7280.

200. Xie Z, Chen C, Xu S, Li J, Zhang Y, Liu S, *et al.* White-light emission strategy of a single organic compound with aggregation-induced emission and delayed fluorescence properties. *Angew Chem Int Ed Engl,* 2015, **54**(24)**:** 7181-7184.

201. Birks JB. *Photophysics of aromatic molecules*. John Wiley & Sons,1970.

202. Boeneman K, Mei BC, Dennis AM, Bao G, Deschamps JR, Mattoussi H, *et al.* Sensing caspase 3 activity with quantum dot− fluorescent protein assemblies. *J Am Chem Soc,* 2009, **131**(11)**:** 3828-3829.

203. Zhang L, Lei J, Liu J, Ma F, Ju H. In situ activation and monitoring of the evolution of the intracellular caspase family. *Chem Sci,* 2015, **6**(6)**:** 3365-3372.

204. Ye D, Shuhendler AJ, Pandit P, Brewer KD, Tee SS, Cui L, *et al.* Caspase-responsive smart gadolinium-based contrast agent for magnetic resonance imaging of drug-induced apoptosis. *Chem Sci,* 2014, **4**(10)**:** 3845-3852.

205. Gu Z, Biswas A, Joo KI, Hu B, Wang P, Tang Y. Probing protease activity by single-fluorescent-protein nanocapsules. *Chem Commun,* 2010, **46**(35)**:** 6467-6469.

206. Yuan Y, Zhang R, Cheng X, Xu S, Liu B. A FRET probe with AIEgen as the energy quencher: dual signal turn-on for self-validated caspase detection. *Chem Sci,* 2016, **7**(7)**:** 4245-4250.

207. Huang Y, Hu F, Zhao R, Zhang G, Yang H, Zhang D. Tetraphenylethylene Conjugated with a Specific Peptide as a Fluorescence Turn-On Bioprobe for the Highly Specific Detection and Tracing of Tumor Markers in Live Cancer Cells. *Chem Eur J,* 2014, **20**(1)**:** 158-164.

208. Zhang XD, Gillespie SK, Hersey P. Staurosporine induces apoptosis of melanoma by both caspase-dependent and-independent apoptotic pathways. *Mol Cancer Ther,* 2004, **3**(2)**:** 187-197.

209. Okada H, Mak TW. Pathways of apoptotic and non-apoptotic death in tumour cells. *Nat Rev Cancer,* 2004, **4**(8)**:** 592-603.

APPENDIX 1 for Chapter 2

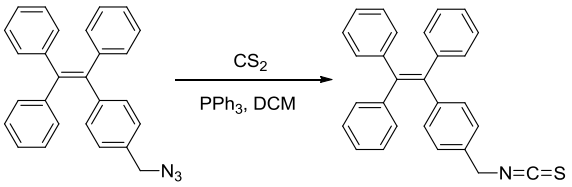

Scheme S2.1 Synthetic route to compound 1-[4-(isothiocyanatomethyl)phenyl]-1,2,2-triphenylethene (TPE-NCS).

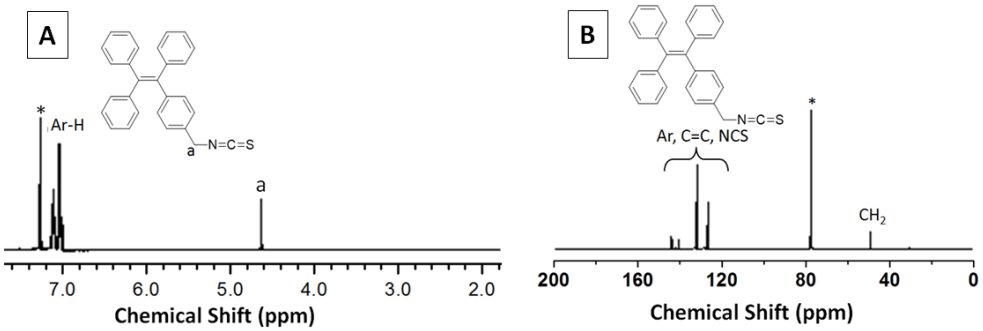

Figure S2.1 ^{1}H NMR and ^{13}C NMR spectra of TPE-NCS in $CDCl_3$.

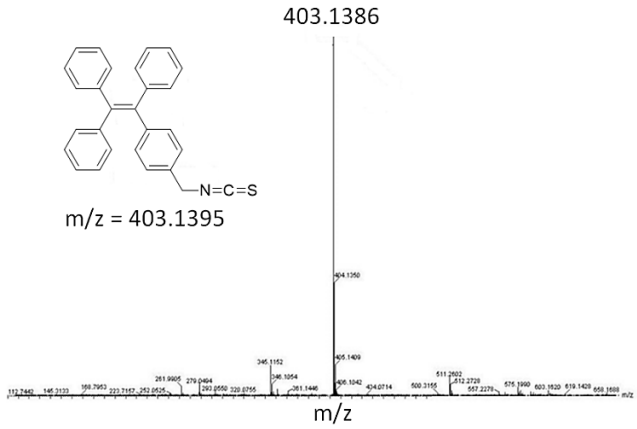

Figure S2.2 High resolution mass spectrum of TPE-NCS.

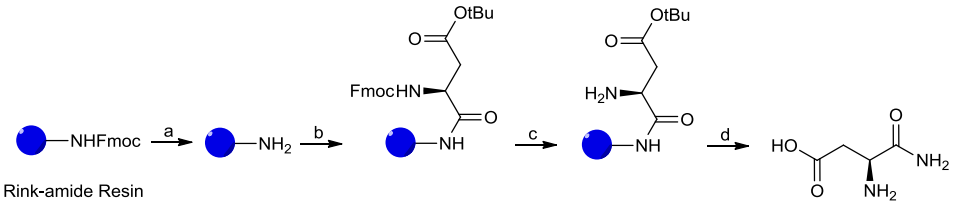

Scheme S2.2 Synthetic route to 2-diamino-4-oxobutanoic acid (amide terminated aspartic acid, D-NH_2). Reagent and conditions: (a) 20% piperidine in DMF; (b) Fmoc-Asp(OtBu)-OH, HBTU, HOBt, DIEA, DMF; (c) 20% piperidine in DMF; (d) TFA/TIS/H_2O (v/v/v = 95/2.5/2.5), 3 h.

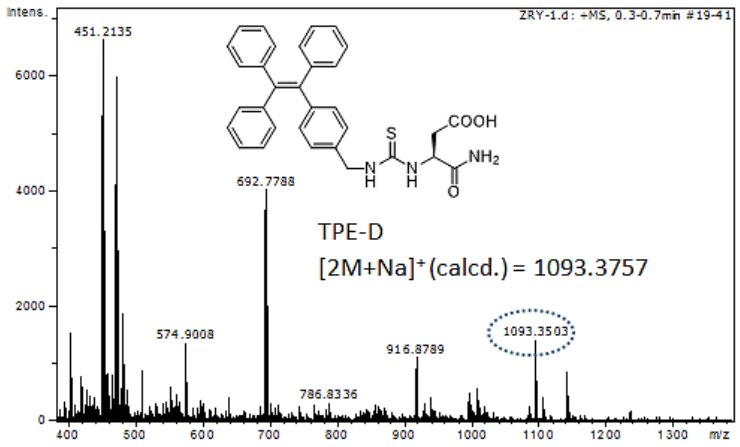

Figure S2.3. ESI-MS spectrum of TPE-D.

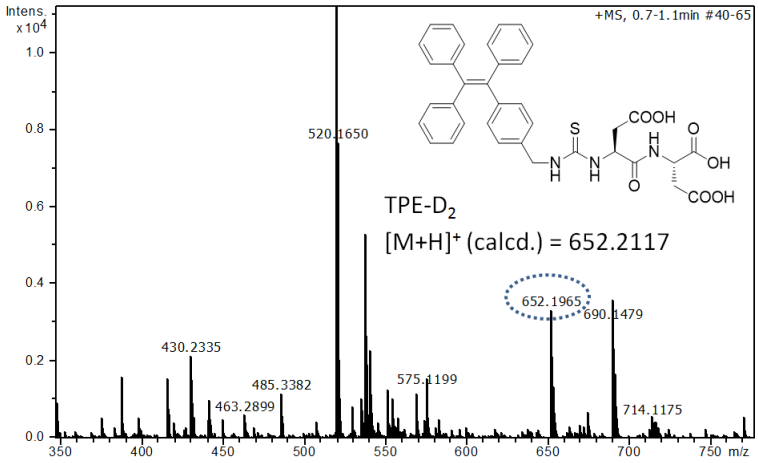

Figure S2.4. ESI-MS spectrum of TPE-D_2.

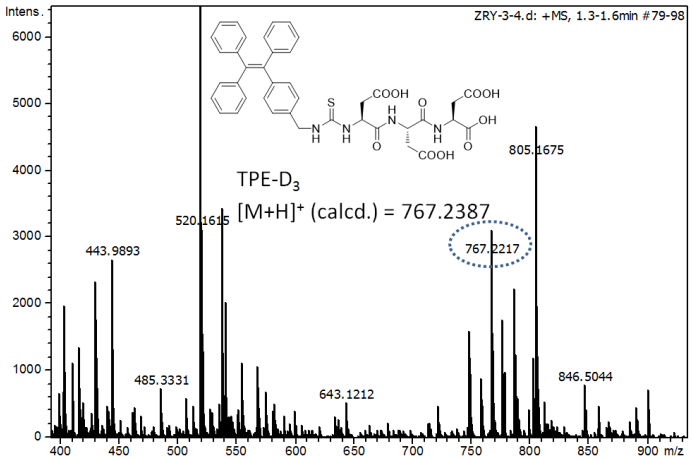

Figure S2.5. ESI-MS spectrum of TPE-D_3.

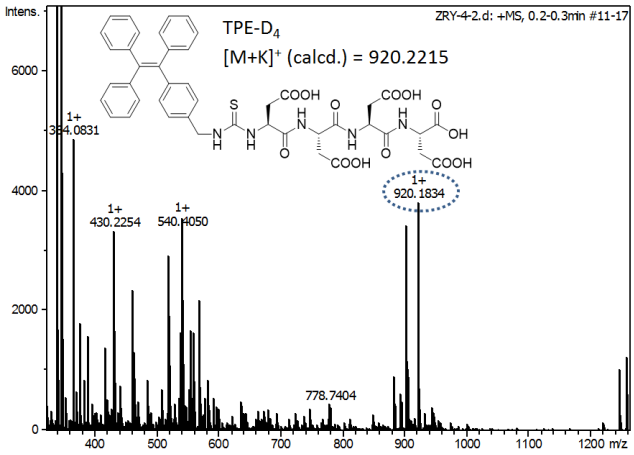

Figure S2.6. ESI-MS spectrum of TPE-D_4.

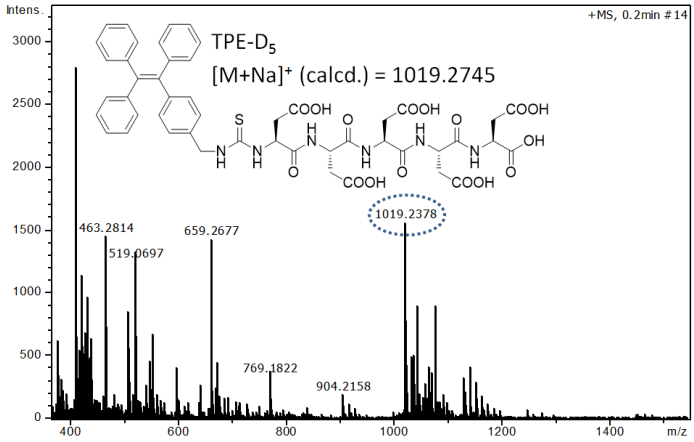

Figure S2.7. ESI-MS spectrum of TPE-D_5.

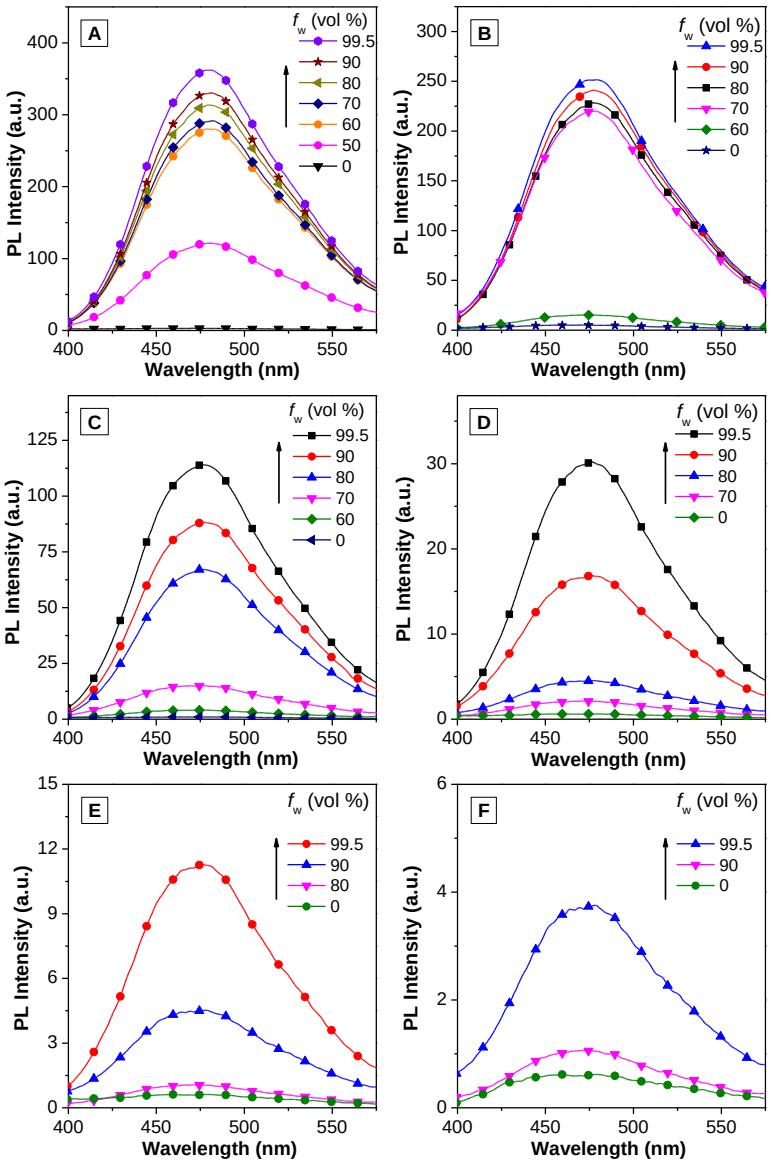

Figure S2.8 PL spectra of (A) TPE-NCS, (B) TPE-D, (C) TPE-D_2, (D) TPE-D_3, (E) TPE-D_4, and (F) TPE-D_5 in DMSO/H_2O mixtures with different water fractions (f_w). (λ_{ex} = 314 nm for TPE-NCS, λ_{ex} = 304 nm for TPE−D_n (n = 1−5), [TPE-NCS] = [TPE-D_n] = 10 μM).

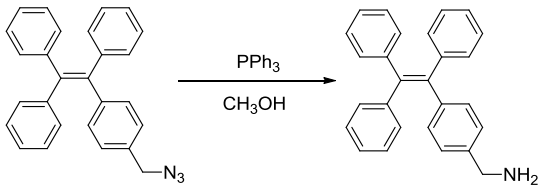

Scheme S2.3. Synthetic route to compound 1-[(4-aminomethyl)phenyl]-1,2,2-triphenylethene (TPE-NH_2).

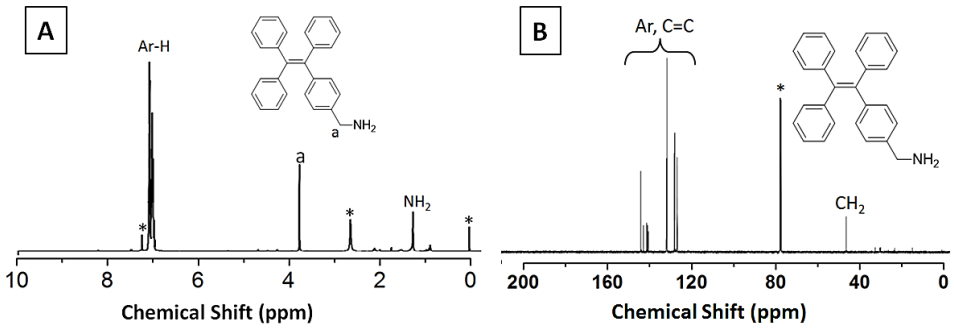

Figure S2.9. ^{1}H NMR and ^{13}C NMR spectra of TPE-NH_2 in $CDCl_3$. [2]

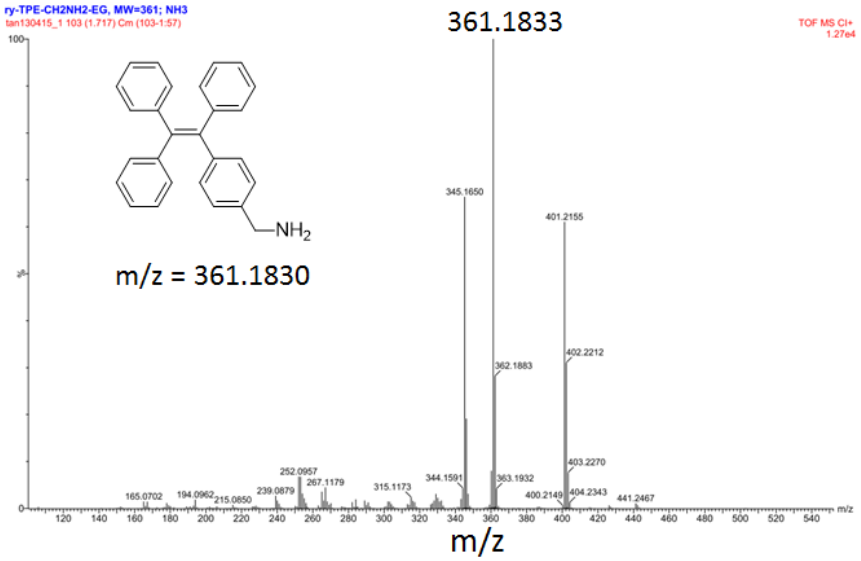

Figure S2.10. High resolution mass spectrum of TPE-NH_2.[2]

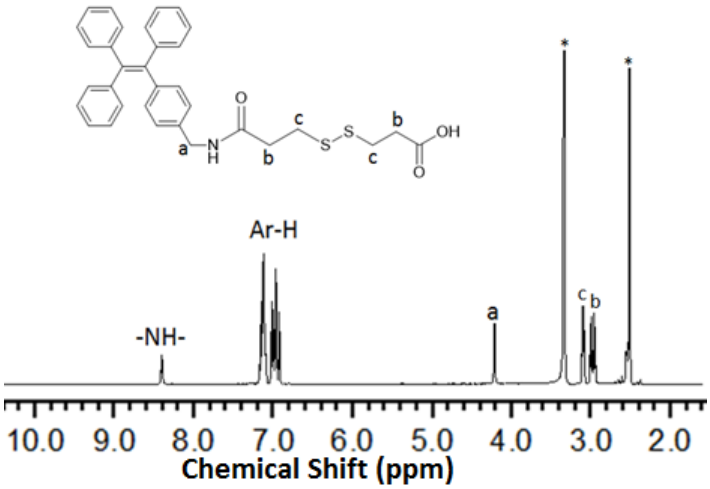

Figure S2.11. ^{1}H NMR spectrum of TPE-SS-COOH in DMSO-d_6.

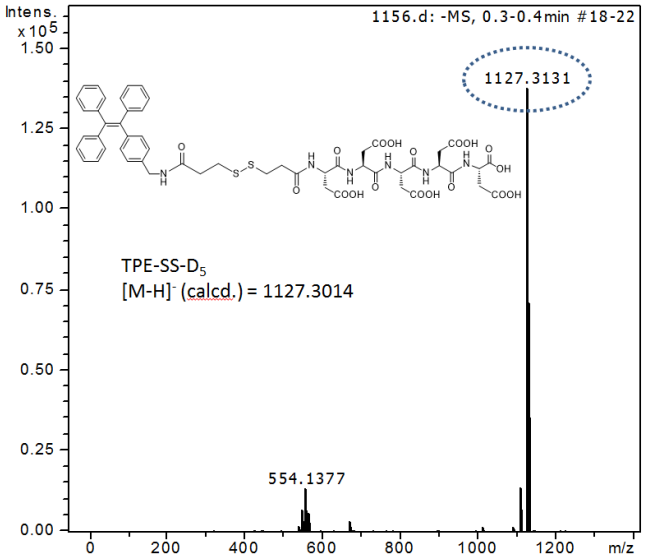

Figure S2.12. ESI-MS spectrum of TPE-SS-D_5.

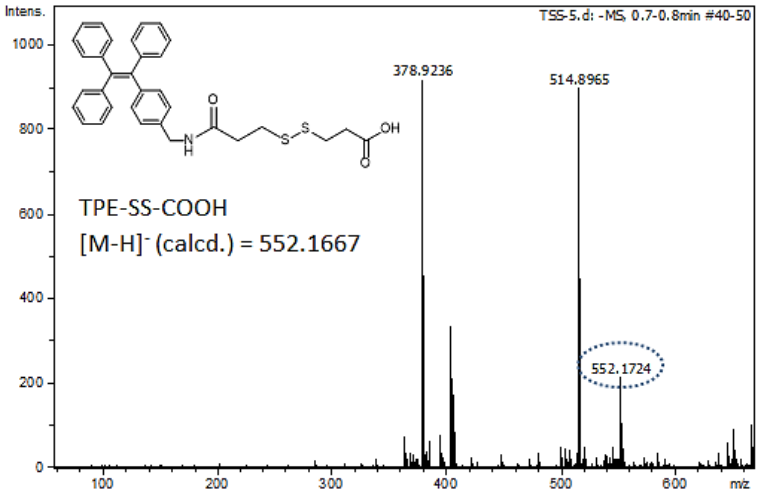

Figure S2.13. ESI-MS spectrum of TPE-SS-COOH.

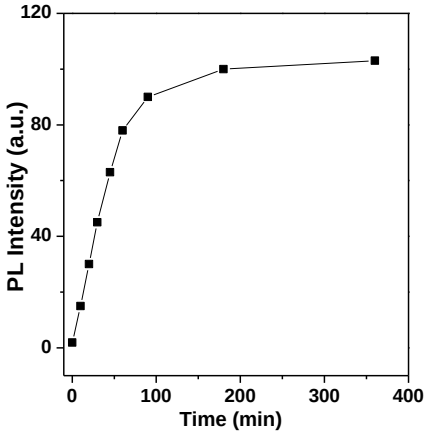

Figure S2.14. The plot of fluorescence intensity versus incubation time for the response of TPE-SS-D_5 to GSH (λ_{ex} = 304 nm).

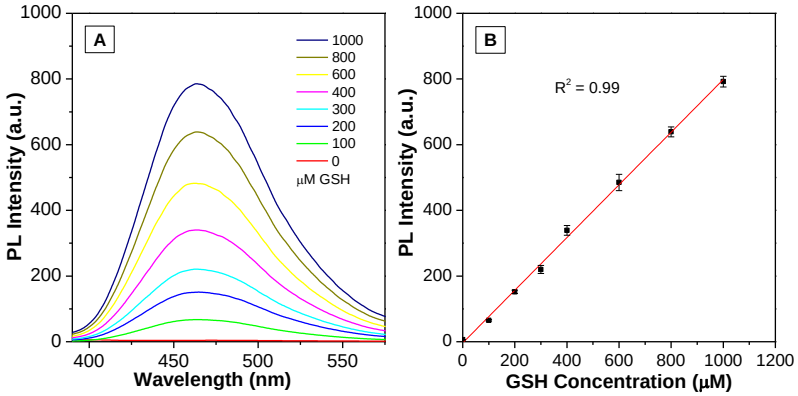

Figure S2.15. (A) PL spectra of 1.0 mM TPE-SS-D_5 upon addition of increasing concentrations of GSH from 0 to 1000 μM, incubation time: 90 min; (B) Plot of PL intensities of 1.0 mM TPE-SS-D_5 in DMSO/H_2O (v/v = 1/199) at 465 nm versus increasing concentrations of GSH (λ_{ex} = 304 nm).

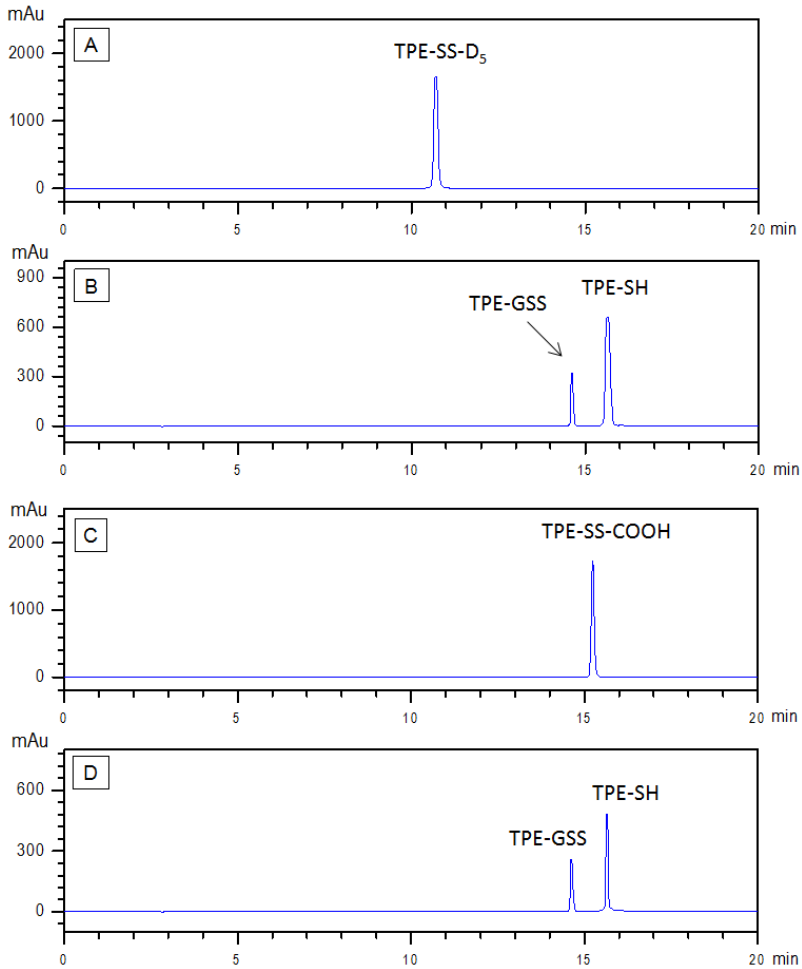

Figure S2.16. HPLC spectra of (A) TPE-SS-D_5 and (B) the product after incubation with GSH; (C) TPE-SS-COOH and (D) the product after incubation with GSH for 3 h. λ_{ex} = 304 nm.

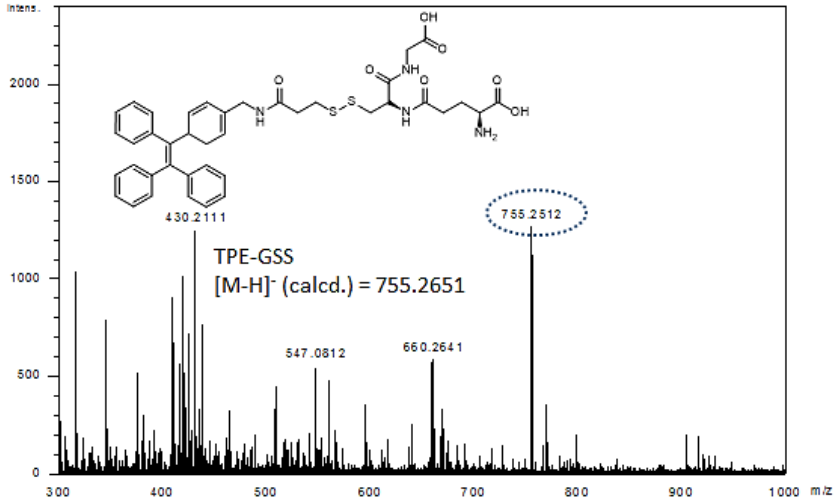

Figure S2.17. ESI-MS spectrum of TPE-GSS.

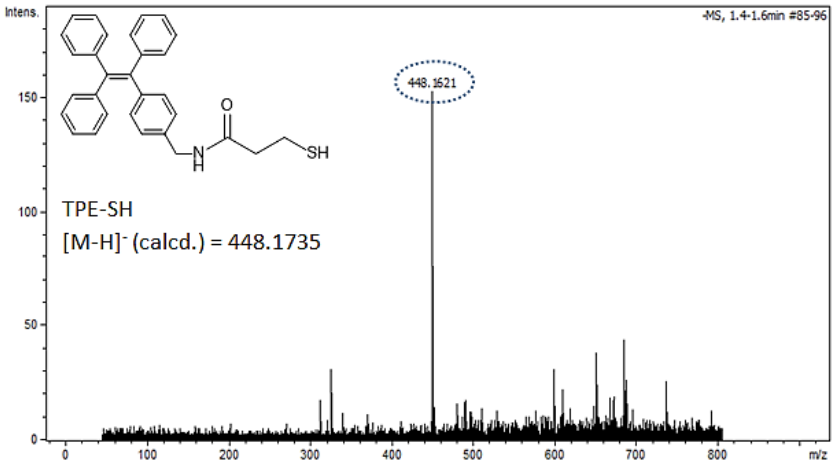

Figure S2.18. ESI-MS spectrum of TPE-SH.

Reference:

1. Wang, Z.; Chen, S.; Lam, J. W.; Qin, W.; Kwok, R. T.; Xie, N.; Hu, Q.; Tang, B. Z. Long-Term Fluorescent Cellular Tracing by the Aggregates of AIE Bioconjugates. *J. Am. Chem. Soc.* **2013,** *135*, 8238-8245.

2. Yuan, Y.; Kwok, R. T.; Feng, G.; Liang, J.; Geng, J.; Tang, B. Z.; Liu, B. Rational Design of Fluorescent Light-up Probes Based on an AIE Luminogen for Targeted Intracellular Thiol Imaging. *Chem. Commun.* **2014,** *50*, 295-297.

APPENDIX 2 for Chapter 3

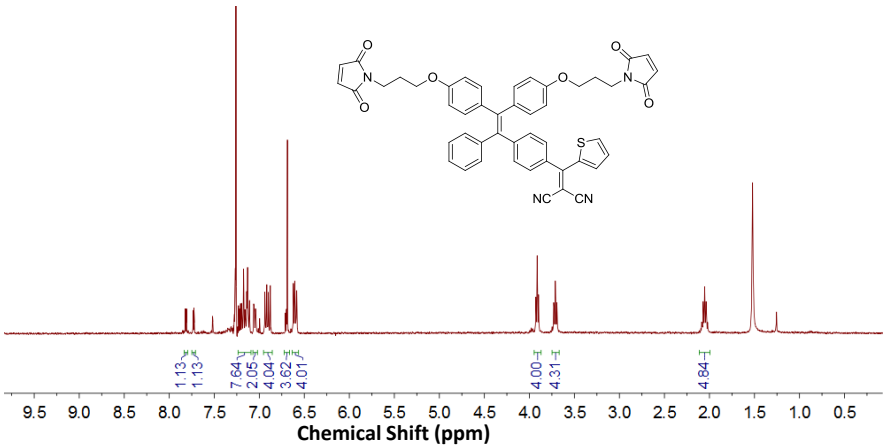

Figure S3.1. ^{1}H NMR spectrum of TPETH-2MAL.

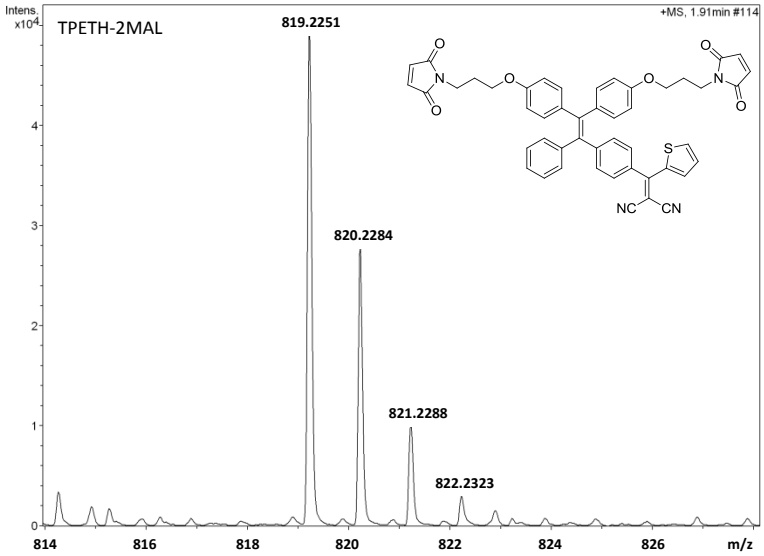

Figure S3.2. HRMS (ESI-MS) spectrum of TPETH-2MAL.

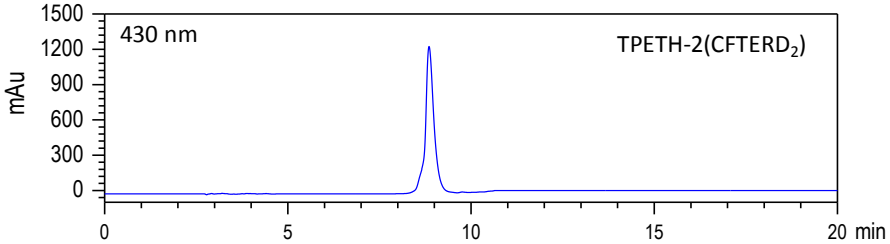

Figure S3.3 HPLC spectrum of the probe TPETH-2(CFTERD$_2$) monitored by absorbance at 430 nm.

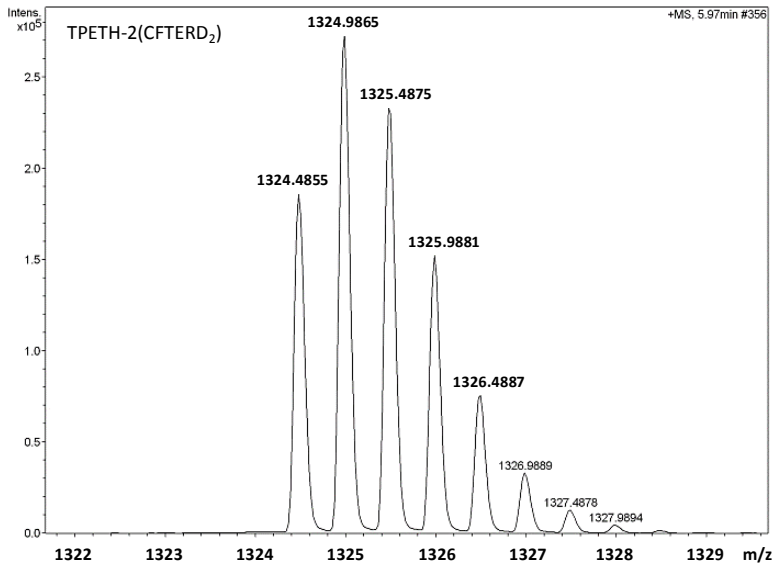

Figure S3.4. HRMS (ESI-MS) spectrum of TPETH-2(CFTERD$_2$).

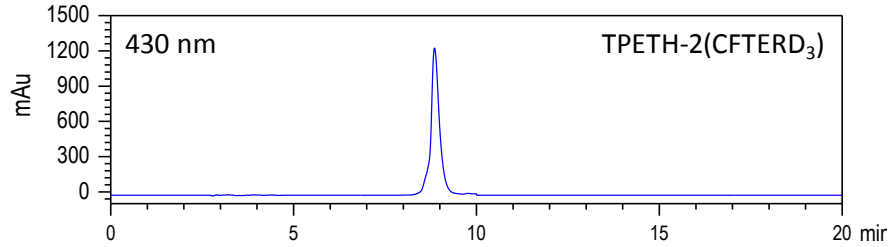

Figure S3.5. HPLC spectrum of the probe TPETH-2(CFTERD$_3$) monitored by absorbance at 430 nm.

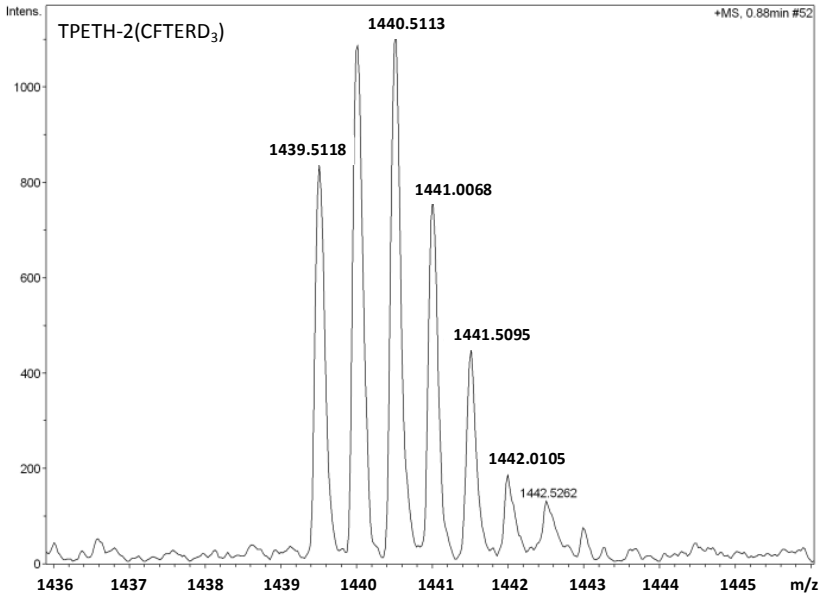

Figure S3.6. HRMS (ESI-MS) spectrum of TPETH-2(CFTERD$_3$).

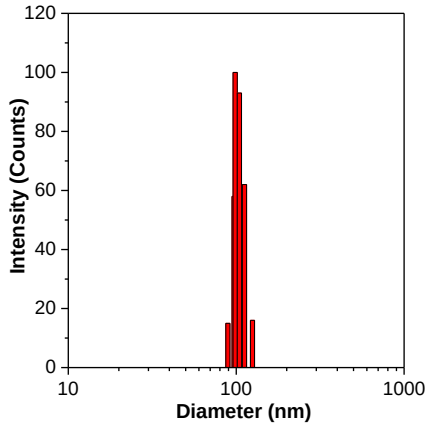

Figure S3.7. Hydrodynamic diameter of TPETH-2MAL in DMSO/PBS (v/v = 1/99) measured by laser light scattering (LLS). [TPETH-2MAL] = 20 μM.

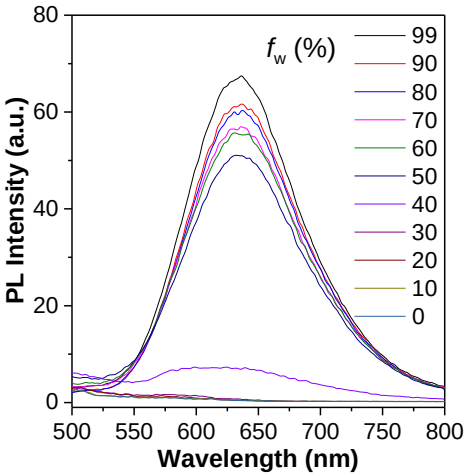

Figure S3.8. PL spectra of TPETH-2MAL (10 μM) in DMSO/H_2O mixture with increasing volume fraction of water.

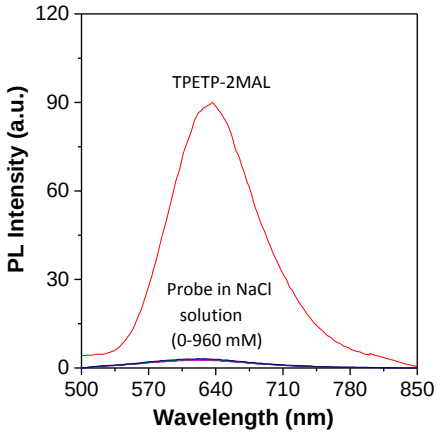

Figure S3.9. PL spectra of the probe TPETH-2(CFTERD$_3$) in aqueous media with increasing NaCl concentration from 0-960 mM. [TPETH-2(CFTERD$_3$)] = 10 μM.

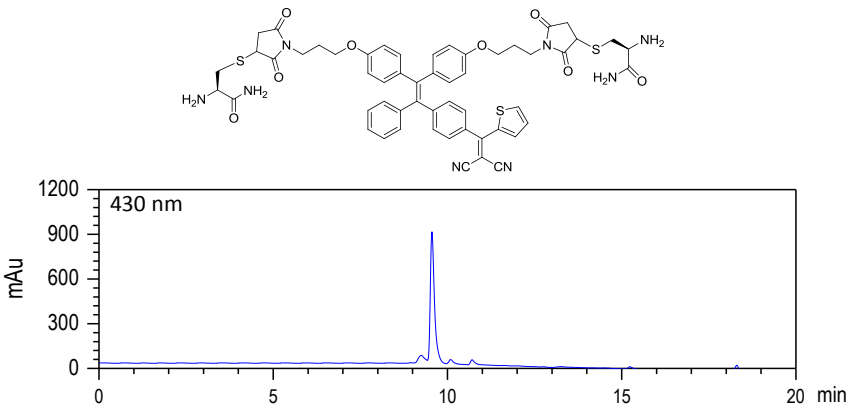

Figure S3.10. HPLC spectrum of the cleavage product TPETH-2C monitored by absorbance at 430 nm.

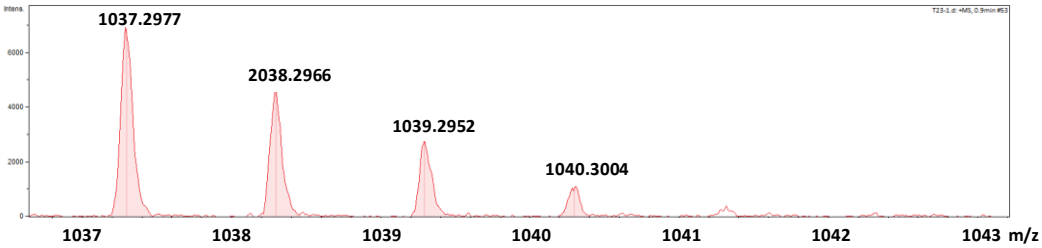

Figure S3.11. HRMS (ESI-MS) spectrum of the cleavage product TPETH-2C, m/z: $[M+H]^+$, calcd for $C_{54}H_{52}N_8O_8S_3$, 1037.3148; found, 1037.2977.

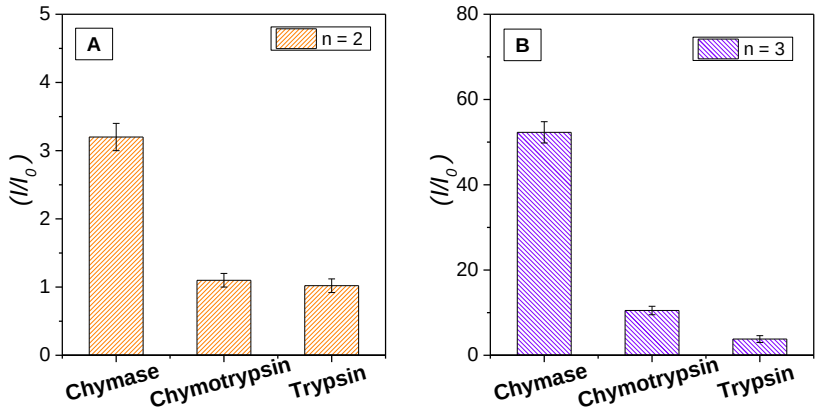

Figure S3.12. Comparison of PL enhancement for the probes TPETH-2($CFTERD_n$) (n = 2 or 3) when they are incubated with enzymes including chymase, chymotrypsin and trypsin. [probe] = 10 μM, [enzymes] = 5 nM.

APPENDIX 3 for Chapter 4

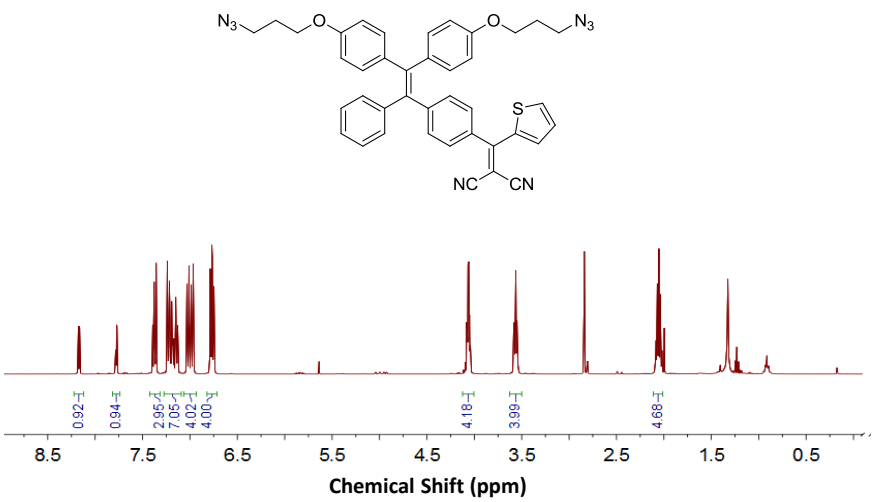

Figure S4.1. ^{1}H NMR spectrum of TPETH-2N$_3$ in d_6-DMSO.

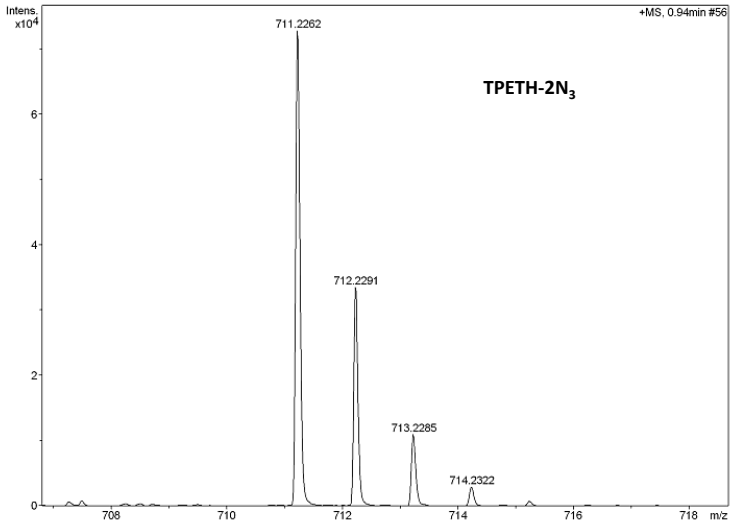

Figure S4.2. HRMS (ESI-MS) spectrum of TPETH-2N$_3$, m/z: [M+Na]$^+$, calcd for $C_{40}H_{32}N_8O_2S$, 711.2261; found, 711.2262.

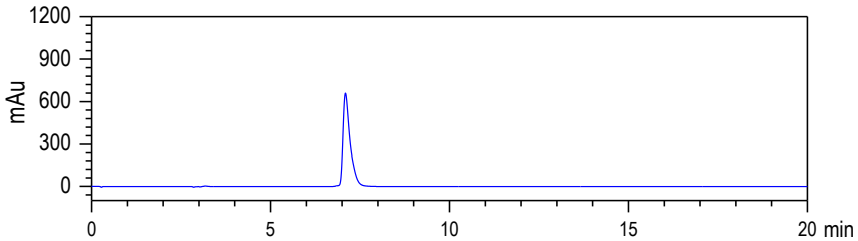

Figure S4.3. HPLC spectrum of the probe TPETH-2T7 monitored by absorbance at 430 nm.

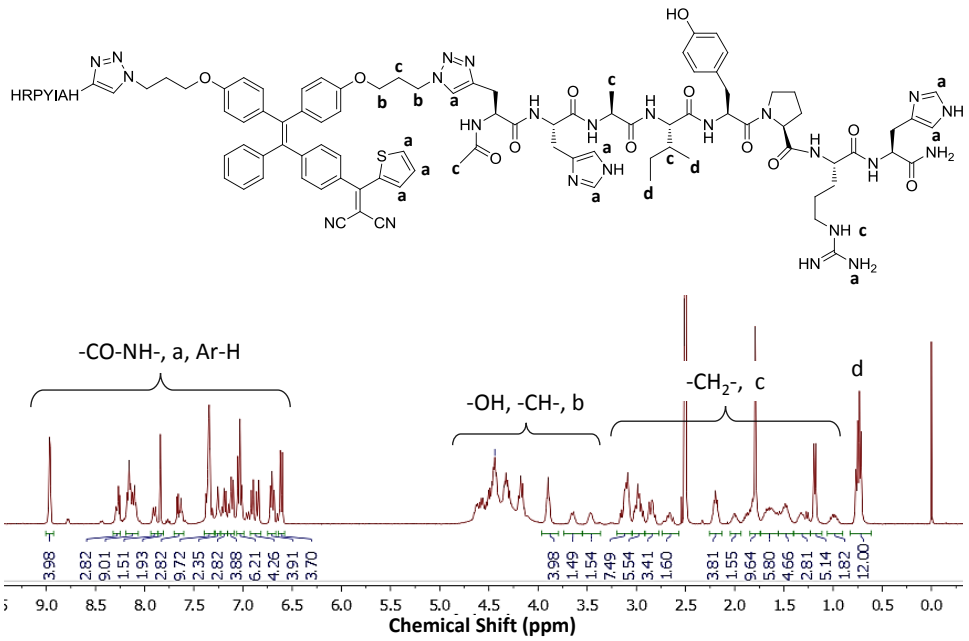

Figure S4.4. ^{1}H NMR spectra of the probe TPETH-2T7 in d_6-DMSO.

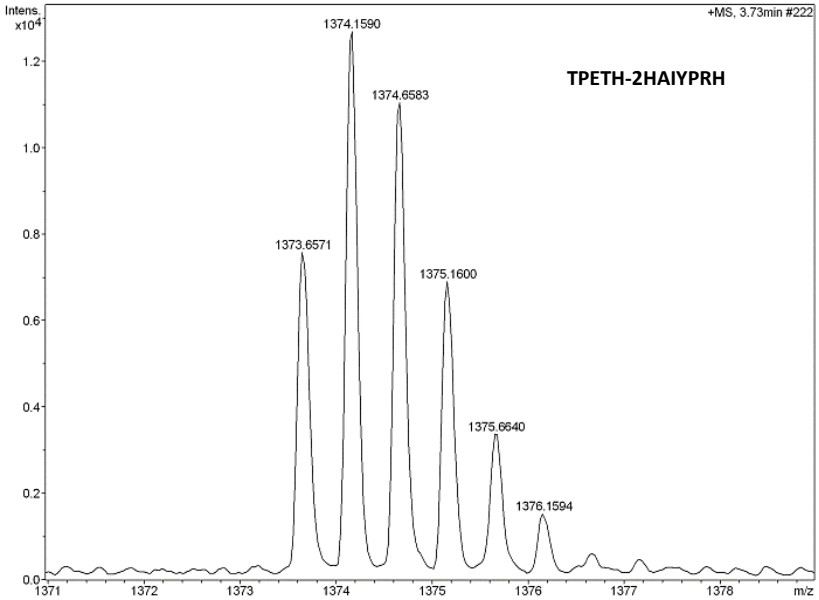

Figure S4.5. HRMS (ESI-MS) spectrum of TPETH-2T7, m/2z: $[M+2H]^{2+}$, calcd for $C_{136}H_{168}N_{40}O_{22}S$, 1373.6562; found, 1373.6571.

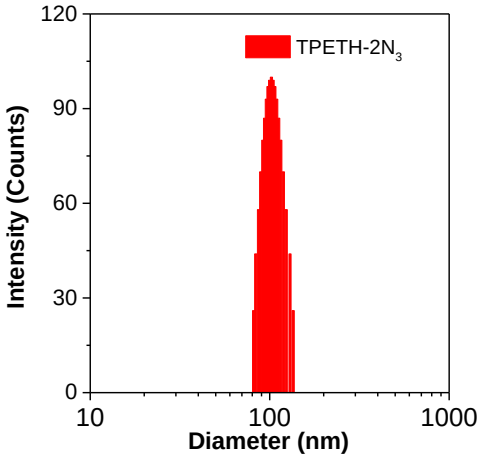

Figure S4.6. Hydrodynamic diameter of TPETH-2N_3 in DMSO/PBS (v/v = 1/99) measured by laser light scattering (LLS). [TPETH-2N_3] = 10 μM.

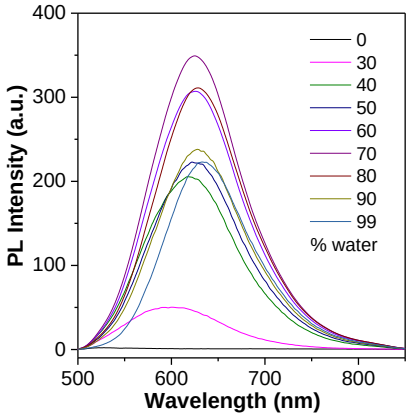

Figure S4.7. PL spectra of TPETH-2N_3 (10 μM) in DMSO/H_2O mixture with increasing proportion of water.

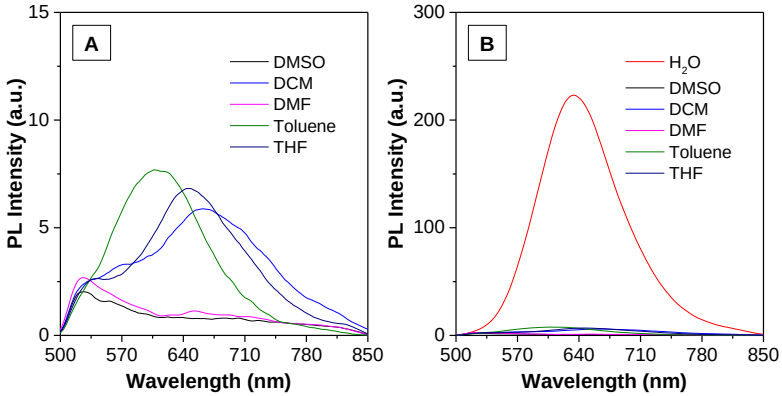

Figure S4.8. PL spectra of TPETH-2N_3 in different organic solvent and H_2O. [TPETH-2N_3] = 10 μM.

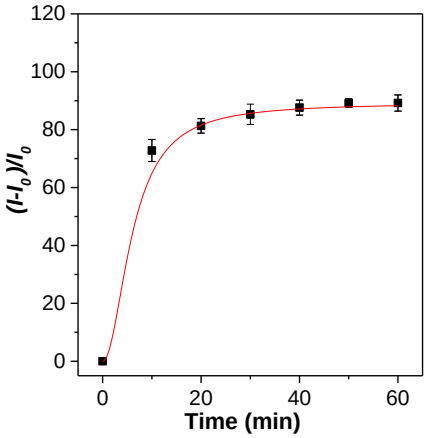

Figure S4.9. Time-dependent PL intensities of the probe TPETH-2T7 upon addition of 100 μg/mL TfR monitored within 60 min.

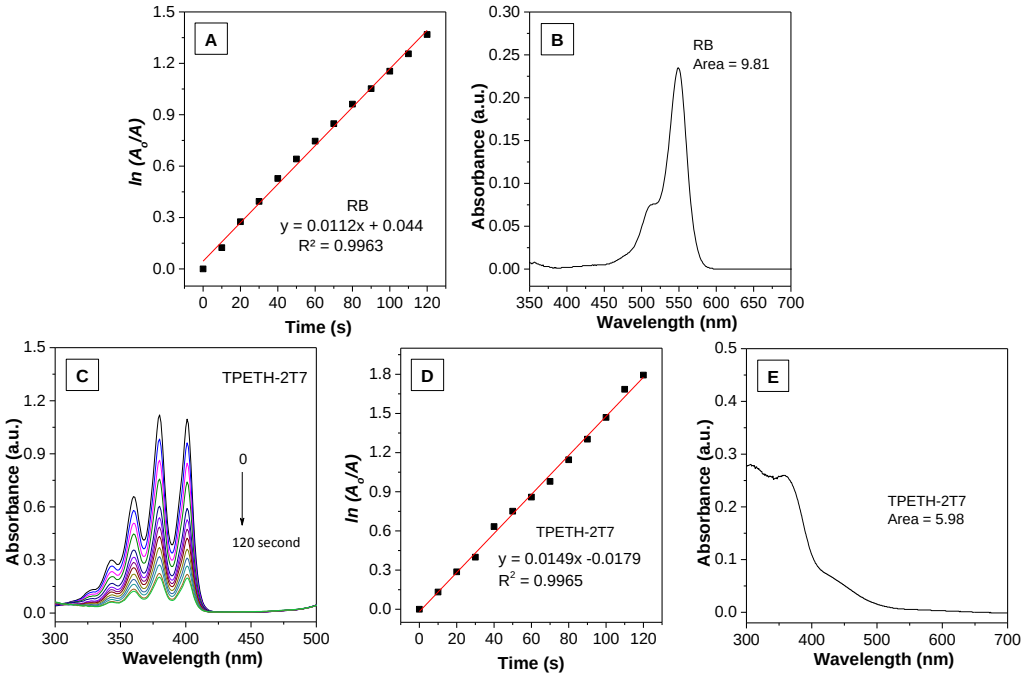

Figure S4.10. (A) Plot of the absorbance at 380 nm of ABDA against exposure time in the presence of Rose Bengal (RB); (B) UV-vis absorption spectrum and integration area of RB; (C) UV-vis spectra of ABDA upon white light irradiation from 0 to 120s in the presence of the 10 μM probe solution; (D) plot of the absorbance at 380 nm of ABDA against exposure time in the presence of probe solution; and (D) UV-vis absorption spectrum and integration area of 10 μM probe.

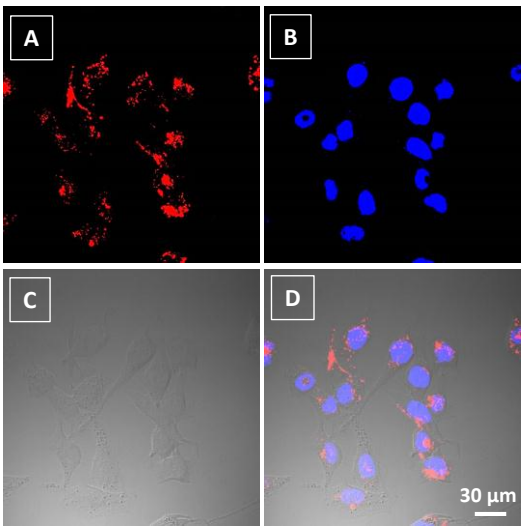

Figure S4.11. Confocal images of MDA-MB-231 cells after incubation with TPETH-2T7 for 0.5 h and removal of free probe followed by incubation for another 4 h at room temperature. The blue fluorescence is from the nuclei stained by Hoechst 33342 and the red fluorescence is from TfR/TPETH-2T7 complex. All the images share the same scale bar of 30 µm.

APPENDIX 4 for Chapter 5

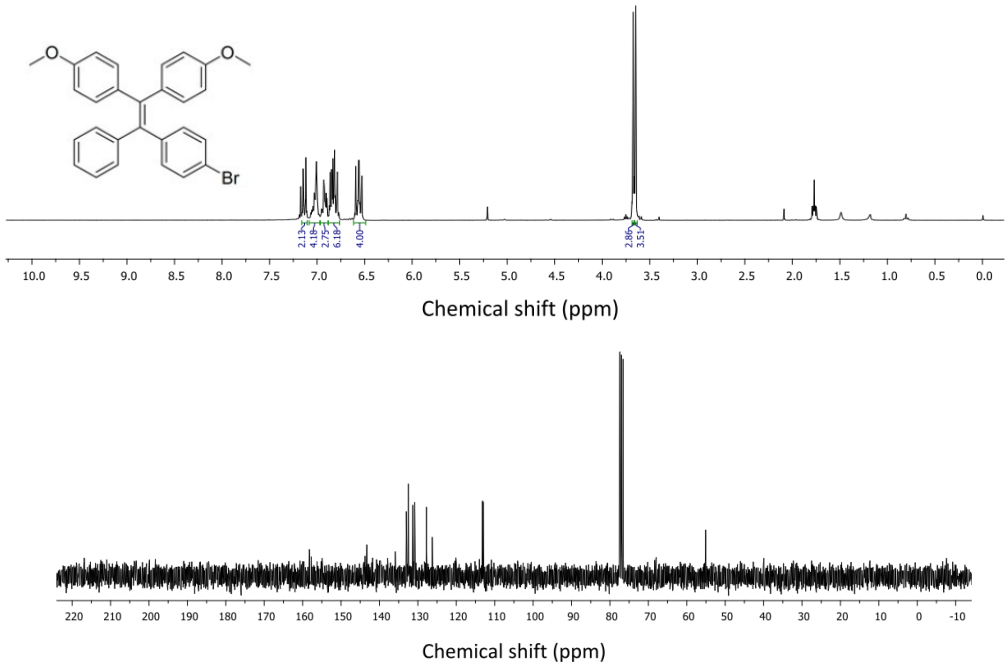

Figure S5.1 ^{1}H NMR and ^{13}C NMR spectra of Compound **1** in $CDCl_3$.

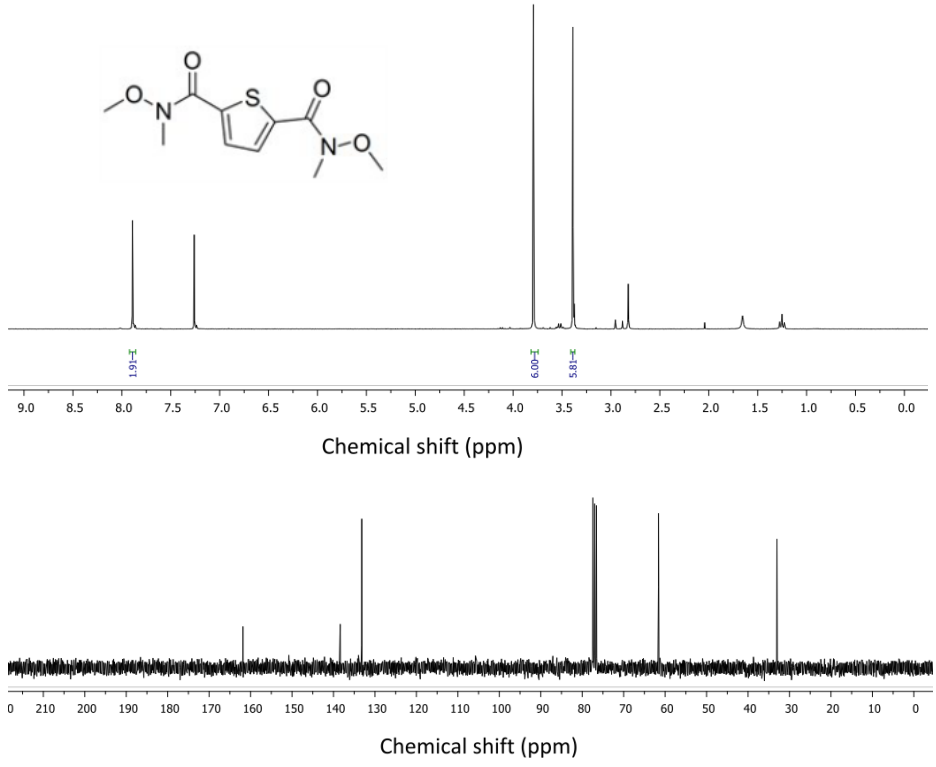

Figure S5.2 ^{1}H NMR and ^{13}C NMR spectra of Compound **2** in $CDCl_3$.

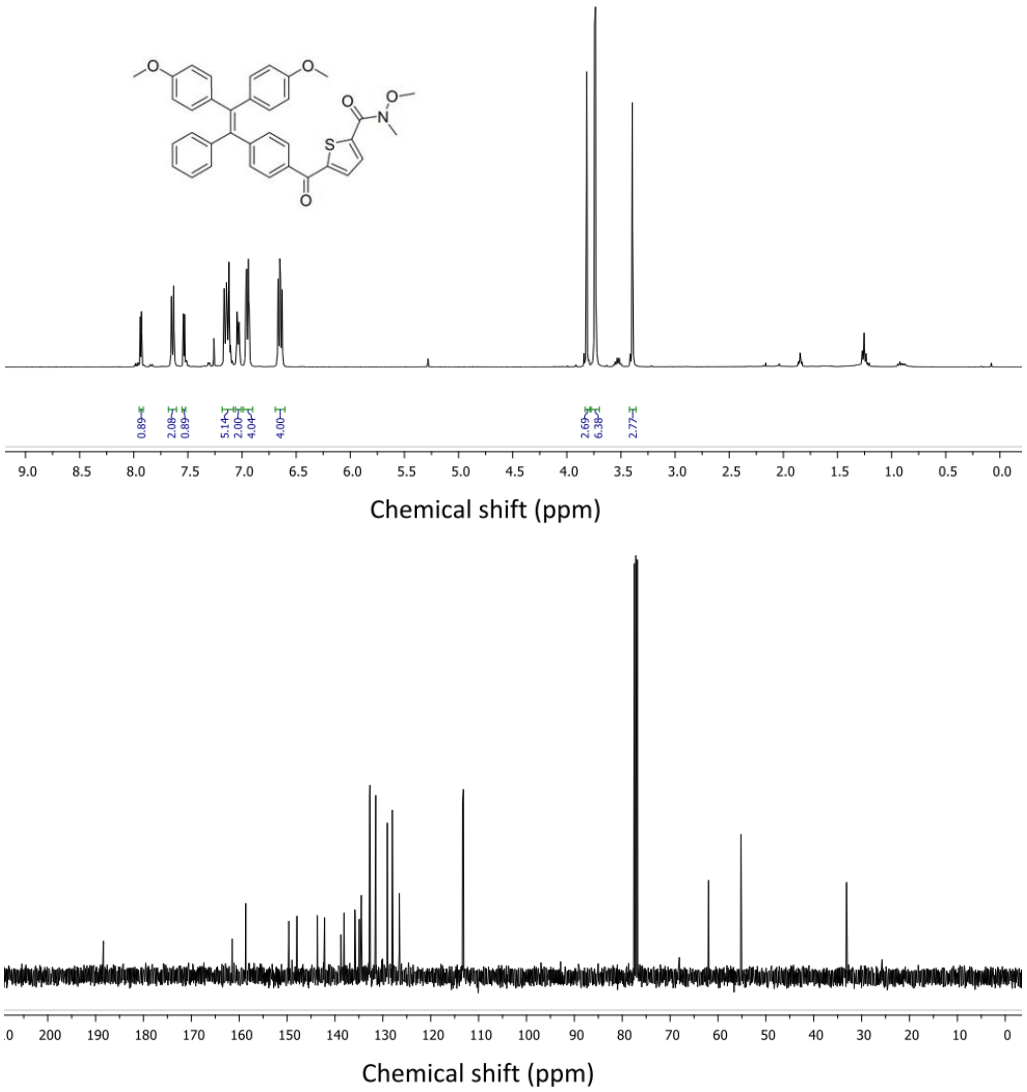

Figure S5.3 ^{1}H NMR and ^{13}C NMR spectra of Compound **3** in $CDCl_3$.

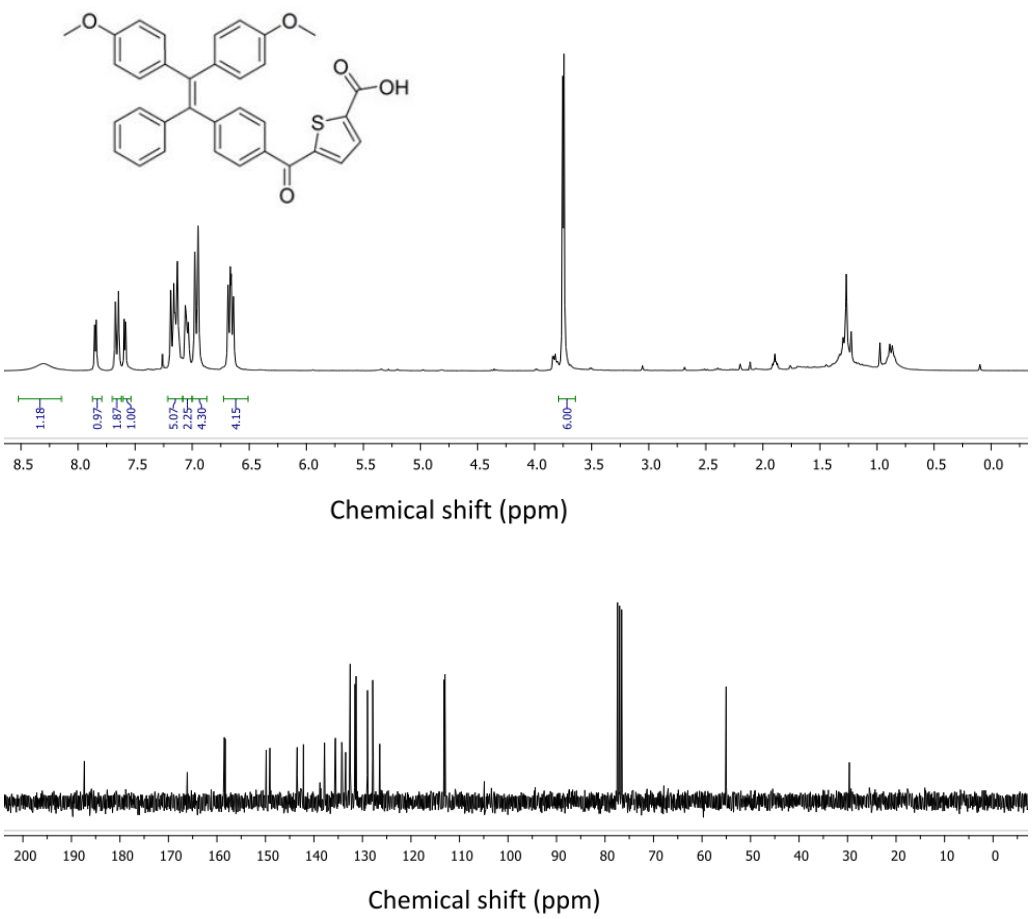

Figure S5.4 ^{1}H NMR and ^{13}C NMR spectra of Compound **4** in $CDCl_3$.

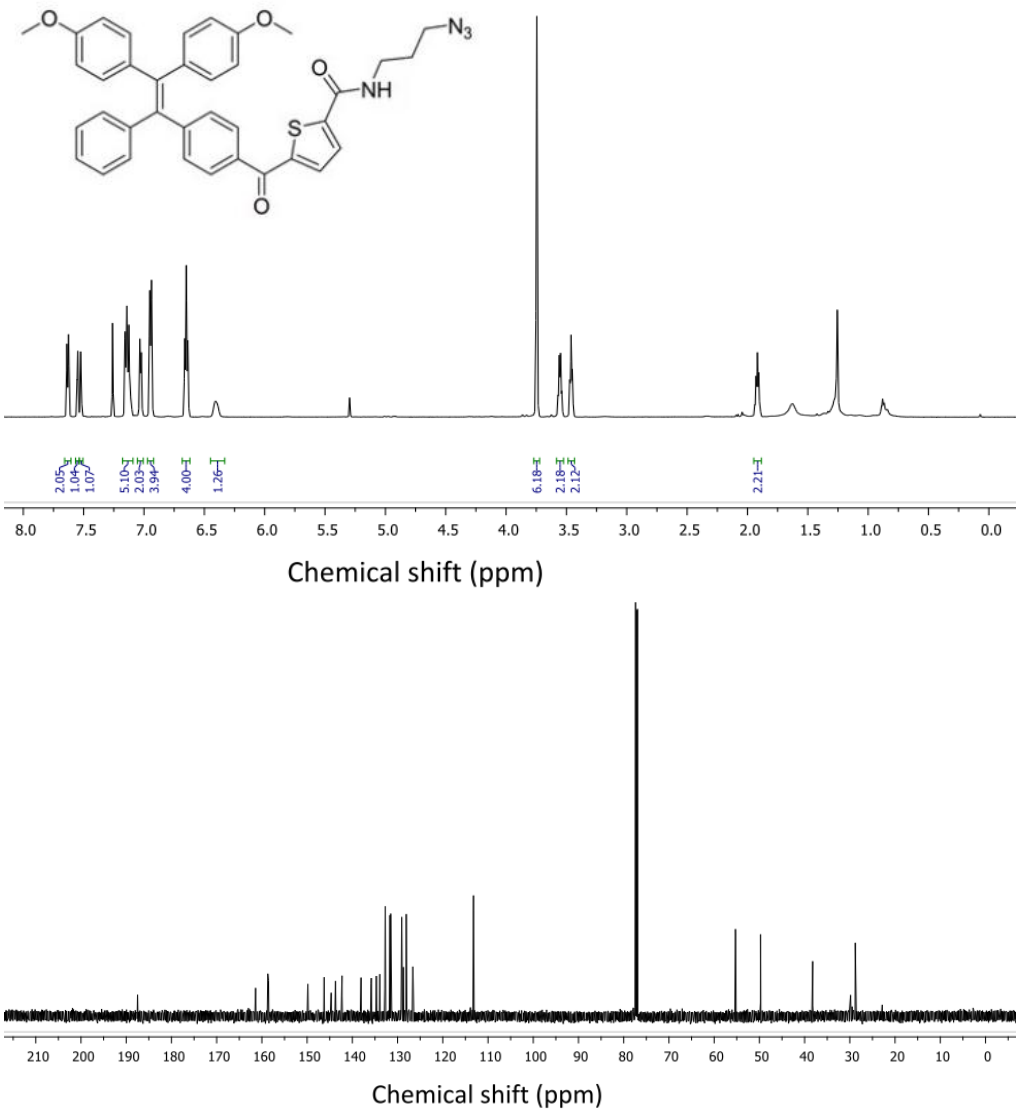

Figure S5.5 ^{1}H NMR and ^{13}C NMR spectra of Compound **5** in $CDCl_3$.

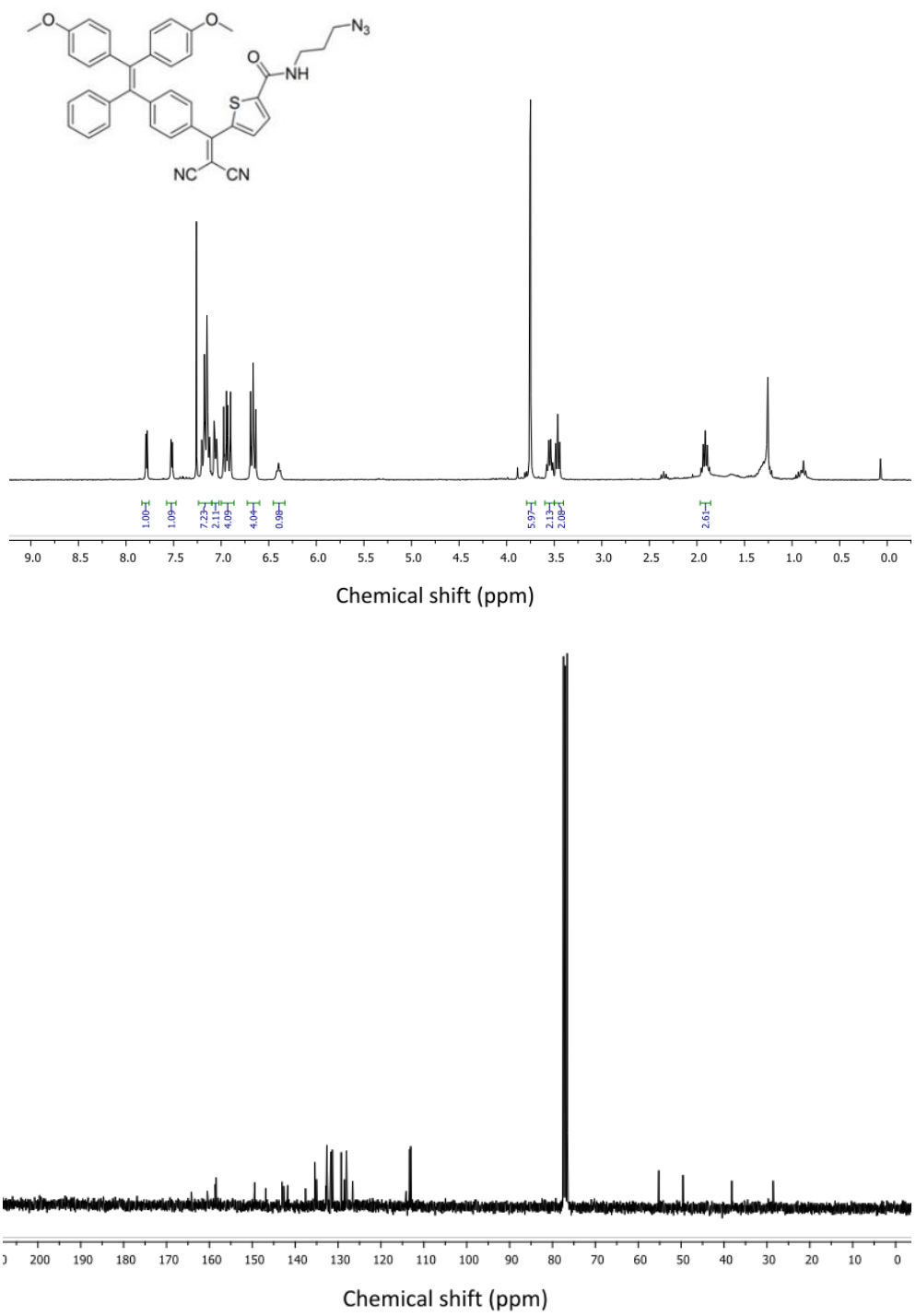

Figure S5.6 ^{1}H NMR and ^{13}C NMR spectra of Compound TPETP-N_3 in $CDCl_3$.

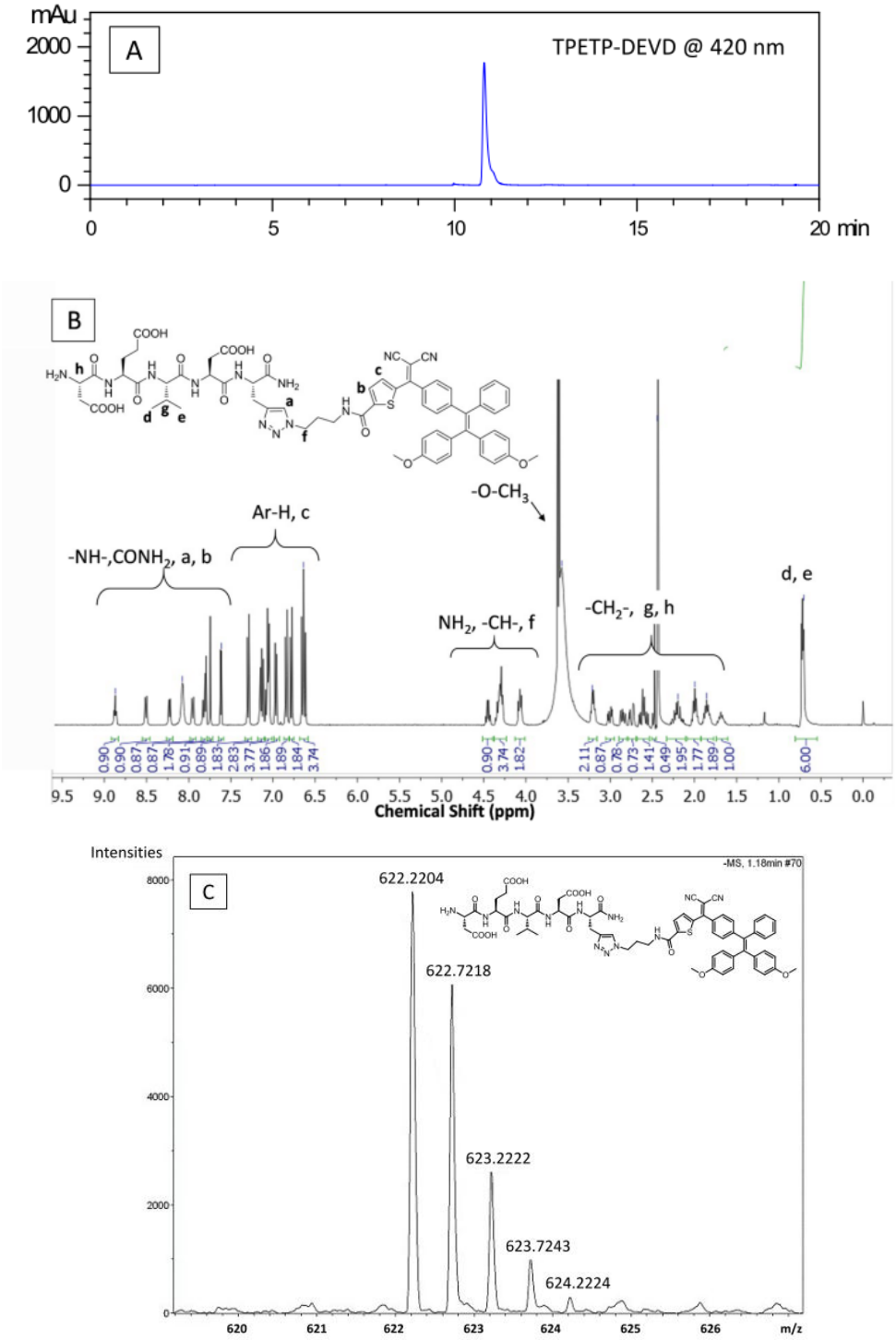

Figure S5.7 HPLC spectrum of TPETP-DEVD; ^{1}H NMR spectrum of TPETP-DEVD in DMSO-*d*$_6$; High resolution mass spectrum (ESI-MS) of TPETP-DEVD. ($C_{63}H_{64}N_{12}O_{14}S$, $[M-2H]^{2-}$,Calcd: 622.2198, measured: 622.2204).

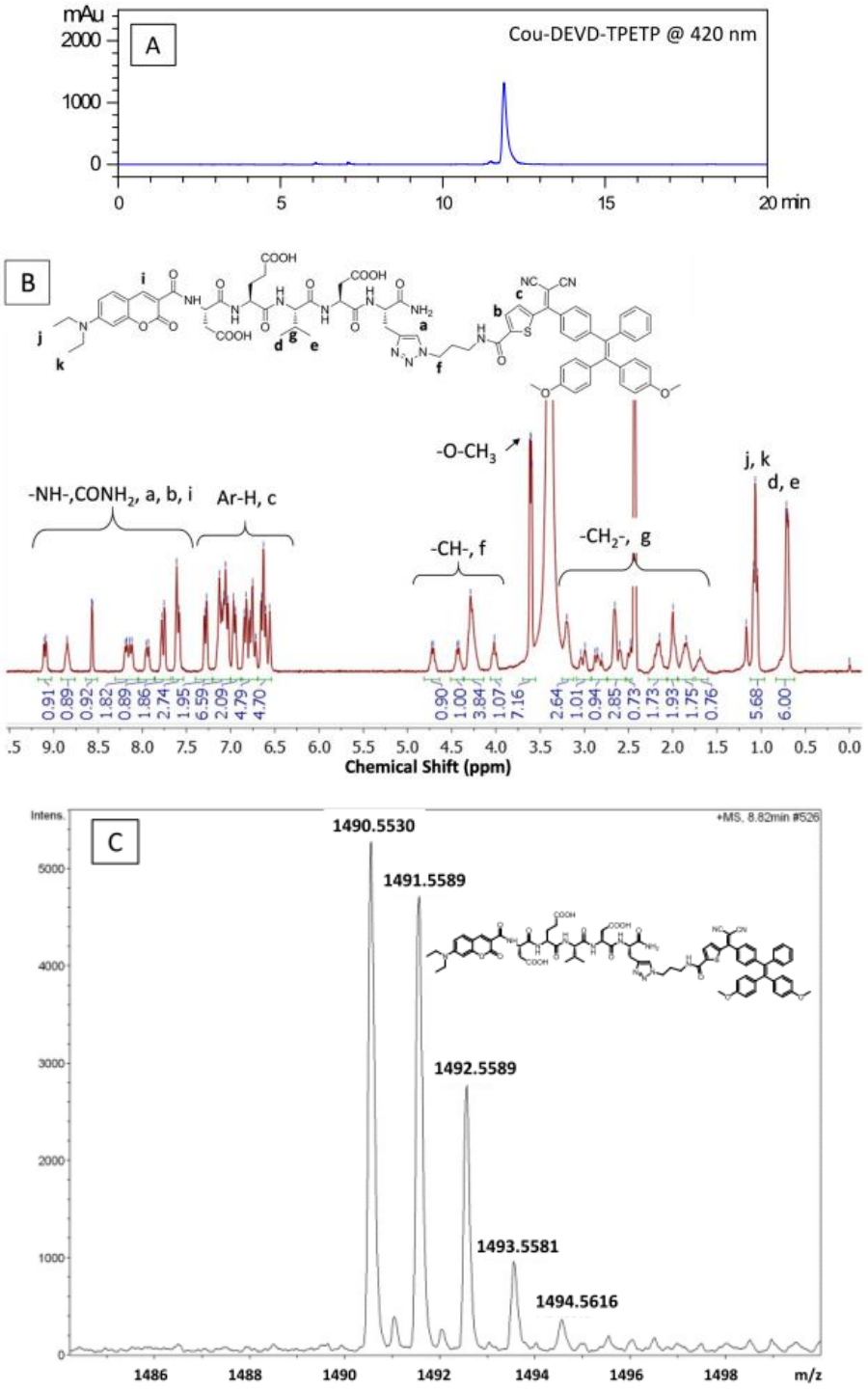

Figure S5.8 HPLC spectra of Cou-DEVD-TPETP; ^{1}H NMR spectrum of Cou-DEVD-TPETP in DMSO-*d*$_6$; High resolution mass spectrum (ESI-MS) of Cou-DEVD-TPETP, $C_{77}H_{80}N_{13}O_{17}S$, $[M+H]^+$ calcd: 1490.5510, Measured: 1490.5530.

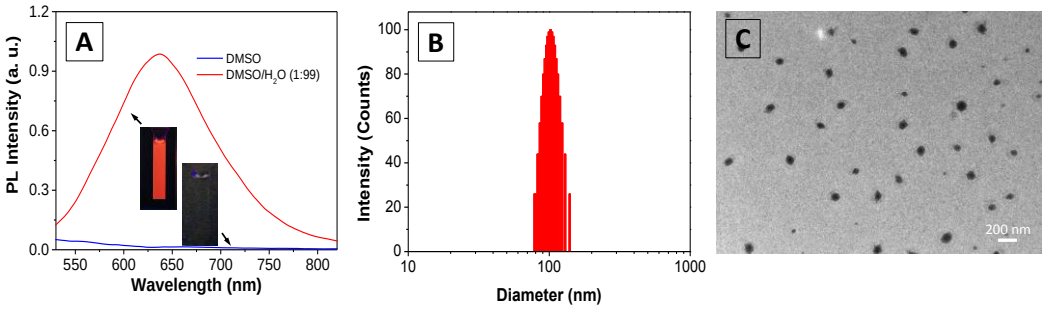

Figure S5.9 (A) Photoluminescence (PL) spectra of TPETP-N_3 (10 μM) in DMSO or DMSO/water mixtures (v/v = 1/99). Inset: the digital photographs of TPETP-N_3 (10 μM) in DMSO or DMSO/water mixtures (v/v = 1/99) under illumination of a UV lamp at 365 nm. (B) Laser light scattering data and (C) TEM image of TPETP-N_3 (10 μM) in DMSO/water mixtures (v/v = 1/99).

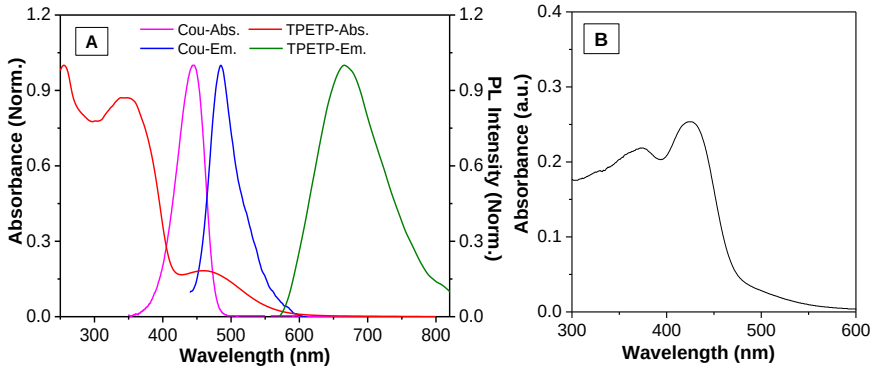

Figure S5.10 (A) Normalized UV-vis absorption and photoluminescence (PL) spectra of Cou and TPETP in DMSO/PBS buffer (v/v = 1/99); (B) UV-vis absorption spectra of the probe Cou-DEVD-TPETP.

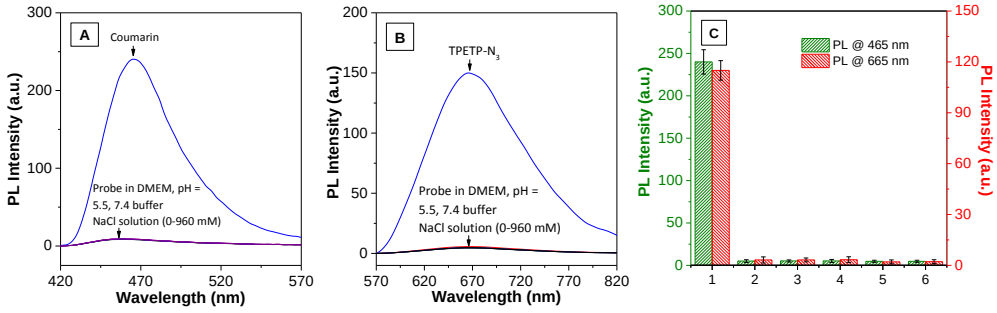

Figure S5.11 PL spectra of the Cou-DEVD-TPETP (10 μM) monitored at 420-570 nm and 570-820 nm upon excitation at 405 nm referenced against free coumarin and TPETP-N_3 in water containing [NaCl] ranging from 0, 250, 500, 960 mM, in cell culture medium (DMEM) or in buffer solutions with pH of 7.4 and 5.5 (C, DMSO/PBS buffer and DMSO/acetate buffer, v/v = 1/99), respectively (Entry 1-8).

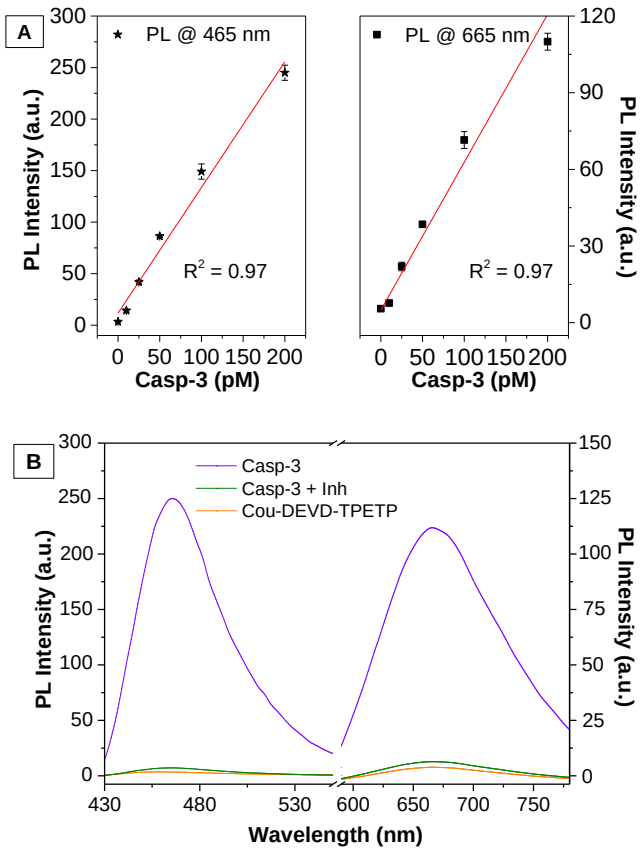

Figure S5.12 (A) PL intensities monitored at 465 nm and 665 nm for Cou-DEVD-TPETP (10 μM) probe upon incubation with caspase-3 at different concentrations; (B) PL spectra of Cou-DEVD-TPETP without and with treatment of caspase-3 in the presence and absence of inhibitor 5-[(S)-(+)-2-(methoxymethyl)pyrrolidino] sulfonylisatin (10 μM). (λ_{ex}: 405 nm, emission collected from 430 - 550 nm is from the Cou-DEVD and that at 590 – 780 nm is from the TPETP residue).

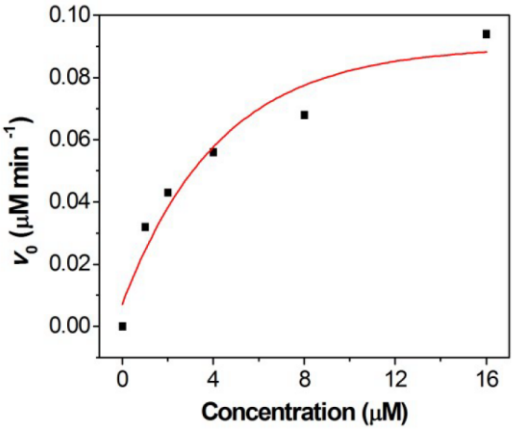

Figure S5.13 Michaelis-Menton plot for the hydrolysis of Cou-DEVD-TPETP at different concentrations by caspase-3 (100 pM).

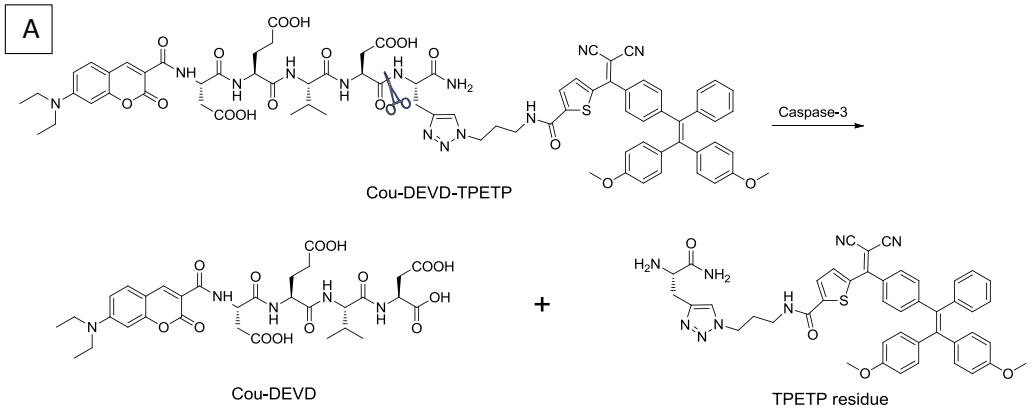
A
Caspase-3
Cou-DEVD-TPETP
Cou-DEVD
TPETP residue

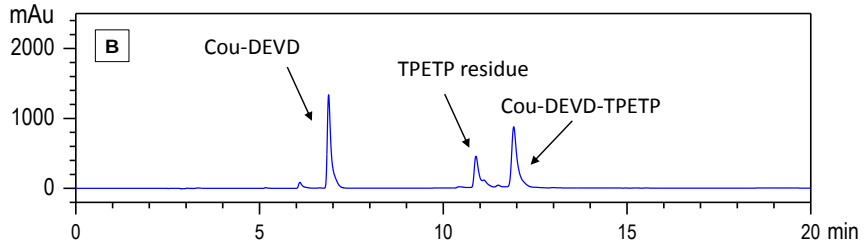
mAu
2000
1000
0
B
Cou-DEVD
TPETP residue
Cou-DEVD-TPETP
0
5
10
15
20 min

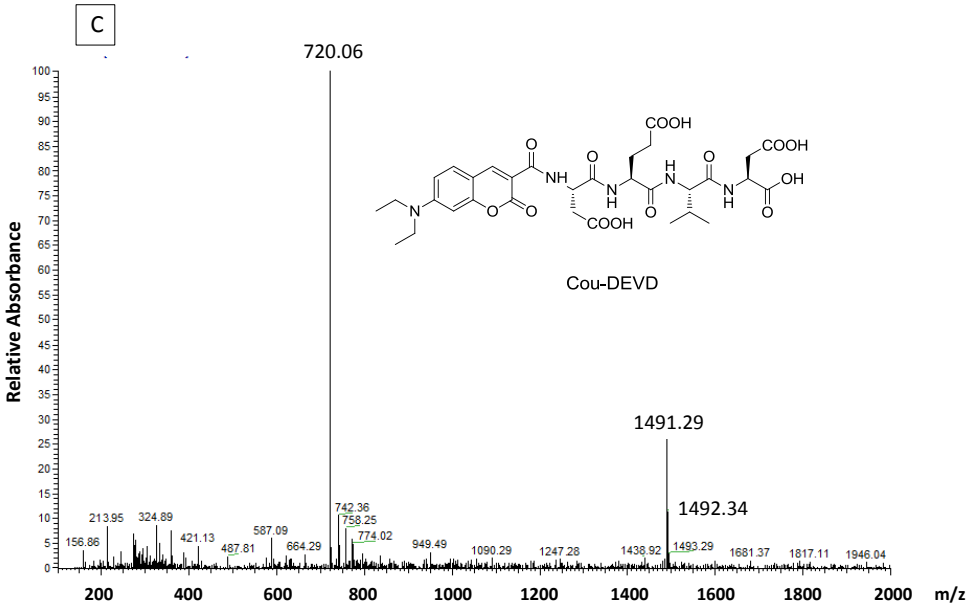
C
720.06
Cou-DEVD
1491.29
1492.34
Relative Absorbance
m/z

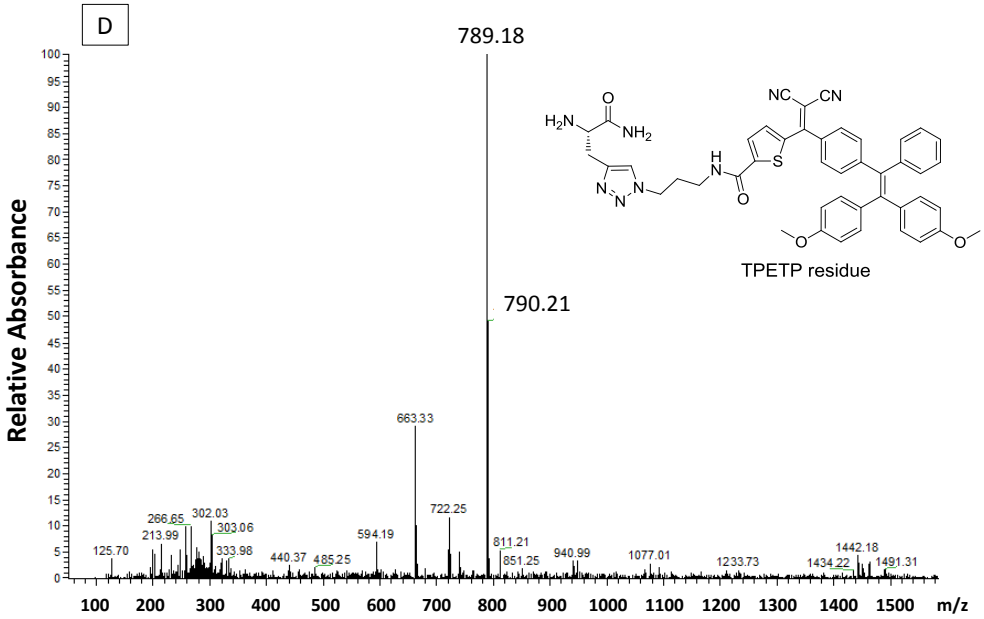

Figure S5.14. The caspase-catalyzed hydrolysis of Cou-DEVD-TPETP (t = 1 h) monitored by reverse phase HPLC; Mass spectra (ESI-MS) of Cou-DEVD ($[M+H]^+$ calcd: 720.28, Measured: 720.06) and TPETP residue ($[M+H]^+$ calcd: 788.29, Measured: 789.18).

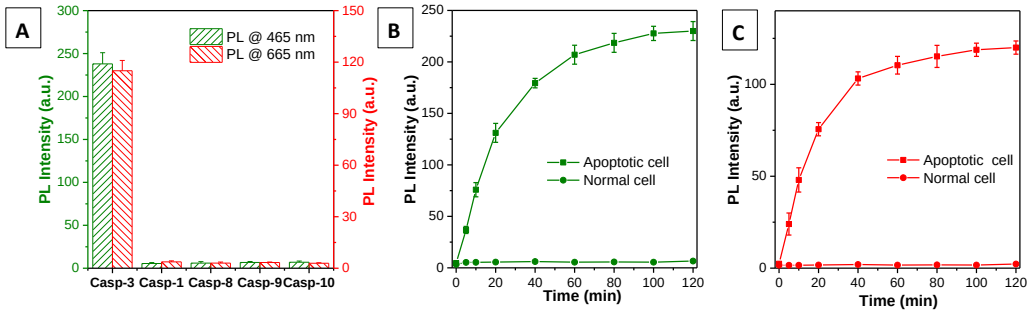

Figure S5.15 (A) PL intensities monitored at 465 nm and 665 nm for Cou-DEVD-TPETP in responsive to different caspase enzymes. (B, C) Time-dependent PL intensity changes of Cou-DEVD-TPETP in apoptotic and normal HeLa cell lysate (B) Monitored at 465 nm, and (C) monitored at 665 nm. Data represent mean values ± standard deviation, n = 3.

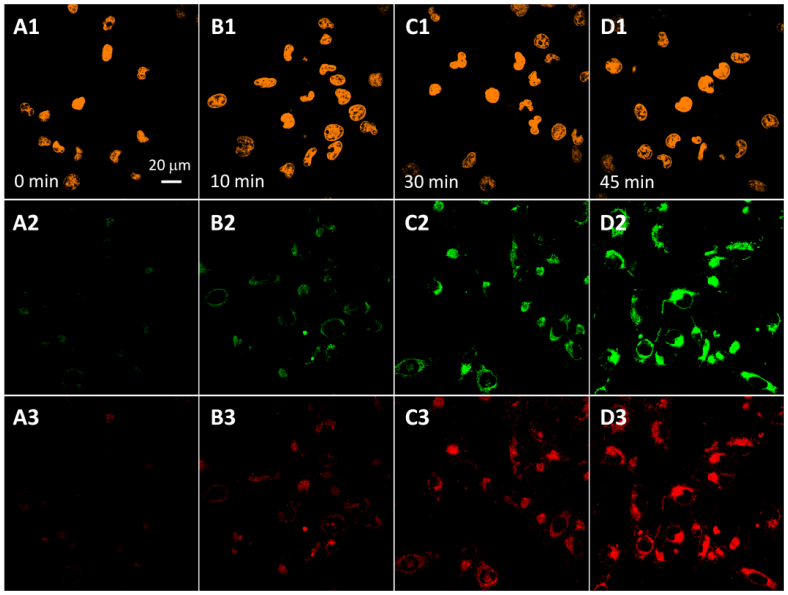

Figure S5.16. Confocal images of Cou-DEVD-TPETP (10 μM) incubated MDA-MB-231 cells treated with STS (1 μM) for (A) 0 min, (B) 10 min, (C) 30 min and (D) 45 min. Orange fluorescence (nucleus dyed with SYTO® orange, A1-D1, E_x: 543 nm, E_m: 610-640 nm); green fluorescence (A2-D2, E_x: 405 nm; E_m: 505-525 nm); red fluorescence (A3-D3, E_x: 405 nm, E_m: > 650 nm).

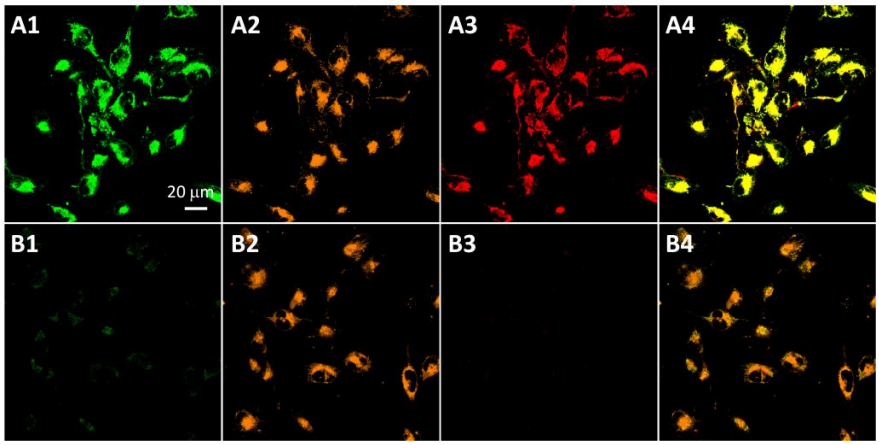

Figure S5.17. Confocal images of apoptotic MDA-MB-231 cells treated with Cou-DEVD-TPETP (10 μM) in the absence (A) and (B) presence of inhibitor and stained with anti-caspase-3 primary antibody and a Texas Red-labeled secondary antibody. Green fluorescence (Cou-DEVD, A1, B1, E_x: 405 nm; E_m: 505-525 nm); orange fluorescence (Texas Red, A2, B2, E_x: 543 nm, E_m: 610−640 nm); red fluorescence (TPETP residue, A3, B3, E_x: 405 nm, E_m: > 650 nm); A4, B4 are the overlay of images A1-A3 and B1-B3, respectively. Due to the low absorbance of TPETP residue at 543 nm, its spectral overlap with Texas Red is negligible.

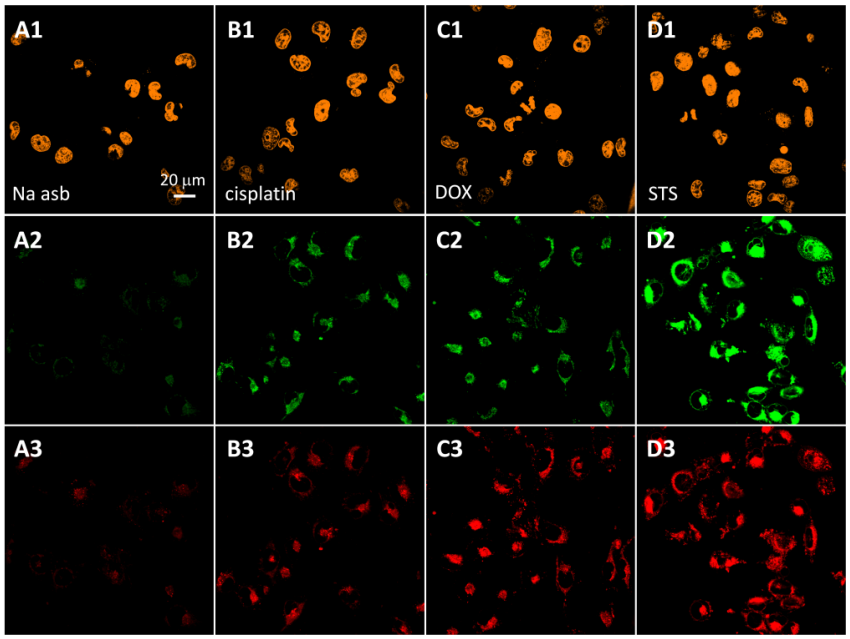

Figure S5.18. Confocal images of Cou-DEVD-TPETP (10 μM) incubated MDA-MB-231 cells upon treatment with (A) sodium ascorbate (Na asb), (B) cisplatin, (C) DOX and (D) STS. Orange fluorescence (nucleus dyed with SYTO® orange, A1-D1, E_x: 543 nm, E_m: 610-640 nm); green fluorescence (Cou-DEVD, A2-D2, E_x: 405 nm; E_m: 505-525 nm); red fluorescence (TPETP residue, A3-D3, E_x: 405 nm, E_m: > 650 nm).

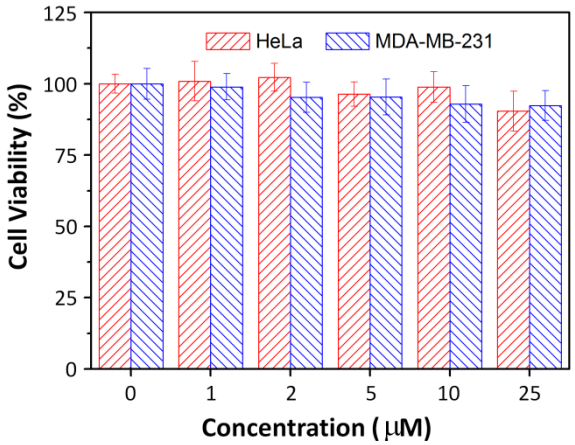

Figure S5.19. The viability of HeLa and MDA-MB-231 cells upon incubation with Cou-DEVD-TPETP at different concentrations for 48 h.

List of Publications

1. **R. Zhang**, Y. Yuan, J. Liang, R. T. K. Kwok, Q. Zhu, G. Feng, J. Geng, B. Z. Tang and B. Liu*; Fluorogen−Peptide Conjugates with Tunable Aggregation-Induced Emission Characteristics for Bioprobe Design; *ACS Appl. Mater. Interfaces*, **2014**, 6, 14302–14310. (Chapter 2)

2. **R. Zhang**, C. J. Zhang, G. Feng, F. Hu, J. Wang and B. Liu*; Specific Light-Up Probe with Aggregation-Induced Emission for Facile Detection of Chymase; *Anal. Chem.*, **2016**, 88, 9111–9117. (Chapter 3)

3. **R. Zhang**, G. Feng, C. J. Zhang, X. Cai, X. Cheng and B. Liu*; Real-Time Specific Light-Up Sensing of Transferrin Receptor: Image-Guided Photodynamic Ablation of Cancer Cells through Controlled Cytomembrane Disintegration; *Anal. Chem.*, **2016**, 88, 4841–4848. (Chapter 4)

4. Y. Yuan, **R. Zhang**, X. Cheng, S. Xu and B. Liu*; A FRET probe with AIEgen as the energy quencher: dual signal turn-on for self-validated caspase detection; *Chem. Sci.*, **2016**, 7, 4245-4250. (Co-first author, Chapter 5).

5. **R. Zhang**, R. T. K. Kwok, B. Z. Tang* and B. Liu*; Hybridization Induced Fluorescence Turn-On of AIEgen–Oligonucleotide Conjugates for Specific DNA Detection; *RSC Adv.*, **2015**, 5, 28332–28337.

6. **R. Zhang**, M. Gao, S. Bai and B. Liu*; A fluorescent light-up platform with "AIE + ESIPT" characteristics for multi-target detection both in solution and on paper strip; *J. Mater. Chem. B*, **2015**, 3, 1590-1596.

7. **R. Zhang,** C. J. Zhang, Z. Song, J. Liang, R. T. K. Kwok, B. Z. Tang and B. Liu*; AIEgens for Real-Time Naked-Eye Sensing of Hydrazine in Solution and on a Paper Substrate: Structure-Dependent Signal Output and Selectivity; *J. Mater. Chem. C*, **2016**, 4, 2834-2842.

8. Y. Yuan, R. T. K. Kwok, **R. Zhang**, B. Z. Tang and B. Liu*; Targeted Theranostic Prodrugs Based on an Aggregation-Induced Emission (AIE) Luminogen for Real-Time Dual-Drug Tracking; *Chem. Commun.*, **2014**, 50, 11465-11468.

9. G. Feng, J. Liu, **R. Zhang** and B. Liu*; Cell Imaging Using Red Fluorescent Light-up Probes Based on an Environment-Sensitive Fluorogen with Intramolecular Charge Transfer Characteristics; *Chem. Commun.*, **2014**, 50, 9497-9500.

10. Y. Yuan, S. Xu, C. J. Zhang, **R. Zhang** and B. Liu*; Dual-Targeted Activatable Photosensitizers with Aggregation-Induced Emission (AIE) Characteristics for Image-Guided Photodynamic Cancer Cell Ablation; *J. Mater. Chem. B*, **2016**, 4, 169-176.

11. W. Shen, J. Yu, J. Ge, **R. Zhang,** F. Cheng, X. Li, Y. Fan, S. Yu, B. Liu and Q. Zhu*; Light-Up Probes Based on Fluorogens with Aggregation-Induced Emission Characteristics for Monoamine Oxidase-A Activity Study in Solution and in Living Cells; *ACS Appl. Mater. Interfaces*, **2016**, 8, 927-935.

12. G. Feng, Y. Yuan, F. Hu, **R. Zhang,** B. Xing, G. Zhang, D. Zhang and B. Liu*; A Light-Up Probe with Aggregation-Induced Emission Characteristics (AIE) for Selective Imaging, Naked-Eye Detection and Photodynamic Killing of Gram-Positive Bacteria; **Chem. Commun., 2015**, 51, 12490-12493.

13. L. Peng, M. Gao, X. Cai, **R. Zhang,** K. Li, G. Feng, A. Tong and B. Liu*; A Fluorescent Light-Up Probe Based on AIE and ESIPT Processes for β-Galactosidase Activity Detection and Visualization in Living Cells; **J. Mater. Chem. B**, **2015**,**3**, 9168-9172.

14. Y. Yuan, C. J. Zhang, M. Gao, **R. Zhang**, B. Z. Tang and B. Liu*; Specific Light-Up Bioprobe with Aggregation-Induced Emission and Activatable Photoactivity for the Targeted and Image-Guided Photodynamic Ablation of Cancer Cells; *Angew. Chem. In.t Ed.*, **2015**, 54, 1780-1786.

15. C. J. Zhang, Q. Hu, G. Feng, **R. Zhang**, Y. Yuan, X. Lu and B. Liu*; Image-Guided Combination Chemotherapy and Photodynamic Therapy Using a Mitochondria-Targeted Molecular Probe with Aggregation-Induced Emission Characteristics; *Chem. Sci.*, **2015**, 6, 4580-4586.

16. Y. Yuan, C. J. Zhang, R. T. K. Kwok, S. Xu, **R. Zhang,** J. Wu, B. Z. Tang* and B. Liu*; Light-Up Probe for Targeted and Activatable Photodynamic Therapy with Real-Time In Situ Reporting of Sensitizer Activation and Therapeutic Responses; *Adv. Funct. Mater.* **2015**, 25, 6586-6595.